THROMBOMODULIN/HEPARIN FUNCTIONALIZED MEMEBRANE-MIMETIC ASSEMBLIES: STRATEGIES FOR GENERATING AN ACTIVELY ANTI-THROMBOGENIC SURFACE

A Thesis
Presented to
The Academic Faculty

By

Po-Yuan Tseng

In Partial Fulfillment
Of the Requirements for the Degree
Doctor of Philosophy in Bioengineering

Georgia Institute of Technology

August 2005

THROMBOMODULIN/HEPARIN FUNCTIONALIZED MEMEBRANE-MIMETIC ASSEMBLIES: STRATEGIES FOR GENERATING AN ACTIVELY ANTI-THROMBOGENIC SURFACE

Approved by:

Dr. Elliot L. Chaikof, Advisor
Department of Surgery and
Biomedical Engineering
Emory University
School of Chemical and
Biomolecular Engineering
Georgia Institute of Technology

Dr. Athanassios Sambanis
School of Chemical and
Biomolecular Engineering
Georgia Institute of Technology

Dr. Stephen R. Hanson
Department of Biomedical Engineering
Oregon Health & Science University

Dr. Ajit Yoganathan
Department of Biomedical Engineering
Georgia Institute of Technology

Dr. John S. "Pete" Lollar
Department of Pediatrics
Emory University

Date Approved: July 11, 2005

ACKNOWLEDGEMENTS

I dedicate this work to my parents, my elder brother, and my sister-in-law, who have been very supportive in Taiwan while I was studying overseas all these years. Also I want to dedicate this to my best friend also my girlfriend, Ivy Ho, and thank for her great patience and encouragement to my long-term study.

I would like to express my most sincere gratitude to my academic advisor, Dr. Elliot Chaikof, for his excellent guidance and bringing extraordinary ideas that could potentially resolve challenging questions in fundamental and applied biomedical research, which is a tremendous impact on the development of my professional career. His excellent work on being an advisor as well as management of his Biomaterials and Tissue Engineering Laboratory within Department of Surgery at Emory University will always be something I am going to remember him by.

I am also very grateful to Drs Stephen Hanson, Pete Lollar, Athanassios Sambanis, and Ajit Yoganathan for serving as my thesis committee and providing valuable suggestions for my thesis.

I wish to extend my appreciation to the Department of Chemical Engineering and Biomedical Engineering at the Georgia Institute of Technology for admitting me in Bioengineering Program so that I can experience to study in two excellent universities: Georgia Tech and Emory.

This work would not have been possible without any aid from a group of people. I would like to thank all my lab members, including former ones, who have been not only very helpful to my research, but also very supportive to cheer me up when things were

getting rough. For my thesis research, I especially thank Dr. June Feng (a former lab member) for her mentoring me in characterizing enzyme activity, Dr. Keith Faucher (a former lab member) for his excellent experience in surface characterization, Dr. Xue-Long Sun for his tremendous contribution to the current basis of membrane-mimetic structure, Dr. Shyam Rele for his great help on synthesis of bio-conjugated materials, and Dr. Matheau Julien for his guidance and help on the radiolabeling technique. In addition, I would like to thank Dr. Howard Rees from the Department of Neurology at Emory for training me on using confocal microscope and Mr. Dale Rice from Medical Engineering at Emory University Hospital for his craftsmanship in building gadgets for my experiments.

I would like to extend my thanks Beverly Noe for her kind help in all the technical accounting and lab logistics, and Valerie Panditaratne for her kindness and help for providing seminar information and organizing special events for the whole lab.

Finally, I would to thank my family and my girlfriend, Ivy Ho, again for their support during the past six years. I would not have survived if it would not have been your caring, affection, and unconditional trust and support in my endeavors.

TABLE OF CONTENTS

ACKNOWLEDGEMENTS iii

LIST OF TABLES ix

LIST OF TABLES ix

LIST OF FIGURES xi

SUMMARY xix

CHAPTER 1. INTRODUCTION 1
1.1 RATIONALE 1
1.2 GOAL AND SPECIFIC AIMS 2

CHAPTER 2. BACKGROUND 4
2.1 OVERVIEW 4
2.2 REGULATION OF BLOOD COAGULATION 6
2.3 THE EFFECT OF FLOW ON BLOOD COAGULATION 8
2.4 SURFACE MODIFICATION OF VASCULAR SUBSTITUTES 9
2.5 BIOMEMBRANE-MIMETIC MODELS 10

CHAPTER 3. FABRICAION AND CHARACTERIZATION OF FUNCTIONAL THROMBOMODULIN-INCORPORATED MEMBRANE-MIMETIC ASSEMBLIES 14
3.1 ABSTRACT 14
3.2 INTRODUCTION 15
3.3 MATERIALS AND METHODS 23
3.3.1 Materials 23
3.3.2 Layer-By-Layer Assembly of an Alkylated Alginate/Poly-L-Lysine (ALG/PLL) Multilayer on a Glass Surface 24
3.3.3 Reconstitution of Thrombomodulin into Lipid Vesicles 24
3.3.4 Formation of a Thrombomodulin Containing Membrane-Mimetic Thin Film 25
3.3.5 Determination of Thrombomodulin Surface Density and Stability within a Polymeric Lipid Membrane 26
3.3.6 Analysis of TM Catalytic Activity 26
3.3.7 Continuous Flow Reactor Assays on Thrombomodulin Containing Membrane-Mimetic Surface 27
3.3.8 Stability Tests on Bioactivity of Thrombomodulin Incorporated Membrane-Mimetic Surface 28
3.4 RESULTS AND DISCUSSION 29
3.4.1 Robust Membrane-Mimetic Films can be Constructed on Planar Substrates with Predictable Surface Concentrations of Catalytically Active TM 30

3.4.2 Theoretical Considerations of the Surface TM-Catalyzed Flow Reactor 35
3.4.3 Experimental Analysis of TM-Mediated Activated Protein C Production Under Laminar Flow Conditions 42
3.4.4 Stability of Surface TM Activity 46
3.5 CONCLUSIONS 50

CHAPTER 4. FABRICATION AND CHARACTERIZATION OF HEPARINIZED SURFACE BASED ON MEMBRANE-MIMETIC ASSEMBLIES 51
4.1 ABSTRACT 51
4.2 INTRODUCTION 52
4.3 MATERIALS AND METHODS 58
4.3.1 Materials 58
4.3.2 Synthesis of Biotin-Conjugated Heparin 59
4.3.3 Purification of Biotin-Conjugated Heparin 63
4.3.4 Determination of Biotin Content From Biotin-Conjugated Heparin 63
4.3.5 Analysis of Biotin-Heparin Activity 64
4.3.6 Fabrication of Biotin-Functionalized Membrane-Mimetic Thin Films 65
4.3.7 Fabrication of a Heparinized Surface Based on a Membrane-Mimetic Thin Film 66
4.3.8 Determination of Heparin Surface Density 66
4.3.9 Continuous Flow Reactor Assays on Heparinized Surface 67
4.4 RESULTS AND DISCUSSION 70
4.4.1 Synthesis of Biotin-Conjugated Heparin 70
4.4.2 Analysis of Biotin-Heparin Activity 77
4.4.3 Determination of Heparin Surface Density 82
4.4.4 Flow Effect on Catalytic Efficiency of Heparinized Surface 86
4.5 CONCLUSIONS 91

CHAPTER 5. FABRICATION AND CHARACTERIZATION OF TISSUE FACTOR-COATED SURFACE BASED ON MEMBRANE-MIMETIC ASSEMBLIES 92
5.1 ABSTRACT 92
5.2 INTRODUCTION 94
5.3 MATERIALS AND METHODS 99
5.3.1 Materials 99
5.3.2 Reconstitution of Tissue factor into Phospholipid vesicles 100
5.3.3 Fabrication of Tissue Factor Containing Membrane-Mimetic Surface 101
5.3.4 Continuous Flow Reactor Assays on Tissue Factor Containing Membrane-Mimetic Surface 101
5.4 RESULTS AND DISCUSSION 103
5.4.1 Fluorescent Images of Lipid Vesicles Bound onto Membrane-Mimetic Films 103
5.4.2 Surface Activity of Tissue Factor Under Flow Conditions 105
5.4 CONCLUSIONS 114

CHAPTER 6. REGULATORY EFFECTS OF THROMBOMODULIN, HEPARIN, AND THROMBOMODULIN/HEPARIN COMPOSITE SURFACES ON TISSUE FACTOR-INDUCED THROMBIN GENERATION 116
6.1 ABSTRACT 116
6.2 INTRODUCTION 118
6.3 MATERIALS AND METHODS 123
6.3.1 Materials 123
6.3.2 Fabrication of Localized Tissue Factor Containing Membrane-Mimetic Surfaces. 124
6.3.3 Determination of Tissue Factor Surface Density and Stability 126
6.3.4 Fabrication of Composite Tissue Factor/Thrombomodulin, Tissue Factor/Heparin, and Tissue Factor/Thrombomodulin-Heparin Containing Membrane-Mimetic Surfaces 126
6.3.5 Continuous Flow Reactor Assays on Immobilized Catalysts-Containing membrane-mimetic surface: Effects of Anticoagulants on Thrombin Generation Triggered by TF 127
6.4 RESULTS AND DISCUSSION 130
6.4.1 Lipid Vesicles Tethered onto Biotin-Functionalized Membrane-Mimetic Films 130
6.4.2 Determination of Tissue Factor Surface Density 132
6.4.3 Surface Activity of Tissue Factor Under Flow Conditions: As a Source of Thrombin Generation From Upstream 135
6.4.4 Effect of Surface Anticoagulants on Tissue Factor-Initiated Thrombin Generation Under Flow Conditions 141

CHAPTER 7 DISCUSSION 168

CHAPTER 8 CONCLUSIONS 16874

CHAPTER 9 FUTURE WORK AND RECOMMENDATIONS 179

APPENDIX A. Standard Protein Concentrations for Chromogenic Assay 181

APPENDIX B. Theoretical Considerations of Transport Effect on Surface Enzymatic Reaction…. 184

APPENDIX C. Activated Protein C Generation Under Flow Conditions 188

APPENDIX D. Purification of Biotin-Conjugated Heparin Through Avidin Column 189

APPENDIX E. Fact Xa and Thrombin Generation From TF-coated (Entire Flow-Exposed) Surface 193

APPENDIX F. Tissue Factor Surface Density 195

APPENDIX G. Thrombin Generation From TF-Coated (Localized at the Upstream) Surface 196

APPENDIX H. *F* Test for Equality of $[T]_{max}$ and $[T]_{ss}$ means among TF+AT, TF/TM+AT, TF/Heparin, and TF/TM-Heparin Systems 198

APPENDIX I. Tukey Multiple Comparison Procedure 200

REFERENCES 202

LIST OF TABLES

Table 1 Damköhler number (Da) at a series of TM surface concentration under flow conditions. Da is defined as the ratio of maximum rate of kinetic reaction (V_{max}) over maximum rate of transport (kC_0). Vmax is obtained from the product of k_{cat} (79) and TM surface concentration ($[E]_t$), while kC_0 is obtained from analytical expression shown in equation (6). 41

Table 2 Parameters of TM Density Titrations. The TM density plots (Lineweaver-Burk plot) of figure 10 were fit to a hyperbola. The maximal APC production rate ($V_{max\ E}$) and the TM density resulting in half-maximal rate of reaction ($K_{1/2\ E}$) are shown. 45

Table 3 Polydispersity and molecular weight of heparin and biotin-heparin from SEC and LLS. Adopted with permission from (136). 76

Table 4 Comparison of experimental values of the second order rate constant between heparin and biotin-heparin. 81

Table 5 Comparison of dissociation constants of heparin-antithrombin (K_{HI}) and the second order rate constants with heparin (k) between current and previous studies. 81

Table 6 Characterization of heparin surface concentration (mean ± standard deviation, n = 6) resulted from biotin-AcPE mole% within membrane-mimetic thin film. 84

Table 7 Parameters of TF Density Titrations. The TF density plots (Lineweaver-Burk plot) of Figure 25 were fit to a hyperbola. The maximal factor Xa production rate ($V_{max\ E}$) and the TF density resulting in half-maximal rate of reaction ($K_{1/2\ E}$) are shown. Data represent mean ± standard deviation (n = 5). 108

Table 8 Steady state concentrations (mean ± standard deviation, n = 5) of thrombin at a series of TF surface densities. 138

Table 9 Steady state rate of thrombin (T) generation (mean ± standard deviation, n = 5) at a series of TF surface densities. Steady state rates of thrombin generation (pmol/min/cm^2) in the presence of more than 50 fmole TF per cm^2 are 2.75 ± 0.25 and 11.77 ± 1.30 at shear rates of 50 and 500 sec-1 respectively 140

Table 10 Summary of thrombin responses from a variety of surface systems, including maximum thrombin generation ($[T]_{max}$, nM) and rate of reaction (RT_{max}, pmole/min/cm^2), steady state thrombin generation ($[T]_{ss}$, nM) and rate of reaction (RT_{ss}, pmole/min/cm^2), and drop % of thrombin generation (mean

value comparison of $[T]_{max}$ or $[T]_{ss}$ with respect to $[T]_{TFss}$). Each data value for $[T]_{max}$, RT_{max}, $[T]_{ss}$, and RT_{ss} is presented as mean ± standard deviation (n = 5). 158

Table 11 Comparisons of transient peak ([T]max) and steady state ([T]ss) using ANOVA with Tukey multiple comparison procedure between test surfaces in the absence and presence of TM (TF+AT vs. TF/TM+AT and TF/Heparin vs. TF/TM-Heparin), and between test surfaces in the absence and presence of heparin, (TF+AT vs. TF/Heparin and TF/TM+AT vs. TF/TM-Heparin). Confidence intervals (C.I.) indicate whether the comparison of [T]max is significantly different or not for confidence coefficient of 95 percent. A value of $P < 0.05$ was used to define statistical significance. 161

Table C APC generation (nM) as a function of perfusion time at a series of TM surface concentrations (fmole/cm^2). Each data point represents the mean ± standard error (n = 5). 188

Table E1 Factor Xa generation as a function of perfusion time at a series of TF surface concentrations (fmole/cm^2). Each data point represents the mean ± standard error (n = 5). 193

Table E2 Thrombin generation as a function of perfusion time at a series of TF surface concentrations (fmole/cm^2). Each data point represents mean ± standard error (n = 5). 194

Table F1 Tissue factor surface density (fmole/cm^2) as a function of TF concentration (nM)[a] within lipid vesicles (1mM of egg PC/brain PS/ biotin-PE, 79:20:1 molar ratio). Stability of TF coated surface was assessed by incubating the sample with PBS at 37 °C over a 28-day period. The samples were transferred to fresh PBS at indicated time points and radioactivity measured in a gamma counter. Each data point represents mean ± standard deviation (n = 6). 195

Table G1 Thrombin generation (nM, mean ± standard error, n = 5) vs. perfusion time for a variety of composite surfaces including TF, TF/TM, TF/heparin, and TF/TM-heparin systems. 196

Table G2 Rate of thrombin generation (pmole/min/cm^2, mean ± standard error, n = 5) vs. perfusion time for a variety of composite surfaces including TF, TF/TM, TF/heparin, and TF/TM-heparin systems. 197

LIST OF FIGURES

Figure 1 The blood coagulation cascades. The intrinsic cascade is initiated when contact is made between blood and surfaces. The extrinsic pathway is initiation upon vascular injury which leads to exposure of tissue factor (TF) (also identified as factor III), a subendothelial cell-surface glycoprotein that binds phospholipid. The two pathways converge at the activation of factor X to Xa. Factor Xa has a role in the further activation of factor VII to VIIa as depicted by the dashed arrow. Active factor Xa hydrolyzes and activates prothrombin to thrombin. Thrombin can then activate factors VIII and V furthering the cascade. Ultimately the role of thrombin is to convert fibrinogen to fibrin and to activate factor XIII to XIIIa. Factor XIIIa cross-links fibrin polymers solidifying the clot. 5

Figure 2 Schematic representation of a polymeric phospholipid monolayer composed of 1-palmitoyl-2-[12-(acryloyloxy) dodecanoyl]-sn-glycero-3-phosphorylcholine supported on an alkylated polyelectrolyte multilayer (Not to scale). 13

Figure 3 Schematic representation of TM functionalized polymeric phospholipid monolayer supported on an alkylated polyelectrolyte multilayer. (Not to scale) 20

Figure 4 Schematic of parallel plate flow reactor (not to scale). The gasket (plastic shim) creates height of the flow channel. TM containing membrane-mimetic construct is immobilized onto a glass substrate. The surface is perfused with reactants and the perfusate is collected at the outlet to determine product concentration. 22

Figure 5 The relationship between the rate of surface mediated protein C activation (nM/min/cm2) and the concentration of TM in the fusion mixture. Adopted with permission from (79). 30

Figure 6 (A) Serial measurements (mean ± S.D.) of the rate of protein C activation for a TM containing lipid film incubated in PBS at 4 °C. (B) Serial measurements (mean ± S.D.) of the rate of protein C activation for a TM containing lipid film incubated in plasma at 37 °C. All values are normalized with respect to the initial rate protein C activation in PBS. Adopted with permission from (79). 32

Figure 7 TM surface density and stability within a polymeric lipid membrane. TM was radiolabeled with 125I and reconstituted into lipid vesicles, and surface concentration was determined after the formation of a polymeric lipid assembly. The stability of this system was assessed in PBS at 37 °C over a 28-

day period. Films were transferred to fresh PBS at indicated time points and radioactivity measured in a gamma counter. 33

Figure 8 Stability of TM surface concentrations for [TM] = 300nM for lipid fusion. The surface samples were incubated with PBS at 37^{o}C and radioactivity was detected at time points up to four weeks..... 34

Figure 9 Schematic of fluid dynamic profiles in a parallel plate flow system for surface catalytic reaction. (Not to scale) 38

Figure 10 Kinetics of APC generation ([APC] vs. perfusion time) at a wall shear rate of (A) 50 sec^{-1} and (B) 500 sec^{-1} with TM surface concentrations of 1351 (●), 764(○), 488 (■), 344 (□), 162 (▲), 82 (Δ), 66 (▼) fmole/cm^2. Each data point represents the mean (n = 5) at perfusion timed points (see Appendix C). 44

Figure 11 Rate of steady state protein C activation as a function of TM surface concentration at two different shear rates 50 and 500 sec-1. Each data point represents the mean ± standard deviation (n = 5). Note: rate of APC generation (pmole/min/cm^2) = APC generation (nM) x flow rate (mL/min) / reactor surface area (cm^2) 45

Figure 12 Stability of TM activities. Surface samples were incubated in phosphate-buffered saline (PBS, 1X) at 37^{o}C (A) steady-state APC generation (nM) and (B) rate of steady state APC generation (pmole/min/cm^2) at shear rates 50 sec^{-1} and 500 sec^{-1}. Each data point represents the mean ± standard deviation (n = 5). 48

Figure 13 Stability of TM activities. Surface samples were incubated within normal pooled human plasma at 37^{o}C. (A) steady-state APC generation (nM) and (B) rate of steady state APC generation (pmole/min/cm^2) at shear rates 50 sec^{-1} and 500 sec^{-1}. Each data point represents the mean ± standard deviation (n = 5). 49

Figure 14 Heparin is a heterogeneous mixture of polysaccharides, which chains are made up of alternating 1 to 4 linked, sulfated monosaccharide residues of L-iduronic acid and D-glucosamine. The most frequent types of disaccharide unit represent up to 90% of the structure of beef-lung heparin, and up to 70% of pig-mucosa heparin (A). The unique pentasaccharide binding site for antithrombin occurs in about one-third of the heparin chains (B). 54

Figure 15 Schematic representation of immobilized heparin on the basis of polymeric phospholipid monolayer supported on an alkylated polyelectrolyte multilayer. (Not to scale)..... 57

Figure 16. Sequential procedure for the synthesis of biotinylated heparin. Adopted with permission from (136)..... 62

Figure 17 Schematic of parallel plate flow reactor (not to scale). The gasket (plastic shim) creates height of the flow channel. Heparin containing membrane-mimetic construct is immobilized onto a glass substrate. The surface was perfused with reactants, thrombin and antithrombin (ATIII) in separate syringes and the perfusate is collected at the outlet to determine product concentration..... 69

Figure 18 ^{1}H NMR spectrum of heparin-lactone (600 MHz/D_2O). Adopted with permission from (136)..... 73

Figure 19 ^{1}H NMR of amine terminated biotin spacer arm in $CD_3OD/CDCl_3$ mixture (600 MHz). Adopted with permission from (136)..... 74

Figure 20 1H NMR spectra of biotin-functionalized heparin D_2O (600 MHz). Adopted with permission from(136). 75

Figure 21 Size Exclusion Chromatography (SEC)/ Laser Light Scattering (LLS) profiles of chemically modified heparin. Adopted with permission from (136). 76

Figure 22 Thrombin inactivation by antithrombin in the presence of various (A) heparin or (B) biotin-heparin concentrations. Results for heparin concentrations ranging from 10 nM to 1 μM are presented: 0 (○),10 nM (■), 40 nM (□), 0.1 μM (▲), 1 μM (Δ). Each data point represents a mean value at each reaction time point (n = 4). 80

Figure 23 Surface density of biotin-heparin as a function of mole% of biotin-AcPE within membrane-mimetic construct. Each data point represents mean ± standard deviation (n = 6). 84

Figure 24 Lineweaver-Burke plot of data points from Figure 21. The linear relationship indicates the binding mechanism might follow Langmuir binding isotherm. 85

Figure 25 Thrombin inactivation at timed points during the perfusion of thrombin and antithrombin over heparinized surface with surface concentrations of 0 (○). 3.47 (●), 4.36 (□), 5.34 (■), and 5.94 pmole/cm^2 (Δ) at shear rates of (A) 50 sec^{-1} (B) 500 sec^{-1}. Each data point represents a mean value (n = 4). 87

Figure 26 Kinetic data of levels of thrombin decay over perfusion time as a function of heparin surface concentrations (3.47 (●), 4.36 (□), 5.34 (■), and 5.94 pmole/cm^2 (Δ)) at shear rates of (A) 50 sec^{-1}and (B) 500 sec^{-1}. Each data point represents a mean value (n = 4). Note: the level of thrombin decay as the difference between the initial thrombin concentration, i.e. 30 nM, and a thrombin response at a timed point from Figure 23..... 88

Figure 27 Rate of thrombin inactivation (= level of thrombin decay x flow rate / flow-exposed heparinized surface area) as a function of heparin surface concentrations (3.47 (●), 4.36 (□), 5.34 (■), and 5.94 pmole/cm^2 (Δ)) at shear rates of (A) 50 sec^{-1}and (B) 500 sec^{-1}. Each data point represents a mean value (n = 4). 89

Figure 28 Steady state rate of thrombin inactivation as a function of heparin surface concentration. Saturated rates of thrombin inactivation were 0.20 ± 0.01 and 0.82 ± 0.03 pmole/min/cm^2 (mean ± standard deviation) in the presence of surface heparin equal to or greater than 4.36 pmole/cm^2 at shear rates of 50 (○) and 500 (●) sec^{-1}. Data points represent the mean values ± standard deviation (n = 4). 90

Figure 29 Schematic representation of immobilized relipidated tissue factor on the basis of polymeric phospholipid monolayer supported on an alkylated polyelectrolyte multilayer. (Not to scale) 98

Figure 30 The fluorescent images (20x) of 1mM lipid vesicle coated surfaces. 0.1 mol% FITC-doped lipid vesicles were coated on surface containing 0 mol% biotin-AcPE/AcPC (control) (A), 5 mol% biotin-AcPE/AcPC (B), 10 mol% of biotin-AcPE/AcPC (C), and 50 mole% biotin-AcPE/AcPC (D) through biotin-streptavidin binding system 104

Figure 31 Factor Xa generation with various TF surface concentrations (9.4 (●) 27.3 (○) 51.2 (■) 69.9 (□) 88.6 (▲) fmole/cm2) at shear rates of (A) 50 sec^{-1} and (B) 500 sec^{-1}. Each data point represents a mean value for five experiments (see Appendix E1 for raw data). 107

Figure 32 Steady state rate of factor Xa production as a function of TF surface concentration at shear rates of 50 sec^{-1}(○) and 500 sec^{-1}(●). Each data point represents a mean ± standard deviation (n = 5). Steady state rate of factor Xa generation (pmole/min/cm^2) = steady state factor Xa generation (nM) x flow rate (mL/min)/reactor surface area cm^2). 108

Figure 33 Thrombin generation with various TF surface concentrations (9.4 (●) 27.3 (○) 51.2 (■) 69.9 (□) 88.6 (▲) fmole/cm^2) at shear rates of (A) 50 sec^{-1} and (B) 500 sec^{-1}. Each data point represents a mean value for five experiments (see Appendix E2 for raw data). 112

Figure 34 (A) Thrombin concentration (nM) and (B) rate of thrombin generation (pmole/min/cm^2) as a function of TF concentration within lipid vesicles at shear rates of 50 (●) and 500 (○) sec^{-1}. Each data point represents a mean ± standard deviation (n =5). 113

Figure 35 Schematic representation of immobilized thrombomodulin (TM), tissue factor (TF), and heparin on the basis of biotin functionalized polymeric phospholipid monolayer supported on an alkylated polyelectrolyte multilayer. Relipidated TF is positioned at the upstream of the flow (Not to scale). 122

Figure 36 (A) Schematic representation for TF-coating process. Supporting substrates were pretreated with biotin-functionalized membrane-mimetic assemblies, followed by immobilization of streptavidin, then the streptavidin-coated surfaces facing inwards were dipped into relipidated tissue factor mixture at room temperature for 30 minutes. (B) The resulting localized TF-coated area (yellow). (Not to scale) 125

Figure 37 Fluorescent images (20x) of FITC-doped biotinylated lipid vesicles on Si coated with membrane-mimetic thin film (90/10 acrylate PC/biotin-acrylate PE) were taken before (A) and after (B) shear flow exposed to PBS at 2000 sec^{-1} for 1 hour. 131

Figure 38 Relipidated TF surface density as a function of TF concentration within lipid vesicles (1mM of egg PC/brain PS/ biotin-PE, 79:20:1 molar ratio). TF was radiolabeled with ^{125}I and reconstituted into lipid vesicles. Surface concentration was determined after immobilizing onto streptavidin-biotinylated polymeric membrane-mimetic constructs. The stability of this system was assessed in PBS at 37 °C over a 28-day period. Films were transferred to fresh PBS at indicated time points and radioactivity measured in a gamma counter. Each data point represents mean ± standard deviation (n = 6) (see Tables in Appendix F)..... 133

Figure 39 Stability of relipidated TF surface density and based on membrane-mimetic thin films. The stability of this system was assessed in PBS at 37 °C over a 28-day period. Note: a series of TF concentrations within lipid vesicles were prepared for immobilization: 6 nM (●),12 nM (○),30 nM (■), 60 nM (□), 90 nM (▲), and 120 nM (Δ). Each data point represents mean ± standard deviation (n = 6) (see Tables in Appendix F). 134

Figure 40 TF-induced thrombin generation at the reactor outlet over perfusion time as a function of surface TF concentrations (TF density: 9.4 (●) 27.3 (○) 51.2 (■) 69.9 (□) 88.6 (▲) fmole/cm2) at wall shear rates of (A) 50 $sec^{-1}$and (B) 500 sec^{-1}. Each data point represents a mean value (n = 5). (see Table G2 in Appendix G)..... 137

Figure 41 Steady state level of thrombin generation as a function of TF surface density at wall shear rates of 50 sec^{-1} and 500 sec^{-1}. Each data point represent a mean value ± standard deviation (n = 5). The results show that thrombin generation becomes saturated in the presence of more than 50 $fmole/cm^2$. 138

Figure 42 Rate of TF-induced thrombin generation at the reactor outlet over perfusion time as a function of surface TF concentrations (TF density: 9.4 (●) 27.3 (○) 51.2 (■) 69.9 (□) 88.6 (▲) fmole/cm^2) at wall shear rates of (A) 50 sec^{-1}and (B) 500 sec^{-1}. Each data point represent a mean value (n = 5). (see Table G2 in Appendix G). Note: rate of reaction = thrombin generation (Figure 40) x flow rate / surface area of reactor (= 0.6 (W, cm) x 3.6 (L, cm) = 2.16 cm^2) 139

Figure 43 Steady-state rate of thrombin generation as a function of TF surface density at wall shear rates of 50 sec^{-1} (●) and 500 sec^{-1} (○). Each data point represent a mean value ± standard deviation (n = 5)..... 140

Figure 44 Thrombin generation at the reactor outlet over perfusion time from TF (●) and TF/TM (○) surfaces TF positioned at the upstream at wall shear rates of (A) 50 sec^{-1} (B) 500 sec^{-1}. Each data point represents a mean value (n = 5) with a standard error less than 10% (see Table G1 in Appendix G)..... 142

Figure 45 Rate of thrombin generation at the reactor outlet over perfusion time from TF (●) and TF/TM (○)surfaces with TF positioned at the upstream at wall shear rates of (A) 50 sec^{-1} (B) 500 sec^{-1}. Each data point represents a mean value (n = 5) with a standard error less than 10%. Note: rate of reaction = thrombin generation (Figure 42) x flow rate / surface area of reactor (= 0.6 (W, cm) x 3.6 (L, cm) = 2.16 cm^2). (see Table G2 in Appendix G) 143

Figure 46 Thrombin generation at the reactor outlet over perfusion time from TF (●), TF/TM (○), and TF+AT (■) surfaces with TF positioned at the upstream at wall shear rates of (A) 50 sec^{-1} (B) 500 sec^{-1}. Each data point represents a mean value (n = 5) with a standard error less than 10%. (see Table G1 in Appendix G1)..... 145

Figure 47 Rate of thrombin generation at the reactor outlet over perfusion time from TF (●), TF/TM (○), and TF+AT (■) surfaces with TF positioned at the upstream at wall shear rates of (A) 50 sec^{-1} (B) 500 sec^{-1}. Each data point represents a mean value (n = 5) with a standard error less than 10% (see Table G2 in Appendix G). Note: rate of reaction = thrombin generation (Figure 44) x flow rate / surface area of reactor (= 0.6 (W, cm) x 3.6 (L, cm) = 2.16 cm^2). 146

Figure 48 Thrombin generation at the reactor outlet over perfusion time from TF (●), TF/TM (○), TF+AT (■), and TF/TM+AT (□) surfaces with TF positioned at the upstream at wall shear rates of (A) 50 sec^{-1} (B) 500 sec^{-1}. Each data point represents a mean value (n = 5) with a standard error less than 10%. (see Table G1 in Appendix G). 148

Figure 49 Rate of thrombin generation at the reactor outlet over perfusion time from TF (●),TF/TM (○), TF+AT (■), and TF/TM+AT (□) surfaces with TF

positioned at the upstream at wall shear rates of (A) 50 sec^{-1} (B) 500 sec^{-1}. Data points represent mean values (n = 5) with a standard error less than 10%. (see Table G2 in Appendix G). Note: rate of reaction = thrombin generation (Figure 46) x flow rate / surface area of reactor (= 0.6 (W, cm) x 3.6 (L, cm) = 2.16 cm^2). 149

Figure 50 Thrombin generation at the reactor outlet over perfusion time from TF (●),TF/TM (○), TF + ATIII (■), TF/TM + ATIII (□), and TF/Heparin (▲) surfaces with TF positioned at the upstream at wall shear rates of (A) 50 sec^{-1} (B) 500 sec^{-1}. Each data point represents a mean value (n = 5) with a standard error less than 10%. (see Table G1 in Appendix G). 151

Figure 51 Rate of thrombin generation at the reactor outlet over perfusion time from TF (●),TF/TM (○), TF + ATIII (■), TF/TM + ATIII (□), and TF/Heparin (▲) surfaces with TF positioned at the upstream at wall shear rates of (A) 50 sec^{-1} (B) 500 sec^{-1}. Each data point represents a mean value (n = 5) with a standard error less than 10% (see Table G2 in Appendix G). Note: rate of reaction = thrombin generation (Figure 48) x flow rate / surface area of reactor (= 0.6 (W, cm) x 3.6 (L, cm) = 2.16 cm^2). 152

Figure 52 Thrombin generation at the reactor outlet over perfusion time from TF (●),TF/TM (○), TF + AT (■),TF/TM + AT (□), TF/Heparin (▲), and TF/TM-heparin (Δ) surfaces with TF positioned at the upstream at wall shear rates of (A) 50 sec^{-1} (B) 500 sec^{-1}. Each data point represents a mean value (n = 5) with a standard error less than 10% (see Table G1 in Appendix G)..... 154

Figure 53 Rate of thrombin generation at the reactor outlet over perfusion time from TF (●),TF/TM (○), TF + ATIII (■), TF/TM + ATIII (□), TF/Heparin (▲), and TF/TM-heparin (Δ) surfaces with TF positioned at the upstream at wall shear rates of (A) 50 sec^{-1} (B) 500 sec^{-1}. Each data point represents a mean value (n = 5) with a standard error less than 10% (see Table G2 in Appendix G). Note: rate of reaction = thrombin generation (Figure 31) x flow rate / surface area of reactor (= 0.6 (W, cm) x 3.6 (L, cm) = 2.16 cm^2). 155

Figure 54 Thrombin responses at (A) peak ([T]max, nM) and (B) steady state ([T]ss, nM) levels from TF surfaces in the presence of ATIII only (TF+AT), surface heparin (TF/Heparin), surface TM (TF/TM+AT) and both surface heparin and TM (TF/TM-Heparin) at shear rates of 50 sec^{-1}. P values are analyzed from comparisons between surfaces in the absence and presence of TM (TF+AT vs. TF/TM+AT and TF/Heparin vs. TF/TM-Heparin), and between surfaces in the absence and presence of heparin, (TF+AT vs. TF/Heparin and TF/TM+AT vs. TF/TM-Heparin). The error bars represent standard deviation (n = 5)..... 159

Figure 55 Thrombin responses at (A) peak ([T]max, nM) and (B) steady state ([T]ss, nM) levels from TF surfaces in the presence of ATIII only (TF+AT), surface heparin (TF/Heparin), surface TM (TF/TM+AT) and both surface heparin and

TM (TF/TM-Heparin) at shear rates of 500 sec^{-1}. P values are analyzed from comparisons between surfaces in the absence and presence of TM (TF+AT vs. TF/TM+AT and TF/Heparin vs. TF/TM-Heparin), and between surfaces in the absence and presence of heparin, (TF+AT vs. TF/Heparin and TF/TM+AT vs. TF/TM-Heparin). The error bars represent standard deviation (n = 5)..... 160

Figure A1 Standard curve of activated protein C. A linear relationship between [APC] (nM) and rate of absorbance change (dA/min) was observed: [APC] (nM) = 3761.8 (dA/min) – 3.0693..... 181

Figure A2 Standard curve of factor Xa. A linear relationship between [Xa] (nM) and rate of absorbance change (dA/min) was observed: [Xa] (nM) = 840.67 (dA/min) – 4.3823..... 182

Figure A3 Standard curve of thrombin. A linear relationship between [thrombin] (nM) and rate of absorbance change (dA/min) was observed: [thrombin] (nM) = 406.09 (dA/min) – 0.0901..... 183

Figure D1 The UV-VIS scanning results demonstrate (A) the complete bound biotin-heparin in avidin column after washing with PBS (step 7) and (B) recovery of the bound compound after washing with Biotin Blocking and Elution Buffer (step 8). For PBS washing, non-bound material was completely removed after the third fraction collection (f#3). As for recovery of the biotin-heparin from the avidin column, scanning curves almost overlap with that of pure biotin blocking buffer after collecting fraction #5 (f#5), indicating the biotin-heparin was fully recovered. 192

SUMMARY

Synthetic materials have been successful in applications requiring large-diameter (>5 to 6 mm) vascular substitutes. However, in smaller diameter applications such as peripheral vascular repair below the knee or coronary bypass are not effective due to serious thrombosis and hemostasis. It has been recognized that established paradigms based on natural systems provide strategies to design functional biomaterials ad hoc to improve the performance of synthetic grafts. Particularly, the biological membrane has been used as a model system for the development of biosensors, drug delivery systems, and surface modified medical devices. We postulate that membrane-mimetic systems, incorporating with biologically functional substances, may offer a useful approach to improve the long- term efficacy of the synthetic grafts by modulating surface-mediated blood coagulation.

The membrane-mimetic construct contains polymeric phospholipid monolayer on an alkylated polyelectrolyte multilayer supported by planar substrate such as glass or silicone. When incorporated with thrombomodulin (TM), a transmembrane protein constitutively expressed by endothelial cells, the model platform exhibited the biological function by facilitating activation of protein C, which is a potent anticoagulant. Surface TM-medicated protein C activation was extensively studied under flow conditions by perfusion of protein mixture at 50 and 500 sec^{-1}, the physiologic venous and arterial shear rates, respectively. Significantly, surface TM activity was limited in the presence of TM surface density more than 800 $fmole/cm^2$ due to a transport limitation. By storing the surface in human plasma and investigating surface activity under the same flow

conditions periodically, we found the stability of TM bioactivity can retain up to two months. In addition to creating a TM- incorporated membrane-mimetic thin film, we also immobilized heparin based on the same membrane-mimetic construct as an alternative for potential antithrombogenic system. The heparinized surface was fabricated by anchoring biotin-conjugated heparin onto biotinylated phospholipid membrane through biotin-streptavidin binding interactions. Surface heparin activity was investigated to determine its catalytic efficiency for thrombin inactivation by perfusion of thrombin and antithrombin at shear rates of 50 and 500 sec^{-1}. The efficiency on thrombin decay can not be improved significantly in the presence of heparin surface density more than 4.4 $pmole/cm^2$, indicating mass transport of reactants onto catalytic surface is the rate-limiting factor.

We designed a membrane-mimetic-system-based tissue factor (TF)-coated surface as a vascular injury-mimetic system to initiate thrombin generation. The purpose of this design was to determine antithrombogenic capacity of the above two surface anticoagulants. We investigated thrombin responses by perfusion of a mixture of relevant coagulation proteins and inhibitors over a composite surface system containing TF positioned at the upstream and TM and/or heparin at the downstream of the flow. Although initial thrombin generation cannot be completely inhibited in the presence of TM and heparin, they have potential to shut down thrombin generation completely at the end of perfusion. Due to the complexity of intertwined effects of transport and surface reactions on regulation of thrombin generation, we attempt to work on a mathematical model to provide in depth analyses of the experimental results as a future work. In addition, we will try to investigate the capacity of the surface anticoagulants to inhibit

coagulation in vitro using human plasma or blood. Ultimately, we are looking forward to applying these membrane-mimetic systems to synthetic vascular grafts for in vivo studies.

CHAPTER 1

INTRODUCTION

1.1 RATIONALE

Atherosclerosis remains a serious source of morbidity and death despite advances in preventive measures and pharmacological therapeutics. Surgical treatment of vascular disease has become a common medical procedure. Nearly 700,000 vascular surgical procedures are performed annually in the United States along with several hundred thousand peripheral and coronary angioplasties(1). Prosthetic bypass grafts and, more recently, arterial stents and other endovascular prostheses have been utilized in association with these reconstructive procedures. Although vascular grafts have been successfully developed from polymers such as polytetrafluoroethylene (PTFE) and polyethylene terephthalate, the use of synthetic materials is limited to large diameter grafts ($\geq$ 6 mm internal diameter) due to the frequency of occlusion observed with synthetic vessels of small caliber. Consequently, significant efforts in the past 20 years have focused on improving clinical durability of small caliber vascular prostheses. Surface modification has become one of proposed approaches, which here particularly involves introducing biological materials that are actively antithrombogenic.

It is recognized that the adverse events leading to the failure of many vascular prostheses are related to maladaptive biological reactions at the blood-material and tissue-material interface. Attempts to improve performance of grafts have been made by coating with clotting inhibitor such as albumin and prostacyclin analogues, or inert materials like polyethylene oxide (2, 3), which turned out to be a failure due to

overwhelming platelet activation and coagulation. An alternative approach has been used to design materials which support the in situ regeneration of an endothelial cell lining in order to create a functional arterial substitute with a durable thromboresistant interface (4, 5), which ironically led to a more thrombogenic surface due to incomplete coverage or loss of cells.

Endothelial cells lining the blood vessels and regulating biological mechanisms in blood leads to the hypothesis that the cell membrane establishes an important paradigm for the design of an antithrombogenic surface because of its capacity to participate in molecular recognition processes that are physiologically relevant to the control of blood coagulation. Based on mechanisms of regulation of blood coagulation, we consider heparin and thrombomodulin, which respectively facilitate inactivation of several coagulation factors and protein C anticoagulant pathway, as critical factors for antithrombogenicity. Consequently, we believe that a membrane-mimetic assembly serving as a platform for the presentation of biological regulators provides a rational design strategy for surface modification of synthetic prostheses.

1.2 GOAL AND SPECIFIC AIMS

Our central hypothesis is that a membrane-mimetic system will provide a route for generating an actively antithrombogenic surface thereby enhancing the patency of small-caliber arterial bioprostheses. In this regard, our goal was to create a well-characterized membrane-mimetic construct featuring immobilized functional anticoagulants and determine their antithrombogenic capacities.

Specific aims of the thesis were (1) Characterizing the catalytic capacity of surface bound TM to catalyze protein C activation, (2) Characterizing surface bound heparin to facilitate thrombin inactivation by antithrombin, (3) characterizing surface bound TF-induced thrombin generation as a vascular injury model, and 4) Determining antithrombogenic capacities of surface bound TM and heparin to inhibit surface TF-induced thrombin generation.

In this thesis, general background information including a membrane-mimetic surface containing physiologically significant regulators for thrombus formation and the effect of flow on surface enzyme activity was introduced in CHAPTER 2. There are four distinct topics presented in CHAPTERS 3-6. Characterization of surface bound thrombomodulin (TM) and heparin based on membrane-mimetic assemblies are presented in CHAPTER 3 and 4, respectively. Specifically, we determined surface densities of both surface anticoagulants and studied surface bioactivity under flow conditions. In CHAPTER 5, we designed a membrane-mimetic construct containing tissue factor (TF), which is a physiologic trigger for blood coagulation, as a vascular injury model. We observed that surface TF can exhibited activity by inducing thrombin generation, which provides strategies for determining antithrombogenic capacities of surface TM and heparin, which is described in CHAPTER 6. A composite system was designed by combining TF, TM and/or heparin on a membrane-mimetic surface in order to investigate effects of surface bound TM and/or heparin on TF-induced thrombin generation. Following these four chapters, applications and limitations of current model systems are discussed in CHPATER 7. Significant outcomes from the results of this research are summarized in CHAPTER 8 and recommendations for future work are in CHAPTER 9.

CHAPTER 2

BACKGROUND

2.1 OVERVIEW

The use of synthetic materials to fabricate a blood vessel substitute began in the 1950s and has led to vascular prostheses made from a wide variety of materials, including nylon, Teflon, Orlon, Dacron, polyethylene, and polyurethane (4). Among them, expanded poly(tetrafluoroethylene) (e-PTFE), and Dacron remain the most widely used synthetic materials. Although these materials have been very successful in the use of large-diameter (> 5 to 6 mm) substitutes (6), their use in small-caliber vascular substitutes remains ineffective (7, 8). Graft failure is associated with thrombogenicity (9-11). Natural blood vessels have endothelial cells (ECs) lining the interior of the vessel wall and these cells synthesize several inhibitors of clot formation such as plasminogen activators, heparin, and thrombomodulin (12). Since ECs are not present in synthetic grafts, no inhibitors are released to stop the clot formation once the coagulation cascade is triggered. This has led to the impetus for developing composite devices incorporating biological substances into the synthetic graft in order to modulate the host response and help prevent graft failure.

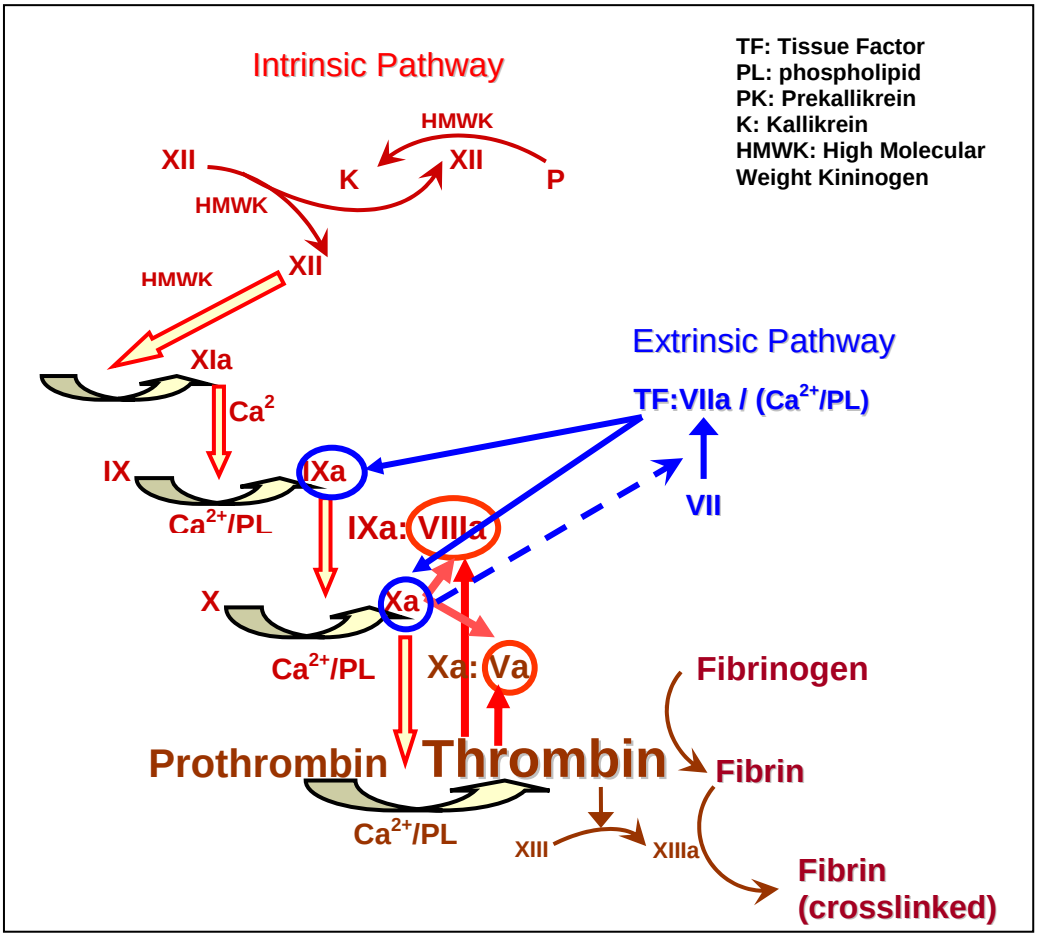

Figure 1 The blood coagulation cascades. The intrinsic cascade is initiated when contact is made between blood and surfaces. The extrinsic pathway is initiation upon vascular injury which leads to exposure of tissue factor (TF) (also identified as factor III), a subendothelial cell-surface glycoprotein that binds phospholipid. The two pathways converge at the activation of factor X to Xa. Factor Xa has a role in the further activation of factor VII to VIIa as depicted by the dashed arrow. Active factor Xa hydrolyzes and activates prothrombin to thrombin. Thrombin can then activate factors VIII and V furthering the cascade. Ultimately the role of thrombin is to convert fibrinogen to fibrin and to activate factor XIII to XIIIa. Factor XIIIa cross-links fibrin polymers solidifying the clot.

2.2 REGULATION OF BLOOD COAGULATION

It is commonly accepted that the blood coagulation cascade (Figure 1) is initiated *in vivo* when subendothelial tissue factor (TF) is exposed and/or expressed to the blood flow following vascular injury (13-17). Tissue factor functions in coagulation by serving as a protein cofactor for the plasma serine protease, factor VIIa, already present in blood (18, 19). The formation of TF-VIIa enzyme complex in turn activates two zymogens, factor IX and factor X (20-23). The serine protease factor Xa induces generation of trace amounts of thrombin (in picomolar scale (14, 24, 25)) in the initial phase of coagulation. Generated thrombin triggers positive feedback reactions by activating coagulation factors V and VIII to form Va and VIIIa (24, 26, 27), which serve as cofactors of Xa to form *prothrombinase* complex and cofactor of IXa to form *tenase* (*intrinsic factor Xase*), respectively. Since *tenase* and *prothrombinase* are primary activators of factor X and prothrombin (28-30), the generation of thrombin is quickly and largely amplified due to activation of factors V and VIII (24, 31) and continuous positive-feedback reactions. Moreover, thrombin activates factor XIII and cleaves fibrinogen (32, 33) to generate insoluble cross-linked fibrin clot (34, 35) and activates platelets by cleaving thrombin receptors on the platelet surface.

In order to attenuate the procoagulant processes, there are two major mechanisms involved: serine protease inhibitors and protein C pathway. Serine protease inhibitors, also called “serpins”, function by formation of stable 1:1 complex with their target enzymes and neutralize them. Antithrombin has been one of classic serpins by being the major inhibitor of several serine proteases produced during the blood coagulation (36), including thrombin, factor IXa and Xa, and some noncoagulation serine proteases, such

as plasmin, kallikrein and the complement enzyme C1. Specifically, thrombin inactivation by antithrombin can be significantly enhanced in the presence of heparin (37, 38), a type of glycosaminoglycan (GAG). To date, the catalysis of the ATIII-thrombin reaction by heparan sulfate has been most thoroughly characterized (39-43). Tissue factor pathway inhibitor (TFPI), another example of stoichiometric inhibitor, serves as an important regulator of serine proteases by inhibiting its principle targets including factor Xa and factor VIIa-TF-factor Xa complex (44-46).

The protein C anticoagulant pathway has emerged as a dynamic inhibitory mechanism for blood coagulation. This "on demand" physiologic anticoagulant pathway is initiated when thrombin binds to thrombomodulin (TM) (47). Thrombomodulin (TM), a 60 kD type I transmembrane protein (human) providing high affinity binding sites for thrombin with dissociation constant (K_d) about 0.7 nM (12), forms a 1:1 molar complex which affects the biological function of thrombin by changing its activity (47). The thrombin-TM complex exhibits dramatically altered macromolecular specificity and rapidly cleaves the plasma zymogen, protein C, to form activated protein C by releasing 12 residue peptides from the heavy chain of the zymogen (48). Activated protein C serves as a robust anticoagulant by interacting with its cofactor protein S on membrane surfaces to catalyze the inactivation of factor Va and VIIIa, thus preventing the generation of Xa and thrombin, which are critical for the amplification of the coagulation cascade (49).

2.3 THE EFFECT OF FLOW ON BLOOD COAGULATION

The coagulation of blood on damaged tissue surfaces has been long recognized to involve the nature of the surface, the blood elements and local flow conditions (50). The processes of hemostasis and its pathological correlate, thrombosis, are dynamic events in nature, meaning they primarily occur in the presence of flow. In a flow regime, the transfer of fluid phase reactants, to a catalytic surface and the removal rate of formed products depends upon the kinetics of molecular adsorption and desorption processes, intrinsic surface reaction rate constants, convection by the fluid flow, and diffusion within the boundary layer region. Therefore, local flow conditions likely have a significant effect on such a surface catalytic reaction in the presence of competing substrates for a given cofactor or an enzyme active site.

The overall reaction rate at which proteins or cells react with an enzymatically active surface usually depends on a combination of kinetics of chemical reactions at the interface and the rate at which molecules arrive at the interface through convection and diffusion. In most cases, fluid dynamics and the kinetic reaction processes are coupled or interdependent. In the presence of solute-interface reaction, the flow pattern in the vicinity of the surface may be altered such that there is a finite velocity component in a direction vertical to the surface, which leads to a net transfer of solutes in this direction required by the reaction. Therefore, both equations of fluid dynamics and mass transfer must be solved simultaneously, which would be exceedingly complex especially when further simultaneous equations are required for each additional reactant and product involved in the reaction. To simplify the above situation, it is commonly assumed that the surface enzymatic reaction is transport-limited.

2.4 SURFACE MODIFICATION OF VASCULAR SUBSTITUTES

To develop a clinically durable small-caliber arterial substitute, modification of a blood-contacting surface to reduce thrombogenicity has been pursued. Affixing antithrombogenic substances experimentally to synthetic materials has been one of the proposed strategies. Heparin binding Dacron prostheses, for example, transiently reduces its thrombogenicity in some models (51). Some animal studies (52) have also demonstrated that heparin is able to improve graft patency rates by immobilizing onto polyurethane and poly(dimethylsiloxane). Besides applying onto synthetic grafts, covalent bonding of nitrite-degraded heparin by end-point attachment applied on membrane oxygenators and tubings makes it possible to maintain a long-lasting extracorporeal circulation without systemic heparinization (53). Direct coating of thrombomodulin onto polymer-based surfaces has been investigated. TM has been conjugated to both aminated and carboxylated surfaces (54-57) and immobilized onto poly(acrylic acid) surface-grafted PTFE (58, 59). *In vitro* studies showed that both clotting time and protein C activation were enhanced.

While immobilization of biologically functional materials has been strategized for medical application, loss of surface bioactivity remains the major issue (54-59). For immobilization of TM through direct covalent binding, TM surface bioactivity in terms of protein C activation rates was increased by only 10 fold compared with 20,000-fold enhancement previously observed when TM is a component of either lipid vesicles or the endothelial cell surface. Since TM's biological properties are closely related to a variety of structural features, including three distal epidermal growth factor (EGF)-like modules that are able to recognize thrombin and a covalently associated chondroitin sulfate moiety

that increases the affinity of thrombin binding to TM (60), altering these properties would lead to the loss of cofactor activity, which may have been due to the protein immobilization by the direct covalent binding procedure. Moreover, random-site reactions to any accessible functional group on the TM surface, including those within the thrombin-binding site, may have inactivated the catalytic domain of TM. Enhancement of TM catalytic activity on lipid surface possibly results from interactions of proteins and lipid, such as protein C through a C-terminal 4-carboxyglutamic acid (Gla) domain binds to the cell membrane and thereby increases its local concentration by confining it to the two-dimensional plane of the lipid bilayer (61-63). In addition, the electrostatic and hydrophobic interactions between protein C and cell membrane may also induce conformational changes that help align the protein C cleavage site with thrombin's proteolytically active domain. Consequently, the inherent strength of a membrane-mimetic based approach may be the capacity to incorporate a variety of physiologically significant processes relevant to the control of blood coagulation, which leads to developing biological regulator-incorporated membrane-mimetic systems.

2.5 BIOMEMBRANE-MIMETIC MODELS

Lipid membranes, as self-organizing noncovalent aggregates, offer a model for molecular engineering in which the constituent members can be controlled, modified, precisely defined, and easily assembled. During the past decade, phospholipids differing in chemical composition, saturation, and size have been utilized as building blocks in the design of a variety of structures of complex geometry. Lipid-based cylinders, cubes, and spheres have found applications in both drug delivery and as templates for composite

molecularly engineered structures (64). Surface-coupled bilayers for biosensor applications have also been produced by assembling a layer of closely packed hydrocarbon chains onto an underlying substrate followed by exposure to either a dilute solution of emulsified lipids or unilamellar lipid vesicles (65-67). In addition, Langmuir-Blodgett techniques have been used as an alternate strategy to construct supported bilayers via a process of controlled dipping of a substrate through an organic amphiphilic monolayer (68). Remarkably, these noncovalent molecular assemblies exhibit a high degree of stability. Israelachvili and others have determined that 26 kT is required to remove a double chained C-16 phosphatidylcholine molecule from a bilayer into water (69, 70). This nearly approximates the biotin-streptavidin bond energy of 35 kT and is several orders of magnitude greater than the affinity of typical monoclonal antibody-antigen interactions. Thus, the significance of these design methodologies lies in the ability to engineer relatively robust materials with an unparalleled level of reproducibility and molecular control over surface order and chemistry.

Membrane-mimetic systems have also had a direct impact on efforts aimed at understanding the mechanisms of blood coagulation at sites of vascular wall injury and on artificial surfaces. In a series of investigations using planar membrane models, Thompson and colleagues (71, 72) have characterized the molecular requirements for prothrombin binding to phospholipid membranes. Most intriguing has been the observation by other investigators that the phosphorylcholine head group appears to limit the induction of blood clot formation on synthetic surfaces (73-75). Although not well understood, it has been speculated that this biological property may be related to the large amount of water bound to this zwitterionic head group, or conceivably, the selective

adsorption to phosphorylcholine of specific plasma proteins that inhibit the blood clotting process (76).

Given the fact that lipid bilayers serve as a critical factor for protein bioactivity by locally concentrating and coordinating appropriate alignment of reacting substrates, we propose that a substrate-supported membrane-mimetic assembly provide a rational design for generating an actively antithrombogenic blood contacting interface. The model construct (Figure 2) coated onto a supporting substrate is composed of polyelectrolyte multilayer of poly-(L-lysine)-alginate as a base layer, an amphiphilic alkylated terpolymer (3-acryloyl-3-oxapropyl-3-(N,N-dioctadecyl-carbamoyl)-propionate))$_3$:(2-hydroxyethyl acrylate)$_6$:sodium styrene sulfonate$_1$ (AOD_3:HEA_6:SS_1), and lipid monolayer comprised of monoacrylate-phospholipids (77-80). Based on such a system, additional substances can be incorporated with the model surface, which provides a high level of molecular control over surface order and chemistry and, as a consequence, facilitates the examination of surface molecular determinants, which are required for efficient antithrombogenicity. In the following parts of the thesis, fabrication and characterization of TM and heparin functionalized surfaces are presented and their potential individual and combined antithrombogenic capacities are investigated using TF-presented surface as a vascular injury model. The mechanisms governing TM-initiated APC generation, heparin-enhanced thrombin inactivation, and their capacities to inhibit TF-initiated thrombin generation under physiologic shear rates in vein and artery were defined.

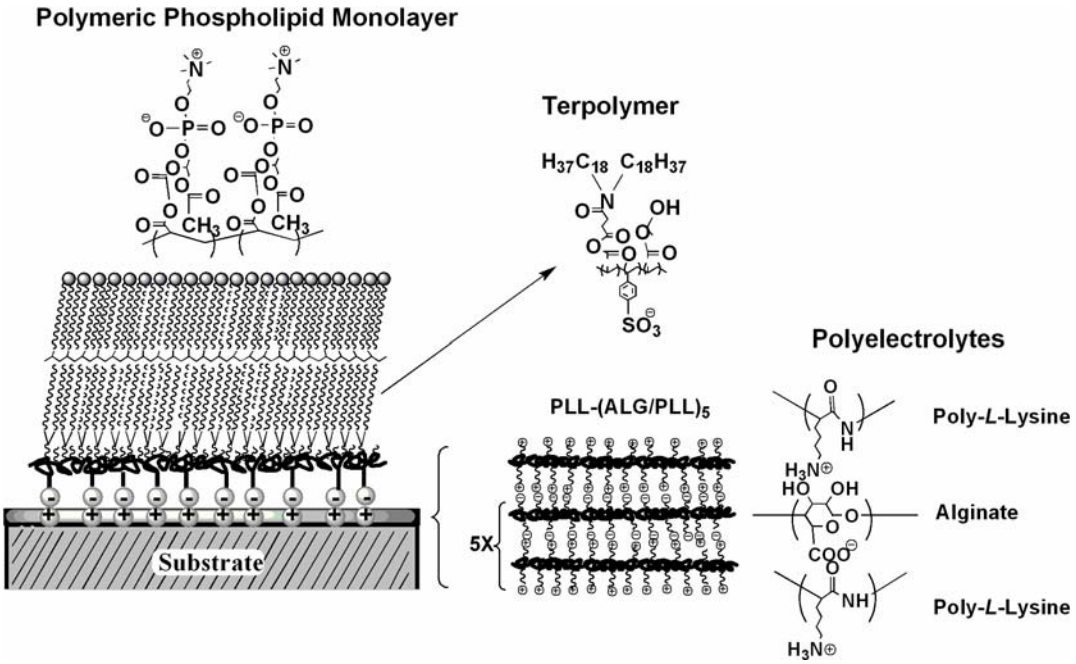

Figure 2 Schematic representation of a polymeric phospholipid monolayer composed of 1-palmitoyl-2-[12-(acryloyloxy) dodecanoyl]-sn-glycero-3-phosphorylcholine supported on an alkylated polyelectrolyte multilayer (Not to scale).

CHAPTER 3

FABRICAION AND CHARACTERIZATION OF FUNCTIONAL THROMBOMODULIN-INCORPORATED MEMBRANE-MIMETIC ASSEMBLIES

3.1 ABSTRACT

The protein C anticoagulant pathway generates an "on demand" physiologic anticoagulant response, which is initiated when thrombin binds to thrombomodulin (TM), a transmemebrane protein constitutively expressed by endothelial cells. A stable, protein C activating membrane-mimetic film was produced on a polyelectrolyte multilayer (PEM) by in-situ photopolymerization of a phospholipid assembly containing TM. The monoacrylated phospholipid monomer was initially synthesized and prepared as unilamellar vesicles with varying molar concentrations of TM. Membrane-mimetic films were constructed on planar substrates with predictable surface concentrations of catalytically active TM. ^{125}I-labeled TM demonstrated little change in TM surface concentration over periods of up to 4 weeks. We have utilized a continuous parallel plate flow reactor to investigate effects of physiologic shear rates (50 sec^{-1} and 500 sec^{-1}) and TM surface concentration (0 - 1400 fmole per cm^2) on activation of protein C. In agreement with an analysis of reaction kinetics and mass transfer, experimental results demonstrated that reaction rates became saturated when TM surface density was equal to or greater than 800 fmole per cm^2. Moreover, steady state rate of activated protein C generation increased with shear rate and TM surface content. Stability tests of TM activity showed that surface TM activity in terms of protein C activation can be preserved for at least a short-term period. We believe that the design of membrane-mimetic films

that have the capacity to activate the protein C pathway will provide a useful strategy for generating "actively" antithrombogenic surfaces.

3.2 INTRODUCTION

It has been postulated that a clinically durable vascular prosthesis may be achievable by controlling thrombus formation on molecularly engineered surfaces through the incorporation of physiologically relevant antithrombogenic mechanisms that are normally operative at the blood-material interface under a range of hemodynamic conditions. The inhibition of blood coagulation is primarily achieved by two complementary mechanisms - serine proteinase inhibitors (serpins) and the protein C pathway (81). Despite the presence of serpin binding sites on heparan sulfates and the well characterized anticoagulant properties of these glycosaminoglycans, the physiological significance of the anticoagulant/antithrombotic functions attributed to heparan sulfates at the endothelial cell surface have not been conclusively established. For example, high affinity antithrombin binding sites have not been localized to heparan sulfates that are in direct contact with blood (82). Moreover, Lollar et al. (83) could not confirm the alleged catalytic effect of heparan sulfate on the ATIII-thrombin reaction in recirculating rabbit Langendorff heart preparations. In contrast, there is growing evidence that thrombomodulin (TM), as a critical regulator of the protein C pathway, represents the major anticoagulant mechanism that is operative in both normal and injured blood vessels under physiologic conditions *in vivo* (84).

TM is a transmembrane glycoprotein of the endothelium of blood and lymphatic vessels and the basis of a major natural anticoagulant system (60). TM has high affinity

for thrombin to form 1:1 stoichiometric complex and in the process turns all known procoagulant/proinflammatory functions of thrombin into anticoagulant/anti-inflammatory activities of the enzyme complex, which initiates protein C anticoagulant system. TM-facilitated protein C activation shows robust physiologic anticoagulant response due to three distinct substrate dependent mechanisms. While free thrombin efficiently converts fibrinogen to fibrin, thrombin bound to TM is no longer capable of cleaving fibrinogen, nor is it able to act on platelets (61). In addition, TM not only enhances the rate of thrombin inactivation by ATIII but also dramatically accelerates the ability of thrombin to activate protein C. APC together with its cofactor protein S inactivates coagulation factors Va and VIIIa (49) which are generated by thrombin-catalyzed activation of factor V and VIII and serve as critical cofactors for generation of thrombin and factor Xa, respectively. Inasmuch as APC functions as a potent inhibitor of blood clot formation by preventing the generation of factor Xa and thrombin which are critical for the amplification of the coagulation cascade, TM apparently plays a key role to regulation of blood coagulation.

Several investigators have described the direct immobilization of thrombomodulin onto polymeric surfaces in order to generate thromboresistant materials for blood contacting applications. Kishida et al. (54-57) have conjugated TM to both aminated and carboxylated surfaces, including poly(vinyl amine) and poly(acrylic acid) surface-grafted polyethylene and a surface-hydrolyzed poly(ether urethaneurea). Similarly, Vasilets et al. (59) have reported the immobilization of TM onto poly(acrylic acid) surface-grafted PTFE. Recently, Li at al. (85) have reported the immobilization of TM onto expanded PTFE utilizing carbodiimide-based coupling reaction. Han et al. (86) have documented

the immobilization of TM onto the cover glass substrates using trichlorotriazine (TCT) and amino-terminated silane as new coupling agents with or without the aid of PEG between TM and substrate. Sperling et al. (87) have reported TM was covalently anchored onto thin films of poly(octadecene *alt* maleic anhydride) covering planar glass substrates, which was achieved by active ester formation at the carboxylic acid terminus of the PEG spacers. While the conjugation schemes in these reports vary TM is always coupled to the substrate via freely available amino or carboxyl functionalities on the protein surface. Characteristically, in vitro studies demonstrated that both clotting time and protein C activation are enhanced and this activity appears to be directly proportional to TM surface density, as determined by a ninhydrin assay. However, the ability to control TM surface concentration was substrate dependent with reported TM densities ranging between 0.15 and 0.45 $\mu g/cm^2$. Furthermore, TM bioactivity was significantly reduced after surface coupling, as evident by protein C activation rates, which were increased only 5 to 10-fold compared with an observed 20,000-fold enhancement when TM is evaluated as a component of either lipid vesicles or the endothelial cell surface. Furthermore, the impact of local flow conditions on the effectiveness of this strategy was not investigated.

These studies confirm that substrate bound TM has the potential to limit thrombus formation on synthetic surfaces that are otherwise thrombogenic. However, the observed reduction in TM bioactivity serves to emphasize that TM's biological properties are intimately tied to a variety of structural features which may be lost upon direct covalent coupling to a biomaterial surface, possibly due to random-site reactions to any accessible functional group on the TM surface, including those within the thrombin

binding site. For example, TM's ability to accelerate the thrombin-dependent activation of protein C requires three tandemly repeated EGF-like domains that serve as a thrombin binding site; a serine/threonine-rich 65 Å spacer between the EGF-like domains and the transmembrane domain (88), a distance similar to the location of the active site of APC above the membrane surface (89), which optimally align thrombin's active site with the critical scissile bond in protein C; and a covalently associated chondroitin sulfate moiety that increases the affinity of thrombin binding to TM by 10- to 20-fold and catalyzes ATIII inactivation of thrombin (60, 90). Furthermore, while some activity is retained even after the solubilization of TM with detergents, membrane association significantly accelerates protein C activation by TM. This is mediated, in part, by the ability of the membrane to locally concentrate and coordinate the appropriate alignment of reacting cofactors and substrates with TM (91). For example, protein C has a C-terminal 4-carboxyglutamic acid (Gla) domain which binds to the cell membrane and presumably increase its local concentration by confining it to the two-dimensional plane of the lipid bilayer (61-63). In addition, the binding of protein C to the plasma membrane may also induce conformational changes that help align the protein C cleavage site with thrombin's proteolytically active domain. Furthermore, direct interaction of the Gla domain of protein C with the phospholipids is augmented by calcium and negatively charged phospholipids are the most active type of lipid (92). Analysis of the membrane binding properties of protein C indicates that this interaction with negatively charged phospholipids probably involves insertion of the very hydrophobic loop of the protein C Gla domain into the hydrophobic regions of the bilayer (93). Presumably, this membrane binding concentrates protein near the activation complex accounting for the observed

decrease in the Km (92). In addition, orientation of the scissile bond on protein C with the active site of thrombin in the thrombin-TM complex probably plays an important role in this process (88). Thus, the lipid bilayer serves as an essential 'cofactor', which in concert with TM accelerates protein C activation and subsequently optimizes APC anticoagulant activity. Given this framework, a membrane-mimetic design strategy not only facilitates the formation of chemically heterogeneous and biologically active thin films through a process of self-assembly, but provides a useful scheme for incorporating TM into blood-contacting interfaces in a manner that provides for optimal anticoagulant activity.

Phospholipid membrane surfaces accelerate TM-facilitated protein C activation by acting as an essential mediator which locally concentrates and coordinate the appropriate alignment of reacting cofactors and substrates (88, 89, 92, 93). Given the molecular basis of protein C activation on the membrane surface, we have postulated that a substrate-supported membrane-mimetic assembly that contains TM provides a rational design for generating an actively antithrombogenic blood contacting interface. We have recently described the formation of a stabilized, membrane-mimetic film containing reconstitution of TM into lipid assemblies composed of 1-palmitoyl-2-[12-(acryloyloxy) dodecanoyl]-sn-glycero-3-phosphorylcholine (monoacrylate-PC) (78, 79, 94, 95) through an optimized polymerization process (Figure 3).

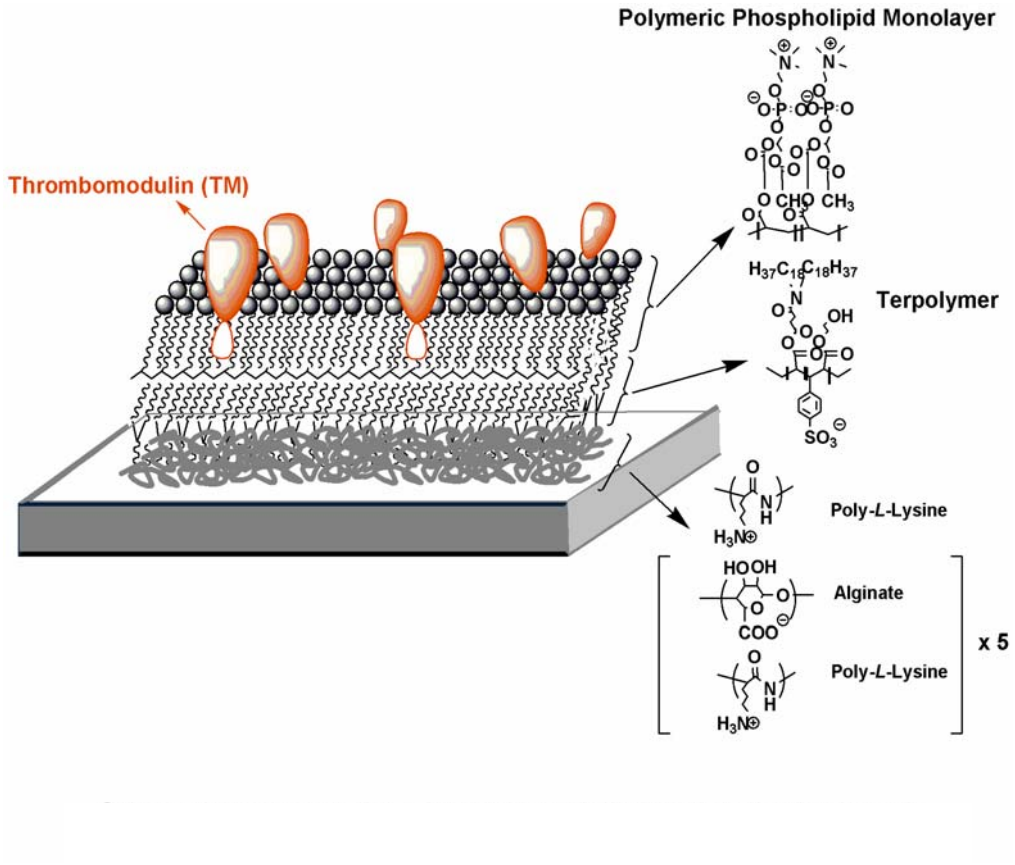

Figure 3 Schematic representation of TM functionalized polymeric phospholipid monolayer supported on an alkylated polyelectrolyte multilayer. (Not to scale)

Although TM containing membrane-mimetic films have been studied under a variety of static conditions (79), the catalytic efficiency of this system under well defined flow conditions has not been previously investigated. In this regard, an analytical model is used to define the mass-transfer limited regime under simulated arterial (500 sec^{-1}) and venous (50 sec^{-1}) conditions in which increases in TM surface concentration do not further enhance local APC production. This was confirmed experimentally in a parallel plate flow chamber (Figure 4). Moreover, preserved TM bioactivity was documented even after prolonged incubation of test surfaces in PBS and human plasma at 37°C.

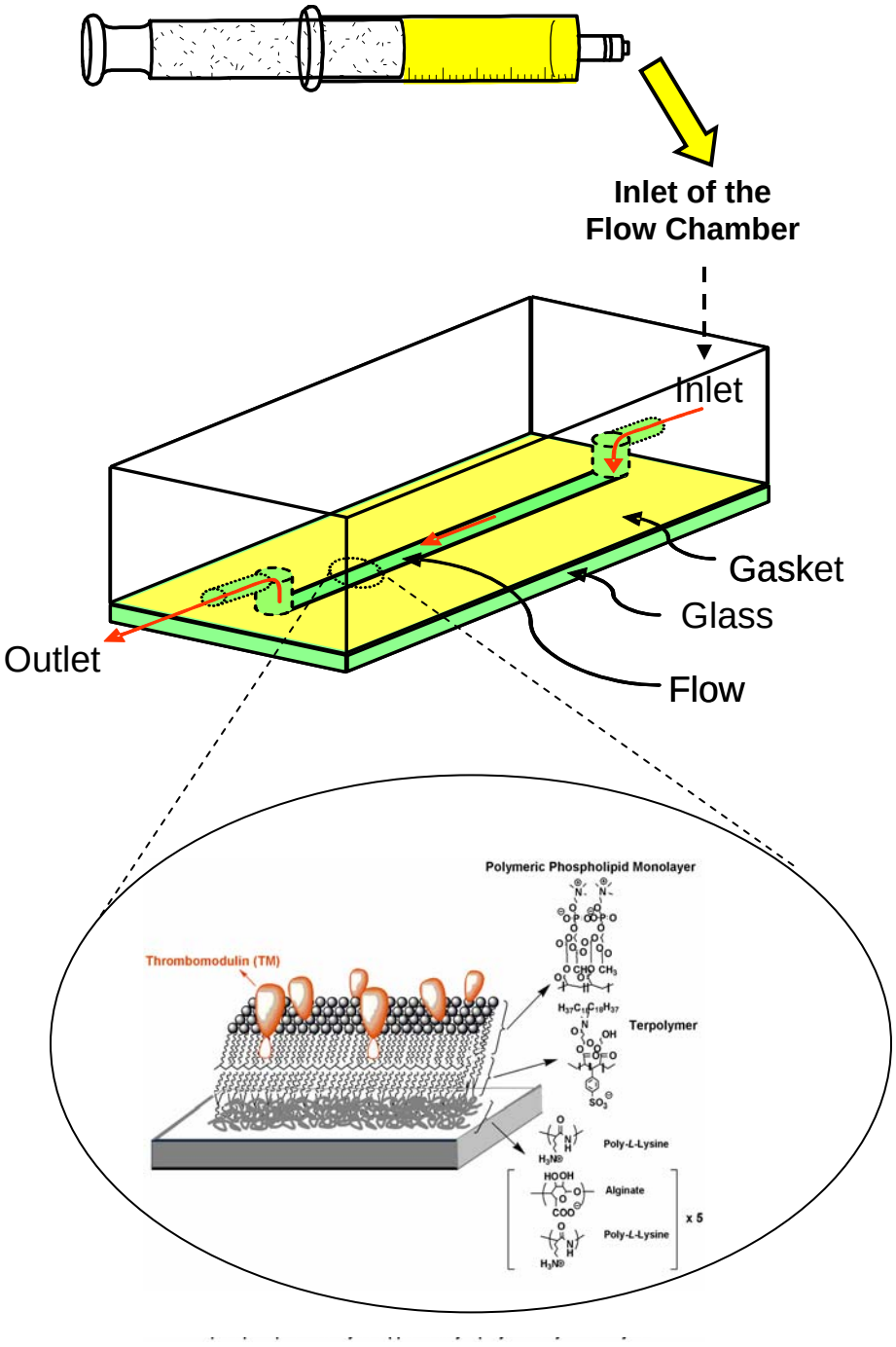

Figure 4 Schematic of parallel plate flow reactor (not to scale). The gasket (plastic shim) creates height of the flow channel. TM containing membrane-mimetic construct is immobilized onto a glass substrate. The surface is perfused with reactants and the perfusate is collected at the outlet to determine product concentration.

3.3 MATERIALS AND METHODS

3.3.1 Materials

Rabbit lung thrombomodulin (single chain containing NH_2-terminal hydrophobic domain, six EGF domains, one O-glycosylation rich domain, one transmembrane domain, COOH-terminal cytoplasmic domain, 74 kD, in 0.02 M Tris, 0.15 M NaCl, pH 7.4 containing 0.05% lubrol PX), human protein C, and human thrombin were obtained from Haematologic Technologies, Inc. Human antithrombin III and Spectrozyme PCa substrate (H-DLys (γ-carbobenzoxy)-Pro-Arg-pNA•2AcOH) were obtained from American Diagnostica Inc. Eosin Y (EY, 5% in water), triethylamine (TEA), 1-vinyl-2-pyrrolidinone (VP) were obtained from Aldrich. Nucleopore polycarbonate filters, circular glass coverslips (15 mm diameter, 0.17 mm thickness) and Contrad 70 detergent were obtained from Fisher. Alginate (ALG; low viscosity, ca. 60% mannuronic acid) was obtained from Pronova Biomedical (Norway). Poly (L-lysine) (PLL, MW > 300 kD) and all buffer salts were obtained from Sigma. Normal pooled human plasma was purchased from George King Biomedicals, Inc. Sodium azide (NaN_3) was purchased from Sigma. Monoacrylate-PC (AcPC, 1-palmitoyl-2-[12-(acryloyloxy) dodeca-noyl]-*sn*-glycero-3-phosphocholine) was synthesized as described previously (77). The synthesis of the terpolymer that consists (3-acryloyl-3-oxapropyl-3-(N,N-dioctadecyl-carbamoyl)-propionate))$_6$:(2-hydroxyethyl acrylate)$_3$:sodium styrene sulfonate$_1$ (AOD$_6$:HEA$_3$:SS$_1$) has been described elsewhere (96).

Instrumentation: Irradiation was performed using a DynaLume quartz halogen illuminator equipped with a heat shield (Scientific Instruments). Light intensity was measured using a radiometer model IL 1400A equipped with a SL021 photodetector and

FQI filter (International Light). Radioactive materials were detected using Gamma counter. All spectrophotometric measurements were executed on a Cary 50 Bio UV-Visible spectrophotometer (Varian) equipped with a temperature-regulated cell compartment.

3.3.2 Layer-By-Layer Assembly of an Alkylated Alginate/Poly-L-Lysine (ALG/PLL) Multilayer on a Glass Surface

Microscope glass slides were cleaned by 30 minutes of sonication in 10% Contrad 70 detergent solution followed by extensive washing and sonication in deionized water. The substrate was then immersed in a solution of 0.10% PLL in 20 mM PBS for 30 seconds and then washed with water. The procedure was repeated using a solution of 0.15% ALG in 20 mM PBS. This process was repeated until a total of 11 layers (six PLL and five alginate layers) were coated, with the top layer comprised of PLL. Samples were then immersed in a 0.1 mM (in [SS]) terpolymer (AOD6:HEA3:SS1) solution in 1% (v/v) DMSO/PBS buffer for 1 minute. After extensive rinsing with water, samples were air-dried. Advancing contact angles of > 100° were characteristic of these substrates. Comprehensive surface analysis of these films with or without a supported lipid assembly, including contact angle goniometry, ellipsometry, external reflectance infrared spectroscopy, and high resolution scanning electron microscopy, has been detailed elsewhere (96).

3.3.3 Reconstitution of Thrombomodulin into Lipid Vesicles

Large unilamellar vesicles (LUV) of 12 mM lipid solution in 20 mM sodium phosphate buffer, pH 7.4, were prepared by four successive freeze/thaw/vortex cycles using liquid N_2 and a 45°C water bath. Thrombomodulin was then added to obtain the

desired thrombomodulin/lipid molar ratio, which ranged in these investigations from 1:4000 to 1:200,000. The lipid/thrombomodulin solution was gently vortexed for 1hr at room temperature before it was extruded 21 times; each through two back-to-back 2000 nm and then 600 nm polycarbonate filters (Avanti Polar Lipids, Inc.). It has been confirmed that 95% of the TM activity was associated with the lipid vesicles (79).

3.3.4 Formation of a Thrombomodulin Containing Membrane-Mimetic Thin Film

Extruded lipid vesicles were diluted to 1.2 mM with 20 mM sodium phosphate buffer containing 150 mM NaCl, pH 7.4. This solution was then purged with argon for 20 minutes. A terpolymer-coated glass slide was completely immersed in 4 mL of vesicle solution, faced upwards, and maintained overnight at 40°C. Photopolymerization of acrylate-PC was carried out as described previously (78) with some modifications. A stock solution of co-initiators was prepared as 10 mM Eosin Y, 225 mM TEA, and 37 mM VP in water, and was stored in an opaque amber bottle. In a glove box purged with argon, the desired amount of initiator stock solution was added to the vial containing the substrate fused with vesicles so that a 12:1 ratio of [AcPC]:[Eosin Y] was achieved. The sample was irradiated for 30 minutes under ambient conditions from above at a distance of approximately 6 cm (light intensity ~ 40 mW/cm^2). Following the photopolymerization period, the sample was removed from the polymerization media and washed extensively with water.

3.3.5 Determination of Thrombomodulin Surface Density and Stability within a Polymeric Lipid Membrane

Rabbit lung thrombomodulin at a concentration of 1 mg/mL was radiolabeled with ^{125}I using Iodobeads (Pierce Chemical Co., Rockford, IL) according to the manufacture's protocol. The concentration of radiolabeled TM was determined by a modification of the Bradford Protein Assay (Bio-Rad) using a TM standard curve. Specific activity of the protein solution averaged 1.8 x 10^7 cpm/μg (1330 cpm/fmole). Cleaned supporting substrates (5x5 mm^2 Si chip) were coated with TM containing membrane-mimetic thin film as described previously. ^{125}I-TM and unlabeled TM were mixed to form 1:16 molar ratio solution, and TM was then added to obtain the desired TM/lipid molar ratio. Planar photopolymerized lipid/TM assemblies were produced as described above and washed extensively with water prior to measuring surface radioactivity in a gamma counter. TM surface density (fmol/cm^2) was calculated as {cpm/(specific activity x sample area)} and specific activity corrected for decay. For stability analysis, samples were stored in PBS at 37 °C and radioactivity periodically measured after extensive washing in water over a 1-month period. Test samples were generated in quadruplicate.

3.3.6 Analysis of TM Catalytic Activity

Activity of TM was accessed via the activation of human protein C by human thrombin-rabbit lung TM complex, as described in the literature with some modification (61). Activation was performed at 37 °C in 20mM Tris-HCl buffer, pH 7.5, containing 100 mM NaCl, 0.1% BSA, and 5 mM Ca^{2+}. A typical activation mixture contains 0.5 nM of TM as a component of LUVs, 5 nM of thrombin, and 0.1 μM of protein C. Incubation periods were adjusted such that less than 10% of protein C was converted to activated

protein C. Activation was terminated by the addition of antithrombin III (300 μg/mL final concentration). Activated protein C concentration was determined using the Spectrozyme PCa substrate (absorbance 405 nm). Km and k_{cat} values were calculated assuming Michaelis-Menton reaction kinetics.

Thrombomodulin activity on glass coverslips coated with a membrane-mimetic thin film was determined in similar fashion in a shaking water bath at 37 °C. For stability tests, samples were incubated in PBS at 4 °C or human plasma at 37 °C for specified time periods prior to measuring TM activity. Fresh samples were used for all stability tests, and a total of six samples were assayed to obtain each data point.

3.3.7 Continuous Flow Reactor Assays on Thrombomodulin Containing Membrane-Mimetic Surface

Microscope glass slides were cleaned and coated with TM-incorporated membrane-mimetic thin film. A parallel plate flow system (0.6 cm (width) x 0.01 cm (height) x 4.5 cm (length), 27μL volume) containing the coated sample was flushed with 20mM Tris-HCl buffer for 1 hours at $\gamma_w = 2000$ sec^{-1}. The reaction was started by perfusing the sample with the Tris-BSA (20mM Tris-HCl + 100 mM NaCl + 0.1 wt% BSA, pH 7.5) containing 5 mM Ca^{2+}, 2 nM of thrombin and 0.1 μM of protein C at 37^{o}C. The entrance length (i.e., the distance from the inlet over which the laminar flow profile becomes fully developed) for the current flow system was estimated by $Le/H = 1 + 0.1Re$, where *Le* is entrance length, H is the height of the channel, and Re is the Reynolds number (97). As the Reynolds numbers in this system were less than 10, the entrance length was less than 0.5% of the total reactor length. Protein C activation was investigated at shear rates of 50 and 500 sec^{-1}, which correspond to flow rates of 0.031

and 0.31 mL/min and residence times over the reactive surface of 53 and 5.3 sec, respectively. The perfusate was collected at timed intervals (every 10 minutes for 50 sec^{-1} and every 5 minutes for 500 sec^{-1}) and quenched by antithrombin III (120 μg/mL, final concentration) for 5 minutes, and assayed by adding Spectrozyme PCa substrate (0.2 mM, final concentration). The concentration of activated protein C (APC) was determined by converting measured absorbance (at 405 nm) from UV-VIS spectrophotometer via a standard curve (see Appendix A1).

3.3.8 Stability Tests on Bioactivity of Thrombomodulin Incorporated Membrane-Mimetic Surface

TM-incorporated membrane mimetic surfaces were incubated with daily fresh phosphate-buffered saline (PBS, 1X) or normal pooled human plasma (replace with fresh plasma every 2~3 days) at 37 °C. The model surface was tested using the same continuous flow assay as described previously at timed points for up to three months.

3.4 RESULTS AND DISCUSSION

The lipid membrane has been considered as an essential cofactor in blood coagulation, mainly due to the central role it plays in assembly of the activation complexes. For example, the formation of the enzyme complex prothrombinase on membrane surface provides a platform for its substrate prothrombin to bind effectively (71, 72). In the absence of membrane, the formation of the complex is either abolished or impaired (29, 98-100). In contrast, catalytic activity of integral membrane proteins is largely enhanced by orders of magnitude comparing to that of pure enzyme (22, 98). Specifically, the assembly of thrombin-TM complex on membrane leads to $> 10^4$ fold in the proteolytic efficiency of activation of protein C (60, 91).

It have been noted that the phosphorylcholine headgroup appears to limit the induction of blood clot formation on synthetic surfaces (73-75). While our group has observed limited thrombus formation and neointimal hyperplasia on phospholipids functionalized surfaces using short-term *in vivo* assays (77, 101), we believe that the inherent strength of a membrane-mimetic-based approach is the capacity to incorporate within these systems a variety of physiologically significant processes relevant to the control of blood coagulation. As a critical regulator of the protein C pathway, TM represents the major anticoagulant mechanism that is operative under physiologic conditions *in vivo* and thereby provides an appropriate target for functionalizing blood contacting membrane-mimetic thin films.

3.4.1 Robust Membrane-Mimetic Films can be Constructed on Planar Substrates with Predictable Surface Concentrations of Catalytically Active TM.

A schematic representation of the membrane-mimetic construct is illustrated in Figure 3, and a detailed description of the surface physiochemical properties of this system have been published elsewhere (96). The molar ratio of TM:phospholipids was systematically varied from 1:4000 to 1:200000 with an observed linear relationship between the concentration of TM in the lipid mixture and the rate of activated protein C formation under static conditions (Figure 5).

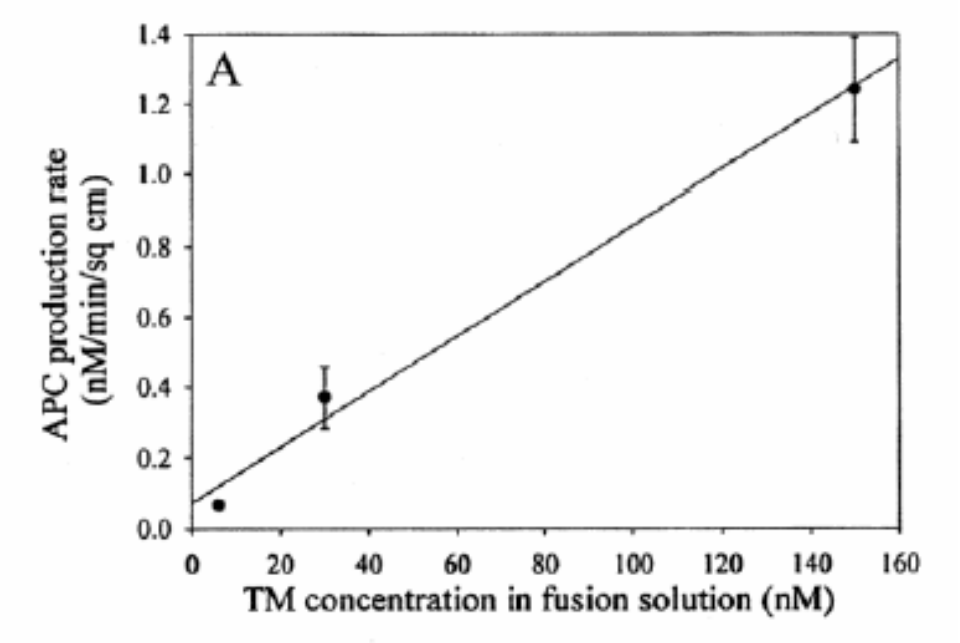

Figure 5 The relationship between the rate of surface mediated protein C activation (nM/min/cm2) and the concentration of TM in the fusion mixture. Adopted with permission from (79).

Moreover, TM activity was unchanged over a 5-day incubation period in PBS at 4°C (Figure 6A). Incubation of films in plasma at 37 °C revealed a small decrease in TM activity (~20%) within 30 min. Nonetheless, continued incubation for an additional 3 days was not associated with any further loss of TM activity (Figure 6B).

^{125}I-protein labeling was used to determine the absolute surface density of TM on planar-supported membranes as a function of its molar concentration in the vesicle solution (Figure 7). A linear relationship was observed over a wide range of TM concentrations. A small decrease in surface concentration was noted within the first 3 days on incubation at 37 °C in PBS with relatively little change observed over a period extending up to 28 days. We speculate that the small decrease TM concentration soon after the initiation of PBS incubation may be related to the loss of partially adsorbed lipid vesicles. Notably, samples were removed from the bathing media on multiple occasions during the incubation period, which emphasizes the relative stability and robustness of this system.

However, for the highest TM concentration, i.e. [TM] = 300 nM in fusion solution, the behavior of TM stability was observed to be a bit more drastic than lower TM concentration (Figure 8). It appears to have more initial loss during the first week of incubation, but became stable after two weeks.

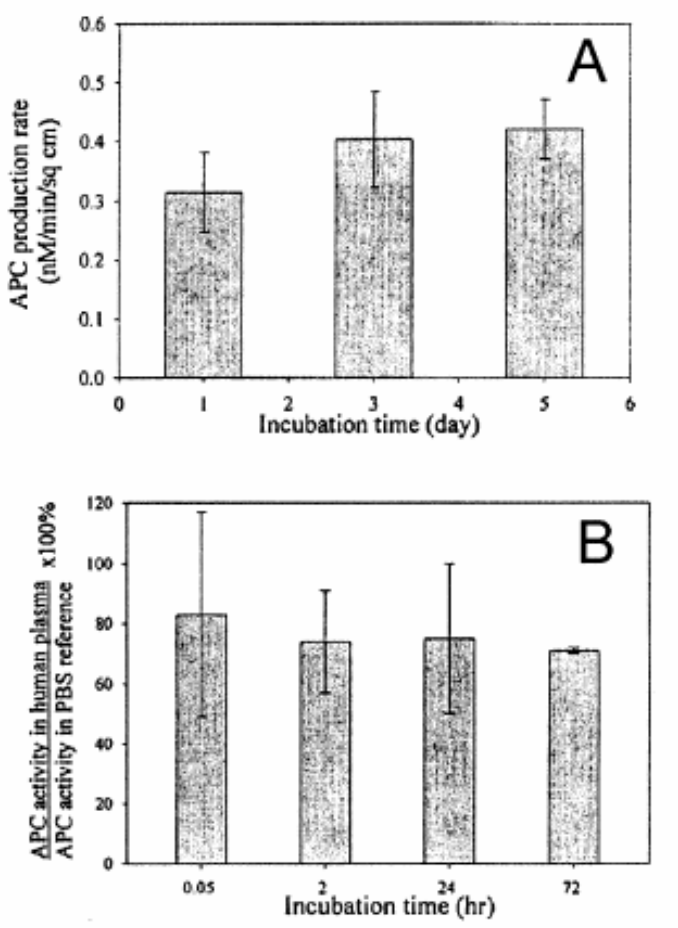

Figure 6 (A) Serial measurements (mean ± S.D.) of the rate of protein C activation for a TM containing lipid film incubated in PBS at 4 °C. (B) Serial measurements (mean ± S.D.) of the rate of protein C activation for a TM containing lipid film incubated in plasma at 37 °C. All values are normalized with respect to the initial rate protein C activation in PBS. Adopted with permission from (79).

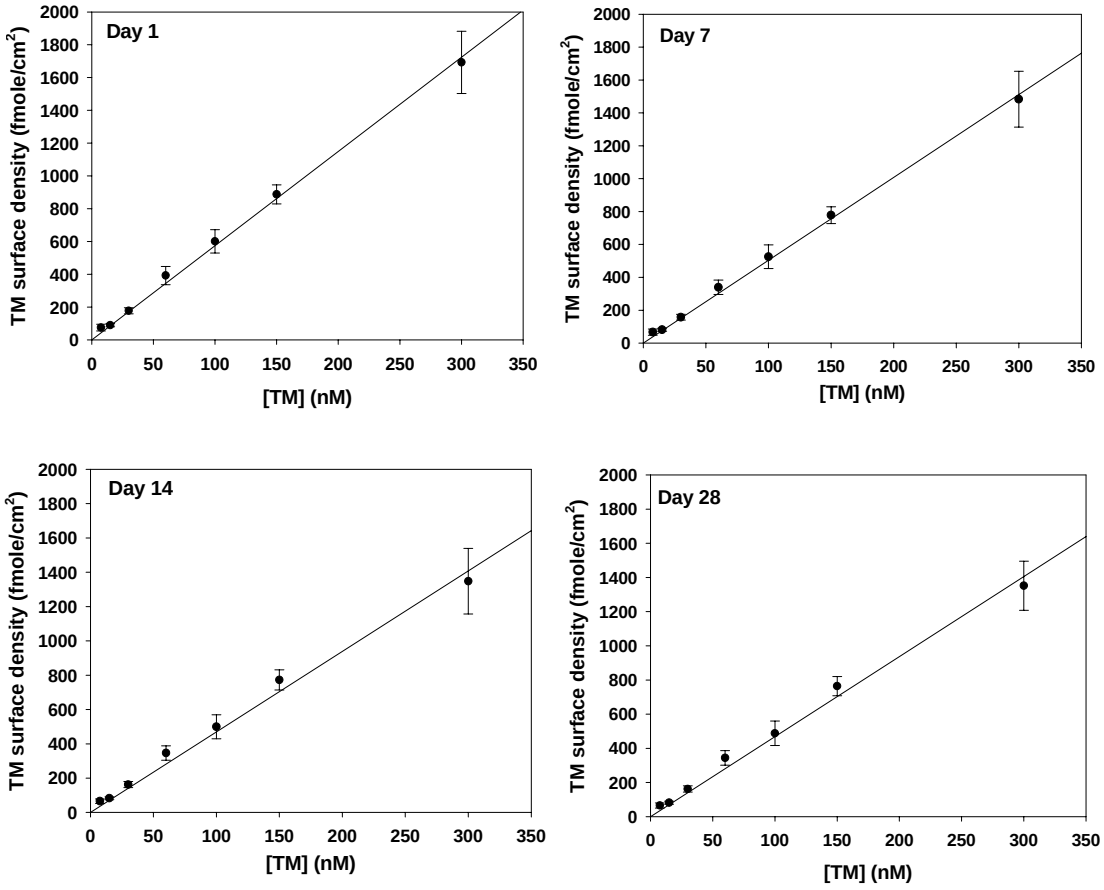

Figure 7 TM surface density and stability within a polymeric lipid membrane. TM was radiolabeled with 125I and reconstituted into lipid vesicles, and surface concentration was determined after the formation of a polymeric lipid assembly. The stability of this system was assessed in PBS at 37 °C over a 28-day period. Films were transferred to fresh PBS at indicated time points and radioactivity measured in a gamma counter.

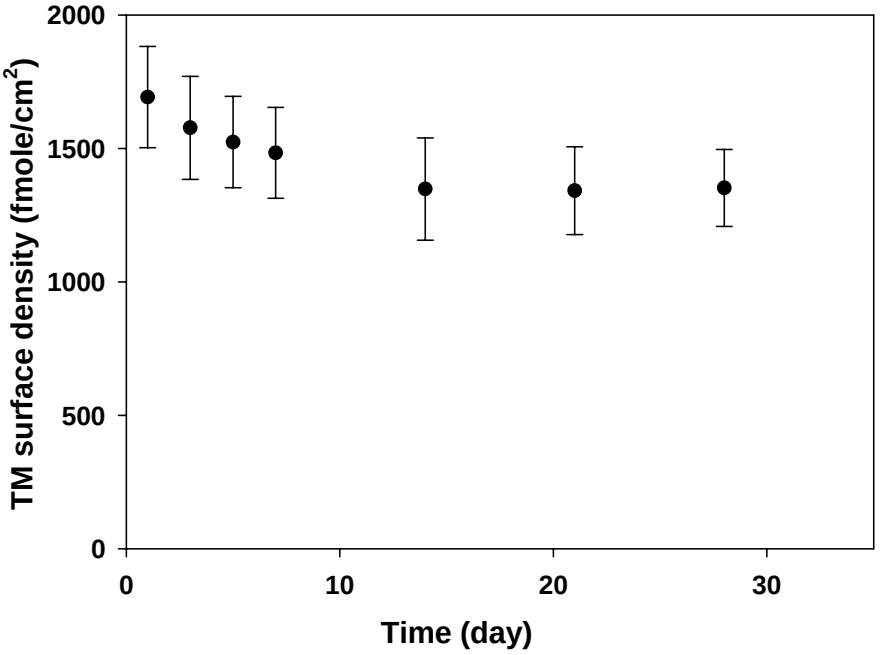

Figure 8 Stability of TM surface concentrations for [TM] = 300nM for lipid fusion. The surface samples were incubated with PBS at 37^{o}C and radioactivity was detected at time points up to four weeks.

3.4.2 Theoretical Considerations of the Surface TM-Catalyzed Flow Reactor

Under flow conditions, the production of TM-catalyzed activated protein C depends upon an intrinsic reaction rate constant, as well as the transport of protein C and thrombin to TM and the subsequent removal of APC. The latter processes are governed by convection in fluid flow and diffusion within the boundary layer region. To simplify the analysis of this system, we have assumed that TM and thrombin for a stable protein C activating complex and that the reaction of protein C with this complex acts as a two-component system consisting of an enzyme and substrate. In addition, we have assumed that TM-catalyzed activation of protein C occurs at the catalytic site within the boundary layer and the bulk concentration of protein C remains constant.

The reaction kinetics for an immobilized enzyme (thrombin-TM complex) bound on the surface of a parallel plate reactor and exposed to substrate (protein C) flowing past under laminar flow conditions has been considered in a similar fashion to a tubular reactor (102, 103) because a parallel plate flow system is highly analogous to a tubular system in terms of fluid dynamic properties (104). The hydrodynamic properties of such a flow system are presented (Figure 9). The flow profile is parabolic across the height and uniform across the width of the flow chamber due to the aspect ratio ($W/H > 10$) of the channel cross section. The substrate concentration behaves in a boundary layer-like fashion base on the following assumptions: (a) steady state and (b) diffusion and convection are radially (y-direction) and axially (z-direction) dominant. The governing equation for the limitations was delineated based on the classic Leveque problem (97) :

$$D\frac{\partial^2 C}{\partial y^2} = v_z \frac{\partial C}{\partial z} \tag{1}$$

$$v_z = v_{\max}\left(1 - \left(\frac{y}{B}\right)^2\right) \tag{2}$$

The appropriate boundary conditions at the surface and in the bulk fluid are:

$$\text{B.C. 1: } C = C_0 \quad \text{at} \quad z = 0 \text{ (at entrance) for all y} \tag{3}$$

$$\text{B.C. 2: } D\frac{\partial C}{\partial y} = f\,(C_w) \quad \text{at y} = \pm B \text{ for all z} \tag{4}$$

$$\text{B.C. 3: } C = C_0 \text{ everywhere but at y} \approx \pm B \tag{5}$$

where C_o is the bulk substrate concentration, C is the substrate concentration within the boundary layer, v_z is the local fluid velocity in the axial direction (z) as a function of the position in the height of the reactor (y), and v_{max} is the maximum fluid velocity.

The first condition describes the initial substrate concentration at the entrance of the flow. The third condition represents the boundary layer-like nature of the mass transport for which changes in substrate concentration occur only in the vicinity of the surface. The second boundary condition indicates diffusive flux is exactly balanced by rate of reaction at the catalytic surface. Under flow conditions in which diffusional transport to the surface is rate-limiting relative to the enzyme kinetics, eq.(4) becomes

$$C = 0 \qquad \text{at y} = \pm B \text{ for all z}$$

The average rate of reaction per unit area at the surface can be shown to be

$$\left(r_p\right)_{d\,iff} = k\,C_0 \tag{6}$$

$$k = 1.68\left(\frac{\gamma_w D^2}{9L}\right)^{1/3} \tag{7}$$

$$\left(r_p\right)_{d\,iff} = Q\,\frac{[P]_{diff}}{A} \tag{8}$$

where

$(r_p)_{diff}$ = rate of surface reaction (flux, pmole/min/cm^2)

D: diffusion coefficient (cm^2/min)

L: length of the reactor (cm)

H: height of the reactor (= 2B) (cm)

k: mass transfer coefficient (cm/min)

W: width of the reactor (cm)

Q: volumetric flow rate (mL/min)

γ_w : wall shear rate = $\frac{3Q}{2B^2 W}$ (sec^{-1}) (9)

$[P]_{diff}$: concentration of product (nM)

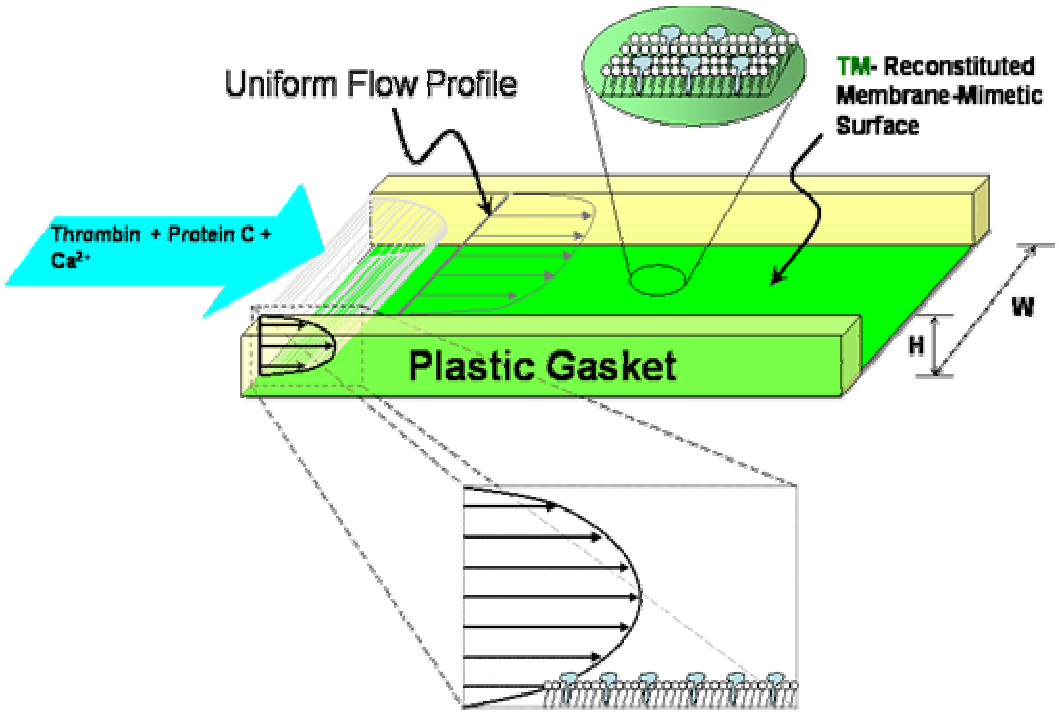

Figure 9 Schematic of fluid dynamic profiles in a parallel plate flow system for surface catalytic reaction. (Not to scale)

Details about solving the above partial differential equation are shown in Appendix B for readers unfamiliar with the field. Given the flow chamber geometry, the wall shear rates of 50 and 500 sec^{-1} require flow rates of 0.031 and 0.31 mL/min, which result in residence time of 53 and 5.3 seconds respectively. The diffusion coefficient of protein C was estimated 7.36 X 10^{-7} cm^2/sec at 37°C using semiempirical equation of Polson (105) for biological molecules since no value for protein C is reported in the literature

$$D = \frac{9.40\ x\ 10^{-15}\ T}{\mu\ M_w^{1/3}} \tag{10}$$

where D is diffusion coefficient in cm^2/sec, M_w is the molecular weight of the molecule in g/gmol, T is temperature in K, and μ is viscosity of solution in g/(cm·sec). For 0.1 μM protein C, theoretical rates of reaction due to transport effect are 0.88 and 1.90 pmole/(min·cm^2) at 50 and 500 sec^{-1}, respectively.

The average thickness (δ_{av})of the concentration boundary layer (106-108) is given by:

$$\delta_{av} \approx 0.75\left(\frac{WH^2DL}{Q}\right)^{1/3} \tag{11}$$

The average thicknesses of boundary layer in our system are 55 and 25 μm for shear rates of 50 and 500 sec^{-1}, respectively. According to the above analytical results (eq. (7) and (11)), both rate of reaction and average thickness of concentration boundary layer are a function of shear rate, given the other fixed parameters including diffusivity, and geometry of reactor vessel, the similar expressions to previous studies (102, 109). Steady state rate of reaction is expected to be higher due to faster transport of materials through a thinner boundary layer.

In order to optimize catalytic surface design in a manner that appropriately matches the enzymatic capacity of a surface with the anticipated level of substrate delivery, it is often useful to define a *mass transfer limited regime* in which the rate of product formation is dictated by the transport of the substrate to surface reactive sites rather than by insufficient surface catalytic activity. Given that the physiologic concentration of protein C is ~ 0.1 μM and varies little, this analysis requires a consideration of both surface reaction kinetics and the rate of substrate transport to the reactive surface at a given shear rate. Assuming Michaelis-Menten kinetics and that all surface sites are catalytically primed through full complexation of TM with thrombin, the relative effects of these parameters can be assessed in a ratio referred to as a Damköhler number (Da). Da is a dimensionless number and its physical significance is emphasized as the ratio of maximum rate of reaction kinetic to maximum rate of transport (110):

$$Da = V_{max} / kC_o$$

where V_{max} (Michaelis-Menten kinetics) = $k_{cat}[E]_t$, $[E]_t$ is the TM surface density, k_{cat} is 23 min^{-1} for TM-reconstituted polymerized lipid vesicles (79), k is the mass transfer coefficient, C_0 is the initial substrate concentration of protein C.

According to the above analytical model (eq. (6)), theoretical calculations of kC_0 are 0.88 and 1.90 (pmole/min/cm^2) for 50 sec^{-1} and 500 sec^{-1} respectively

Characteristically, at a Da >> 1 a transport-limited regime exists, while conversely a reaction-limited regime occurs at a Da << 1. Thus, Damköhler numbers as a function of TM surface density can be determined and are summarized in Table 1. At TM concentrations between 66 and 800 fmol/cm^2, Da varies between 1 and 10, which suggests that both diffusive transport and surface kinetics dictate product formation and

that maximum protein C activation would not be achieved. However, if surfaces were designed at a TM surface density $\geq$ 800 fmole/cm^2, our analysis predicted that a transport-limited regime (Da > 10) would be attained at both target shear rates. In addition, at the same TM surface concentration, Da is smaller at higher shear rate due to higher rate of transport effect. Since no Da is much less than unity in all given TM surface concentrations, there is no pure kinetic-limited regime.

Table 1 Damköhler number (Da) at a series of TM surface concentration under flow conditions. Da is defined as the ratio of maximum rate of kinetic reaction (V_{max}) over maximum rate of transport (kC_0). Vmax is obtained from the product of k_{cat} (79) and TM surface concentration ($[E]_t$), while kC_0 is obtained from analytical expression shown in equation (6).

TM (fmole/cm^2)	$V_{max} = k_{cat}\,[E]_t$	Da (50 sec^{-1})	Da (500 sec^{-1})
1351	31.05	35.22	16.35
764	17.57	19.93	9.25
488	11.22	12.73	5.91
344	7.91	8.98	4.17
162	3.73	4.23	1.96
82	1.89	2.14	0.99
66	1.52	1.72	0.80

3.4.3 Experimental Analysis of TM-Mediated Activated Protein C Production Under Laminar Flow Conditions

Activated protein C production as a function of TM surface density at shear rates of 50 and 500 sec^{-1} are shown in Figure 10. APC generation increased with increasing perfusion time until a steady-state concentration of APC was observed. After initiating perfusion at shear rate of 50 and 500 sec^{-1}, the time to reach steady-state level was approximately 40 min and 5 min, respectively. Of note, the concentration of APC measured at the outlet varied inversely with wall shear rate, which is consistent with what equations (6)-(9) reflect. As summarized in Figure 11, the rate of protein C activation increases with TM surface concentration and reaches a maximum at a TM surface density equal to or greater than 800 $fmole/cm^2$, which is also in agreement with Da analysis. The TM density plots (Figure 3) were fit to the equation for a hyperbola, thereby defining two parameters, $K_{1/2\ E}$, the density required for half-maximal rates, and $V_{max\ E,}$ the predicted maximal rate of reaction, both are summarized in Table 2. Values of $K_{1/2\ E}$ reflect the activation rates of protein C with 106 and 127 $fmol/cm^2$ TM were 0.23 and 0.69 $pmole/(min \cdot cm^2)$ respectively. These values are equivalent to a turnover of 2.17 and 5.43 molecules per min per TM-thrombin complex at shear rates of 50 and 500 sec^{-1} respectively. In contrast, within a regime characterized by excess TM, as exemplified by a TM surface concentration of 1350 $fmol/cm^2$, respective turnover rates were 0.33 and 1.01 molecules per min per TM-thrombin complex., showing the excess catalytic capacity at high TM densities. The average steady-state rates of APC generation in the presence of TM surface density = 1350 $fmole/cm^2$ were 0.44 (n = 5) and 1.35 $pmole/(min \cdot cm^2)$ at shear rates of 50 and 500 sec^{-1}, respectively, which are close to the $V_{max\ E}$ value determined by the curve fitting. The ratio of $V_{max\ E}$ at 50:500 sec^{-1} is

approximately 1:3, while theoretical ratio based on transport limitation is 1: 2.2 (= $50^{1/3}$:$500^{1/3}$).

Although the empirical rate of APC as a function TM surface density indicates that the rate of reaction is higher at higher shear rate and the system reaches the limit of catalytic efficiency at high TM surface content, there is discrepancy between theoretical and experimental values. Compared to theoretical values of rate of APC generation, experimental results show approximately 50% (0.45/0.88 pmole/(min·cm^2)) and 72% (1.37/1.90 pmole/(min·cm^2)) of those anticipated (k·C_o) at wall shear rates of 50 and 500 sec^{-1}, respectively. The analytical model assumes that the substrate concentration in the center core of the chamber remains constant and only substrate molecules in the substrate boundary layer, which is typically quite small compared to the chamber thickness, are involved in the reaction. However, calculated average boundary layer thicknesses at shear rates of 50 and 500 sec^{-1} are approximately one-half and one-quarter of the flow chamber height, respectively. Thus, the theoretical flux may be overestimated due to a greater level of transport resistance than otherwise anticipated providing one possible explanation for the observed discrepancy between measured and predicted rates of APC production. It is also plausible that these differences may be related to a disparity in estimated and actual k_{cat} values, as well as the possibility that the local shear environment induces a conformational change in the catalytic site of TM and, as a consequence, k_{cat}. More detailed studies will be required to address these issues. Nevertheless, it is consistent with the hydrodynamic theory that the rate of the reaction is higher at higher shear rate due to less transport resistance (smaller δ), which also has been observed in other surface enzymatic reactions under flow (109, 111, 112).

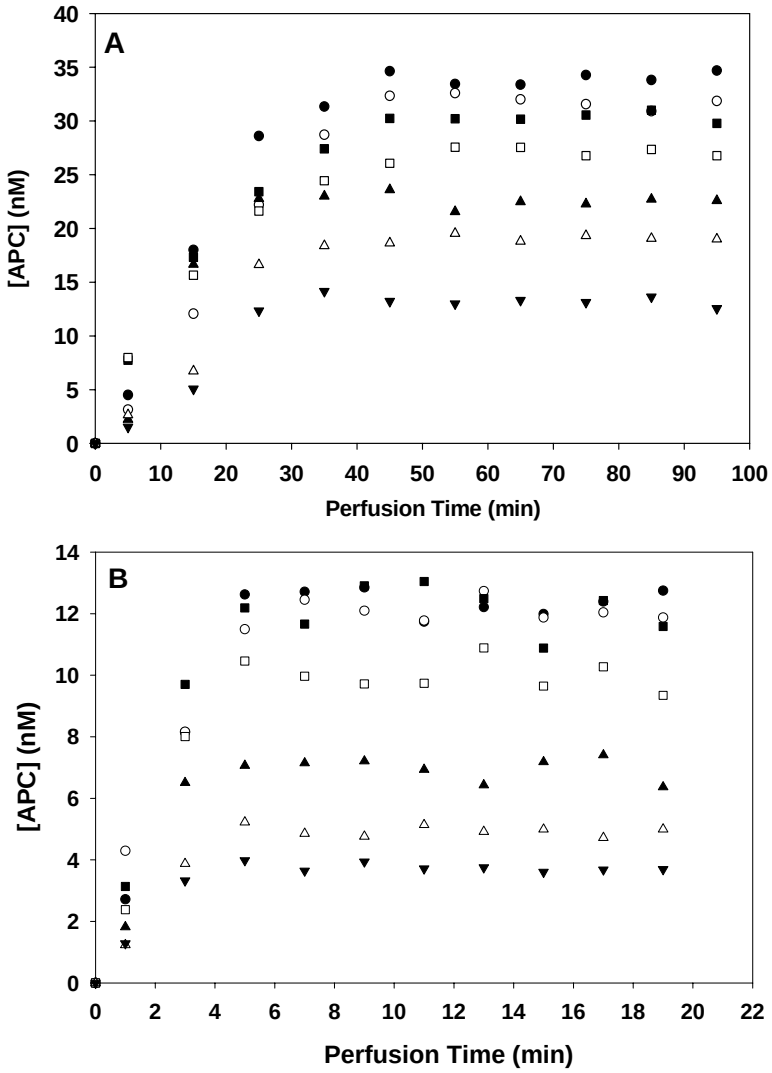

Figure 10 Kinetics of APC generation ([APC] vs. perfusion time) at a wall shear rate of (A) 50 sec^{-1} and (B) 500 sec^{-1} with TM surface concentrations of 1351 (●), 764(○), 488 (■), 344 (□), 162 (▲), 82 (Δ), 66 (▼) $fmole/cm^2$. Each data point represents the mean (n = 5) at perfusion timed points (see Appendix C).

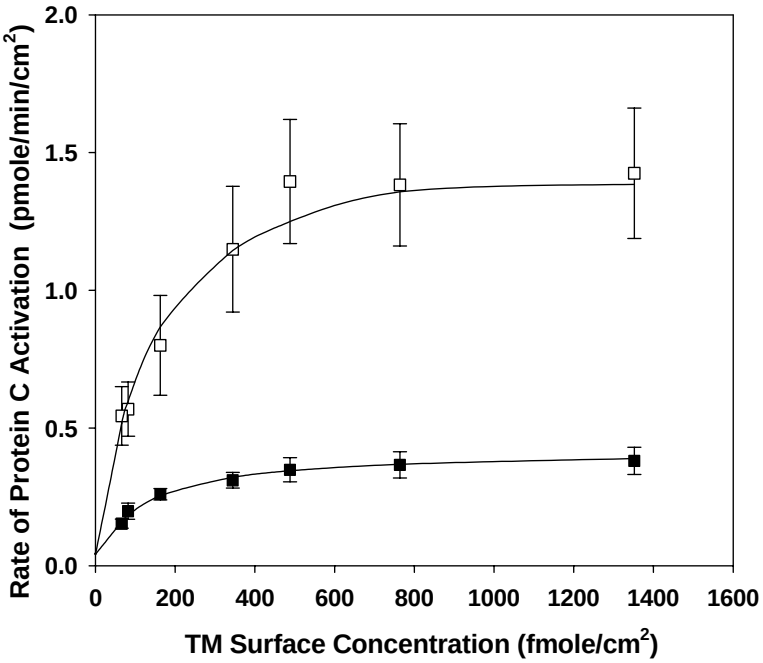

Figure 11 Rate of steady state protein C activation as a function of TM surface concentration at two different shear rates 50 (■) and 500 (□) sec^{-1}. Each data point represents the mean ± standard deviation (n = 5). Note: rate of APC generation (pmole/min/cm^2) = APC generation (nM) x flow rate (mL/min) / reactor surface area (cm^2)

Table 2 Parameters of TM Density Titrations. The TM density plots (Lineweaver-Burk plot) of figure 10 were fit to a hyperbola. The maximal APC production rate ($V_{max\ E}$) and the TM density resulting in half-maximal rate of reaction ($K_{1/2\ E}$) are shown.

γ_w (sec^{-1})	$K_{1/2\ E}$ (fmole/cm^2)	$V_{max\ E}$ (pmole/min/cm^2)
50	105.65 ±11.80	0.45 ±0.05
500	126.62 ±19.63	1.37 ± 0.23

3.4.4 Stability of Surface TM Activity

The biostability of TM containing membrane-mimetic films was assessed using test samples containing TM at a density of 1350 fmole/cm^2. Films were stored in PBS or human plasma at 37 °C and APC generation measured under flow over a three month period. Upon incubation in PBS, TM activity appeared to be relatively stable after 1-week with little change over a subsequent four week period (Figure 4). In plasma, TM activity decreased during the first two-weeks, but displayed little change over a subsequent 3 month observation period (Figure 5). A prior report from our group, reported the stability of these assemblies using ^{125}I-TM (79). Consistent with the current set of bioactivity studies a decrease in surface concentration was observed within the first 3 days of incubation in PBS with relatively little change observed thereafter. Since high shear flow (2000 sec^{-1} for 1 h) was applied to wash away non-fused, loosely associated surface TM/lipid vesicles before conducting activity tests, we have assumed that the effect of TM/vesicle desorption can be largely neglected and the loss in activity primarily reflects direct enzyme inactivation. As anticipated, a greater loss of TM activity was noted for test samples stored in plasma. We suspect that this effect is due, at least in part, to the existence of plasma protein inhibitors of TM. For example, the protein C inhibitor (PCI), known as an inhibitor of activated protein C, is also a potent inhibitor of the thrombin-thrombomodulin complex (113, 114). In addition, homocysteine, a sulfur containing amino acid in plasma that plays an important role in methionine and folate metabolism, has been reported as a possible factor of inactivating the cofactor activity of thrombomodulin by reducing the disulfide-bond rich epidermal growth factor-like structures of thrombomodulin (115).

There is growing evidence that immobilized proteins and enzymes have been found useful in many bioanalytical and biomedical applications (116). Among those enzyme-immobilized systems, enzyme-incorporated lipid membrane constructs have been broadly used for biosensors and bioreactors (116-118), such as liposome-encapsulated enzymes for disease treatment. While the stability of the immobilized enzyme as an application for biosensors in medicine can retain months in most cases (116), the current model system is considerably stable for at least a short-term period.

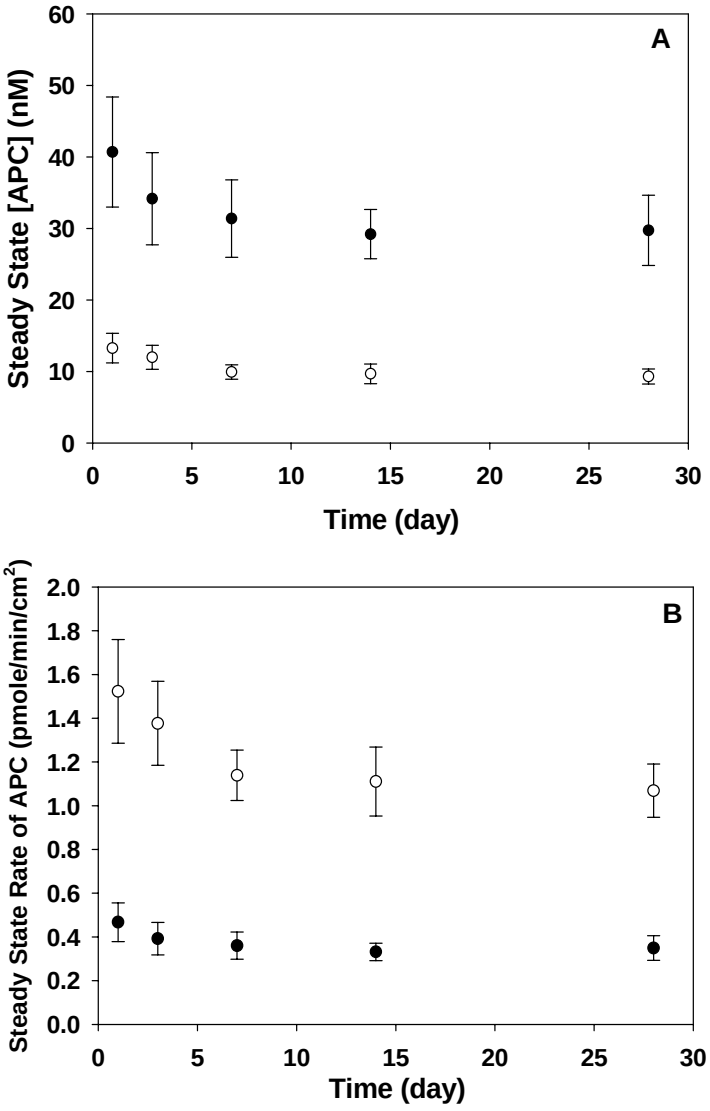

Figure 12 Stability of TM activities. Surface samples were incubated in phosphate-buffered saline (PBS, 1X) at 37°C (A) steady-state APC generation (nM) and (B) rate of steady state APC generation (pmole/min/cm^2) at shear rates 50 (●) and 500 (○) sec^{-1}. Each data point represents the mean ± standard deviation (n = 5).

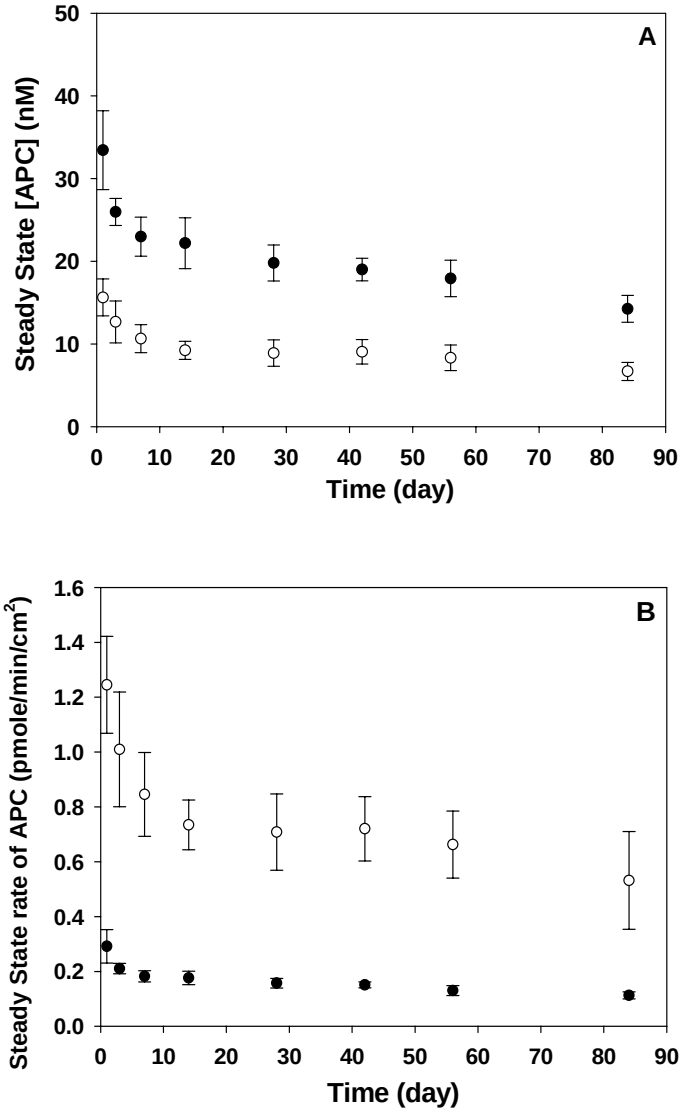

Figure 13 Stability of TM activities. Surface samples were incubated within normal pooled human plasma at 37°C. (A) steady-state APC generation (nM) and (B) rate of steady state APC generation (pmole/min/cm^2) at shear rates 50 (●) and 500 (○) sec^{-1}. Each data point represents the mean ± standard deviation (n = 5).

3.5 CONCLUSIONS

Conclusively, membrane-mimetic films can be constructed on planar substrates with predictable surface concentrations of catalytically active TM. Under flow conditions, APC production increased with increasing TM surface density, but the catalytic capacity of TM was exceeded when TM surface density is greater than 800 fmole per cm^2, indicating that a transport limit takes effect on the rate of reaction. The persistence of TM activity was investigated by incubating test films in human plasma at 37^oC with periodic testing up to three months. Durable surface bound TM activity was observed.

CHAPTER 4

FABRICATION AND CHARACTERIZATION OF HEPARINIZED SURFACE BASED ON MEMBRANE-MIMETIC ASSEMBLIES

4.1 ABSTRACT

A functional heparinized surface based on biomimetic assemblies was fabricated as a potential system to improve hemocompatibility of blood contacting devices. Heparin was chemically modified by end-point conjugation of biotin. Soluble biotinylated heparin was tested for catalytic activity on thrombin inactivation by antithrombin (ATIII). Significantly, catalytic efficiency of biotin-heparin increased with increasing heparin concentration in a range of 10 nM to 1 μM (Mw ~ 14kDa). Immobilization of biotin-heparin onto membrane-mimetic surfaces was achieved through biotin-streptavidin binding interactions. ^{3}H-Heparin was used to determine surface concentration of heparin and the results showed that correlation between surface concentration and biotin content within membrane-mimetic assemblies were fit to binding isotherm. Activity of surface heparin was investigated under well-defined flow conditions by the use of a parallel plate flow chamber at wall shear rates of 50 sec^{-1} and 500 sec^{-1}. Significantly, rate of thrombin decay becomes saturated at surface heparin concentrations equal to or greater than 4.4 pmole per cm^2, indicating catalytic efficiency of surface heparin is exceeded due to a transport limit of reactants toward as well as removal of the products from the catalytic surface.

4.2 INTRODUCTION

Clinically used since 1930s (119), heparin has become a common anticoagulant for preventing blood clotting during surgery and in the treatment of postoperative thrombosis and embolism. Heparin is a strongly negatively charged glycosaminoglycan (GAG) and a polymer of alternating hexuronic acid residues, which can be either D-glucuronic acid or L -iduronic acid, and D-glucosamine residues (Figure 14A). The resulting polysaccharide chain is highly sulfated, with N-sulfate groups on the glucosamine residues and O-sulfate groups in various positions on both the hexuronic acid and glucosamine residues. Both the distribution of glucuronic acid and iduronic acid unit and the sulfation pattern are variable, which results in a considerable structural heterogeneity (120, 121). Heparin has been found in mast cells in a large number of mammalian and nonmammalian vertebrates and is located mainly in tissues/organs that are in direct contact with the environment (i.e. lung, skin and intestine) (122).

Pharmacologically, the well-known anticoagulant activity of heparin is due predominantly to the ability of the polysaccharide to accelerate greatly the rate by which antithrombin inactivates clotting proteinases including thrombin, factor Xa, and factor IXa (81, 123). The mechanism is primarily through initial binding of a unique antithrombin-binding pentasaccharide sequence (Figure 14B) in a heparin GAG chain to antithrombin, which induces a conformational change in the antithrombin molecule, and then greatly facilitates the antithrombin inhibition of its target enzymes (124, 125). The reaction for the inactivation of thrombin is accelerated 2000- to 4000- fold: the apparent second-order rate constant increases from 0.7 to 1.4 x 10^4 $M^{-1}s^{-1}$ at 25 to 37^{o}C in the

absence of heparin to 1.5 to 4 x 10^7 $M^{-1}s^{-1}$ in the presence of optimal concentrations of the polysaccharide (37, 126-130).

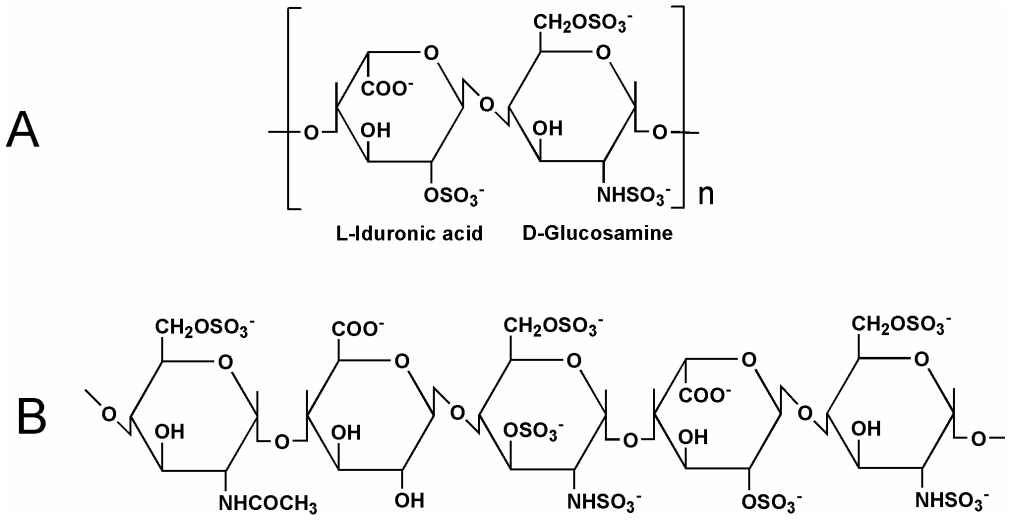

Figure 14 Heparin is a heterogeneous mixture of polysaccharides, which chains are made up of alternating 1 to 4 linked, sulfated monosaccharide residues of L-iduronic acid and D-glucosamine. The most frequent types of disaccharide unit represent up to 90% of the structure of beef-lung heparin, and up to 70% of pig-mucosa heparin (A). The unique pentasaccharide binding site for antithrombin occurs in about one-third of the heparin chains (B).

Heparinization of artificial surfaces has been studied and shown to be a successful way to prevent surface-induced thrombus formation and improve the hemocompatibility of blood-contacting surfaces in a variety of studies. Among those studies, heparin immobilized onto surfaces using spacer groups has been largely reported. Covalent bonding of nitrite-degraded heparin by end-point attachment applied on membrane oxygenators and tubings makes it possible to maintain a long-lasting extracorporeal circulation without systemic heparinization (53). Heparin immobilized through poly(ethylene oxide) (PEO) spacer groups onto polyurethane surfaces consistently enhanced bioactivity in *in vitro*, *ex vivo*, and *in vivo* experiments (52, 131). It was demonstrated that the activity of immobilized heparin increased with increasing length of the alkyl spacer group (132). Heparin coupled to surface through a spacer system was found to be more active than direct coupling due to accelerated antithrombin binding to heparin, leading to enhanced inactivation of coagulation protease. Specifically, the dominant mechanism for spacer-immobilized heparin was binding to antithrombin, followed by thrombin binding to the heparin-antithrombin complex (133, 134).

Our group has recently reported cytomimetic biomaterials as model platforms which can potentially improve the clinical performance characteristics of blood-contacting artificial organs and other implantable medical devices by modulating maladaptive processes at the blood material and tissue-material interfaces (77-80, 95, 96). Such a model construct provides strategies for generating biologically functional systems by incorporating transmembrane protein (79), as well as peptide or carbohydrate lipophilic conjugates (80). In addition, we have recently described and characterized a membrane-mimetic thin film composed of mixed polymerizable lipids containing

phosphatidylcholine or biotin headgroups (80, 94), which leads to fabrication of heparinized surface based on membrane-mimetic assemblies (Figure 15).

Heparin was chemically modified by oxidation and lactonization at the terminal position, followed by conjugation of biotinylated linker which was synthesized by reacting 2-(4-aminophenyl) ethylamine with N-biotin succinimide. Before applied for coating, biotinylated heparin was characterized by determining the extent of biotinylation and the catalytic efficiency on thrombin inactivation by antithrombin in a solution form. The results showed that there was more than 90% of biotinylation and the activity was comparable to that of original heparin extracted from porcine intestinal mucosa. Heparinized surface was then fabricated by coupling biotinylated heparin to biotinylated lipid thin film bridged by streptavidin. Surface concentration of heparin was determined and found to be a function of biotinylated lipid surface content. A parallel plate flow reactor containing heparin-coated surface was used to investigate heparin-mediated thrombin inactivation by antithrombin at shear rates of 50 sec^{-1} and 500 sec^{-1}. Under such circumstances, the kinetics of thrombin inactivation at a heparinized surface is not only dependent on inherent reactions among thrombin, antithrombin, and heparin, but also influenced by the transport of reactant toward and removal of products from the catalytic surface, which is determined by convection in bulk and diffusion within boundary layer under laminar flow conditions. Steady-state rates of thrombin decay were higher at higher shear rate and became saturated in the presence of heparin surface content equal to or greater than 4.4 $pmole/cm^2$, indicating that capacity of surface heparin to facilitate thrombin neutralization can not be further enhanced by increasing heparin surface density due to transport limitation.

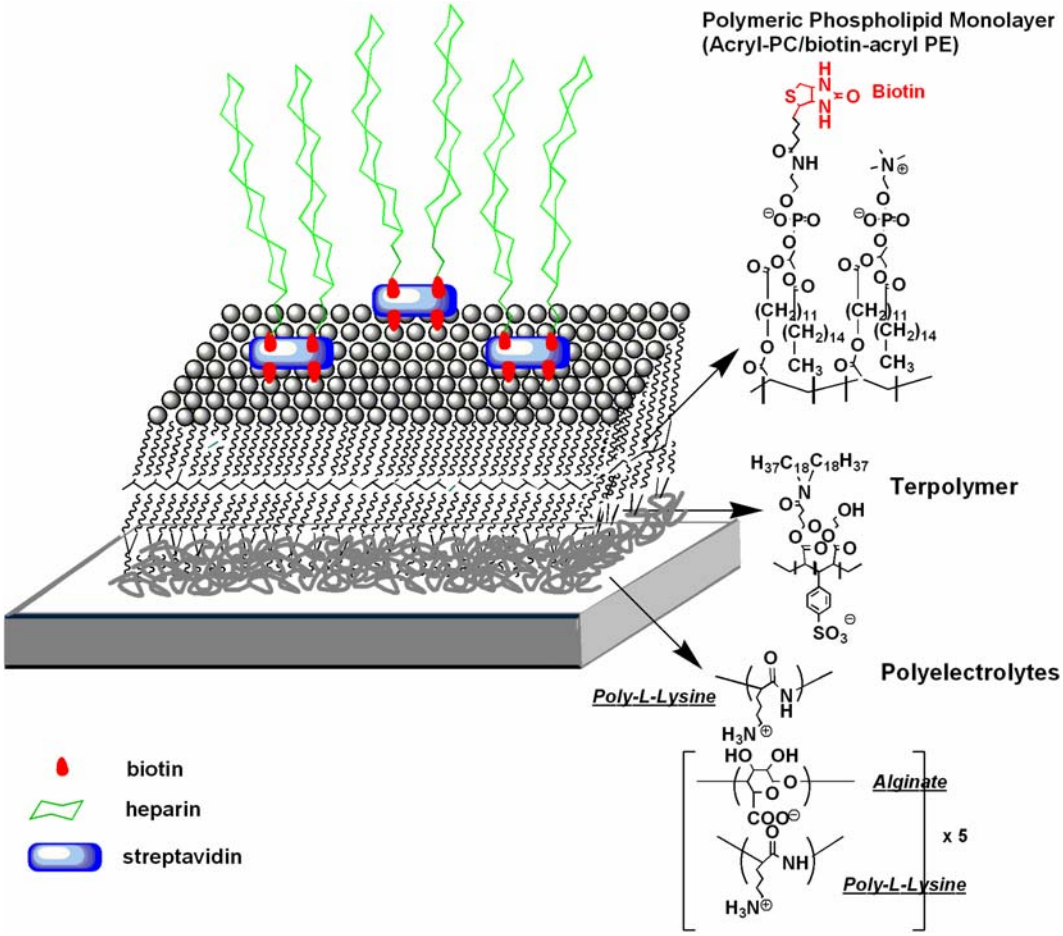

Figure 15 Schematic representation of immobilized heparin on the basis of polymeric phospholipid monolayer supported on an alkylated polyelectrolyte multilayer. (Not to scale)

4.3 MATERIALS AND METHODS

4.3.1 Materials

Human thrombin and antithrombin III (ATIII) were obtained from Haematologic Technologies, Inc. Heparin (sodium salt, porcine intestinal mucosa, Mw: 12,000-14,000) and streptavidin was obtained from Calbiochem. N-hydroxysuccinmido biotin (active ester) and polybrene (1,5-Dimethyl-1,5-diazaundecamethylene polymethobromide) were obtained from Sigma. Tritiated heparin (Heparin sodium salt,[3H(G)]- M.W. 6,000-20,000) was purchased from PerkinElmer. Chromogenic substrate for thrombin Spectrozyme TH: H-D-hexahydrotyrosyl-L-alanyl-L-arginine-p-nitroanilide-diacetate salt was purchased from American Diagnostica, Inc. Eosin Y (EY, 5% in water), triethylamine (TEA), 1-vinyl-2-pyrrolidinone (VP) were obtained from Aldrich. Nucleopore polycarbonate filters, circular glass coverslips (12 mm diameter, 0.17 mm thickness from Fisher) and Contrad 70 detergent are obtained from Fisher. Alginate (ALG; low viscosity, ca. 60% mannuronic acid) was obtained from Pronova Biomedical (Norway). Poly (L-lysine) (PLL, MW > 300 kD) and all buffer salts were obtained from Sigma. Synthesis of monoacrylate-PC (AcPC, 1-palmitoyl-2-[12-(acryloyloxy)dodeca-noyl]-*sn*-glycero-3-phosphocholine), monoacrylate-PE (AcPE, 1-palmitoyl-2-(12-(acryloyloxy)dodecanoyl)-*sn*-glycero-3-phosphoethanolamine) and its biotin derivative (biotin-AcPE, mono-acryl PE-biotin) have been described previously (77, 94). The synthesis of the terpolymer that consists (3-acryloyl-3-oxapropyl-3-(N,N-dioctadecyl-carbamoyl)-propionate))$_6$:(2-hydroxyethyl acrylate)$_3$:sodium styrene sulfonate$_1$ (AOD_6:HEA_3:SS_1) has been described elsewhere (135).

Instrumentation. Biotinylated heparin was characterized by NMR spectroscopy for component analysis. ^{1}H NMR spectra was recorded on a Varian INOVA 400 MHz or on 600 MHz NMR spectrometer. For ^{1}H NMR spectra recorded in $CDCl_3$, D_2O and CD_3OD chemical shifts (δ) are given in ppm relative to solvent peaks (for $CDCl_3$, ^{1}H $\delta = 7.26$, for D_2O ^{1}H $\delta = 4.85$, for CD_3OD ^{1}H $\delta = 4.87$ & 3.32) as internal standard. Coupling constants (*J*) are reported in Hertz (Hz). Size exclusion chromatography/laser light scattering (SEC/LLS) was used to determine molecular weight and polydispersity. ^{3}H-labeled materials were detected using a scintillation counter (Beckman LS 6000IC). UV-Visible spectrophotometric measurements were executed on a Cary 50 Bio spectrophotometer (Varian) equipped with a temperature-regulated cell compartment.

4.3.2 Synthesis of Biotin-Conjugated Heparin

The procedure for the preparation of biotinylated heparin is illustrated in the Figure 16. Three reaction steps were sequentially conducted:

Step I: Oxidization of Heparin

Heparin sodium salt **1**, was dissolved in water and passed through the protonated Dowex resin (50X8 H^{+}) and eluted with water. The eluate was dialyzed and lyophilized to obtain Heparin (protonated form). The heparin-lactone was then prepared by oxidizing the reducing end of HMW protonated heparin (0.0392 mmol, 550 mg) by iodide (20 eq.) in 20% aqueous MeOH solution (100 mL) for 6–8 h at room temperature. The completion of the oxidation process was assessed by 3,5-dinitrosalicylcic acid method.* The reaction solution was then added to a ethanolic 4% KOH solution (100 mL). The mixture was allowed to stand for 30-45 min and then the supernatant solution was decanted and centrifuged. The collective white residue obtained was dissolved in water and subjected

to dialysis (MWCO ~ 3500) for 24 h. The sample solution was freeze dried and lyophilized to obtain the oxidized heparin product **2** (370 mg) [******3,5-dinitrosalicylcic acid method*: 3 mL of sugar solution + 3 mL of DNS reagent. Heat the mixture for 5 – 15 min at 90 °C. The color of the solution changes from orange to reddish brown. 3,5-dinitrosalicylcic acid reagent (1%) was prepared by dissolving 10 g of 3,5-DNSA, 2 g of Phenol, 0.5 g of Sodium sulfite Na_2SO_3, and 10 g of NaOH in 1 L of deionized water].

Step II: Preparation of Heparin-lactone

The oxidized heparin product **2** was subsequently dissolved in distilled water and passed through a protonated Dowex resin (50X8 H^+) and stirred for 30 min. The eluant was then filtered and washed with water several time (the eluant was checked regularly with litmus paper to ensure that the washing is complete). The sample solution was freeze dried and lyophilized to obtain the heparin lactone 3 (300 mg).

Amine-terminated biotin linker **6** was synthesized before conjugated with the heparin-lactone: to a solution of 2-(4-aminophenyl)-ethylamine **4** (1.2 eq., 3.51 mmol, 478 mg) in dry DMF was added triethylamine Et_3N (1.25 eq., 3.662 mmol, 510 μl) and the solution was stirred at room temperature for 20 min under Argon atmosphere. To this mixture, N-biotin succinimide **5** (2.93 mmol, 1.0 g) dissolved in DMF was added and the reaction was allowed to stir at room temperature for 24 h. Removal of the solvent under vacuum afforded a residue which was purified by silica gel column chromatography using 10% $CHCl_3$ + MeOH mixture as the eluent. The lyophilized product was orange yellow solid (510 mg, yield: 45 – 50%); TLC: 20% MeOH/$CHCl_3$. ^{1}H NMR (400 MHz, 9:1 CD_3OD + $CDCl_3$) δ 6.93 (d, 2 H, *J* = 5.6 Hz), 6.63 (d, 2 H, *J* = 5.6 Hz), 4.43 (dd, 1H, *J* = 3.2 Hz, NH-*CH*), 4.21 (m, 1H, *J* = 3.2 Hz, NH-*CH*), 3.1 (m, 1H, S-*CH*), 2.86 (dd, 1H, *J* = 3.2

Hz), 2.67 - 2.59 (5H, Ar-*CH*$_2$ + NH-*CH*$_2$ + S-*CH*), 2.09 (t, 2H, *J* = 4.4 Hz, CO-*CH*$_2$), 1.68-1.52 (m, 4H, (*CH*$_2$)$_2$), 1.15 (m, 2H, *CH*$_2$).

Step III: *Coupling of aminated biotin with heparin Lactone*

Amine terminated biotin **6** (10 eq., 0,22 mmol, 75 mg) dissolved in DMF was added to a solution of heparin-lactone **3** (0.022 mmol, 300 mg) in DMF containing diisopropylethylamine (10 eq., 40 µl). The reaction mixture was stirred for 8 h at 55 – 60 °C. The reaction mixture was concentrated and washed with $CHCl_3$/MeOH mixture to remove the excess aminated biotin. The subsequent residue was dissolved in water, dialyzed (36 h, MWCO ~ 3500) and freeze dried to obtain the biotinylated heparin. Finally, the biotinated heparin was purified by Gel permeation chromatography (Sephadex G-25) using water as an eluant. The water fractions containing the product were pooled together and lyophilized to afford a pale yellow biotin-functionalized heparin derivative 7 (180 mg, yield: 60%). ^{1}H NMR of **7** (600 MHz, D_2O) δ 7.6 – 7.2 (m, ArH), 5.72 – 4.91 (m, ring protons), 4.75 – 4.1 (m, ring protons + NH-CH), 4.08 – 3.35 (m, ring protons), 3.06 – 2.76 (m, Ar-CH_2 + NH-CH_2 + S-CH), 2.09 (s, CO-CH_2), 2.01 (s, NH-Ac), 1.6 – 1.2 (m, $(CH_2)_n$ protons).

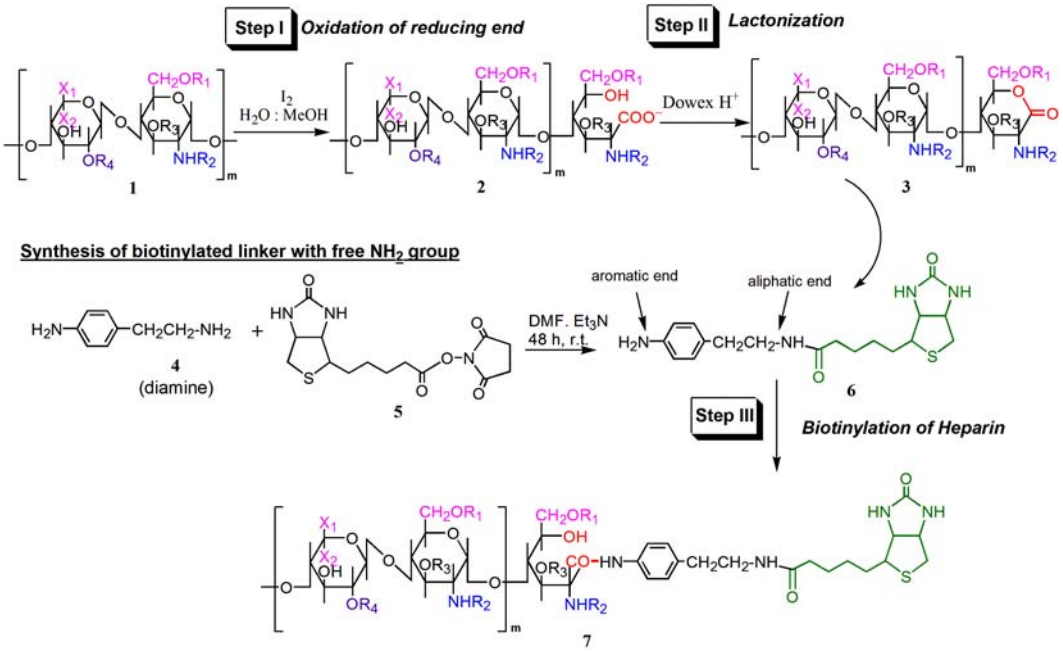

Figure 16. Sequential procedure for the synthesis of biotinylated heparin. Adopted with permission from (136).

4.3.3 Purification of Biotin-Conjugated Heparin.

ImmunoPure® Immobilized Monomeric Avidin, a commercially available kit obtained from Pierce, was used for purification. The principle of the kit is using immobilized polymeric forms of avidin with strong binding characteristics to biotinylated molecules (137-139). In brief, these high affinity biotin-binding sites are first blocked with a biotin-containing buffer. Biotin molecules are eluted from the monomers with a glycine solution revealing only the reversible binding sites. The biotinylated molecule of interest may then be applied to the support for purification and then eluted by ligand competition using a biotin-containing buffer. Since the final eluted materials contain biotin, extraneous sources of biotin were removed by dialysis in order to obtain optimal binding capacity.

4.3.4 Determination of Biotin Content From Biotin-Conjugated Heparin

Biotin content from biotinylated heparin was determined using HABA assay which has been considered suitable for the spectrophotometric determination of the extent of biotinylation. The assay reagent, HABA/Avidin, contains 0.3 mM HABA (4-Hydroxyazobenzene-2-carboxylic acid), 0.45 mg/ml avidin, 0.3 M NaCl, 0.01 M HEPES (N-[2-Hydroxyethyl] piperazine-NN-[2-ethanesulfonic acid], a buffer with pKa = 7.5), 0.01 M $MgCl_2$, 0.02% sodium azide (as a preservative), pH 7.3 when reconstituted with 10 mL deionized water. The assay was run by following the manufacture protocols (Sigma). Briefly, the following samples were measured at 500 nm by UV-VIS spectroscopy: (a) 900 μL HABA reagent, (b)100 μL biotinylated heparin + 900 μL buffer (50 mM NaH_2PO_4/150 mM NaCl, pH 7.4), and (c) 900 μL HABA reagent + 100 μL biotinylated heparin. Then the absorbance difference ΔA_{500} defined as 0.9(a) + (b) – (c)

(0.9 is dilution factor of HABA reagent upon addition of sample) was calculated. The amount of biotin is defined as μmole biotin/mL, which is equal to ($\Delta A_{500}/34$) X 10 (34 is mM extinction coefficient at 500nm, 10 is dilution factor of sample into cuvette). Biotin content of biotinylated heparin is defined as mole biotin/mole heparin, which is equal to (μmole biotin/mL sample)/(μmole heparin/mL sample) (140).

4.3.5 Analysis of Biotin-Heparin Activity

The heparin activity test was conducted based on its catalytic capacity to facilitate thrombin inactivation by antithrombin in a solution form, and activity of biotinylated heparin was investigated and compared to that of heparin (porcine mucus heparin, Calbiochem) in order to determine the effect of biotinylation on heparin activity. To perform thrombin inactivation assay, Hepes buffer (20 mM Hepes + 100 mM NaCl + 0.5 wt% BSA) containing heparin was incubated with 10 nM human ATIII at 37^{o}C for 5 min, followed by adding 10 nM human thrombin to start the reaction. At timed intervals, aliquots were withdrawn and assayed by adding to Tris buffer (50 mM Tris-HCl + 175 mM NaCl + 0.05 wt% BSA, pH 7.9) containing 1 mg/mL Polybrene (141, 142) and chromogenic substrate Spectrozyme TH (0.2 mM final). The residual thrombin was determined by converting measured absorbance from UV-VIS spectrophotometer via a standard curve (see Appendix A).

4.3.6 Fabrication of Biotin-Functionalized Membrane-Mimetic Thin Films

Preparation of a (PLL-ALG)5-PLL Terpolymer Film on Circle Coverglass. Circle coverslip substrates (12 mm dia., Fisher) was cleaned by 30 minutes of sonication in 10% Contrad 70 detergent solution followed by extensive washing and sonication in deionized water. PLL and ALG were prepared at concentrations of 0.10 and 0.15 w/v % in phosphate-buffered saline (PBS; 20 mM NaH_2PO_4, 0.9 w/v % NaCl, pH 7.4), respectively. The cleaned substrates were then coated by PLL and ALG alternating monolayers to form 11 layers (six PLL and five alginate layers) were coated, with the top layer comprised of PLL. The $(PLL\text{-}ALG)_5$-PLL-coated substrates were then exposed to a 0.1 mM solution of terpolymer (AOD_6:HEA_3:SS_1) dissolved in a mixture of 20 mM NaH_2PO_4/DMSO (99:1 v/v), pH 7.4 for 90 s. The $(PLL\text{-}ALG)_5$-PLL terpolymer coated samples were then rinsed 7-10 times with deionized water.

Vesicle Fusion. Large unilamellar vesicles (LUVs) totaling 12 mM lipid (in either 0, 2, 5, 10, 20, or 50 mol % biotin-AcPE) in 20 mM sodium phosphate buffer (pH 7.4) were prepared by four successive freeze/thaw/vortex cycles using liquid N_2 and a 65 °C water bath. The LUVs were then extruded 21 times each through 2.0 μm and 0.6 μm polycarbonate filters (Millipore), and the solution was diluted to 1.2 mM with 20 mM sodium phosphate buffer (pH 7.4) and 150 mM NaCl. The $(PLL\text{-}ALG)_5$-PLL terpolymer coated substrates were then incubated with the vesicle solution at 43 °C overnight for 14 to 16 hours.

In Situ Photopolymerization of a Supported Lipid Film. Details of the photopolymerization of lipid films on alkylated glass and silicon have been reported elsewhere (78, 135). Briefly, a stock solution of coinitiators was prepared as 10 mM

Eosin Y (EY), 225 mM triethanolamine (TEA), and 37 mM VP in water. A 10:1 (mol/mol) monomer/EY ratio was used for photopolymerization. After lipid fusion, the samples were placed into an Ar-purged atmosphere at 30% relative humidity and 10 μL of initiator was added per 1 mL of sample solution. The initiator was gently mixed by slowly rotating the vial in a horizontal circular motion without lifting it from the bench surface. The sample was then irradiated with a Dynalume visible light lamp at an intensity of approximately 40 mW/cm^2. Following photopolymerization, the samples were washed with deionized water 6-8 times and stored for further processes.

4.3.7 Fabrication of a Heparinized Surface Based on a Membrane-Mimetic Thin Film

Streptavidin binding onto a biotin-functionalized lipid membrane. Streptavidin was prepared in PBST (50 mM NaH_2PO_4 and 150 mM NaCl, pH 7.4) at a concentration of 5μg/mL. Streptavidin-containing solutions were incubated with biotin-functionalized substrates for 15 min on a horizontal rotating platform, followed by rinsing with deionized water extensively (~ 10 times).

Biotinylated heparin binding to a streptavidin-functionalized surface. Streptavidin-coated lipid membranes were incubated with biotin-conjugated heparin at a concentration of 0.1 mg/mL in PBST overnight at 4^oC on a horizontal rotating platform. The membrane was then rinsed with deionized water extensively (~ 10 times).

4.3.8 Determination of Heparin Surface Density

^3H-heparin and unlabeled heparin were mixed to form a mass ratio of 1: 160 for biotinylation as described previously (4.3.2). The biotinylated compound was purified (4.3.3) and determined the extent of biotinylation with more than 95%. Specific activity

(cpm/μg or cpm/pmole) of ^{3}H-heparin was determined by measuring radioactivity of 5, 10, 15, 20, and 30 μL (5 replicates each) from a mixed ^{3}H-heparin and unlabeled heparin solution prepared in PBST at a concentration of 1 mg/mL. Surface density of heparin was determined by incubating streptavidin-coated membrane-mimetic thin films with the ^{3}H-heparin solution. Briefly, circle cover glasses (12 mm diameter) were cleaned and coated with membrane-mimetic constructs as described previously. A series of biotin contents in mixed lipids, 2, 5, 10, 20, 50 mole% of biotin-AcPE mixed with AcPC, were prepared for heparinization as described previously (4.3.7). The heparinized samples were placed in scintillation vials filled with scintillation liquid (BD Biosciences) and ^{3}H activity was counted by scintillation counter (Beckman LS 6000IC). Heparin surface density (pmol/cm^{2}) was calculated as (cpm/specific activity/sample area) and specific activity corrected for decay. Test surface samples were fabricated in six replicates for each lipid composition.

4.3.9 Continuous Flow Reactor Assays on Heparinized Surface

Heparinized surface was fabricated on a microscope glass slide (2.6 cm x 4.6 cm, Fisher) by anchoring biotinylated heparin onto streptavidin-coated membrane-mimetic thin film as previously described. In order to accommodate different surface amount of heparin, we selected 5, 10, 20, and 50 mol% of biotin-AcPE functionalized membrane-mimetic surfaces for heparinization. Surface heparin activity was investigated under unidirectional flow conditions with shear rates 50 sec^{-1} and 500 sec^{-1}. A parallel plate flow system (0.6cm (width) x 0.01 cm (height) x 3.6 cm (length), 22 μL volume, Figure 17) containing coated samples was flushed with 20 mM Hepes buffer for 1 hours at γ_w = 2000 sec^{-1}. The reaction was started by perfusing the surface with HBSA (20 mM Hepes

+ 190 mM NaCl + 0.05 wt% BSA, pH 7.5) (143) containing thrombin (30 nM, final) and antithrombin (30 nM, final) in two syringes separately at 37^{o}C. At pre-selected timed points, aliquots were withdrawn from the outlet of the reactor and assayed by adding to Tris buffer/EDTA (50 mM Tris-HCl + 175 mM NaCl + 0.05 wt% BSA + 20 mM EDTA, pH 7.9) containing Spectrozyme TH substrate (0.2 mM final) (143). The residual thrombin was determined by converting measured absorbance from UV-VIS spectrophotometer via a standard curve.

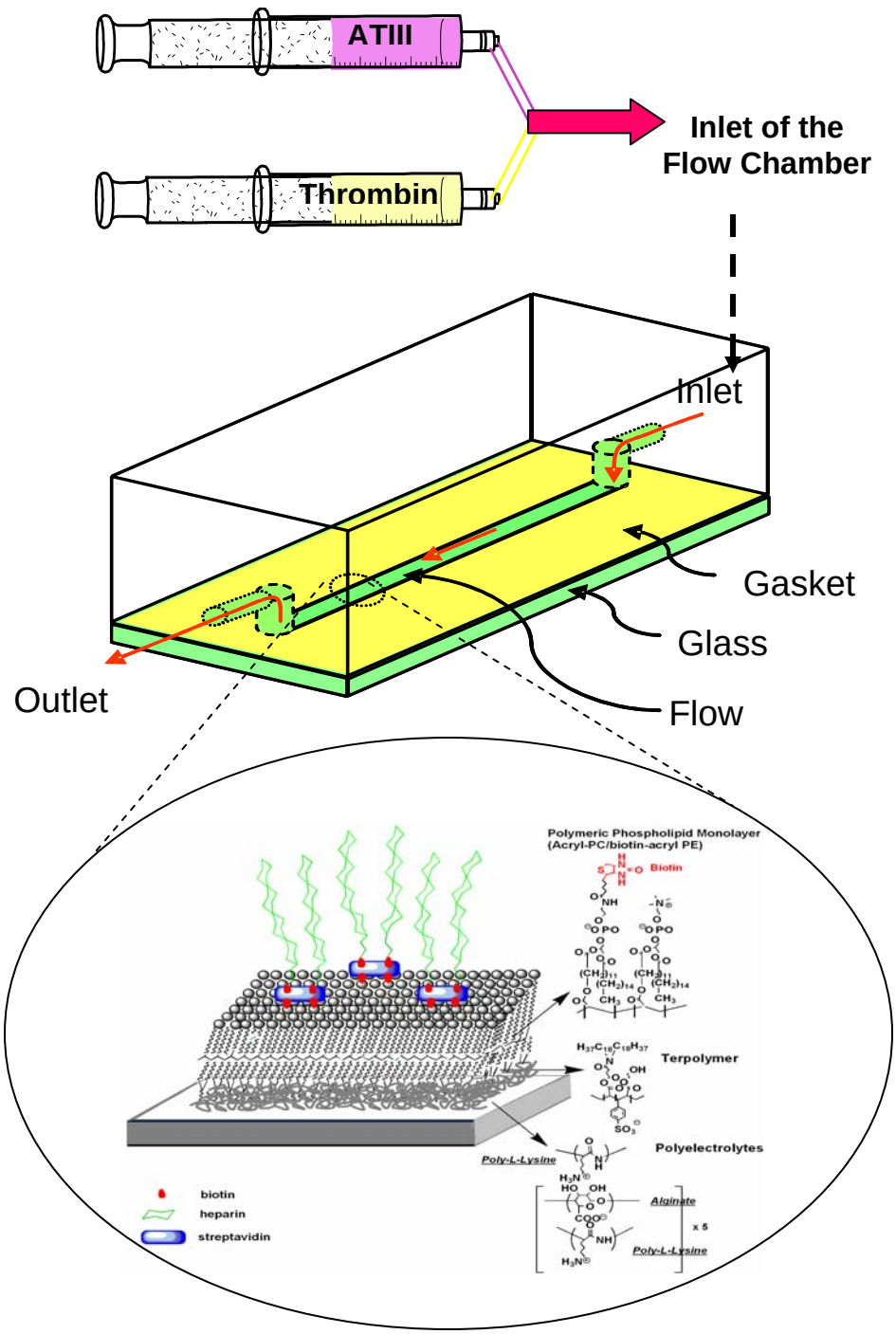

Figure 17 Schematic of parallel plate flow reactor (not to scale). The gasket (plastic shim) creates height of the flow channel. Heparin containing membrane-mimetic construct is immobilized onto a glass substrate. The surface was perfused with reactants, thrombin and antithrombin (ATIII) in separate syringes and the perfusate is collected at the outlet to determine product concentration.

4.4 RESULTS AND DISCUSSION

4.4.1 Synthesis of Biotin-Conjugated Heparin

The rationale behind biotinylated Heparin is that biotin bound to an oligosaccharide moiety is available for noncovalent high affinity interaction with avidin or streptavidin. The affinity constant between biotin and the glycoprotein avidin is one of the largest free energies of association known for noncovalent binding of a protein and a small ligand in aqueous solution. This complex is extremely stable over a wide range of temperature and pH.

Three reaction steps were sequentially conducted: I) iodide cleavage of the terminal reducing end, II) Lactone ring formation, and finally II) bioconjugation of the amine-functionalized biotin with Heparin lactone via ring opening of the terminal pyranose ring to generate terminal biotin-tagged heparin construct. Heparin sodium salt was passed through the protonated Dowex resin (50 X 8 H^+), eluted with water, dialyzed and lyophilized to obtain the protonated form of heparin. The heparin-lactone was prepared by oxidation of the aldehyde at the reducing end by iodide, which cleaves the pyranose ring at the C-O bond resulting in the formation of acid (COO^-). The completion of the oxidation process was assessed by 3,5-dinitrosalicylcic acid. The acid so formed, reacts with the 5-hydroxyl group of the reducing end sugar in presence of an H^+ ion exchange Dowex resin to form the cyclic lactone. The lactonized heparin was analyzed by NMR (Figure 18). It was noticed that although the purity of the lactone could not be determined by NMR, size exclusion chromatography (SEC, gel permeation) analyses (Figure 21) before and after the modification showed that there was little significant change between

the GPC pattern of lactone and heparin, indicating that oxidative cleavage of glycosidic bonds in the main backbone did not occur.

Generating a biotin terminated spacer-arm capable of conjugating to heparin necessitated the utilization of a linker possessing two functional groups. Based on our initial assessment, we devised a simple strategy which involved regioselective amide bond formation at one end of a diamine with the active ester of biotin. As such a diamine derivative having a free aliphatic and aromatic amine group at opposite ends (*para*-positions) of the aromatic skeleton was thought to be the ideal candidate for the coupling reaction. For example, based on the preferential selectivity of the two amines, reaction of N-hydroxysuccinmido biotin (active ester) with the diamine 2-(4-aminophenyl)-ethylamine (NH_2-Ar-R-NH_2, where R = -CH_2-CH_2) resulted in regioselective amide bond formation at the aliphatic end of the primary amine (R-NH_2) affording the desired free amine terminated biotin spacer (Yield 50%). The expected product was confirmed by NMR analysis (Figure 19).

Subsequent reaction of the lactone with the amine-terminated biotin was carried out in presence of a base triethylamine (Et_3N) and dry dimethylformamide (DMF) at 55 ºC for 10 h under Argon atmosphere. Anhydrous solvents and condition are required for this reaction considering the hygroscopic and water labile nature of the lactone. In order to drive the reaction and to ensure that the amide bond coupling between the lactone and the amine is complete, a 10 molar excess of amine is added. On completion, the crude mixture was concentrated in vacuum and washed with 10% $CHCl_3$/MeOH mixture in order to remove the excess of biotin linker. The orange-brown residue obtained was dissolved in distilled water, dialyzed extensively (MWCO 6000-8000) for a period of 48

h and lyophilized. Final purification by gel permeation chromatography (Sephadex G25) of the product using distilled water as eluant followed by lyophilization furnished the biotinylated-heparin as a fluffy pale yellow solid. Analyses of the ^{1}H NMR (Figure 20) of the product indicated the characteristic presence of aromatic protons at 7.2 ppm, keto-methyl (CO$\underline{CH_2}$) group from the spacer arm at around 2.1 ppm. Additionally, the aliphatic methylene protons ($\underline{CH_2}$, 1.4–1.6 ppm) while the resonance signals of other methylene protons attached to N-$\underline{CH_2}$, S-$\underline{CH_2}$, Ar-$\underline{CH_2}$ could be observed between 2.8-3.2 ppm. Though the anomeric protons could be observed between 5.0–5.8 ppm, a characteristic peak at 2.00 ppm was assigned to the N-acetyl group (NH-$\underline{COCH_3}$) from heparin. In order to determine the coupling efficiency of the process, integration values of the peak heights between the aromatic protons and the N-acetyl resonance signal was calculated. The yield of the reaction was ~60% while the conversion efficiency (calculated from ^{1}H NMR) of the coupled product was found to be more than 90%. Moreover, in order to ascertain that incorporation of amine-terminated biotin via covalent functionalization of native heparin does not afford degraded byproducts due to competing side reactions resulting in loss of glycosidic moiety sequence (responsible for its antithrombogenic activity) from the parent polysaccharide chain, the molecular weight of the resultant biotinylated heparin was assessed by size-exclusion chromatography (SEC) coupled with refractive index (RI) and laser-light scattering (LLS) detectors (Figure 21 and Table 3). To this end, analysis of heparin-lactone and biotinylated heparin in comparison with that of native heparin on the basis of its molecular weight demonstrated that covalent biomolecular modification of the heparin backbone resulted in significant retention of the sequence specificity and structural integrity.

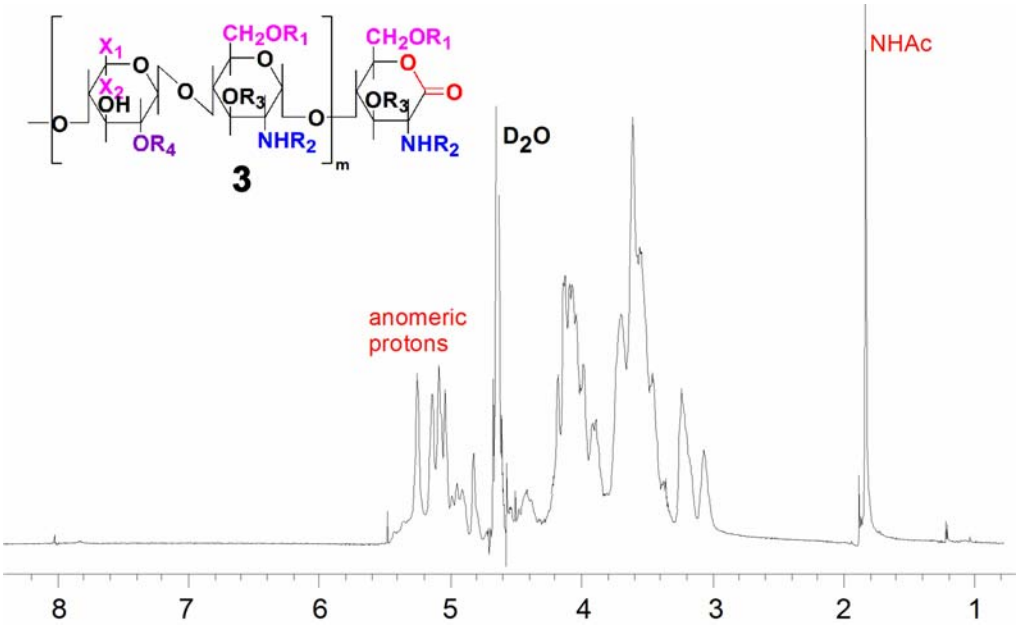

Figure 18 ^{1}H NMR spectrum of heparin-lactone (600 MHz/D_2O). Adopted with permission from (136).

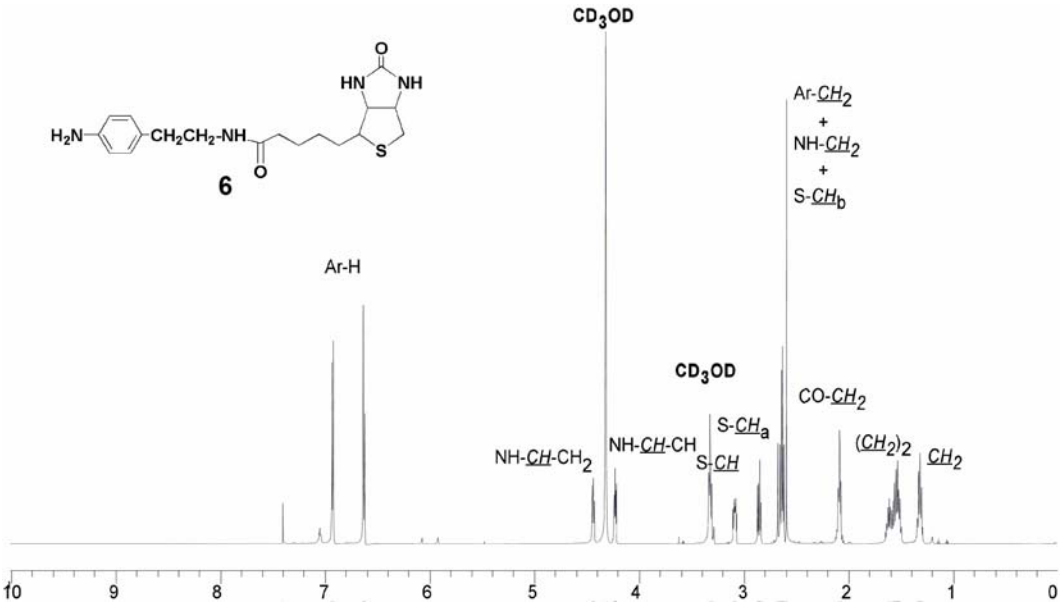

Figure 19 ^{1}H NMR of amine terminated biotin spacer arm in $CD_3OD/CDCl_3$ mixture (600 MHz). Adopted with permission from (136).

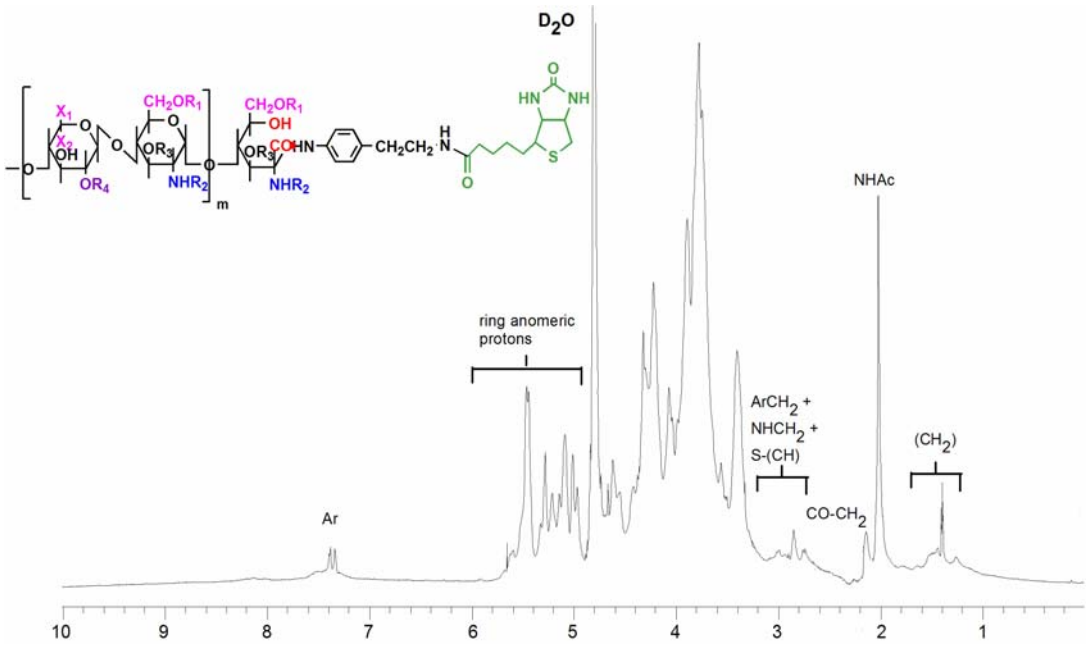

Figure 20 1H NMR spectra of biotin-functionalized heparin D_2O (600 MHz). Adopted with permission from(136).

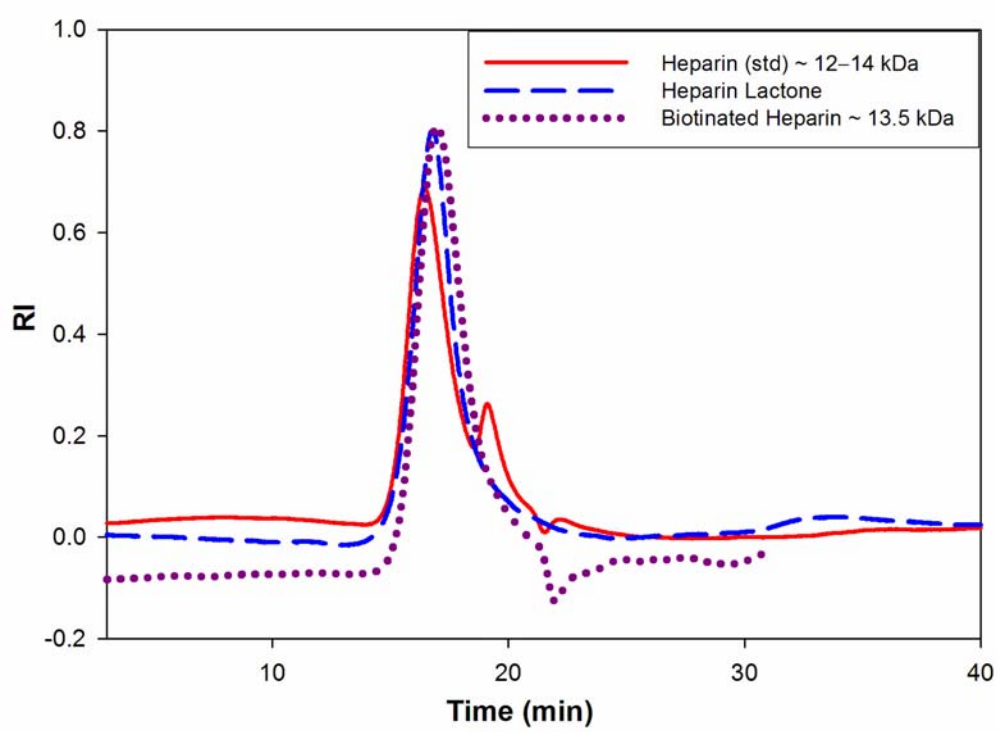

Figure 21 Size Exclusion Chromatography (SEC)/ Laser Light Scattering (LLS) profiles of chemically modified heparin. Adopted with permission from (136).

Table 3 Polydispersity and molecular weight of heparin and biotin-heparin from SEC and LLS. Adopted with permission from (136).

	Polydispersity Index (*PDI*)	Molar Mass Moments (g/mol) *Mw* (kDa)	Mz *(kDa)*
Heparin	1.084	14.3	15.1
Biotin-Heparin	1.115	13.8	15.3

The biotinylated heparin was purified by running through an avidin column (4.3.3) to assure optimal binding capacity. The process of purification was monitored by measuring absorbance of eluted substances at wavelength of 500 nm (see Appendix D). After purification, the extent of biotinylation of the compound was determined by HABA assay following the manufacture protocols (Sigma). The results (n = 5) are shown in the following:

(a) A_{500} of HABA reagent = 1.074 ± 0.008

(b) A_{500} of biotinylated heparin + buffer = 0.067 ± 0.005

(c) A_{500} of HABA + biotinylated heparin = 0.892 ± 0.012

(d) ΔA_{500} (biotinylated heparin) = 0.9(a) + (b) +(c) = 0.229 ± 0.016

(e) μmole biotin/mL (biotinylated heparin) = (ΔA_{500}/34 X 10) = 0.067 ± 0.005

(f) 1mg/mL heparin solution = 0.072 (μmole/mL) (Mw = 13,800).

Biotin levels from biotinylated-heparin, defined as mole biotin/mole heparin = (e)/(f) = 0.92 ± 0.03, showing extent of biotinylation was 92%.

4.4.2 Analysis of Biotin-Heparin Activity

Activity of biotinylated heparin was analyzed based on its catalytic capacity to facilitate thrombin inactivation by ATIII. The results showed that thrombin decay was dependent on the heparin or biotinylated heparin concentration ranging from 10 nM to 1 μM. A linear relationship between the reciprocal of the residual thrombin concentration and the incubation time (Figure 22) was found and the kinetic analysis demonstrated that thrombin decay fits the second order reaction (130). The slope of the curve represents the

second order rate constant (k_{app}). By comparing the second order rate constants between heparin and biotin-heparin (Table 4), heparin activity was considered well preserved after biotinylation.

It was postulated that the reaction mechanisms include direct inactivation of thrombin by ATIII, formation of heparin-ATIII complex, and inactivation of thrombin by the complex. When heparin concentration varied from 1 nM to 1 μM, we assume that any heparin-thrombin complex formation would be negligible (144):

$$\text{ATIII} + \text{T} \xrightarrow{k_0} \text{ATIII-T} \qquad k_0\text{: } 2^{nd} \text{ – order rate constant without heparin}$$

$$\text{b-H-ATIII} + \text{T} \xrightarrow{k} \text{ATIII-T} + \text{b-H} \qquad k\text{: } 2^{nd}\text{- order rate constant with heparin}$$

$$\text{b-H} + \text{ATIII} \xleftrightarrow{K_{HI}} \text{b-H-ATIII} \qquad K_{HI}\text{: the dissociation constant of the b-H-ATIII complex}$$

The apparent rate constant k_{app} is a function of k_0, k, K_{HI}, and $C_{b\text{-}H}$ (130):

$$k_{app} = (k_0 K_{HI} + k C_{b\text{-}H})/(K_{HI} + C_{b\text{-}H}) \qquad C_{b\text{-}H}\text{ : concentration of biotin-heparin}$$

After rearrangement, k_{app} can expressed as:

$$k_{app} = -K_{HI} (k_{app} - k_0)/C_{b\text{-}H} + k$$

K_{HI} and k can be determined by experimental k_{app} values obtained at the corresponding $C_{b\text{-}H}$ values, i.e. plotting k_{app} vs. $(k_{app} - k_0)/C_{b\text{-}H}$. The two parameters, k_{app} and $(k_{app} - k_0)/C_{b\text{-}H}$, were found to be linearly correlated, which determined the values of K_{HI} and k as $(2.30 \pm 0.55) \times 10^{-7}$ M and $(2.42 \pm 0.17) \times 10^{9}$ $M^{-1}min^{-1}$, respectively. In the absence of heparin, k_0 (= k_{app}) is 2.2×10^{6} $M^{-1}min^{-1}$ which is three orders of magnitude less than k. The good correlation observed between the kinetic model and experimental data suggests that the heparin-accelerated thrombin-inhibitor reaction be a two-step mechanism when heparin concentration ranges from 10 nM to 1 μM, including the rapid formation of a heparin-inhibitor complex and the complex reacts with free thrombin. The reaction occurs more rapidly than that of the free inhibitor with the free protease in the absence of heparin. Comparing K_{HI} and k with other studies (Table 5), we found there is no significant difference between the values computed from current experimental results and those from previous research, despite using different types of heparin (low molecular weight vs. unfractionated) and different methodologies to determine kinetic parameters.

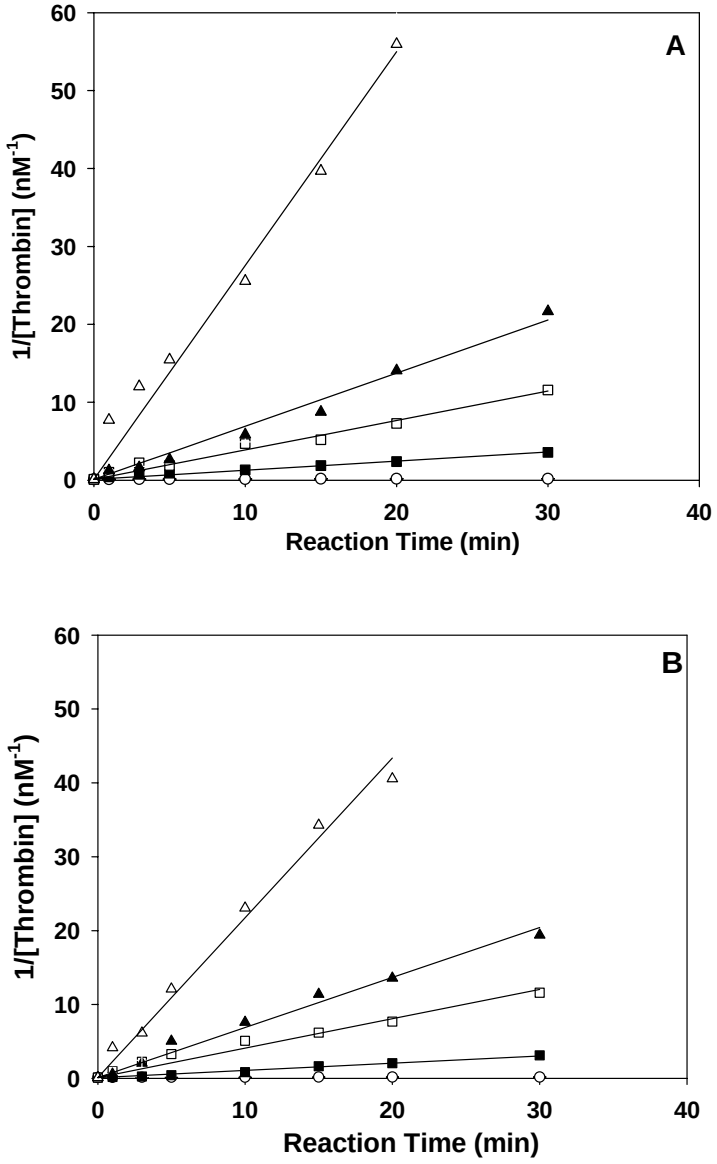

Figure 22 Thrombin inactivation by antithrombin in the presence of various (A) heparin or (B) biotin-heparin concentrations. Results for heparin concentrations ranging from 10 nM to 1 μM are presented: 0 (○),10 nM (■), 40 nM (□), 0.1 μM (▲), 1 μM (Δ). Each data point represents a mean value at each reaction time point (n = 4).

Table 4 Comparison of experimental values of the second order rate constant between heparin and biotin-heparin.

concentration		Heparin	Biotin-heparin
µg/mL	µM	k_{app} ($M^{-1}min^{-1}$)	k_{app} ($M^{-1}min^{-1}$)
14	1	(2.69±0.30) x 10^9	(2.01±0.38) x 10^9
1.4	0.1	(7.11± 0.99) x 10^8	(6.50±0.14) x 10^8
0.56	0.04	(3.58±0.81) x 10^8	(3.13±0.32) x 10^8
0.14	0.01	(1.08±0.30) x 10^8	(1.03±0.24) x 10^8
0.014	0.001	(2.87±0.12) x 10^7	(6.87±1.88) x 10^6
0	0	(2.20±0.46) x 10^6	(2.20±0.46) x 10^6

Table 5 Comparison of dissociation constants of heparin-antithrombin (K_{HI}) and the second order rate constants with heparin (k) between current and previous studies.

	K_{HI} (M)	k (M^{-1} min^{-1})
Maaroufi et al. (130) (UFH[1])[a]	3.7 x 10^{-7}	1.3 x 10^9
Jordan et at. (144) (LMWH[2])[b]	1.0 x 10^{-7}	1.9 x 10^9
Olson (145) (LMWH[3])[b]	2.3 x 10^{-7}	N/A
Griffith (128, 141)(UFH[1])[b]	1.0 x 10^{-7}	N/A
Our results	2.3 x 10^{-7}	2.4 x 10^9

1. UFH (unfractionated heparin,): Mw ~ 15 kDa
2. LMWH (low molecular weight heparin): Mw ~ 6.5 kDa
3. LMWH: ~ 8 kDa

a. K_{HI} was computed from experimental data

b. K_{HI} was determined directly from the change in the intrinsic fluorescence of AT observed during the formation of the heparin-ATIII complex.

4.4.3 Determination of Heparin Surface Density

Mixed ^{3}H-heparin and unlabeled heparin was biotinylated and its specific activity of the heparin solution averaged 324.6 CPM/μg. The extent of biotin levels was determined using HABA assay and the result showed that the biotin level is 0.975 ± 0.025 mole biotin/mole heparin (n = 5), approximately 1:1 molar ratio of biotin to mixed heparin.

According to specific activity, surface mass of heparin was determined based on radioactivity from surface ^{3}H-heparin and was found to be a function of surface biotin content (mol% of biotin-AcPE). The corresponding heparin surface concentration to biotin content within membrane-mimetic thin film is summarized in Table 6. Surface heparin content became saturated when biotin content within membrane-mimetic surface is larger than 50% (Figure 23). Heparin surface concentration as a function of biotin content within membrane-mimetic construct was expressed in a double reciprocal plot (Lineweaver-Burke plot), i.e. 1/[heparin surface concentration] vs. 1/[biotin mole%] (Figure 24) and a linear relationship was found. From intercept of the fitted equation, the saturated heparin surface concentration is approximately 6.6 pmole/cm^2, or equivalent to 92.4ng/cm^2 (Mw = 13.8 kDa).

Previous studies about binding kinetics between streptavidin (SA) and biotin-containing alkylated monolayers (146-148) which constructs were similar to current model systems showed that the amount of SA adsorption increases with surface mole fraction of biotin at low surface biotin concentrations, which provides more binding sites for anchoring biotin or biotinylated molecules. The amount of SA adsorption maximizes at ~230 ng/cm^2 (~ 4 pmole/cm^2) in the presence of 50 mole% of surface biotin (146). The gradual saturation of surface heparin possibly results from saturating surface SA. This

phenomenon may be explained by two reasons: the conformational and orientational disorder of the lipid hydrocarbon chains and the formation of biotin microdomains increase with increasing mole fraction of biotinylated lipids (80), and crowding biotin molecules on the surface may become less accessible to protrude deep enough into the binding site of SA (146). Indeed, it was observed that saturation coverage of SA decreases at high surface biotin concentrations (146, 149).

Given the fact that streptavidin binding to biotin-containing monolayer normally exposes two of its binding sites away from the surface (149-151), the maximum surface content of biotinylated heparin onto streptavidin-biotinylated membrane-mimetic surface could double the amount of SA surface concentration. The accessibility for biotin-heparin to streptavidin binding sites and desorption of surface streptavidin by biotin-heparin could lower the maximum surface content of heparin, indicating the current experimental data fall within a reasonable range.

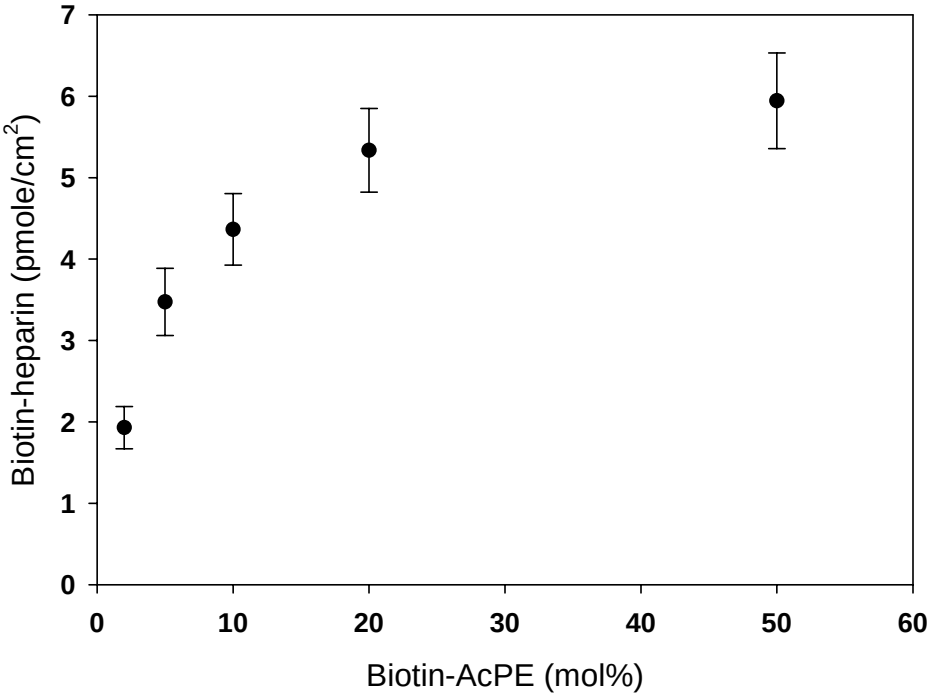

Figure 23 Surface density of biotin-heparin as a function of mole% of biotin-AcPE within membrane-mimetic construct. Each data point represents mean ± standard deviation (n = 6).

Table 6 Characterization of heparin surface concentration (mean ± standard deviation, n = 6) resulted from biotin-AcPE mole% within membrane-mimetic thin film.

Biotin-AcPE mole%	b-heparin (pmole/cm^2)
2	1.93 ± 0.26
5	3.47 ± 0.41
10	4.36 ± 0.44
20	5.34 ± 0.51
50	5.94 ± 0.59

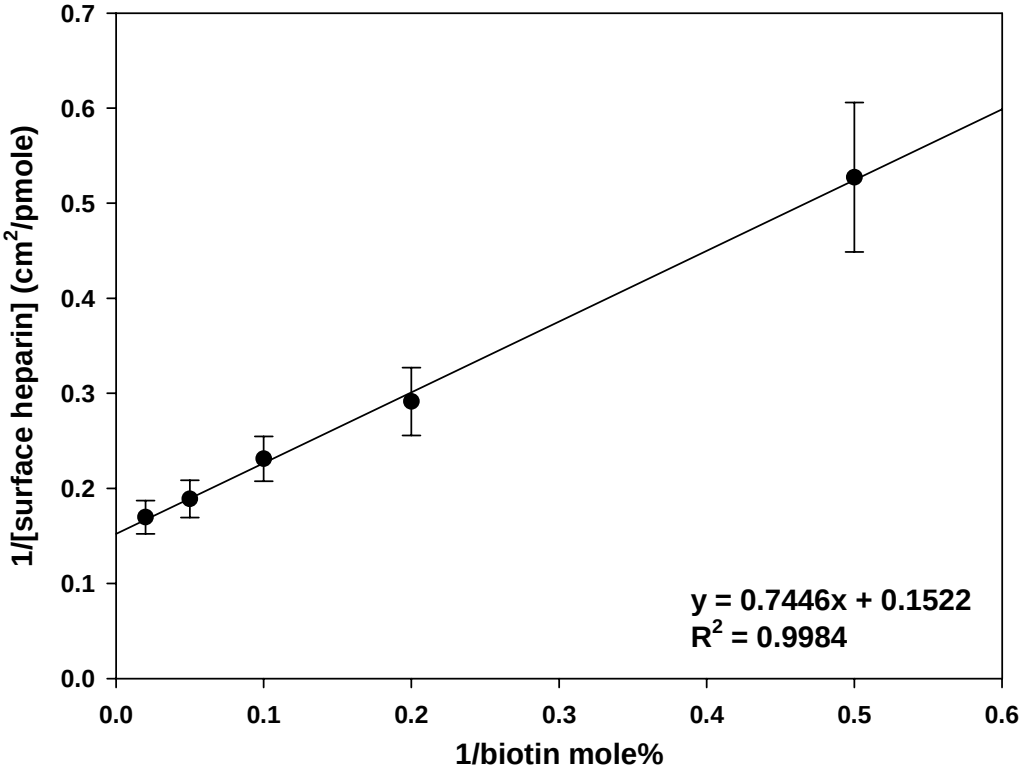

Figure 24 Lineweaver-Burke plot of data points from Figure 21. The linear relationship indicates the binding mechanism might follow Langmuir binding isotherm.

4.4.4 Flow Effect on Catalytic Efficiency of Heparinized Surface

After characterizing the surface concentration of heparin by altering biotin-AcPE content within membrane-mimetic construct, we further investigated how heparin density would affect thrombin inactivation by antithrombin under flow conditions.

Thrombin decay curves in the presence of different surface densities of biotinylated heparin are shown (Figure 25). In the absence of surface heparin, thrombin responses at both shear rates of 50 sec^{-1} and 500 sec^{-1} stabilized after 20 min of perfusion showed 1.9-2.5 nM of thrombin was inactivated, which were 6-8% of initial thrombin concentration (30 nM). In the presence of surface heparin, 35 to 50 % and 15 to 21 % of thrombin was inactivated at shear rates of 50 sec^{-1} and 500 sec^{-1}, respectively, demonstrating surface heparin was catalytically active. In addition, time to reach the steady state level of thrombin decay (Figure 26 & 27) was shorter for higher shear rate, which were approximately 20 and 15 min after starting the flow at shear rates 50 sec^{-1} and 500 sec^{-1} respectively). Moreover, the results revealed that no discernible effect on rate of thrombin decay when surface heparin was equal to or greater than 4.4 $pmole/cm^2$, corresponding to immobilization of biotinylated heparin onto 10 mole% of biotin-AcPE within membrane-mimetic thin film, indicating possible mass transfer limitation for thrombin and antithrombin to reach surface heparin for reaction (102, 103, 108, 112) (Figure 28).

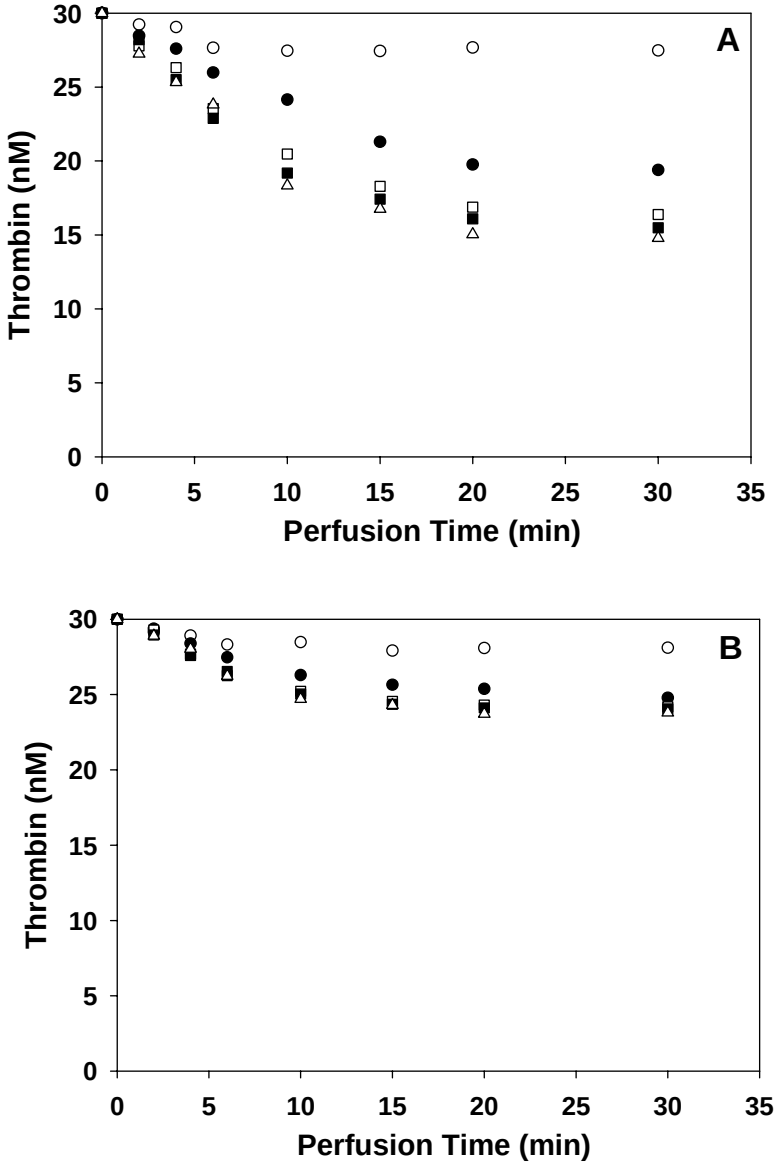

Figure 25 Thrombin inactivation at timed points during the perfusion of thrombin and antithrombin over heparinized surface with surface concentrations of 0 (○). 3.47 (●), 4.36 (□), 5.34 (■), and 5.94 pmole/cm^2 (Δ) at shear rates of (A) 50 sec^{-1} (B) 500 sec^{-1}. Each data point represents a mean value (n = 4).

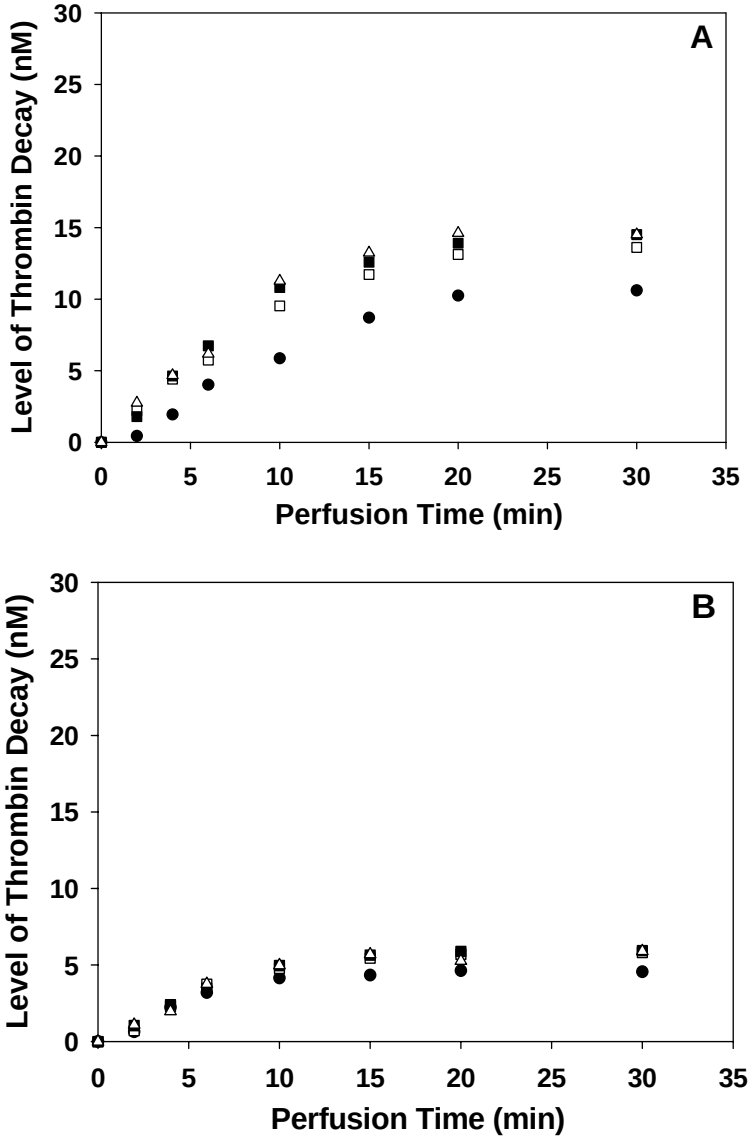

Figure 26 Kinetic data of levels of thrombin decay over perfusion time as a function of heparin surface concentrations (3.47 (●), 4.36 (□), 5.34 (■), and 5.94 pmole/cm^2 (Δ)) at shear rates of (A) 50 sec^{-1}and (B) 500 sec^{-1}. Each data point represents a mean value (n = 4). Note: the level of thrombin decay as the difference between the initial thrombin concentration, i.e. 30 nM, and a thrombin response at a timed point from Figure 23.

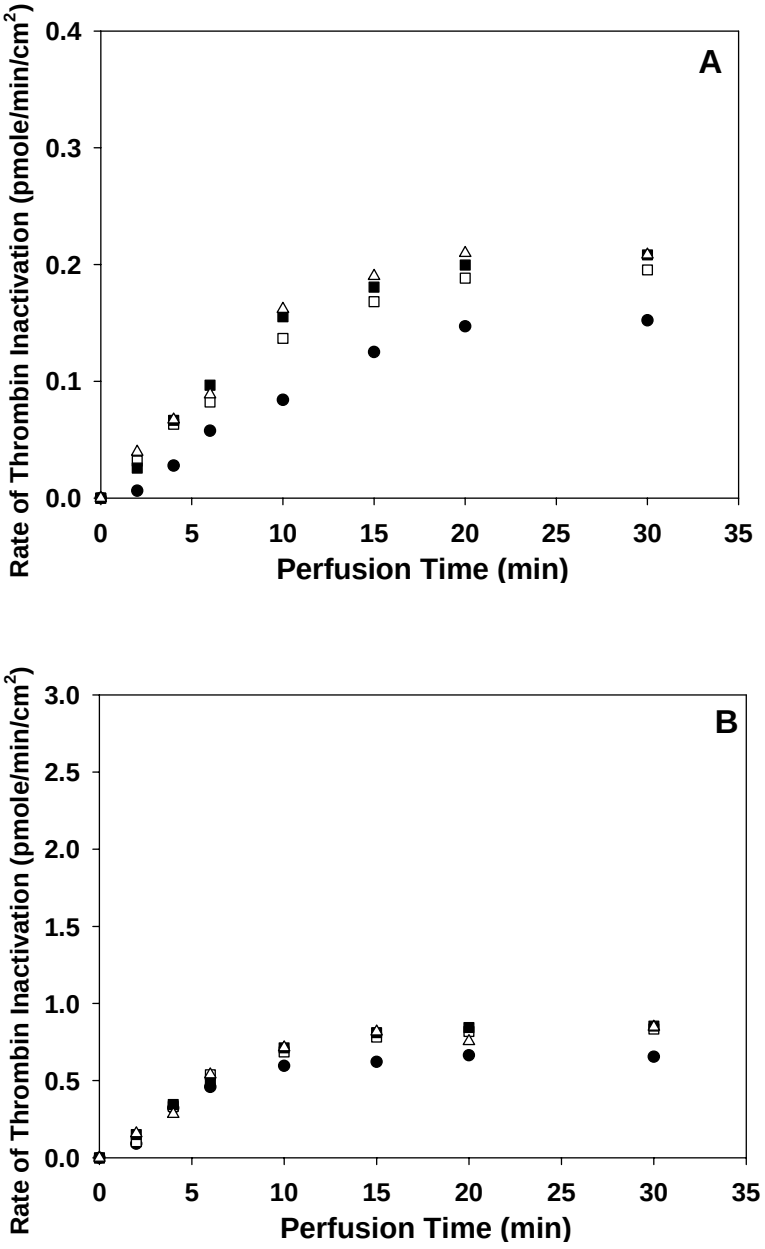

Figure 27 Rate of thrombin inactivation (= level of thrombin decay x flow rate / flow-exposed heparinized surface area) as a function of heparin surface concentrations (3.47 (●), 4.36 (□), 5.34 (■), and 5.94 pmole/cm^2 (Δ)) at shear rates of (A) 50 sec^{-1}and (B) 500 sec^{-1}. Each data point represents a mean value (n = 4).

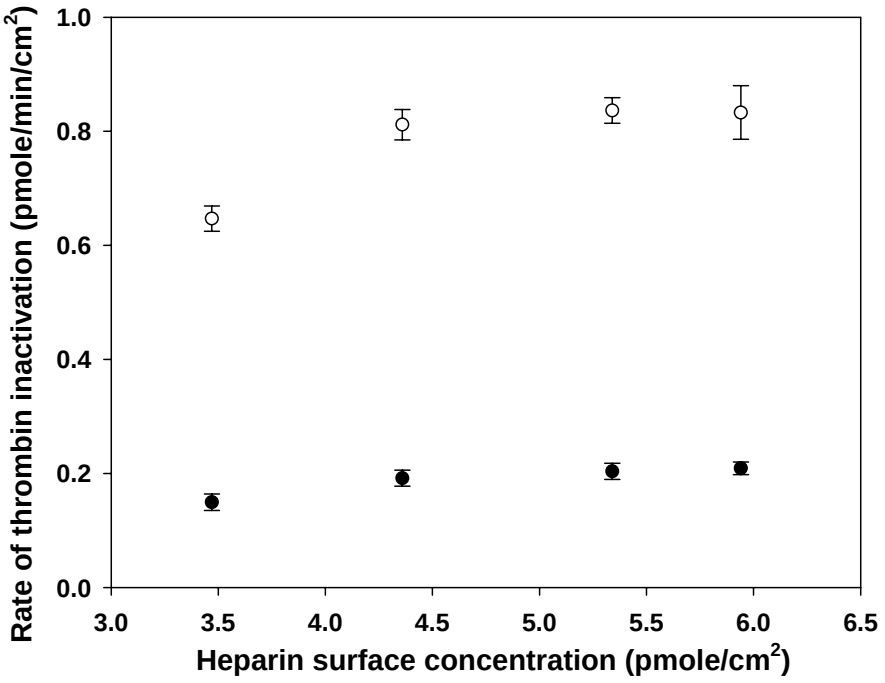

Figure 28 Steady state rate of thrombin inactivation as a function of heparin surface concentration. Saturated rates of thrombin inactivation were 0.20 ± 0.01 and 0.82 ± 0.03 pmole/min/cm^2 (mean ± standard deviation) in the presence of surface heparin equal to or greater than 4.36 pmole/cm^2 at shear rates of 50 (○) and 500 (●) sec^{-1}. Data points represent the mean values ± standard deviation (n = 4).

4.5 CONCLUSIONS

Heparin was chemically modified by conjugation of biotin spacer group at the terminal position without significantly compromising its catalytic capacity of thrombin inactivation by ATIII. Biotinylated heparin was further utilized for the fabricating the heparinized surface by immobilizing the compound onto streptavidin functionalized membrane-mimetic thin films. Surface concentration of heparin was characterized using ^{3}H-labeled heparin and found to be directly related to the surface density of biotin-conjugated AcPE. Significantly, surface concentration of heparin increases with increasing surface content of biotinylated lipids and tends to reach saturation in the presence of biotinylated lipids more than 50 mole% of the total surface lipids.

In the absence of surface heparin, limited thrombin inactivation by antithrombin at a concentration of 30 nM was observed. However, it is anticipated that thrombin activity will be tremendously diminished in a short period of time in the presence of physiologic concentration of antithrombin, ranging from 1.5 to 2.5 μM (152-154), hence the contribution of the heparinized surface to the inactivation of thrombin might be negligible. Nevertheless, the current system shows that surface heparin is catalytically active under flow conditions, yet its catalytic efficiency is limited by transport rates of reactants and products toward and removal from the surface. Inasmuch as membrane-mimetic assemblies can be easily controlled and modified as previously described (78-80, 94-96), we may create a potentially robust antithrombogenic environment by immobilizing heparin along with other anticoagulants such as thrombomodulin for future work.

CHAPTER 5

FABRICATION AND CHARACTERIZATION OF TISSUE FACTOR-COATED SURFACE BASED ON MEMBRANE-MIMETIC ASSEMBLIES

5.1 ABSTRACT

Tissue factor (TF), an integral membrane protein located on subendothelial cells, is the physiologic trigger of the blood coagulation during normal hemostasis when it is exposed to the blood following vascular injury. A TF-coated surface based on membrane-mimetic assemblies, which have been developed from our laboratory, was fabricated as a model that functions to activate coagulation proteins. A continuous flow parallel plate enzyme reactor was used to investigate the effects of shear rate, surface density of tissue factor, and mass transport on the activation of factor X and thrombin generation initiated by the complex of TF-factor VIIa. For factor X activation, production of factor Xa at the outlet of the reactor was monitored with time during perfusion of the flow chamber with 160 nM factor X in the presence of 10 nM VIIa at physiologic shear rates of 50 and 500 sec^{-1} in vein and artery, respectively. The results showed that time to reach steady-state factor Xa generation was shorter and the reaction rates are higher at higher shear rate. In addition, rate of factor X activation becomes saturated in the presence of more than 50 fmole of TF per cm^2, indicating the activation of factor X is controlled by the transport of reactants toward as well as removal of the products from the catalytic surface . For thrombin generation, the reaction is initiated by perfusing the TF-coated surface with coagulation factors V, VII, VIIa, VIII, IX, X, and prothrombin prepared at mean plasma concentrations. Kinetic behavior of thrombin production showed that the steady-state

levels were reached more rapidly at the higher shear rate and increased with increasing TF surface concentration. In contrast to thrombin generation in a static well mixed model studied by many researchers, the experimental results confirm that as anticipated local hemodynamic conditions play a key role in tissue factor induced Xa and thrombin generation. The reaction rates of thrombin generation became saturated at higher TF surface density in a manner similar to Xa generation, consistent with previous studies that indicate Xa generation is a critical step for thrombin generation.

5.2 INTRODUCTION

The blood coagulation process *in vivo* is initiated when subendothelial tissue factor is exposed to the blood flow following either the damage or activation of the endothelium (155). Tissue factor, a critical mediator in hemostasis and thrombosis, is an integral membrane glycoprotein that is normally presented on the surface of certain cell types located outside the vasculature. Since the appropriate spatial and temporal expression of TF is essential for thrombosis and hemostasis, TF expression *in vivo* is highly cell type-specific (156). Instead of constitutive expression by endothelium or by cellular components of blood, TF is expressed strongly in the tunica adventitia, which ensures prompt initiation of coagulation in the event of vascular injury. In addition, induction of TF synthesis *in vivo* can occur during activation of endothelial cells and monocytes/macrophages by cytokines such as interleukin-1 and tumor necrosis factor, endotoxin, and anoxia (157-160) and is implicated in the onset of thrombosis in conditions as diverse as atherosclerosis (161), disseminated intravascular coagulation (DIC), malignancy (162) and hyperacute rejection of xenografts (163).

Tissue factor functions in coagulation by serving as a protein cofactor for a plasma serine protease, factor VIIa. Although the vast majority of factor VII in plasma circulates as a zymogen, all normal individuals have been found to have low levels of factor VIIa in their plasma (~1% or less of the total VII) (164). At the site of a vascular injury, factor VII and VIIa bind TF and form a TF-factor VIIa complex (TF:VIIa), which triggers the blood clotting cascade in two ways. One is to directly activate factor X to Xa. The other is to activate factor IX to IXa which can, in turn, activate factor X in the presence of its protein cofactor, factor VIIIa, on a phospholipids surface. Interestingly, factor X appears

to be the preferred substrate for TF:VIIa under *in vitro* conditions, although which mechanism predominates *in vivo* may depend on local factors, which are not entirely understood (16). Newly formed Xa assembles on phospholipid surfaces with its protein cofactor, factor Va, to catalyze the conversion of prothrombin to thrombin, which is responsible for fibrin clot formation and serves as a potent platelet activator.

Additional details regarding the initiation and propagation phases of the coagulation phases are worth noting. During the "initiation phase" (26) of the blood coagulation process, limited activation of the coagulation zymogens such as IX and X occurs in the absence of their cofactors. Nonetheless, trace amounts of initial thrombin can be produced (~ picomolar concentration). Significantly, the newly formed thrombin accelerates further thrombin generation by feedback activation of cofactors V and VIII, which leads to explosive generation of thrombin during the "propagation phase" (26) of the process. In addition , factor VII can be further activated by factors IXa, Xa, XIIa, thrombin and plasma (165-171) to enhance the amplification of coagulation protease generation.

TF-initiated blood coagulation has been well investigated using several *in vitro* models under nonflow conditions (20-27, 172), which has revealed much about the biochemistry of coagulation. However, several reports have documented that shear flow is a critical regulator of surface TF reactivity (109, 112, 173-175). Specifically, it has been demonstrated that K_m decreased and V_{max} increased with increasing shear rate in TF:VIIa-catalyzed activation of factor X (112, 175), indicating enzymatic efficiency is enhanced by flow. In addition, the rate of the surface reaction is limited at an upper level

of TF surface density, suggesting that a transport-limited effect plays a dominant role in determining the maximum levels of local thrombin production.

As a transmembrane protein, TF can maintain its activity only when incorporated into phospholipid vesicles or supported membranes (176). Significantly, TF activity in terms of catalyzing activation of factor X is maximal when relipidated TF contains 20 mole% of phosphatidylserine, a negatively charged phospholipid (164). Previous studies have shown that a TF containing phospholipid bilayer can be immobilized on a glass surface and thereby utilized as a continuous flow enzyme reactor for simulating TF-initiated blood coagulation (50, 109, 112, 174). Inasmuch as we consider TF to be the major trigger of coagulation and neighboring lipid membranes as an essential cofactor for such surface reactions, a TF-coated surface based on the membrane-mimetic assembly described in the previous chapters was developed. The main purpose of creating such a system was to determine the antithrombogenic capacity of anticoagulants incorporated into membrane-mimetic thin film, such as surface heparin and thrombomodulin. In this chapter, TF-coated surfaces are described and surface TF activity in the absence of anticoagulants is characterized.

TF-reconstituted lipid vesicles, composed of phosphatidylcholine, phosphatidylserine, and phosphatidylethanolamine, were anchored via biotin-streptavidin binding interactions on membrane-mimetic constructs containing a mixture of polymerizable phospholipids, monoacrylate-phosphatidylcholine and biotin-conjugated monoacrylate-phosphatidylethanolamine (Figure 29). Instead of varying surface biotin content within membrane-mimetic thin film, we characterized TF surface concentration by changing molar ratios of TF to lipid (TF:PL)vesicles at fixed surface biotin content of 10 mol%. TF

surface concentration was found to increase with increasing TF:PL at fixed lipid vesicle concentration. TF-coated surfaces were fabricated as a continuous flow enzyme reactor in a parallel plate flow chamber and the catalytic efficiency of TF-mediated factor X activation and thrombin generation was defined under wall shear rates of 50 and 500 sec^{-1}. Our studies revealed that the capacity of TF to induce factor Xa and thrombin was dependent upon shear rate and TF surface concentration. Saturated levels of factor Xa and thrombin were reached at surface TF concentrations equal to or greater than 50 fmole of TF per cm^2. As compared to previous studies under nonflow conditions, flow studies confirm that thrombin is not only dependent on inherent reactions among zymogens and their enzyme complexes, but also influenced by the transport of macromolecules from the fluid phase to the catalytically active surface.

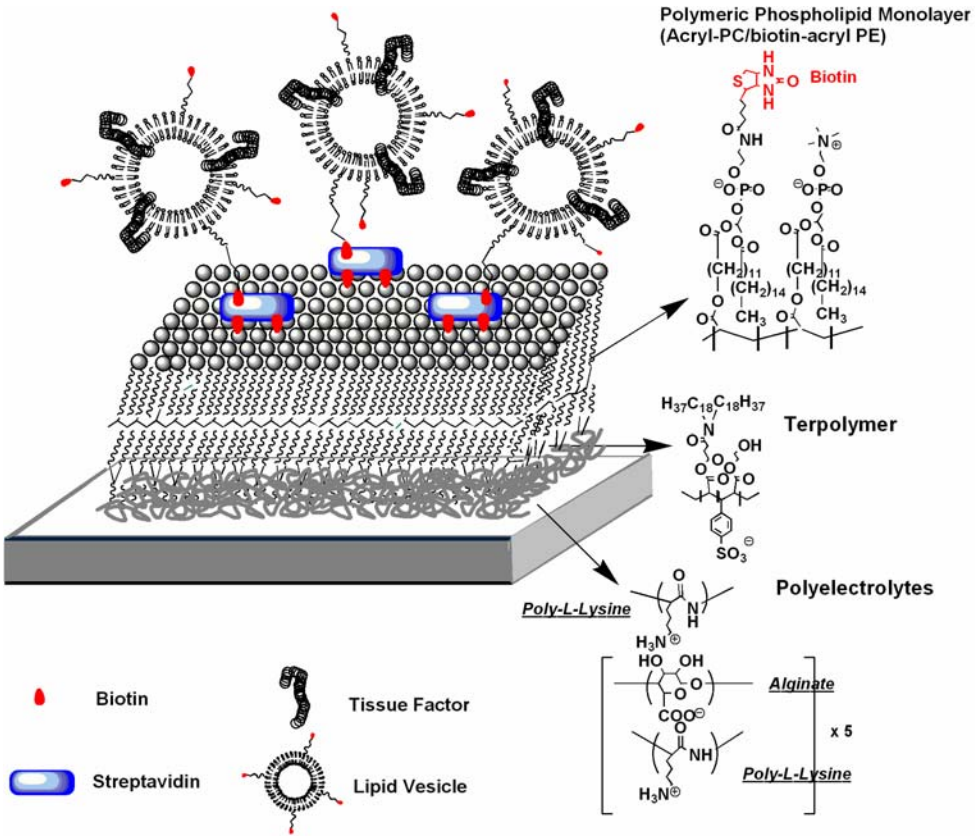

Figure 29 Schematic representation of immobilized relipidated tissue factor on the basis of polymeric phospholipid monolayer supported on an alkylated polyelectrolyte multilayer. (Not to scale)

5.3 MATERIALS AND METHODS

5.3.1 Materials

Human coagulation factors V, VII, VIIa, IX, X, prothrombin, human antithrombin III, and human protein C were obtained from Haematologic Technologies, Inc. Human coagulation factor VIII, tissue factor (full length recombinant human tissue factor, TF, 43 kD, lyophilized from 0.01 M Tris, 0.15 M NaCl, pH 8.0 containing 0.01% CHAPS and 200 mM mannitol), and Spectrozyme TH substrate for thrombin (H-D-hexahydrotyrosyl-L-alanyl-L-arginine-p-nitroanilide-diacetate salt) were obtained from American Diagnostica Inc. S-2222 substrate for factor Xa (Bz-IIe-Glu(γ-OR)-Gly-Arg-pNA•HCl) was purchased from Chromogenix. Eosin Y (EY, 5% in water), triethylamine (TEA), 1-vinyl-2-pyrrolidinone (VP) were obtained from Aldrich. Nucleopore polycarbonate filters and Contrad 70 detergent were obtained from Fisher. Detergent OG (*n*-octyl-β-D-glucopyranoside) was obtained from Sigma. Chicken egg PC (L-α-Phosphatidylcholine), porcine brain PS (L-α-Phosphatidylserine, sodium salt), N-Biotinyl Cap-PE (18:1) (1,2-Dioleoyl-*sn*-Glycero-3-Phosphoethanolamine-N-Cap Biotinyl), and fluorescent PE (1,2-Dioleoyl-sn-Glycero-3-Phosphoethanolamine-N-Carboxyfluorescein) were purchased from Avanti Polar Lpids, Inc. Alginate (ALG; low viscosity, ca. 60% mannuronic acid) was obtained from Pronova Biomedical (Norway). Poly (L-lysine) (PLL, MW > 300 kD) and all buffer salts are obtained from Sigma. Synthesis of monoacrylate-PC (AcPC, 1-palmitoyl-2-[12-(acryloyloxy)dodeca-noyl]-*sn*-glycero-3-phosphocholine), monoacrylate-PE (AcPE, 1-palmitoyl-2-(12-(acryloyloxy)dodecanoyl)-*sn*-glycero-3-phosphoethanolamine) and its biotin derivative (biotin-AcPE) have described previously (77, 94) . The synthesis of the terpolymer that

consists (3-acryloyl-3-oxapropyl-3-(N,N-dioctadecyl-carbamoyl)-propionate))$_6$:(2-hydroxyethyl acrylate)$_3$:sodium styrene sulfonate$_1$ (AOD_6:HEA_3:SS_1) has been described elsewhere (96).

5.3.2 Reconstitution of Tissue factor into Phospholipid vesicles

TF was reconstituted within lipid vesicles as described in the literature with some modification (18, 177).Phospholipids (dissolved in chloroform) consisting of 79 mole% egg PC, 20 mole% brain PS, and 1 mole% biotin-cap-PE were dispensed in a glass test tube. The resulting solution was dried by N_2, followed by high vacuum SpeedVac for 2 hours. Fresh OG/HBS, buffer solution, containing 100mM *n*-octyl-β-D-glucopyranoside and HBS (20 mM Hepes, 100 mM NaCl, and 0.02% (w/v) sodium azide, pH 7.5), was prepared and added with vortexing to completely dissolve the dried lipid mixture. Sonication was occasionally necessary to dislodge any residual pellet at the bottom of the test tube. Once dissolved, the lipid mixture was kept at room temperature for subsequent relipidation of TF. TF was dissolved in the lipid mixture and HBSA, 0.1% (w/v) bovine serum albumin in HBS, added to produce a desired TF:lipid molar ratio, ranging from 1:8000 to 1:160000, at a fixed lipid concentration of 5 mM. The whole mixture was mixed well and incubated for 30 min at room temperature. The sample was dialyzed (Mw cutoff: 12,000) at room temperature against three changes of HBS (24 hr each, for a total of 72 hr). Final TF concentrations ranging from 6 to 120 nM in 1mM lipid were prepared for surface samples. The relipidated TF was extruded 21 times each, through 0.6 μm and 0.1μm polycarbonate filters (Avanti Polar Lipids, Inc.) and used for coating of test samples.

5.3.3 Fabrication of Tissue Factor Containing Membrane-Mimetic Surface

Microscope glass slides (2.6 cm x 4.6 cm, Fisher) were cleaned and coated with biotin-functionalized membrane-mimetic thin film (molar ratio of AcPC: biotin-AcPE = 90:10), followed by coating with streptavidin, as previously described (80). TF-coated surfaces were fabricated by immersing the entire glass slide in the TF-reconstituted lipid mixture on a rotating platform. The coating time was 30 min at room temperature, followed by rinsing extensively using deionized water. Fluorescent PE (fluorescein, 0.1 mole% final) was doped within lipid vesicles (starting from removing chloroform step) for fluorescent microscopy studies.

5.3.4 Continuous Flow Reactor Assays on Tissue Factor Containing Membrane-Mimetic Surface

Surface TF bioactivity was characterized in terms of factor X activation and thrombin generation under flow conditions.

Xa Generation—Surface TF-catalyzed factor X activation was investigated at shear rates of 50 sec^{-1} and 500 sec^{-1}. A parallel plate flow system (0.6 cm (width) x 0.01 cm (height) x 3.6 cm (length), 22 μL volume) containing the coated sample was flushed with 20 mM Hepes buffer for 1 hours at γ_w = 2000 sec^{-1} (flow rate of 1.24 mL/min). The reaction was started by perfusing the coated slides with a reaction mixture containing factor VIIa (10 nM, final), factor X (160 nM, final), and $CaCl_2$ (5 mM, final) in Hepes buffer/BSA (10 mM Hepes + 140 mM NaCl + 0.1 wt% BSA, pH 7.5) (109). At pre-selected timed points, aliquots were withdrawn from perfusate at the reactor outlet and quenched in Hepes buffer/EDTA (20 mM Hepes + 150 mM NaCl + 50 mM EDTA + 0.1 wt% BSA, pH 7.5). Samples were assayed for Xa after adding S-2222 (0.2 mM, final). Xa

concentration was determined by monitoring the change in absorbance at 405 nm using UV-VIS spectrophotometer and calculating via a standard curve (see Appendix A).

Thrombin Generation —Surface TF-initiated thrombin generation was investigated at shear rates of 50sec^{-1} and 500 sec^{-1}. The parallel plate flow system containing a coated test sample was flushed with 20 mM Hepes buffer for 1 hour at γ_w = 2000 sec^{-1}. The reaction was started by perfusing the surface with Hepes buffer/BSA (20 mM Hepes + 150 mM NaCl, pH 7.4) (25, 172) containing coagulation factors (V, VII, VIIa, VIII, IX, X, prothrombin) and 2 mM $CaCl_2$ at 37^{o}C (14, 26). The final concentrations of the proteins in the reaction were chosen to represent mean plasma values: 20 nM factor V, 10 nM factor VII, 0.1 nM factor VIIa, 0.7 nM factor VIII, 90 nM factor IX, 160 nM factor X, and 1.4 μM prothrombin (14, 26). At pre-selected timed points, aliquots withdrawn from the perfusate at the reactor outlet were quenched in Tris-buffer/EDTA (50 mM Tris-HCl + 150 mM NaCl + 20 mM EDTA, pH 7.4), and assayed by adding Spectrozyme TH (0.2mM final). Thrombin concentration was determined by monitoring the change in absorbance at 405 nm using UV-VIS spectrophotometer and calculating via a standard curve.

5.4 RESULTS AND DISCUSSION

5.4.1 Fluorescent Images of Lipid Vesicles Bound onto Membrane-Mimetic Films

TF containing surfaces were fabricated by tethering TF reconstituted lipid vesicles, composed of 79 mol% phosphatidylcholine (PC), 20 mol% phosphatidylserine (PS), and 1 mol% biotin- phosphatidylethanolamine (b-PE), to biotinylated membrane-mimetic thin films through biotin-streptavidin binding interactions. Doped with 0.1 mol% of fluorescein-labeled PE, immobilized lipid vesicles were visualized using fluorescent microscopy for initial characterization of the surface.

Images (Figure 30) demonstrate that fluorescent intensity increases with increasing concentrations of biotin-PE, indicating that more vesicles adsorbed to those surfaces with increasing biotin-PE on glass substrates. While lipid vesicles appear to be evenly distributed on surfaces containing less than 10 mole% of biotin-AcPE, clustering of vesicles was observed on thin films containing 50 mole% of biotin-AcPE. .

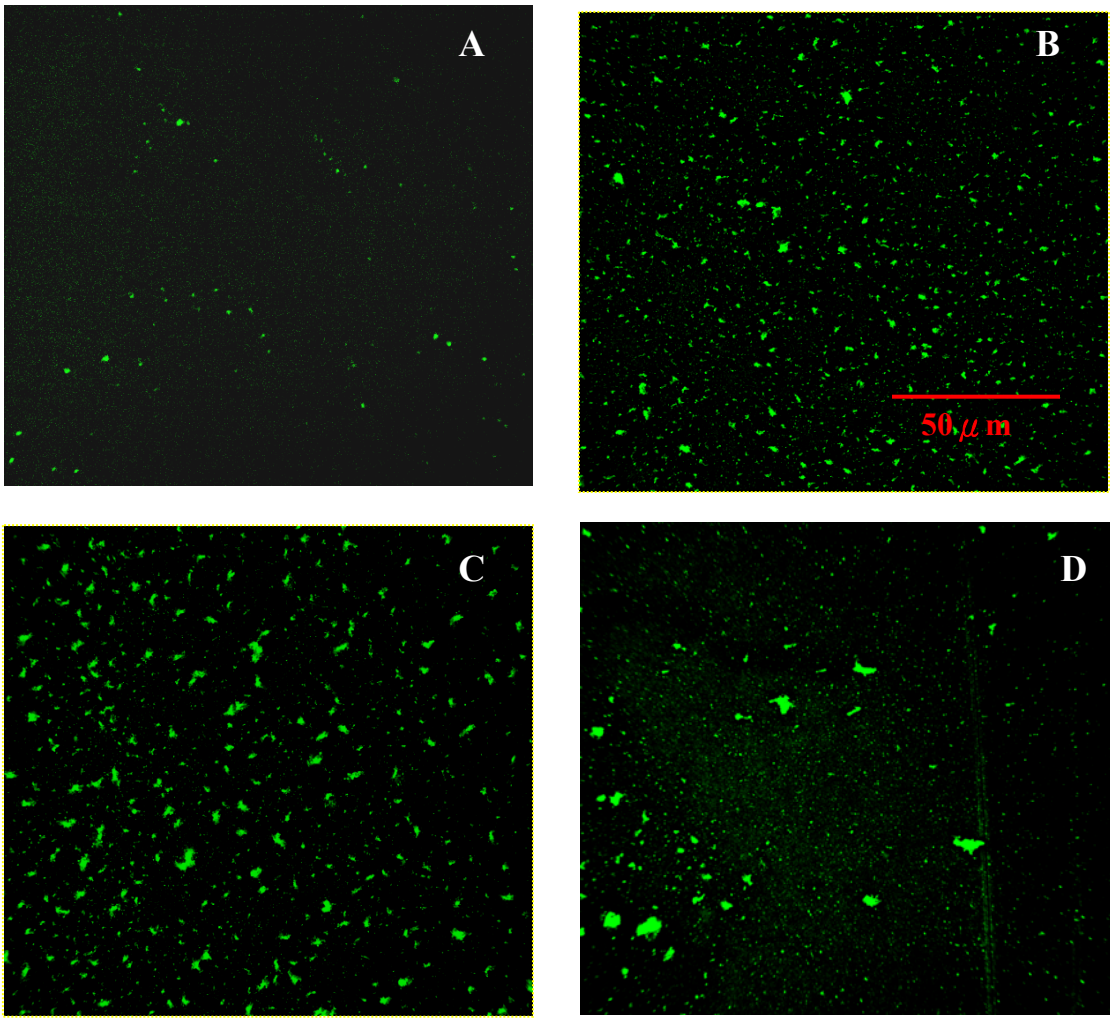

Figure 30 The fluorescent images (20x) of 1mM lipid vesicle coated surfaces. 0.1 mol% FITC-doped lipid vesicles were coated on surface containing 0 mol% biotin-AcPE/AcPC (control) (A), 5 mol% biotin-AcPE/AcPC (B), 10 mol% of biotin-AcPE/AcPC (C), and 50 mole% biotin-AcPE/AcPC (D) through biotin-streptavidin binding system

Such phenomena might be associated with microphase separation of the PC and biotinylated lipids, as well as incomplete vesicle fusion at high biotin-AcPE surface concentrations (80). In order to have well-distributed TF coated region, we proposed to utilize lipid composition of 10 mol% biotin-AcPE/90 mol% AcPC as our model platform for the following studies.

5.4.2 Surface Activity of Tissue Factor Under Flow Conditions

Since tissue factor is involved in a number of haemostatic reactions, we selectively investigate activation of factor X and generation of thrombin initiated by surface TF. Presumably, TF surface density ($[TF]_{surface}$) is a function of relipidated TF concentration ($[TF]_{lipid}$) within biotinylated lipid vesicles (egg PC/brain PS/biotin-PE = 79/20/1) given the fixed biotin content of the lipid monolayer, which contains10 mol% biotin-AcPE. To determine TF surface density, we used radiolabeled TF, detected radioactivity from the coated surface, and converted to surface mass from specific activity. The details will be described in Chapter 6 (section 6.4.2). At this point, we apply the results which show $[TF]_{surface}$ ranging from 9 to 90 fmole/cm^2 corresponding to 6 to 120 nM of TF within 1mM lipid to represent TF surface content. The effect of $[TF]_{surface}$ on these two critical coagulation factors under flow conditions is presented in the following.

Xa generation

Kinetic data (Figure 31) reveal that Xa generation reaches a maximum level with a shorter lag period at the higher shear rate and the level is higher at lower shear rate. Times to reach maximum Xa generation are approximately 12 and 7 minutes at 50 and

500 sec^{-1}, respectively. An exception was noted for the lowest $[TF]_{surface}$ of 9.4 fmole/cm^2, which takes 2 to 3 minute longer to reach the steady state. While the time to reach steady state Xa generation appears to be slow at a $[TF]_{surface}$ of 9.4 fmole/cm^2, there is no significant shear effect on the time to reach steady state when TF density is greater than $[TF]_{surface}$ of 51.2 fmole/cm^2. Steady state Xa generation as a function of TF density (Figure 32) shows steady state values increase with increasing TF density and tends to be saturated in the presence of high TF density. Significantly, steady-state Xa generation plateaus at a $[TF]_{surface}$ of 51.2 fmole/cm^2, indicating a transport-limit is reached.

Activation of factor X as a function of TF surface density is analyzed in a similar fashion to activation of protein C described in Chapter 3. The relationship between rate of reaction and TF density was fit to the equation for a hyperbola to determine kinetic parameters: rate of reaction in the presence of saturated TF, $V_{max\ E}$, and TF density required to reach half-maximal rates, $K_{1/2E}$ (Table 7). At 15.0 and 22.6 fmole of TF/cm^2, the half-maximal activation rates of factor X were 0.45 and 1.13 pmole/(min·cm^2) respectively, which are equivalent to 30.1 and 49.8 conversions per min per enzyme molecule at shear rates of 50 and 500 sec^{-1} respectively, as compared to 10.1 (500 sec^{-1}) and 25.4 (500 sec^{-1}) conversions per min per enzyme molecule at 88.6 fmol/cm^2 TM, showing the excess catalytic capacity at high TF densities. According to the theoretical analysis of average transport rate limit (eq. (7), Chapter 3), the ratio of $V_{max\ E}$ at 500:50 sec^{-1} is approximately 2.2 ($500^{1/3}$:$50^{1/3}$), while experimental results show a ratio of 2.5, indicating the reaction is mass transfer limited in presence of excessive surface TF.

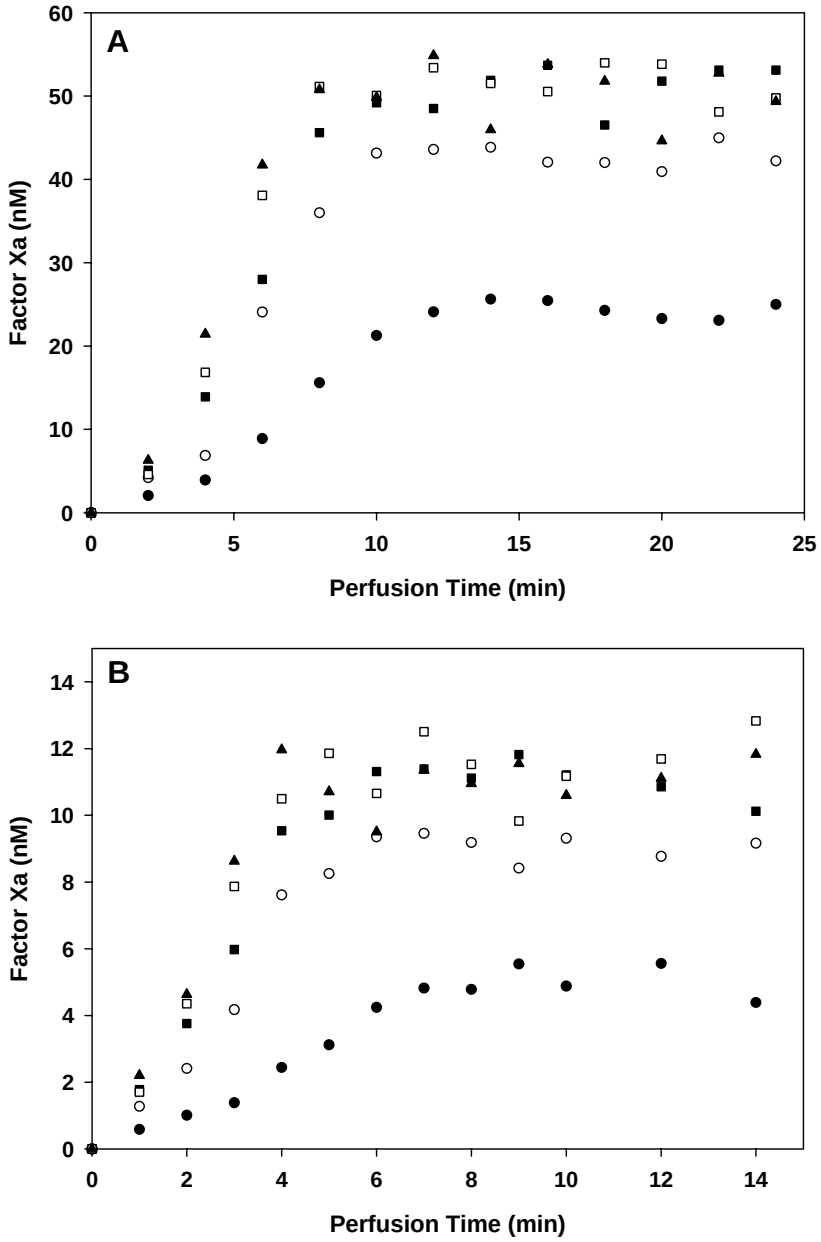

Figure 31 Factor Xa generation with various TF surface concentrations (9.4 (●) 27.3 (○) 51.2 (■) 69.9 (□) 88.6 (▲) fmole/cm2) at shear rates of (A) 50 sec^{-1} and (B) 500 sec^{-1}. Each data point represents a mean value for five experiments (see Appendix E1 for raw data).

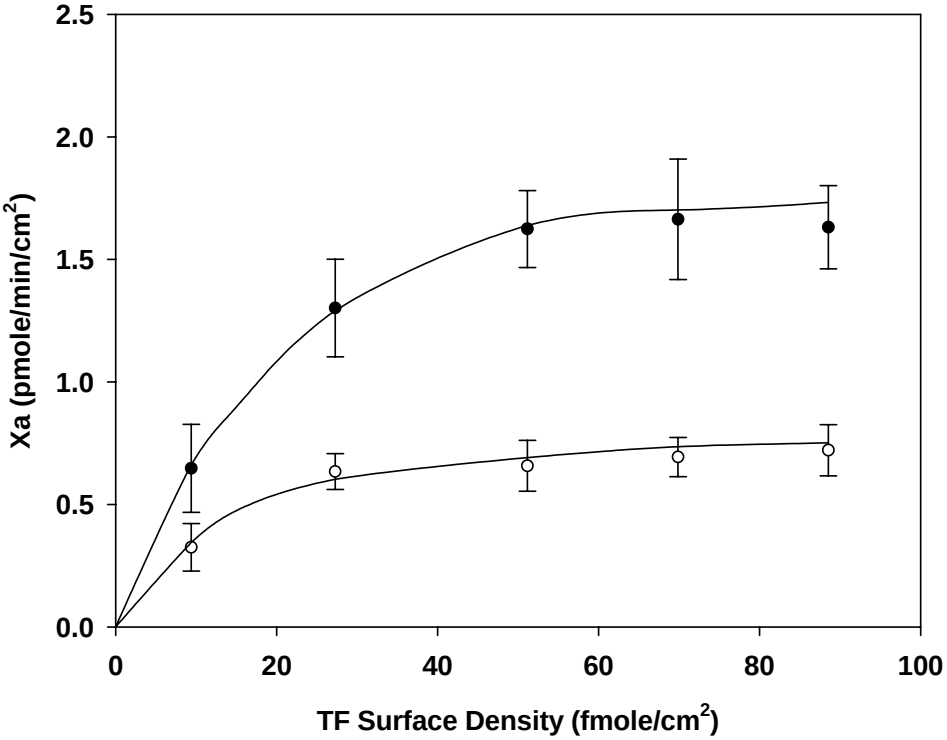

Figure 32 Steady state rate of factor Xa production as a function of TF surface concentration at shear rates of 50 (○) and 500 sec^{-1}(●). Each data point represents a mean ± standard deviation (n = 5). Steady state rate of factor Xa generation (pmole/min/cm^2) = steady state factor Xa generation (nM) x flow rate (mL/min)/reactor surface area cm^2).

Table 7 Parameters of TF Density Titrations. The TF density plots (Lineweaver-Burk plot) of Figure 25 were fit to a hyperbola. The maximal factor Xa production rate ($V_{max\ E}$) and the TF density resulting in half-maximal rate of reaction ($K_{1/2\ E}$) are shown. Data represent mean ± standard deviation (n = 5).

γ_w (sec^{-1})	$K_{1/2\ E}$ (fmole/cm^2)	$V_{max\ E}$ (pmole/min/cm^2)
50	14.96 ± 1.61	0.89 ± 0.10
500	22.62 ± 1.91	2.03 ± 0.19

Thrombin generation

Similar to characterizing factor X activation from surface TF, the effects of shear rates and TF surface density on surface TF-induced thrombin generation were investigated. Generally, thrombin generation started to accelerate within minutes of perfusion and steady state levels were reached at 10 and 5 minutes after starting the perfusion at shear rates of 50 and 500 sec^{-1}, respectively. An exception was noted for the lowest TF surface density (9.4 $fmole/cm^2$), which takes 2 to 3 minutes longer to reach steady state (Figure 33). Steady state thrombin concentrations were higher at lower shear rate, which was also observed for factor Xa generation. Thrombin generation increases with increasing TF surface density and plateaus when TF concentration is more than 51.2 $fmole/cm^2$ (Figure 32), which was also observed for factor Xa generation. Steady state levels of thrombin generation are 472.20 ± 35.24 nM and 190.37 ± 25.36 nM at shear rates of 50 and 500 sec^{-1}, respectively. Since TF-initiated thrombin generation under flow conditions involves at least twenty kinetic rate constants (178) and also requires a consideration of transport properties of reactants and products towards and away from the catalytic surface, it is beyond the scope of this study to explore all of these potential factors. Nonetheless, these experimental results indicate that TF containing surfaces can be produced and exhibit prothrombotic activity for our intended antithrombogenic test system.

Previous studies on thrombin generation under nonflow conditions (26, 178) show that a rapid thrombin production occurs within 1.5 minute and reaches the plateau after 2 minutes of reaction with ~ 1.5 μM of thrombin generation. The slower thrombin response and lower level of thrombin generation from the current flow experiments demonstrate

the effect of shear rate and transport of reactants and products on surface enzymatic reactions related to blood coagulation. An *in vitro* flow study from van't Veer et al. (179) has shown that TF surface activity on stimulated human umbilical vein endothelial cells can trigger activation of factor X as well as thrombin production by perfusion of coagulation protein mixture similar to current studies. Specifically, steady state rate of thrombin generation from a stimulated endothelial cell-coated surface was around 10 pmole/min/cm^2 at shear rate of 100 sec^{-1}, while we observed around 6.8 pmole/min/cm^2 at shear rate of 50 sec^{-1} from the current TF-coated surface (the plateau in Figure 34B). A stimulated rate vascular smooth muscle cell-coated surface in an *in vitro* flow system (180) showed human factor Xa flux was approximately 0.14 pmole/min/cm^2 at shear rate of 80 sec^{-1}, while our studies showed that saturated rate of factor Xa generation was around 0.68 pmole/min/cm^2 at shear rate of 50 sec^{-1}. These demonstrate surface TF activity is cell-type specific and surface TF from our model system can exhibit comparable even greater activity than active cell surfaces. Although surface concentration of tissue factor expressed at vascular injury sites has not been well characterized, we speculate surface tissue factor activity on membrane-mimetic thin film to induce activation of factor X and thrombin generation from the current study may provide a potential model system for investigating blood coagulation on live cell membranes and its regulation using anticoagulants and/or inhibitors for future applications.

We demonstrated surface bound TF is active due to its catalytic ability to initiate generation of Xa and thrombin. Previous studies (27) suggests that concentration of Xa is the rate-limiting component of prothrombinase complex formation and the ultimate

generation of thrombin activity. Since the involved reaction mechanisms intertwined with transport of substances makes thrombin generation under flow a complex issue, mathematical simulation is planned in future work.

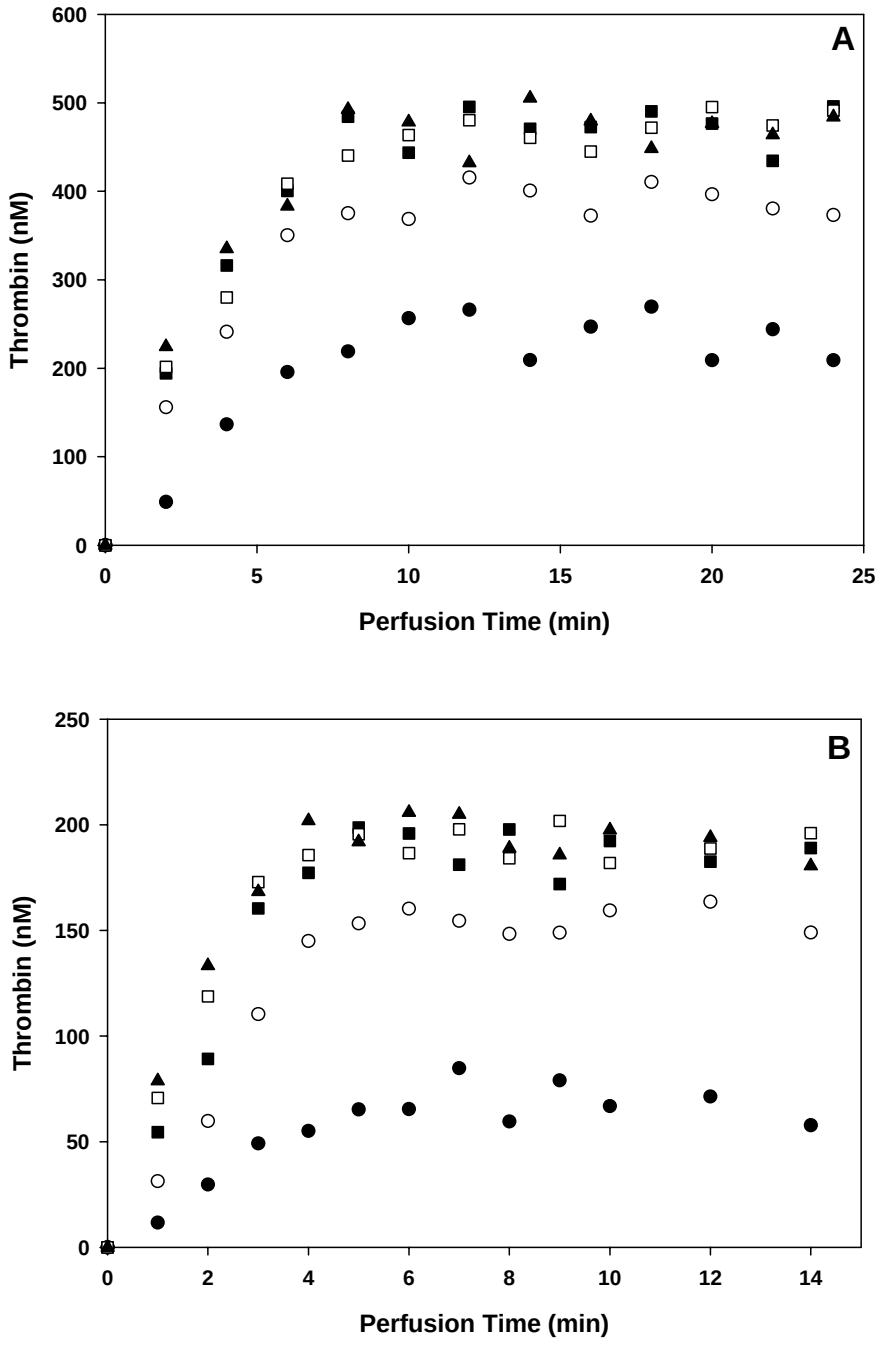

Figure 33 Thrombin generation with various TF surface concentrations (9.4 (●) 27.3 (○) 51.2 (■) 69.9 (□) 88.6 (▲) fmole/cm^2) at shear rates of (A) 50 sec^{-1} and (B) 500 sec^{-1}. Each data point represents a mean value for five experiments (see Appendix E2 for raw data).

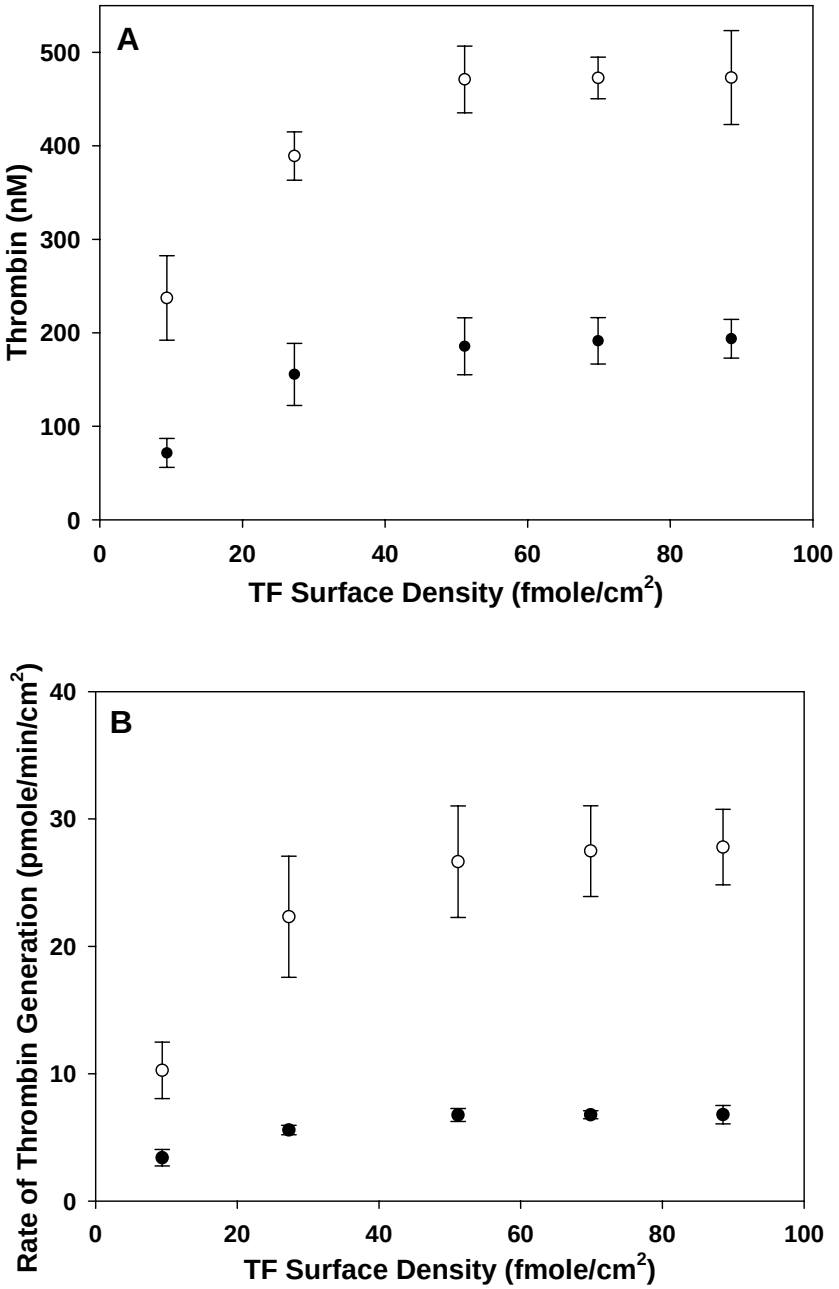

Figure 34 (A) Thrombin concentration (nM) and (B) rate of thrombin generation (pmole/min/cm^2) as a function of TF concentration within lipid vesicles at shear rates of 50 (●) and 500 (○) sec^{-1}. Each data point represents a mean ± standard deviation (n =5).

5.4 CONCLUSIONS

In summary, a TF containing membrane-mimetic thin film can be produced with predictable surface concentrations of TF. We demonstrated surface bound TF is active due to its ability to initiate generation of Xa and thrombin. We have utilized a parallel plate continuous flow reactor to investigate the effect of TF surface density on behavior of activation of factor X and thrombin generation at physiologic relevant shear rates. Factor Xa production increases with increasing TF surface density when surface concentration is less than 50 fmol/cm^2, beyond which the catalytic capacity of TF is exceeded, indicating that reaction velocity will not increase because of a transport limitation. Similar responses of Xa and thrombin are consistent with the view that the generation of thrombin is dependent upon Xa. Indeed, previous studies (27) suggests that concentration of Xa is the rate-limiting component of prothrombinase complex formation and the ultimate generation of thrombin activity.

Recent studies have reported that physiologically active TF is found circulating in blood of healthy individuals either as a component of blood cells and microparticles or as a soluble plasma protein (181), it is speculated these forms of TF do not trigger blood coagulation because the activation threshold condition is not exceeded, and activated enzyme, such as factor VIIa, could safely circulate without initiating explosive coagulation. Substantial exposure of surface TF to blood due to vascular injury is largely responsible for thrombin generation. Trauma substantial enough to raise TF levels beyond the transition level would elicit a very strong response, primed by the interaction of the circulating factor VIIa with the newly exposed TF. That response would be localized to the immediate vicinity of surfaces on which the binding-site density was high.

Since surface density of TF from vascular injury site has not been reported, the current *in vitro* studies provide a strategy for generating TF-coated surface as a model to mimic vascular damage.

CHAPTER 6

REGULATORY EFFECTS OF THROMBOMODULIN, HEPARIN, AND THROMBOMODULIN/HEPARIN COMPOSITE SURFACES ON TISSUE FACTOR-INDUCED THROMBIN GENERATION

6.1 ABSTRACT

The ability to design blood contacting surfaces that limit tissue factor (TF)-induced thrombin generation by activating protein C and ATIII was evaluated in a continuous flow system. Tissue factor along with thrombomodulin (TM) and heparin was immobilized in a spatially distinct manner onto a planar surface as components of a membrane-mimetic film. Specifically, TF positioned over a 2 x 6 mm^2 upstream region as a trigger for thrombin generation and TM and/or heparin positioned over the remaining downstream (34 x 6 mm^2) portion of the test film. In the absence of TM and heparin, thrombin generation was investigated as a function of TF surface density at shear rates of 50 and 500 sec^{-1}. At both shear rates, the limit of thrombin generation was attained at TF densities equal to or greater than 51.2 fmole per cm^2. However, the lag time to reach steady state and the steady state concentration of thrombin were reduced at increasing shear rate. Peak ($[T]_{max}$) and steady state ($[T]_{ss}$) concentrations of thrombin were reduced by ATIII and in the presence of surface bound TM and/or heparin. Although ATIII alone reduced thrombin levels, this effect was significantly enhanced by surface bound TM and heparin. At shear rate of 50 sec^{-1}, the steady state concentration of thrombin in the absence ATIII or protein C was approximately 29.8 ± 2.0 nM (mean ± standard deviation, n = 5). In the presence of ATIII, but in the absence of surface bound TM or heparin, the steady state concentration of thrombin was profoundly reduced to 8.4 ± 0.7 nM.

Incorporating heparin or TM into a membrane-mimetic film reduced thrombin levels to 6.3 ± 1.1 nM and 3.9 ± 1.0 nM, respectively. Compared to a TF surface in the presence of ATIII only, lowest levels of thrombin, which were reduced about three times, were observed when films contained both heparin and TM. Similar responses were observed at 500 sec^{-1}. These studies are the first to demonstrate the additive effect of surface bound heparin and TM as a combined interactive strategy to limit TF-induced thrombin formation.

6.2 INTRODUCTION

Tissue factor pathway has been commonly accepted as a major mechanism responsible for blood coagulation which is initiated by exposure of subendotheilial integral membrane protein tissue factor (TF) to blood due to vascular injury (14-16, 155). The procoagulant reaction starts with the binding of activated factor VII (factor VIIa) to TF to form VIIa-TF enzyme complex which activates the zymogens factor X and IX by limited proteolysis (182). Factor IXa combines with its cofactor factor VIIIa on the membrane surface to form a second complex that activates factor X. Once activated, factor Xa associates with its cofactor factor Va on a membrane surface to form prothrombinase, which converts prothrombin into thrombin (98, 183).The thrombin initially formed accelerates further thrombin generation by feedback activation of the procofactors factor V and factor VIII. Thrombin may also activate factor XI (184, 185), which, in turn, activates more factor IX.

Thrombin stimulates platelets, which secrete their granule contents and aggregate, cleaves fibrinogen to generate the fibrin network, and activates the protransglutaminase factor XIII. The fibrin-platelet aggregate, stabilized by factor XIIIa-catalyzed cross-links, forms the haemostatic plug. Without regulatory systems of blood coagulation, amplified thrombin generation leading to overwhelmed blood clot formation would be detrimental due to severely constricted blood fluidity.

Normal endothelium performs anticoagulant functions to balance thrombin generation by producing thrombin inhibitors, including endothelial surface-bound thrombomodulin (TM) and heparan sulfate (HS). TM functions as a critical regulator to trigger protein C activation. By binding to thrombin, TM converts procoagulant thrombin into

anticoagulant TM-thrombin complex which enhances activation of protein C. The product APC can exhibit its inhibitory effect on coagulation by proteolytically inactivating factor Va and factor VIIIa so that ultimate thrombin generation can be reduced. Moreover, previous studies showed that an individual suffering from thrombosis associated with a TM mutation leading to a defective protein (186) and the embryonic lethality in mice lacking the TM gene (187) identify the significance of TM as a natural anticoagulant.

Heparan sulfate, a glycosaminoglycan, activates ATIII to catalyze the inhibition of thrombin and factor Xa. To date, heparin, a derivative of HS, has been largely used as an anticoagulant drug. According to ATIII-heparin binding mechanisms (120), sulfate groups on heparin pentasaccharide are essential to the high-affinity binding of ATIII. Extensive sulfation makes heparin a more potent catalyst to activate ATIII than HS. Heparin is also known to have a wide variety of biological actions independent of its anticoagulant effects, including interactions with endothelial cell growth factors (188), inhibition of smooth muscle cell proliferation (189), activation of lipoprotein lipase (190), suppression of aldosterone secretion, and interactions with platelets (191).

Interactions among ATIII, heparin, and protein C pathway on regulation of coagulation were studied. The most significant observation was that coagulation time can be markedly prolonged in the presence of APC, ATIII, and heparin simultaneously compared to the effect by ATIII, APC, and heparin individually (192, 193). However, the molecular basis behind such phenomena remains indecisive. Hirahara et al. (192) found that the generation of prothrombinase was strongly suppressed by APC in the presence of heparin, leading to reduced thrombin generation. Petaja et al. (193) suggested that

synergistic effect of APC and heparin can enhance inhibition of thrombin generation by inactivation of factor V instead of Va. In contrast, Nicolaes et al. (194) suggested that APC-mediated inactivation of factor Va was enhanced by heparin on the basis on heparin-bound APC promoting association between factor Va and APC at position Arg306. Some previous studies (195, 196) even revealed thrombin inhibitors and heparin could compromise protein C activation by reducing affinity of thrombin for TM.

In order to determine capacity of immobilized heparin and TM to inhibit surface TF-initiated thrombin generation, we designed an *in vitro* model to mimic vascular implantation. Membrane-mimetic constructs containing TF, TM, and heparin were fabricated on a planar substrate (Figure 35) and investigated using a continuous flow system. Specifically, TF positioned over a 2 x 6 mm^2 upstream region as a trigger for thrombin generation and TM and/or heparin positioned over the remaining downstream (34 x 6 mm^2) portion of the test film. The surface systems are referred to as TF/TM, TF/Heparin, or TF/TM-Heparin. At shear rates of 50 and 500 sec^{-1}, the surface was perfused with a protein mixture containing mean plasma concentrations of coagulation factors, along with physiologic concentrations of antithrombin and protein C when appropriate. In the absence of ATIII, TM or heparin, thrombin rapidly reached a steady state level of production ($[T]_{TFss}$) which increased with increasing TF surface content. Significantly, $[T]_{TFss}$ was independent of TF surface density equal to or greater than 51.2 $fmole/cm^2$, which is possibly due to transport limitation effect on surface catalytic activity. After defining the upper limit of thrombin generation, we started to investigate the effect of surface anticoagulants on thrombin responses under the same flow conditions.

Acute initial thrombin generation was observed in the presence of ATIII, surface TM or heparin, indicating that ATIII and protein C pathway have no significant influence upon the initial phase of reaction. However, thrombin generation thereafter was reduced considerably, especially when the perfusate contained ATIII. Compared to steady state concentration of thrombin from TF surface with perfusate containing ATIII, $[T]_{ss}$ was further reduced with addition of surface TM and/or heparin. According to statistical analyses among TF+AT, TF/TM+AT, TF/Heparin, TF/TM-Heparin systems, surface TM appeared to more effective in reducing thrombin generation than surface heparin.

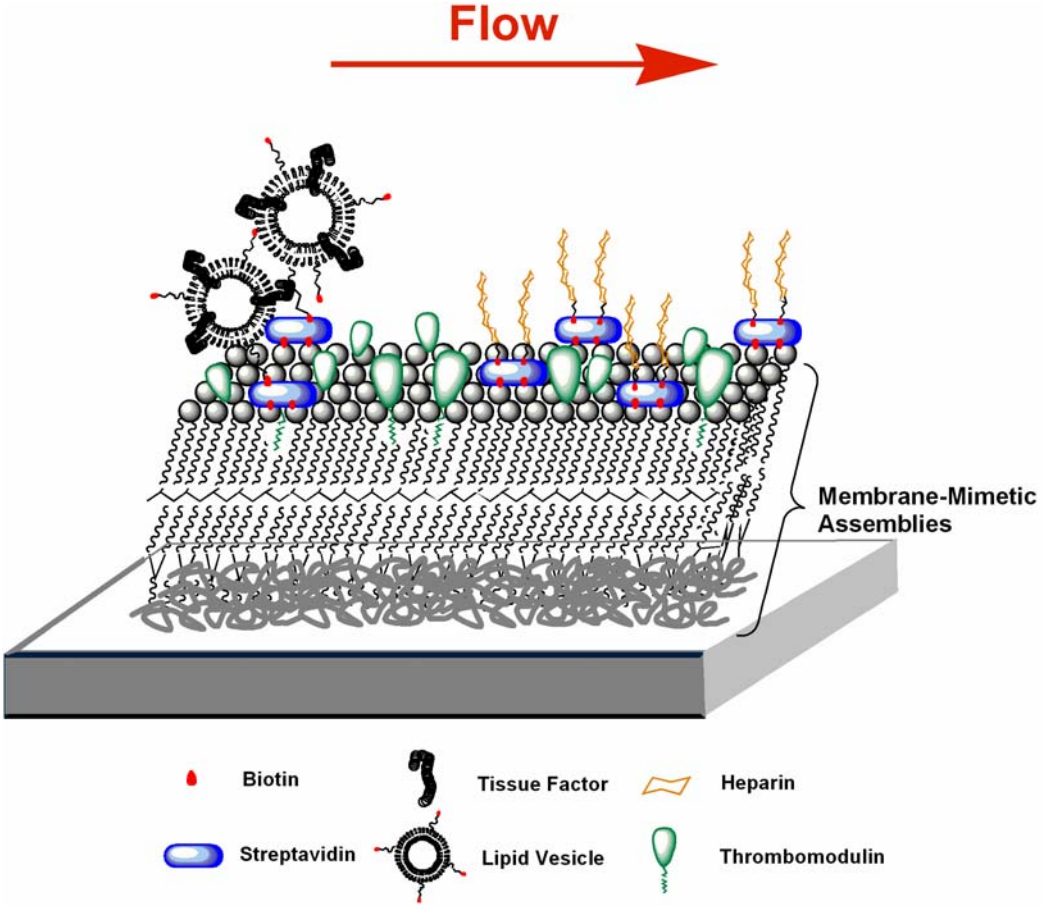

Figure 35 Schematic representation of immobilized thrombomodulin (TM), tissue factor (TF), and heparin on the basis of biotin functionalized polymeric phospholipid monolayer supported on an alkylated polyelectrolyte multilayer. Relipidated TF is positioned at the upstream of the flow (Not to scale).

6.3 MATERIALS AND METHODS

6.3.1 Materials

Human coagulation factors V, VII, VIIa, IX, X, prothrombin, human antithrombin III, human protein C, and rabbit lung thrombomodulin (single chain containing NH_2-terminal hydrophobic domain, six EGF domains, one O-glycosylation rich domain, one transmembrane domain, COOH-terminal cytoplasmic domain, 74 kD, in 0.02 M Tris, 0.15 M NaCl, pH 7.4 containing 0.05% lubrol PX) were obtained from Haematologic Technologies, Inc. Human coagulation factor VIII, tissue factor (full length recombinant human tissue factor, TF, 43 kD, lyophilized from 0.01 M Tris, 0.15 M NaCl, pH 8.0 containing 0.01% CHAPS and 200 mM mannitol), and Spectrozyme TH substrate for thrombin (H-D-hexahydrotyrosyl-L-alanyl-L-arginine-p-nitroanilide-diacetate salt) were obtained from American Diagnostica Inc. Eosin Y (EY, 5% in water), triethylamine (TEA), 1-vinyl-2-pyrrolidinone (VP) were obtained from Aldrich. Nucleopore polycarbonate filters and Contrad 70 detergent were obtained from Fisher. Detergent OG (*n*-octyl-β-D-glucopyranoside) was obtained from Sigma. Chicken egg PC (L-α-Phosphatidylcholine), porcine brain PS (L-α-Phosphatidylserine, sodium salt), N-Biotinyl Cap-PE (18:1) (1,2-Dioleoyl-*sn*-Glycero-3-Phosphoethanolamine-N-(Cap Biotinyl), and fluorescent PE (1,2-Dioleoyl-sn-Glycero-3-Phosphoethanolamine-N-(Carboxyfluorescein) were purchased from Avanti Polar Lipids, Inc. Alginate (ALG; low viscosity, ca. 60% mannuronic acid) was obtained from Pronova Biomedical (Norway). Poly (L-lysine) (PLL, MW > 300 kD) and all buffer salts are obtained from Sigma. Synthesis of monoacrylate-PC (AcPC,1-palmitoyl-2-[12-(acryloyloxy)dodeca-noyl]-*sn*-glycero-3-phosphocholine), monoacrylate-PE (1-palmitoyl-2-(12-

(acryloyloxy)dodecanoyl)-*sn*-glycero-3-phosphoethanolamine) and its biotin derivative (biotin-AcPE, mono-acrylPE-biotin) have described previously (77, 94) . The synthesis of the terpolymer that consists (3-acryloyl-3-oxapropyl-3-(N,N-dioctadecyl-carbamoyl)-propionate))$_6$:(2-hydroxyethyl acrylate)$_3$:sodium styrene sulfonate$_1$ (AOD$_6$:HEA$_3$:SS$_1$) has been described elsewhere (96). Heparin (sodium salt, porcine intestinal mucosa, Mw: 13,500-15,000) and streptavidin (Avidin, *Streptomyces avidinii*, Mw: 60 kDa) was obtained from Calbiochem. Synthesis of biotin-conjugated heparin was described in Chapter 4.

6.3.2 Fabrication of Localized Tissue Factor Containing Membrane-Mimetic Surfaces.

Microscope glass slides (2.6 cm x 4.6 cm, Fisher) were cleaned and coated with biotin-functionalized membrane-mimetic thin film (molar ratio of AcPC: biotin-AcPE = 90:10), followed by coating with streptavidin as previously described (80). TF-coated surfaces were fabricated by dipping the glass slides vertically in a glass jar (2.6 x 2.6 cm^2 bottom area, Wheaton) containing 4.5 mL of a well stirred mixture of TF-constituted lipid vesicles (Chapter 5, section 5.3.2) (Figure 36). The incubation time was 30 min at room temperature, followed by rinsing extensively using deionized water. Fluorescent PE (fluorescein, 0.1mole% final) was doped within lipid vesicles for fluorescent microscopy studies.

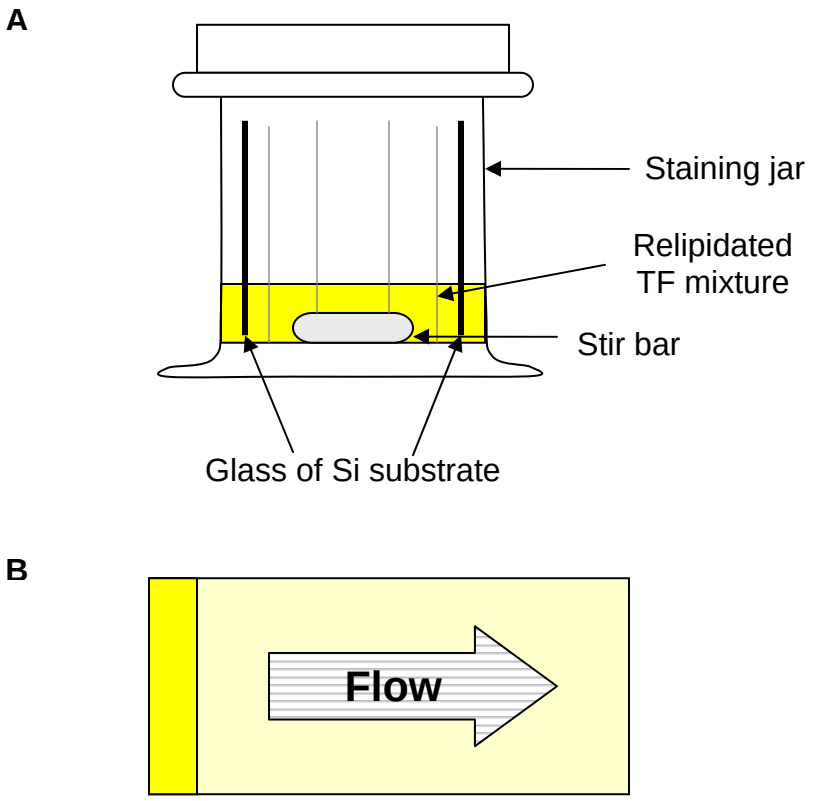

Figure 36 (A) Schematic representation for TF-coating process. Supporting substrates were pretreated with biotin-functionalized membrane-mimetic assemblies, followed by immobilization of streptavidin, then the streptavidin-coated surfaces facing inwards were dipped into relipidated tissue factor mixture at room temperature for 30 minutes. (B) The resulting localized TF-coated area (yellow). (Not to scale)

6.3.3 Determination of Tissue Factor Surface Density and Stability

Recombinant human tissue factor at a concentration of 0.1 mg/mL was radiolabeled with ^{125}I using Iodobeads (Pierce Chemical Co., Rockford, IL) according to the manufacture's protocol. The concentration of radiolabeled TF was determined by a modification of the Bradford Protein Assay (Bio-Rad) using a TF standard curve. Specific activity of the protein solution averaged 7.03 x 10^7 cpm/μg (3022 cpm/fmole). Cleaned supporting substrates (5x5 mm^2 Si chip) were coated with membrane-mimetic thin film containing streptavidin (Chapter 5, section 5.3.3). ^{125}I-TF and unlabeled TF were mixed to form 1:30 molar ratio solution, and TF was then added to obtain the desired TF/lipid molar ratio (Chapter 5, section 5.3.2). The coated silicon chips were attached to glass slides and dipped into relipidated ^{125}I-TF/unlabeled TF mixture, followed by rinsing extensively with deionized water prior to measuring surface radioactivity in a gamma counter. TF surface density (fmol/cm^2) was calculated as {cpm/(specific activity x sample area)} and specific activity corrected for decay. Test samples were generated in six replicates for each TF/lipid molar ratio. For stability analysis, samples were stored in fresh PBS at 37 °C and radioactivity was measured periodically after extensive washing in deionized water over a one-month period.

6.3.4 Fabrication of Composite Tissue Factor/Thrombomodulin, Tissue Factor/Heparin, and Tissue Factor/Thrombomodulin-Heparin Containing Membrane-Mimetic Surfaces.

TF/TM composite surface — Microscope glass substrates (2.6 cm x 4.6 cm, Fisher) were cleaned and coated with TM-incorporated biotin-functionalized membrane-mimetic thin film, followed by immobilizing streptavidin. TF-reconstituted lipid vesicles were tethered onto the above surfaces by dip-coating process (section 6.3.2).

TF/heparin composite surface — A membrane-mimetic thin film containing streptavidin was fabricated on a glass slide surface, followed by dip coating in relipidated TF mixture as described previously. After rinsing extensively, the TF-coated surface was then incubated with biotin-conjugated heparin (0.1 mg/mL) in PBST (50 mM NaH_2PO_4 and 150 mM NaCl, pH 7.4) overnight at 4^oC on a horizontal rotating platform, and rinsed with deionized water extensively.

TF/TM-heparin composite surface—The coating procedure followed the order of immobilizing TM, TF, and heparin. Extensive rinsing with deionized water was performed between immobilization of each component.

All the above surface samples were stored in PBS (1X with 0.02% NaN_3) at 4^{o}C for the following flow studies and experiments were conducted 2 days after fabrication.

6.3.5 Continuous Flow Reactor Assays on Immobilized Catalysts-Containing membrane-mimetic surface: Effects of Anticoagulants on Thrombin Generation Triggered by TF

TF-coated area (0.6 (W) x 0.2 (L) cm^2) positioned at the upstream of the flow served as an inducer for thrombin generation. A parallel plate flow system (0.6cm (width) x 0.025cm (height) x 3.6cm (length), 54.9 μL volume) containing coated sample was flushed with 20 mM HEPES buffer for 1 hours at γ_w = 2000 sec^{-1}. Given the dimension of flow chamber and a shear rate of 50 sec^{-1}, the residence times, defined as time spent by flow through exposed areas, were calculated (eq. (9) in Chapter 3) to be 0.94 sec for TF coated area and 16.06 sec for none-TF area, which simulates the same condition for a 40 cm-long vascular graft (4mm i.d.) with a 2 cm-long injury. Residence times were 0.09 sec

for TF coated area and 1.61 sec for none-TF area at 500 sec^{-1}. We determined the capacities of surface anticoagulants to inhibit TF-induced thrombin generation by conducting the following experiments.

TF-Initiated Thrombin generation — Reaction was started by perfusing the surface with the reaction mixture HBS (20 mM Hepes + 150 mM NaCl, pH 7.4) containing coagulation factors (V, VII, VIIa, VIII, IX, X, prothrombin) and 2 mM $CaCl_2$ at 37^oC (Chapter 5, section 5.3.4). At pre-selected timed points, aliquots withdrawn from the perfusate at the reactor outlet were quenched by TBS/EDTA (50 mM Tris-HCl + 175 mM NaCl + 20 mM EDTA, pH 7.4), and assayed after adding Spectrozyme TH (0.2 mM final) (25, 172). When the reaction mixture contained 2 μM of ATIII, aliquoted samples were withdrawn into TBS/EDTA containing Spectrozyme TH and assayed immediately for thrombin activity otherwise the measured thrombin concentration was not accurate due to rapid inactivation by ATIII (172). Thrombin concentration was determined by monitoring the hydrolysis of the substrate by the change in absorbance at 405 nm using UV-VIS spectrophotometer. Thrombin generation was calculated from a standard curve prepared using serial dilutions of human α-thrombin.

Effect of Surface Bound TM on TF-Initiated Thrombin Generation—Reaction was started by perfusing TF/TM surface with the same reaction mixture containing 0.1 μM protein C. Detection of thrombin generation during perfusion followed the same procedure as described above.

Effect of Surface Heparin on Thrombin Generation Initiated by Surface TF— Reaction was started by perfusing TF/Heparin surface with the same reaction mixture including ATIII (2 μM, final). At pre-selected timed points, aliquots withdrawn from the perfusate at the reactor outlet were assayed by adding TBS/EDTA (50 mM Tris-HCl + 175 mM NaCl + 20 mM EDTA, pH 7.4) containing Spectrozyme TH (0.2 mM final).

Effect of Composite TM/Heparin on Thrombin Generation Initiated by Surface TF– Reaction was started by perfusing TF/TM-Heparin surface with the same reaction mixture containing 0.1 μM protein C and 2 μM ATIII. Detection of thrombin generation during perfusion followed the same procedure as described above.

6.4 RESULTS AND DISCUSSION

6.4.1 Lipid Vesicles Tethered onto Biotin-Functionalized Membrane-Mimetic Films

Doped with fluorescent PE, immobilized lipid vesicles fabricated by the dip-coating process were examined by fluorescent microscopy for initial characterization. To assess the stability of immobilized vesicles, we conducted flow tests by exposing the coated surface to phosphate-buffered saline at a wall shear rate of 2000 sec^{-1} for 1 hour. Fluorescence imaging of test surfaces (Figure 37) demonstrates that there is a sharp boundary between vesicle-coated and uncoated regions and no discernible loss of vesicles after high shear flow.

Previous studies have suggested that adhesion of lipid vesicles (with average diameter of 100 nm) doped with less then 1 mol% biotin appeared to reach saturation within a short time period (148, 197). The biotinylated phospholipid vesicles bind intact onto the streptavidin-coated surfaces without significant vesicle leakage or disruption (198, 199).

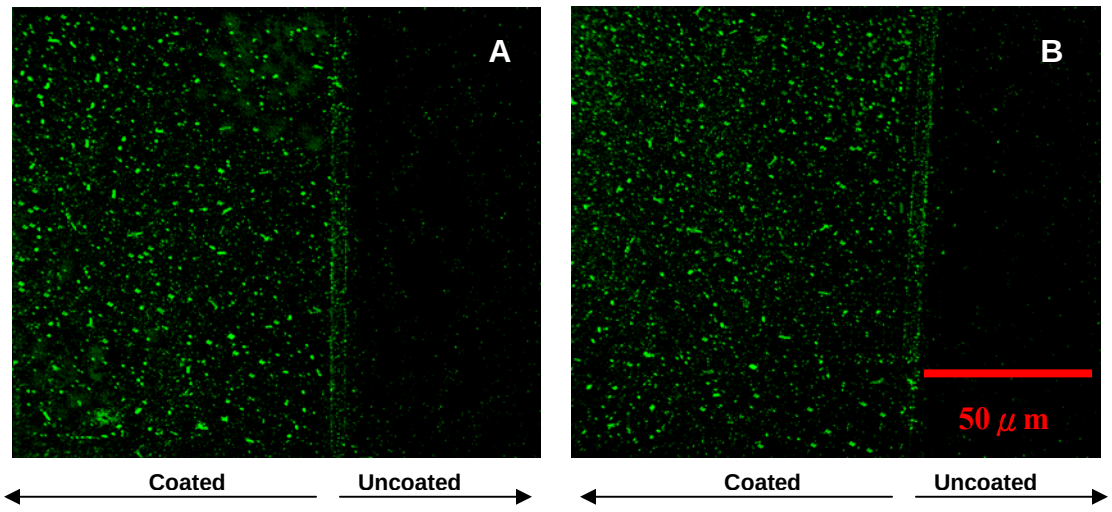

Figure 37 Fluorescent images (20x) of FITC-doped biotinylated lipid vesicles on Si coated with membrane-mimetic thin film (90/10 acrylate PC/biotin-acrylate PE) were taken before (A) and after (B) shear flow exposed to PBS at 2000 sec^{-1} for 1 hour.

6.4.2 Determination of Tissue Factor Surface Density

^{125}I-labeled TF was used to determine absolute surface concentration of TF on a planar substrate-supported membranes containing lipid composition of 10 mol% biotin-AcPE/90 mol% AcPC. A linear relationship was observed between TF surface density and TF concentration reconstituted within vesicles (Figure 38). Stability of immobilized TF/lipid vesicle was studied by incubating samples in PBS at 37^{o}C and measuring surface concentration periodically over a one month period. Generally, dramatic decrease in surface concentration was noted within the first week with little change thereafter up to 28 days (Figure 39). The stabilized TF density ranges from 9.4 ± 3.9 fmole/cm^2 to 88.6 ± 7.5 fmole/cm^2 (n = 6), corresponding to 6 nM to 120 nM TF reconstituted within lipid vesicles. Specifically, more dramatic decreases in surface concentration from TF concentration higher than 60 nM in vesicles were observed than other cases. We speculate that the decrease of TF concentration soon after the initiation of PBS incubation may be related to the loss of nonspecific binding of lipid vesicles. Notably, samples were removed from the bathing media on multiple occasions during the incubation period, which emphasizes the relative stability and robustness of this system.

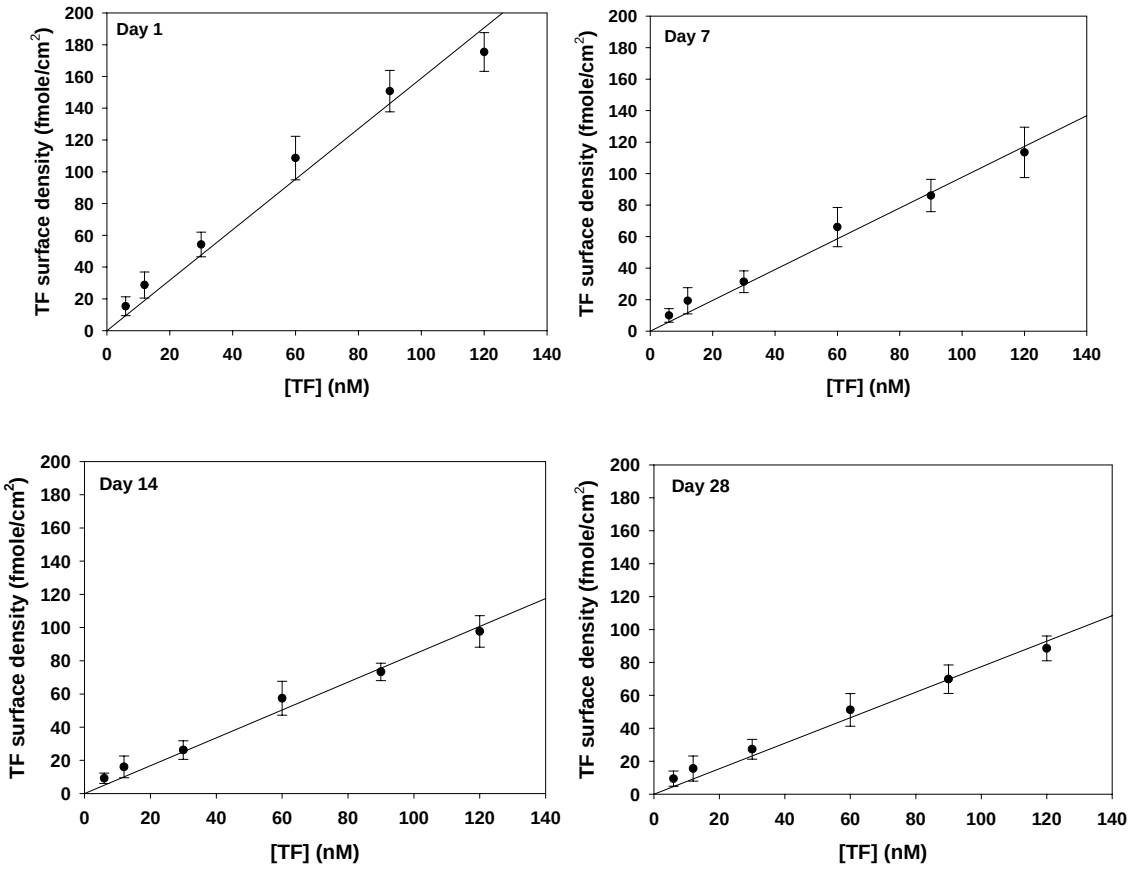

Figure 38 Relipidated TF surface density as a function of TF concentration within lipid vesicles (1mM of egg PC/brain PS/ biotin-PE, 79:20:1 molar ratio). TF was radiolabeled with ^{125}I and reconstituted into lipid vesicles. Surface concentration was determined after immobilizing onto streptavidin-biotinylated polymeric membrane-mimetic constructs. The stability of this system was assessed in PBS at 37 °C over a 28-day period. Films were transferred to fresh PBS at indicated time points and radioactivity measured in a gamma counter. Each data point represents mean ± standard deviation (n = 6) (see Tables in Appendix F)

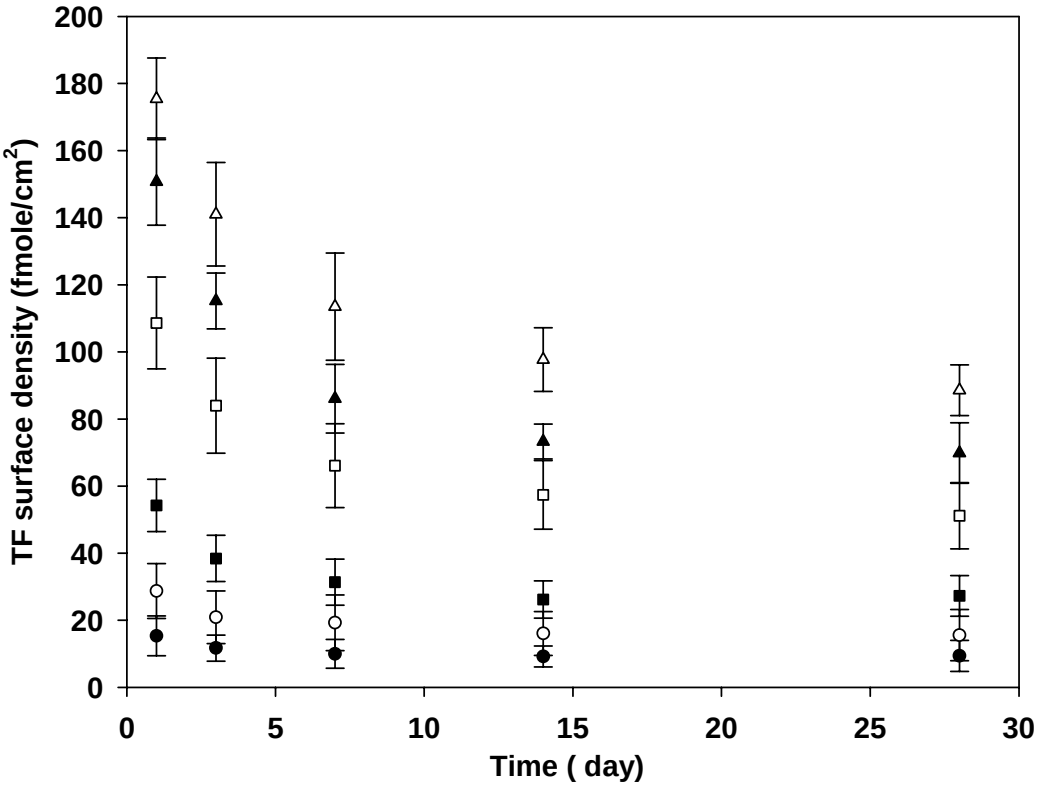

Figure 39 Stability of relipidated TF surface density and based on membrane-mimetic thin films. The stability of this system was assessed in PBS at 37 °C over a 28-day period. Note: a series of TF concentrations within lipid vesicles were prepared for immobilization: 6 nM (●),12 nM (○),30 nM (■), 60 nM (□), 90 nM (▲), and 120 nM (Δ). Each data point represents mean ± standard deviation (n = 6) (see Tables in Appendix F).

6.4.3 Surface Activity of Tissue Factor Under Flow Conditions: As a Source of Thrombin Generation From Upstream

The rationale behind the design of immobilized TF surface is to mimic a focal vascular wall injury site. In order to design a realistic representation of an anastomotic site between a host artery and synthetic vascular graft, the residence times were calculated as a function of shear rate and size of a given test region (e.g. TF vs. none-TF domain). For example, coating one area of 2 (length) x 6 (width) mm^2 with TF and the other of 34 (length) x 6 (width) mm^2 without TF which is associated with a shear rate of 50 sec^{-1} leads to residence times of 0.94 second and 16.06 seconds for TF-coated and none-TF coated areas, respectively. These residence times are equivalent to a 2 cm injury site followed by a 4mm i.d., 40 cm-long vascular graft. At shear rate of 500 sec^{-1}, the residence times are one tenth of those at 50 sec^{-1}.

Thrombin generation induced by a series of TF surface densities was investigated at shear rates of 50 and 500 sec^{-1}. Kinetics of thrombin generation (Figure 40) showed that the lag times to reach steady state concentrations of thrombin were 8-10 min and 4-6 min at shear rates of 50 sec^{-1} and 500 sec^{-1}, respectively. Significantly, steady state thrombin levels (average 30.7nM and 12.7 nM at shear rates of 50 and 500 sec^{-1}, respectively. Table 8) were attained at TF densities equal to or greater than 51.2 fmole per cm^2 (Figure 41), indicating that the transport of reactants and products towards and removal from the catalytic surface might play a crucial role in the overall reaction.

Thrombin generation initiated by TF pathway under flow conditions shows distinct behavior from previous studies in static well-mixed models (26, 172, 178). While static models revealed identical saturated levels of thrombin generation in the presence of a wide range of TF concentrations, current flow studies showed that steady state thrombin

generation was dependent of TF surface density except more than certain surface content. After defining the saturated level of thrombin generation, we started to investigate the ability of surface TM and heparin to inhibit thrombin responses associated with the upper limit of thrombin generation triggered by surface TF with density of 51.2 fmole/cm^2.

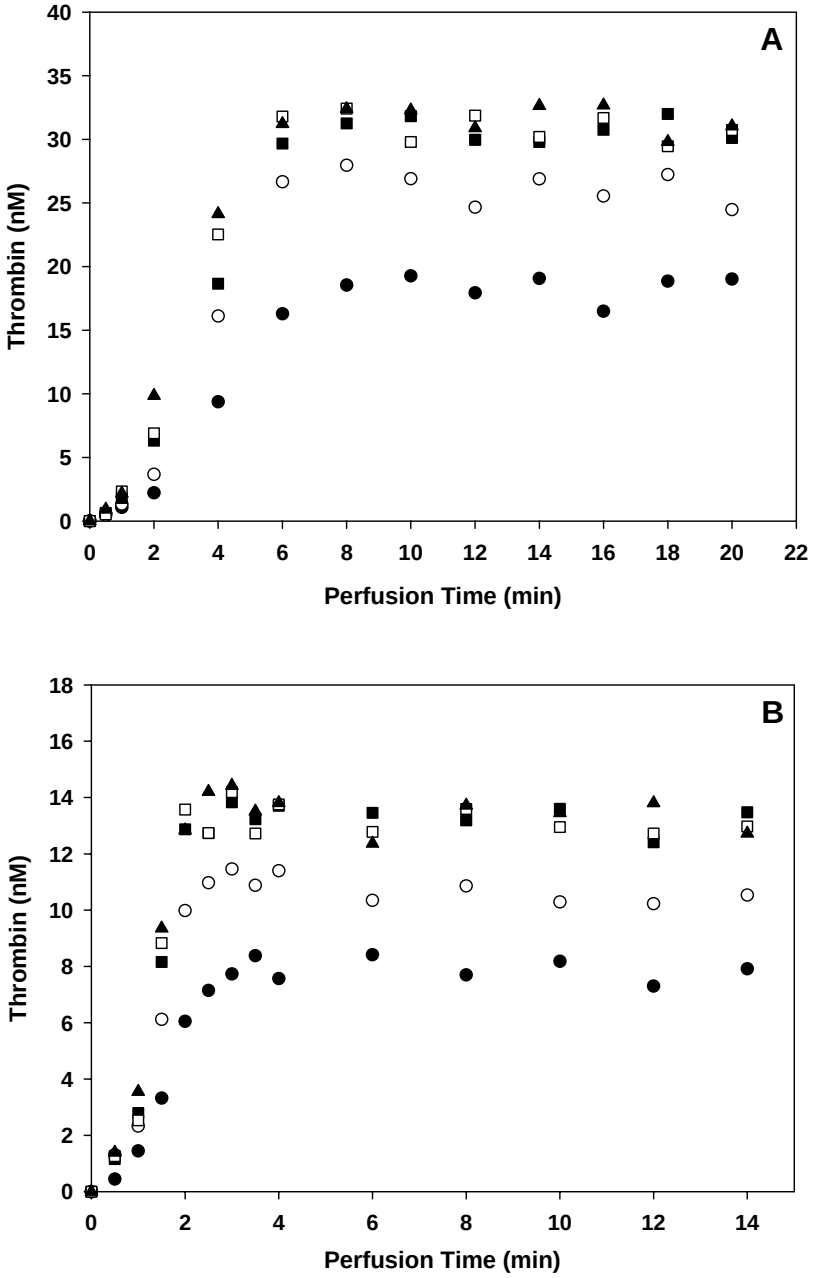

Figure 40 TF-induced thrombin generation at the reactor outlet over perfusion time as a function of surface TF concentrations (TF density: 9.4 (●) 27.3 (○) 51.2 (■) 69.9 (□) 88.6 (▲) fmole/cm2) at wall shear rates of (A) 50 sec^{-1} and (B) 500 sec^{-1}. Each data point represents a mean value (n = 5). (see Table G2 in Appendix G)

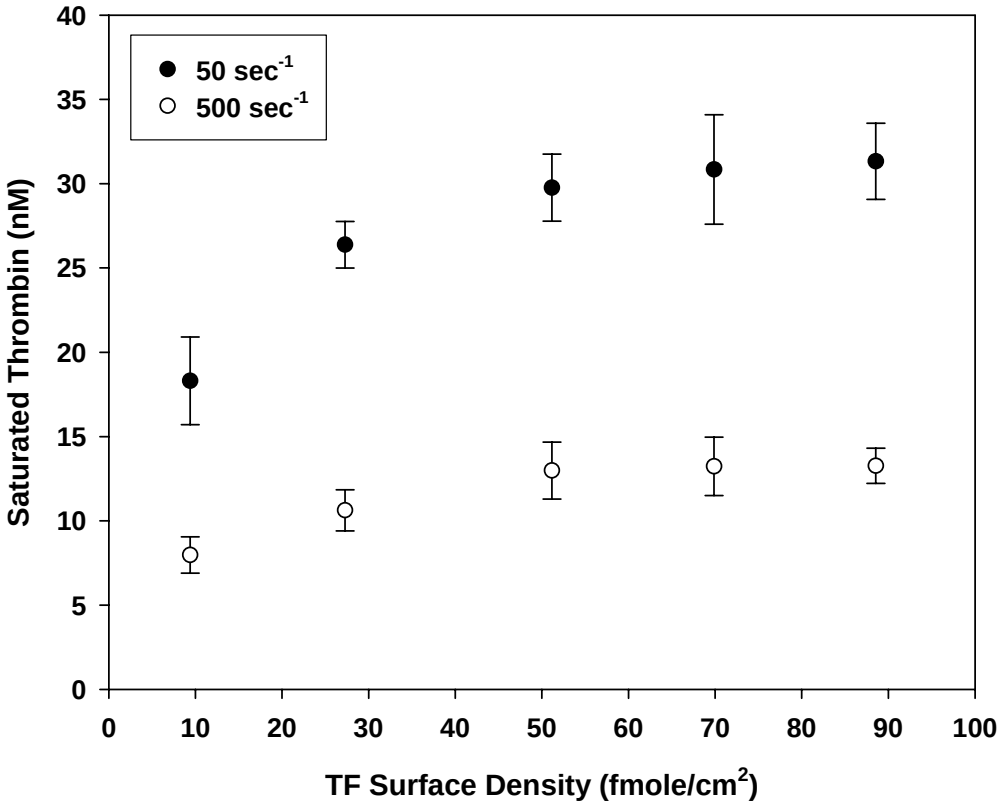

Figure 41 Steady state level of thrombin generation as a function of TF surface density at wall shear rates of 50 sec^{-1} and 500 sec^{-1}. Each data point represent a mean value ± standard deviation (n = 5). The results show that thrombin generation becomes saturated in the presence of more than 50 fmole/cm^2.

Table 8 Steady state concentrations (mean ± standard deviation, n = 5) of thrombin at a series of TF surface densities.

[TF] (fmole/cm^2)	Thrombin (nM), 50 sec^{-1}	Thrombin (nM), 500 sec^{-1}
9.4	18.31 ± 2.54	7.97 ± 1.07
27.3	26.38 ± 1.38	10.63 ± 1.22
51.2	29.76 ± 1.98	12.98 ± 1.69
69.9	30.84 ± 3.24	13.24 ± 1.73
88.6	31.33 ± 2.26	13.27 ± 1.04

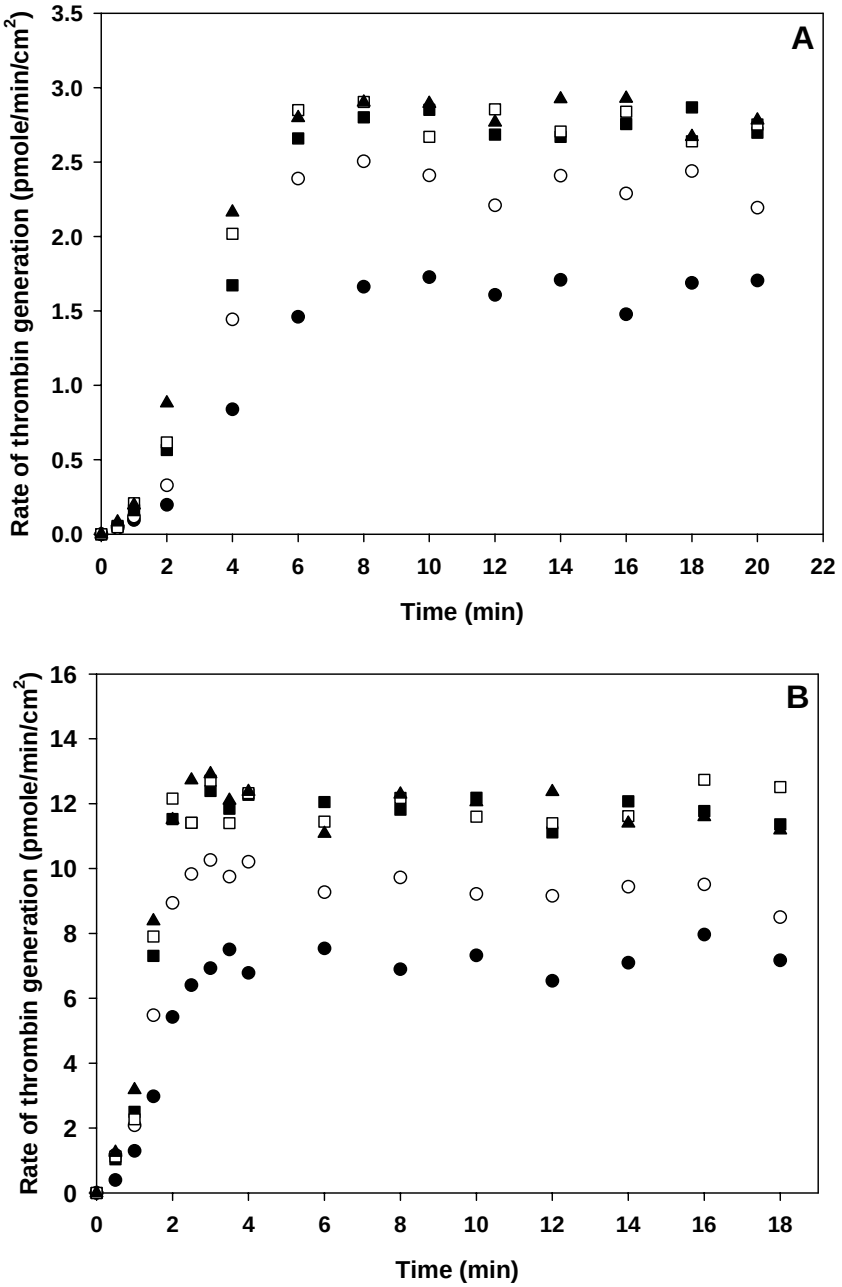

Figure 42 Rate of TF-induced thrombin generation at the reactor outlet over perfusion time as a function of surface TF concentrations (TF density: 9.4 (●) 27.3 (○) 51.2 (■) 69.9 (□) 88.6 (▲) fmole/cm^2) at wall shear rates of (A) 50 sec^{-1}and (B) 500 sec^{-1}. Each data point represent a mean value (n = 5). (see Table G2 in Appendix G). Note: rate of reaction = thrombin generation (Figure 40) x flow rate / surface area of reactor (= 0.6 (W, cm) x 3.6 (L, cm) = 2.16 cm^2)

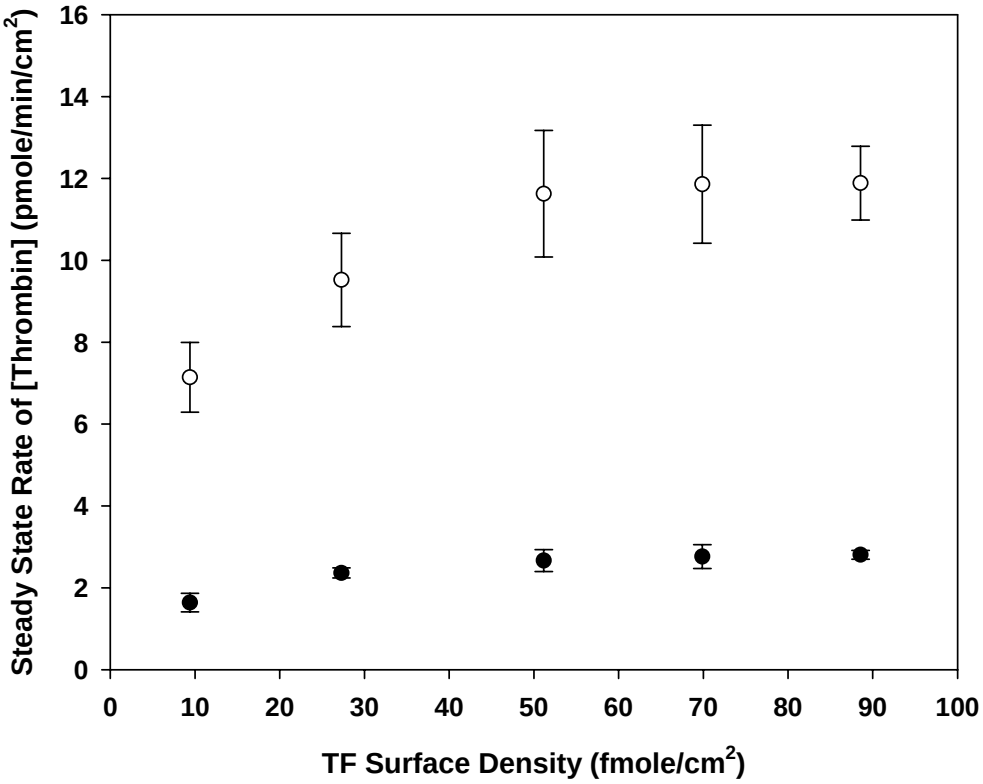

Figure 43 Steady-state rate of thrombin generation as a function of TF surface density at wall shear rates of 50 sec^{-1} (●) and 500 sec^{-1} (○). Each data point represent a mean value ± standard deviation (n = 5).

Table 9 Steady state rate of thrombin (T) generation (mean ± standard deviation, n = 5) at a series of TF surface densities. Steady state rates of thrombin generation (pmol/min/cm^2) in the presence of more than 50 fmole TF per cm^2 are 2.75 ± 0.25 and 11.77 ± 1.30 at shear rates of 50 and 500 sec-1 respectively

[TF] (fmole/cm^2)	T (pmole/min/cm^2), 50 sec^{-1}	T (pmole/min/cm^2), 500 sec^{-1}
9.4	1.64 ± 0.23	7.14 ± 0.85
27.3	2.18 ± 0.12	9.52 ± 1.14
51.2	2.67 ± 0.27	11.63± 1.55
69.9	2.76 ± 0.29	11.86± 1.44
88.6	2.83 ± 0.11	11.89 ± 0.90

6.4.4 Effect of Surface Anticoagulants on Tissue Factor-Initiated Thrombin Generation Under Flow Conditions

A tissue factor-immobilized membrane-mimetic thin film with TF surface density of 51.2 fmole/cm^2, the threshold to induce transport limited thrombin generation, was used to investigate antithrombogenic capacity of surfaces containing TM and heparin. Based on the observed transport limit of TM-induced activation of protein C and heparin-catalyzed ATIII inactivation of thrombin, surface concentrations of TM and heparin were fixed at 1.35 pmole/cm^2 (Ch 3, section 3.4.4) and 4.4 pmole/cm^2 (Ch 4, section 4.4.6), respectively.

Effect of Surface Bound TM on TF-Initiated Thrombin Generation

The effect of surface TM on TF-initiated thrombin generation was studied by perfusion of a defined protein solution, which included protein C over test surfaces consisting of TF and TM over defined upstream and downstream regions, respectively. Thrombin responses were characterized by a rapid initial reaction, a transient peak, and gradual decay to a steady state level (Figure 44 & 45). Maximum ($[T]_{max}$) and steady state ($[T]_{ss}$) values of thrombin concentration are summarized in Table 10. When compared to test surfaces that did not contain TM, average $[T]_{max}$ and $[T]_{ss}$ were, respectively, 18% and 53% less at a shear rate of 50 sec^{-1} , and 16% and 45% less at a shear rate of 500 sec^{-1}. Since the protein C pathway is not activated in the absence of thrombin, the capacity to reduce initial thrombin production is limited. These finding are consistent with other reports in which TM and TF were studied in a well mixed system of isolated vesicles (25). Thrombin decay in our system is likely due to the expected APC inactivation of factor Va (25, 49) with reduced prothrombinase activity.

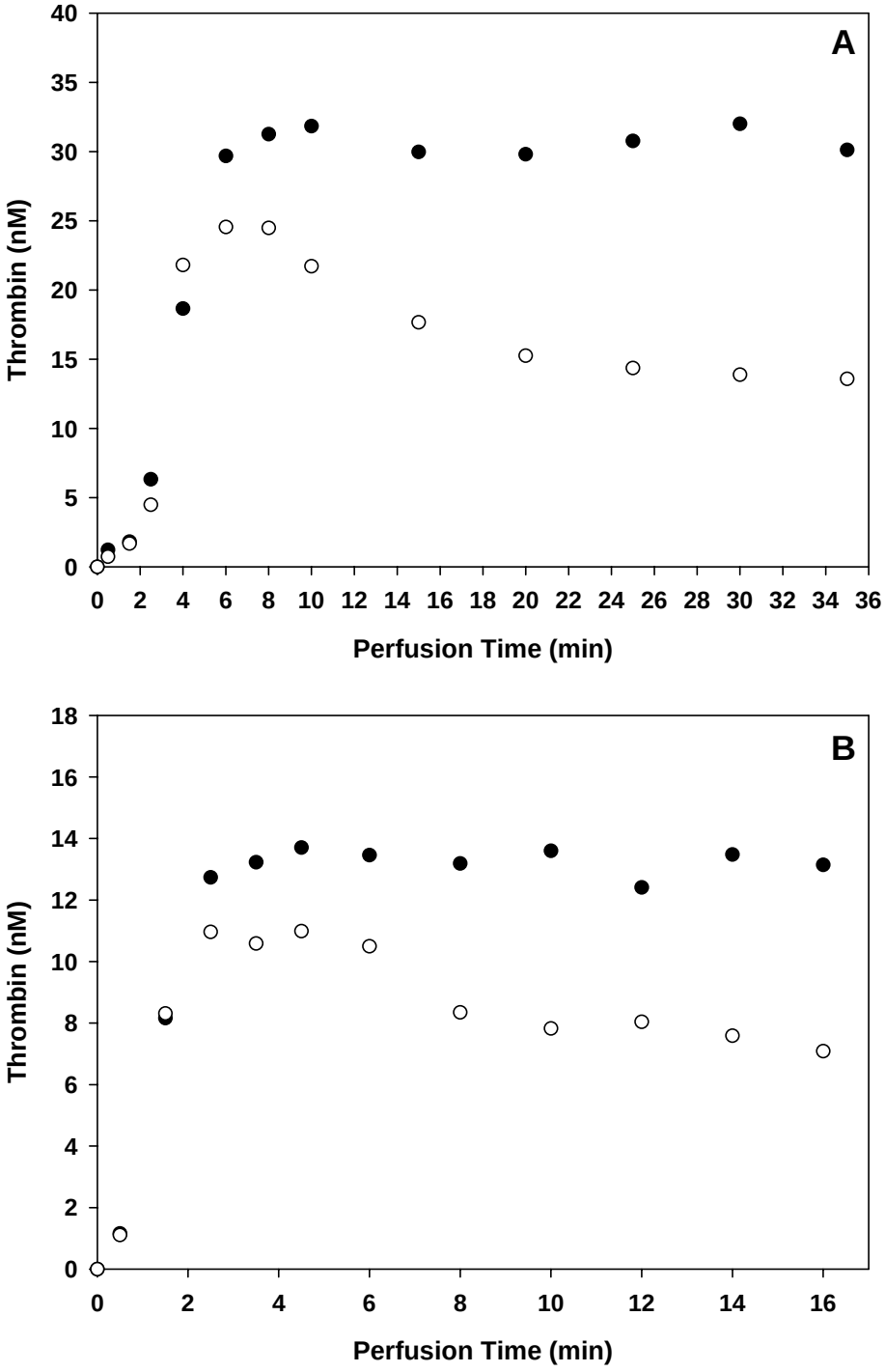

Figure 44 Thrombin generation at the reactor outlet over perfusion time from TF (●) and TF/TM (○) surfaces TF positioned at the upstream at wall shear rates of (A) 50 sec^{-1} (B) 500 sec^{-1}. Each data point represents a mean value (n = 5) with a standard error less than 10% (see Table G1 in Appendix G)

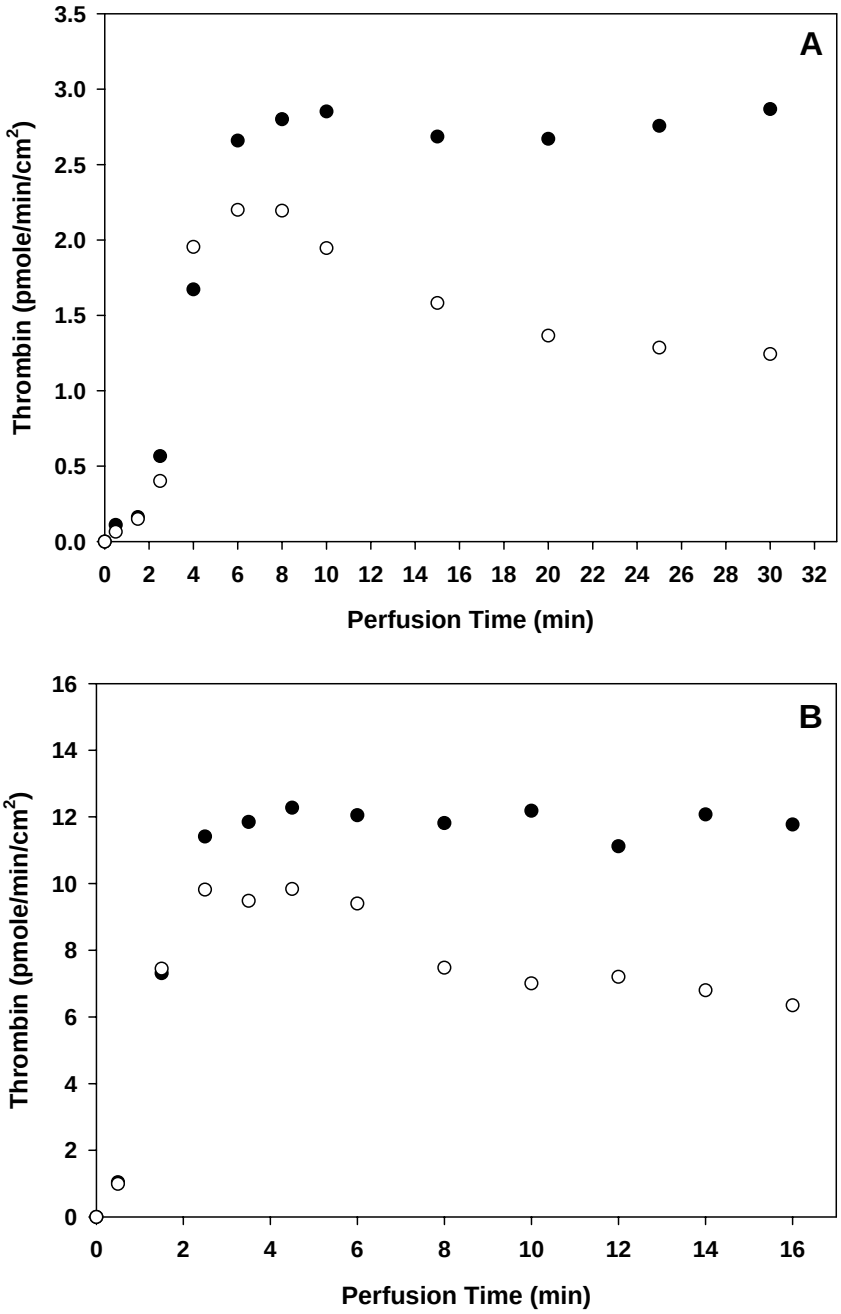

Figure 45 Rate of thrombin generation at the reactor outlet over perfusion time from TF (●) and TF/TM (○)surfaces with TF positioned at the upstream at wall shear rates of (A) 50 sec^{-1} (B) 500 sec^{-1}. Each data point represents a mean value (n = 5) with a standard error less than 10%. Note: rate of reaction = thrombin generation (Figure 42) x flow rate / surface area of reactor (= 0.6 (W, cm) x 3.6 (L, cm) = 2.16 cm^2). (see Table G2 in Appendix G)

Effect of Antithrombin (ATIII) on TF-induced Thrombin Generation

Since physiologic concentration of ATIII ranges from 1.5 to 2.5 μM (152-154), we anticipated that ATIII would have a substantial inhibitory effect on thrombin activity. The effect of ATIII on TF-triggered thrombin generation (TF+AT), was studied using a protein mixture containing 2 μM of ATIII.

Thrombin generation displayed a similar pattern to that of the TF/TM system with lower observed values for $[T]_{max}$ and $[T]_{ss}$ (Fig. 46 & 47, Table 10). When compared to $[T]_{TF\ ss}$ produced by test surfaces containing TF alone, average $[T]_{max}$ and $[T]_{ss}$ at shear rate of 50 sec^{-1} were 35% and 72% lower, respectively, while 29% and 65% lower at a shear rate of 500 sec^{-1}. Moreover, average $[T]_{max}$ and $[T]_{ss}$ were approximately 15% and 20% less than comparable values observed from the TF/TM system.

The initial explosive thrombin generation was not reduced in the presence of ATIII, indicating ATIII is not an efficient inhibitor of TF:VIIa enzyme complex (200). Although ATIII alone is unable to influence the initiation phase of thrombin generation in the presence of low levels of TF:VIIa, ATIII is able to largely reduce even has a potential to completely inhibit thrombin activity afterwards (172). In addition, ATIII is also an inhibitor of factor Xa; with this effect occurring within minutes (172, 200, 201). Although factor Va can protect Xa from inactivation by ATIII (202, 203), inactivation of Xa can still occur prior to V activation and/or prothrombinase complex formation.

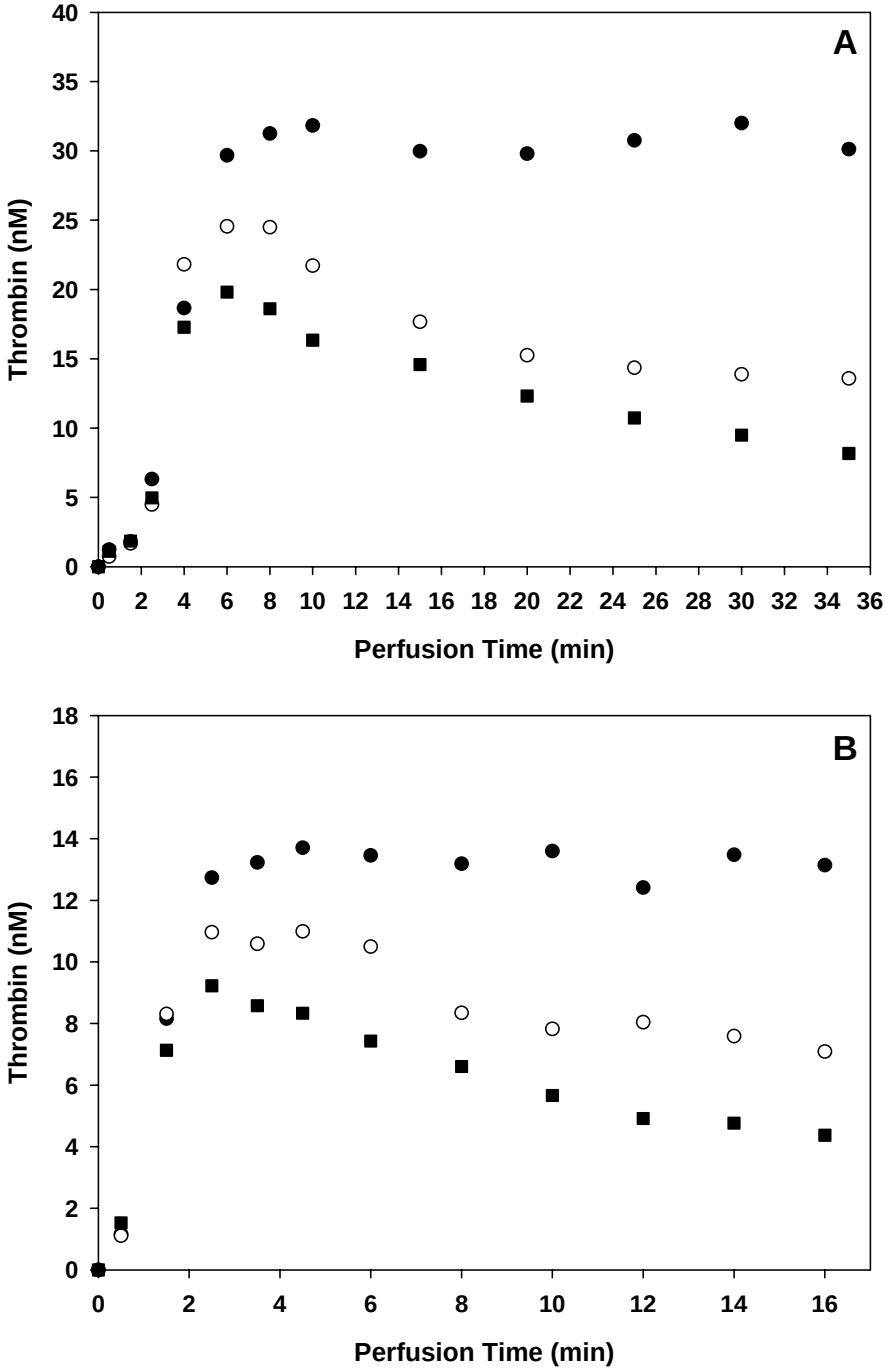

Figure 46 Thrombin generation at the reactor outlet over perfusion time from TF (●), TF/TM (○), and TF+AT (■) surfaces with TF positioned at the upstream at wall shear rates of (A) 50 sec^{-1} (B) 500 sec^{-1}. Each data point represents a mean value (n = 5) with a standard error less than 10%. (see Table G1 in Appendix G1).

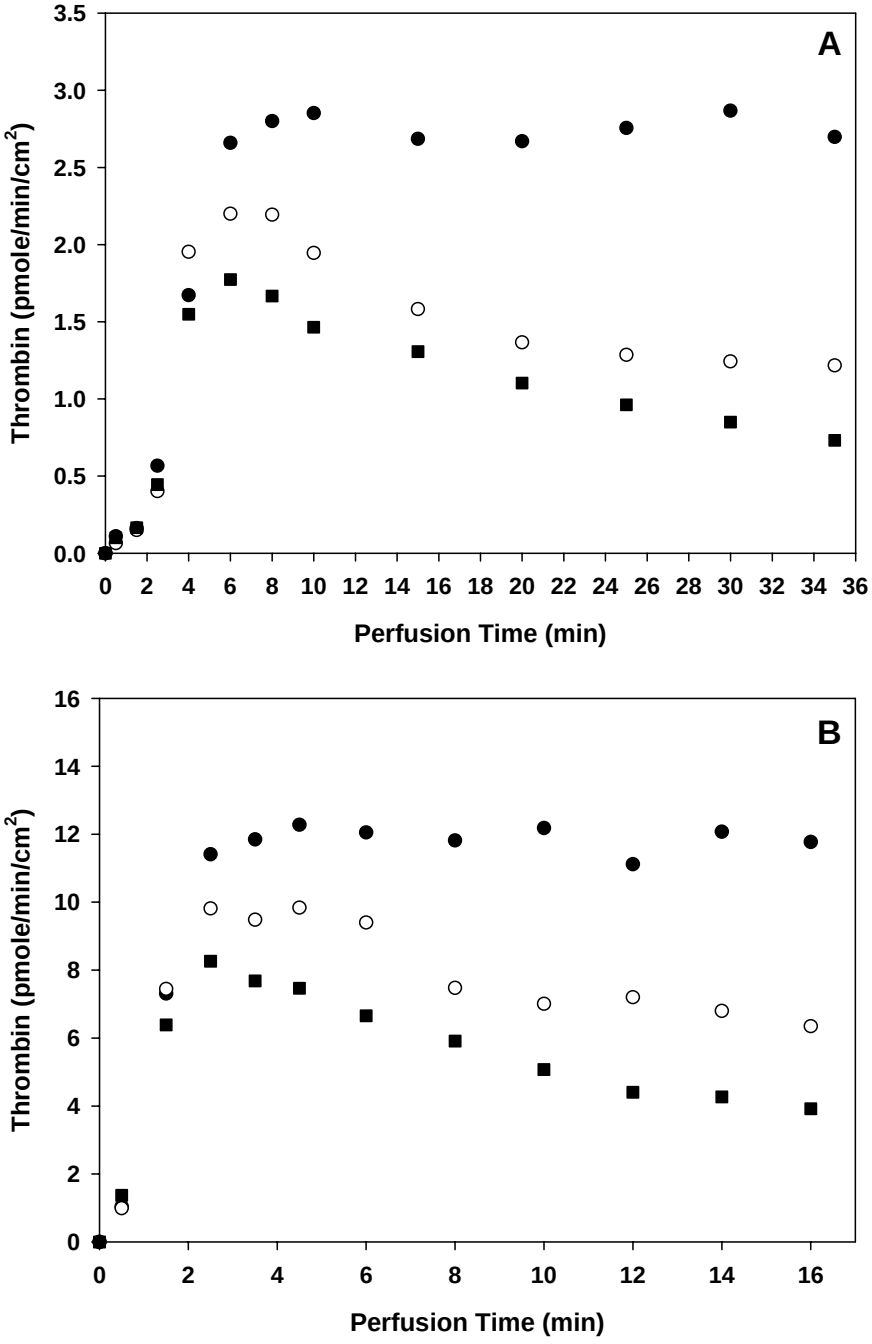

Figure 47 Rate of thrombin generation at the reactor outlet over perfusion time from TF (●), TF/TM (○), and TF+AT (■) surfaces with TF positioned at the upstream at wall shear rates of (A) 50 sec^{-1} (B) 500 sec^{-1}. Each data point represents a mean value (n = 5) with a standard error less than 10% (see Table G2 in Appendix G). Note: rate of reaction = thrombin generation (Figure 44) x flow rate / surface area of reactor (= 0.6 (W, cm) x 3.6 (L, cm) = 2.16 cm^2).

Effects of ATIII and Surface Bound TM on TF-Induced Thrombin Generation

The effect of ATIII and surface bound TM on TF-induced thrombin generation (TF/TM+AT) was studied using the patterned TF/TM surface, as described previously. The presence of TM further reduced thrombin generation when compared to the effect of ATIII alone (Figure 48 & 49). Specifically, average $[T]_{max}$ and $[T]_{ss}$ values were approximately 21% and 14% lower.

It has been noted that ATIII at physiological concentrations decreases the binding of thrombin to TM on endothelial cells and consequently reduces the production of APC (60, 204, 205). However, the rate of inactivation of thrombin by ATIII is stimulated several-fold by the presence of TM (206-208). Despite competitive binding of thrombin between ATIII and TM, we suspect that residual thrombin in the vicinity of the surface has sufficiently high affinity to TM to allow protein C activation to proceed. A reduction in thrombin levels is mediated by direct thrombin inactivation by ATIII, TM-mediated thrombin inactivation by ATIII, and protein C activation. Significantly, the presence of TM promotes a further reduction in thrombin concentration.

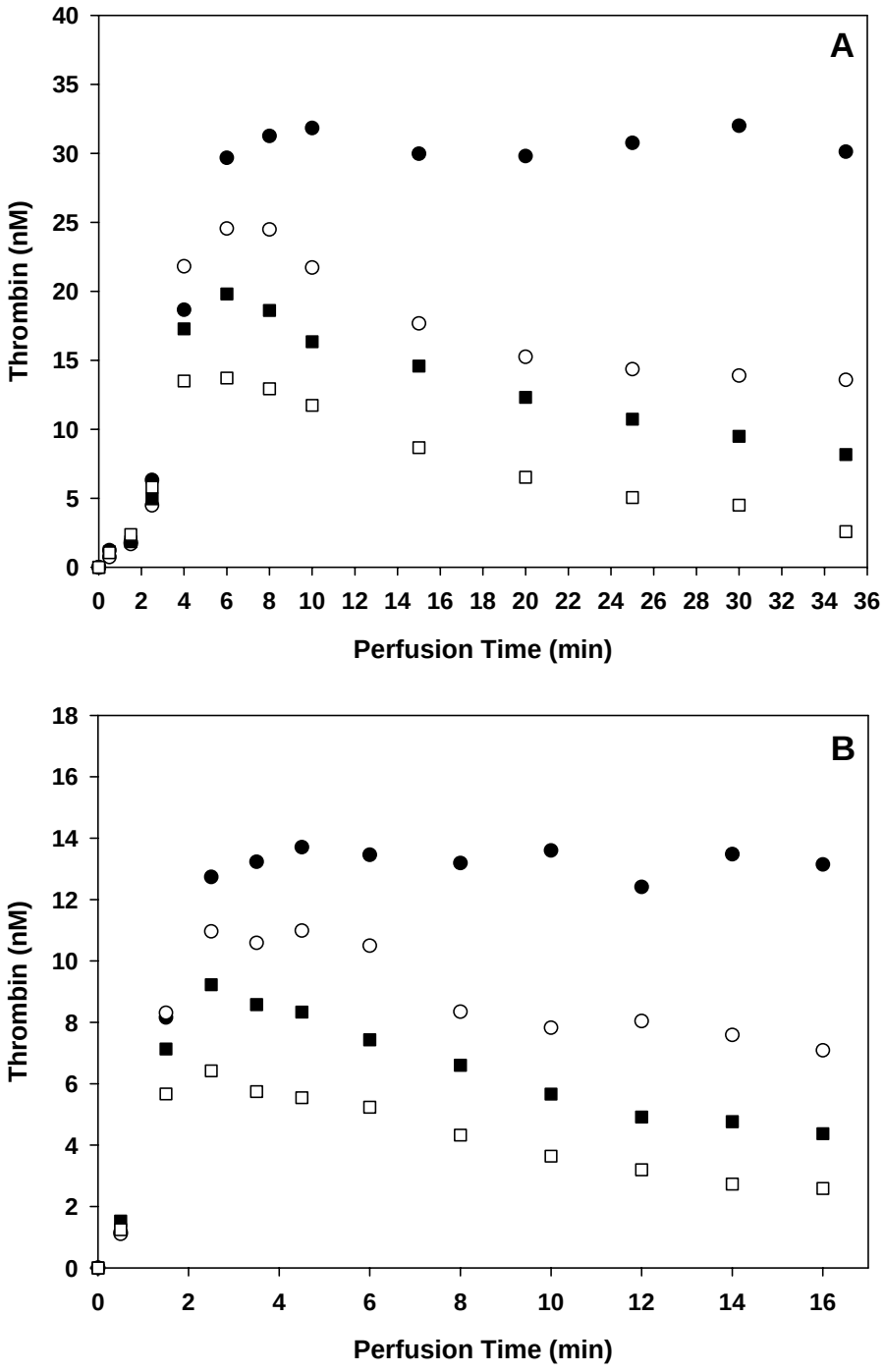

Figure 48 Thrombin generation at the reactor outlet over perfusion time from TF (●), TF/TM (○), TF+AT (■), and TF/TM+AT (□) surfaces with TF positioned at the upstream at wall shear rates of (A) 50 sec^{-1} (B) 500 sec^{-1}. Each data point represents a mean value (n = 5) with a standard error less than 10%. (see Table G1 in Appendix G).

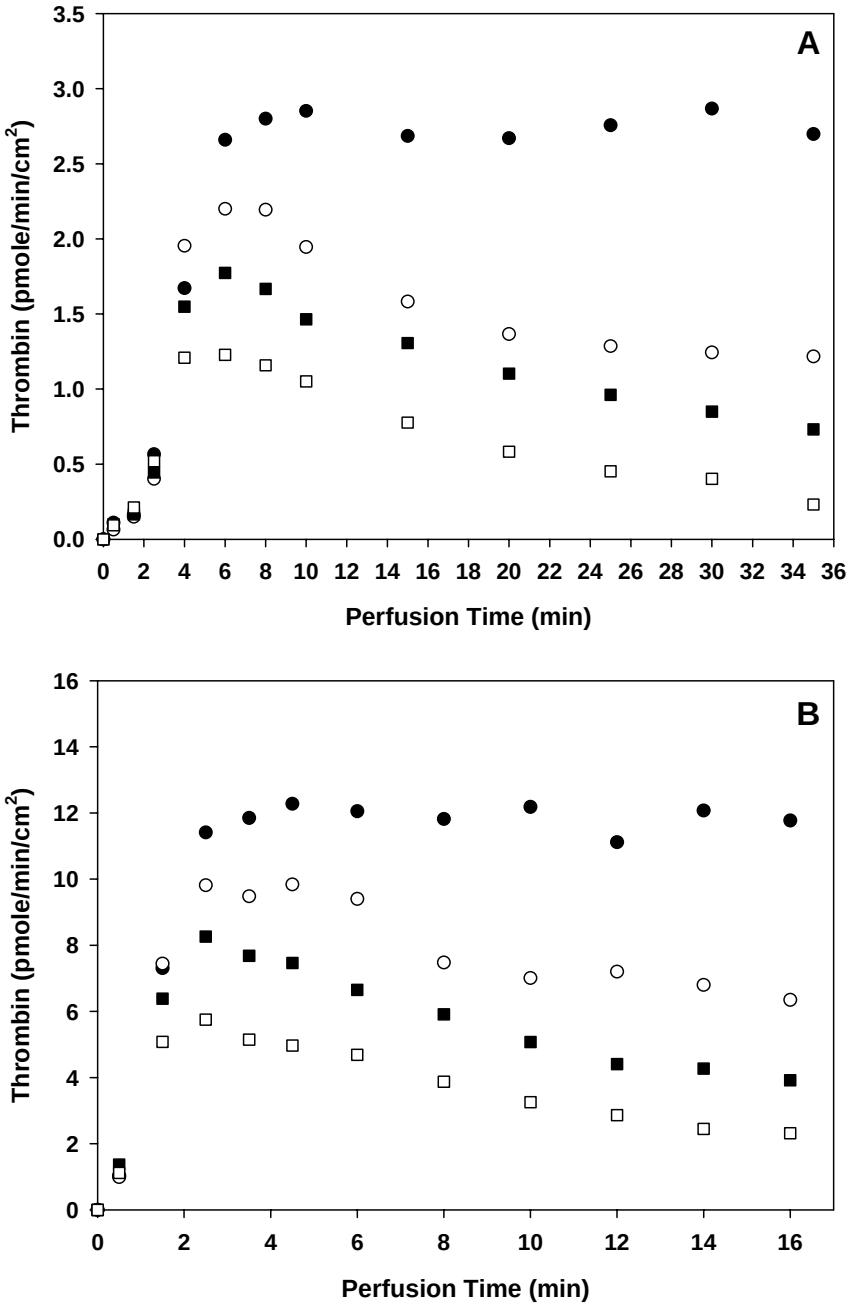

Figure 49 Rate of thrombin generation at the reactor outlet over perfusion time from TF (●),TF/TM (○), TF+AT (■), and TF/TM+AT (□) surfaces with TF positioned at the upstream at wall shear rates of (A) 50 sec^{-1} (B) 500 sec^{-1}. Data points represent mean values (n = 5) with a standard error less than 10%. (see Table G2 in Appendix G). Note: rate of reaction = thrombin generation (Figure 46) x flow rate / surface area of reactor (= 0.6 (W, cm) x 3.6 (L, cm) = 2.16 cm^2).

Effect of Surface Bound Heparin on TF-induced Thrombin Generation

The effect of surface bound heparin on TF-initiated thrombin generation (TF/Heparin) was studied using a protein mixture containing 2 μM ATIII. Test surfaces contained discrete upstream and downstream regions with TF and heparin, respectively. Average $[T]_{max}$ and $[T]_{ss}$ (Fig. 50, 51, Table 10) were reduced by 14% and 22%, respectively, when compared to concentrations observed in systems containing ATIII but without surface bound heparin. Interestingly, thrombin generation from the TF/TM+AT system was lower than that observed from TF/heparin + ATIII. This suggests that, TM may be more effective in inhibition of initial thrombin production than surface bound heparin.

It has been noted that the anticoagulant activity of heparin is a direct result of its ability to greatly (~1000-fold) accelerate the rate at which antithrombin reacts with thrombin (120). In our test system, ATIII has a dominant inhibitory effect on thrombin activity. The presence of surface bound heparin further reduces thrombin generation by at most 10-20%. We suspect that transport limitations associated with the diffusive flux of ATIII and thrombin to surface bound heparin yields a relatively small effect on thrombin inactivation.

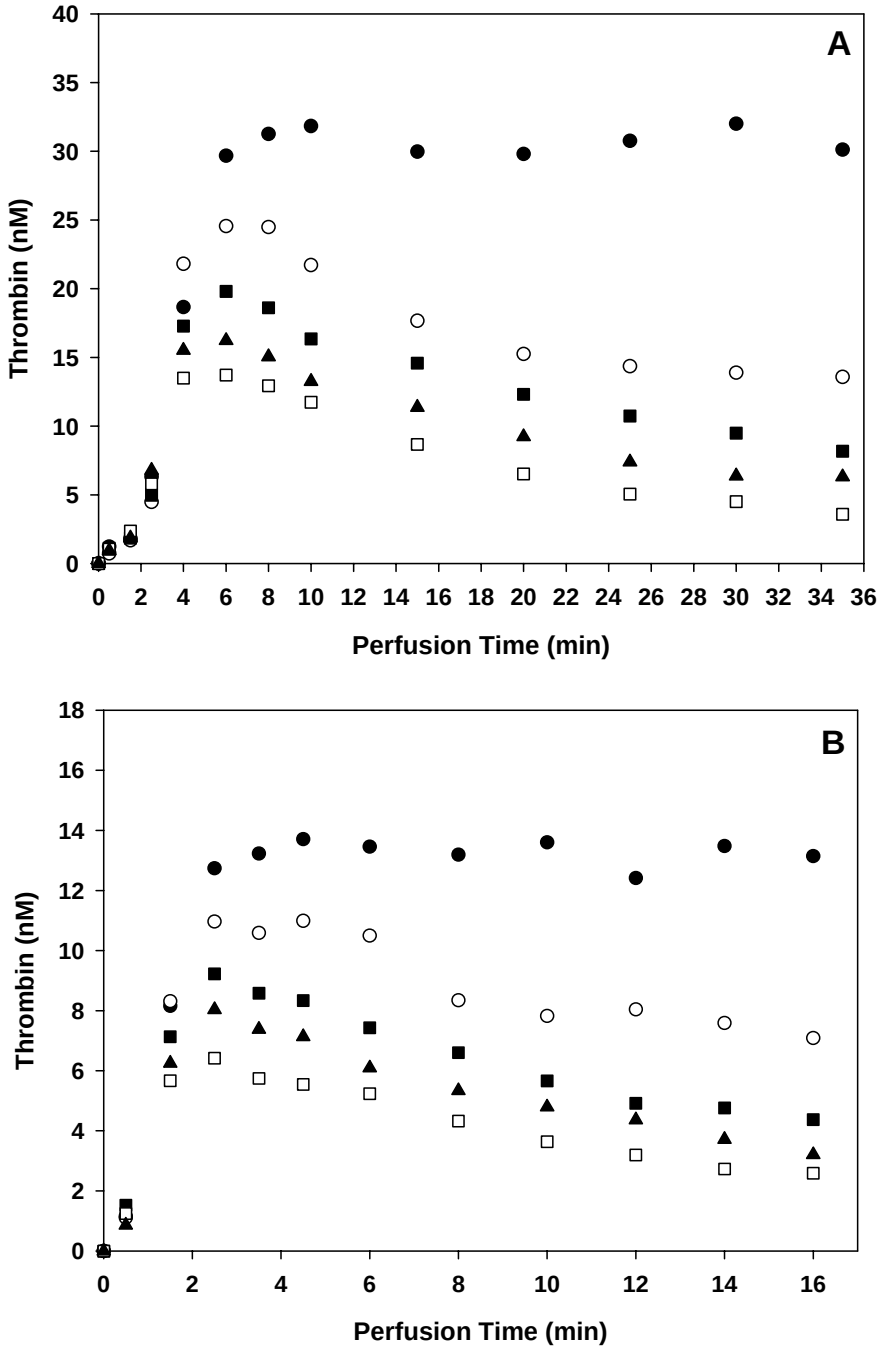

Figure 50 Thrombin generation at the reactor outlet over perfusion time from TF (●),TF/TM (○), TF + ATIII (■), TF/TM + ATIII (□), and TF/Heparin (▲) surfaces with TF positioned at the upstream at wall shear rates of (A) 50 sec^{-1} (B) 500 sec^{-1}. Each data point represents a mean value (n = 5) with a standard error less than 10%. (see Table G1 in Appendix G).

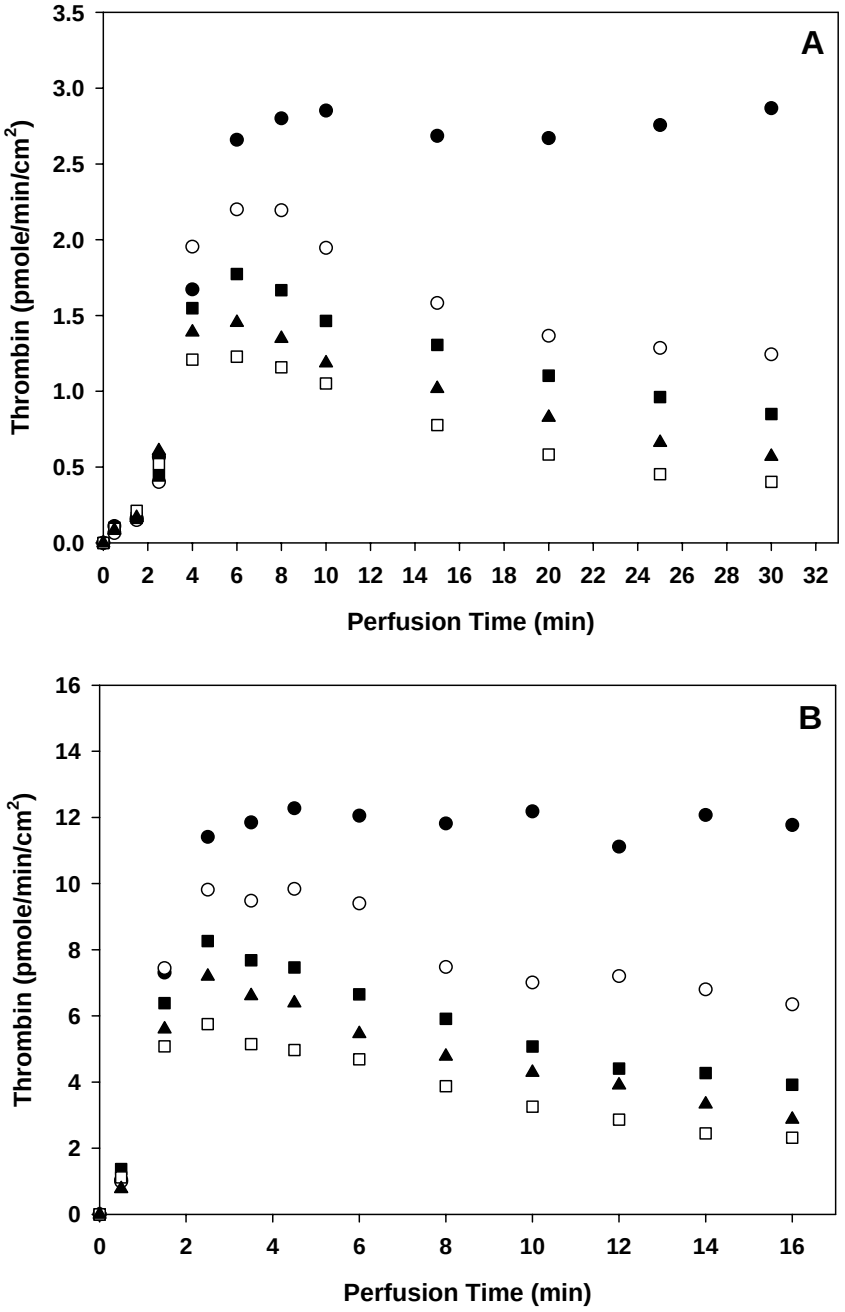

Figure 51 Rate of thrombin generation at the reactor outlet over perfusion time from TF (●),TF/TM (○), TF + ATIII (■), TF/TM + ATIII (□), and TF/Heparin (▲) surfaces with TF positioned at the upstream at wall shear rates of (A) 50 sec^{-1} (B) 500 sec^{-1}. Each data point represents a mean value (n = 5) with a standard error less than 10% (see Table G2 in Appendix G). Note: rate of reaction = thrombin generation (Figure 48) x flow rate / surface area of reactor (= 0.6 (W, cm) x 3.6 (L, cm) = 2.16 cm^2).

Effect of Combined Surface Bound TM and Heparin on TF-Induced Thrombin Generation

The effect of combined surface bound TM and heparin on TF-induced thrombin generation (TF/TM-Heparin) was studied by perfusion of a protein mixture containing ATIII and protein C over test surfaces in which TF was deposited in an upstream region and TM and heparin largely confined to a downstream section. Kinetic data of thrombin responses are presented in Figure 52 and 53.

Average $[T]_{max}$ and $[T]_{ss}$ values were reduced by 55% and 85% (Table 10), respectively, at both shear rates of 50 sec^{-1} and 500 sec^{-1} when compared to concentrations observed in test systems which did not contain either ATIII or surface bound TM or heparin. Moreover, we observed that thrombin generation was considerably lower when compared to systems containing ATIII with (13-15% reduction) or without (20-25% reduction) surface bound heparin.

The combination of both surface bound TM and heparin appears to be the most efficient in inhibiting TF-induced thrombin generation. Indeed, heparin and activated protein C (APC) exhibit significant anticoagulant synergy in plasma (192, 193) due to three mechanisms: heparin enhancement of ATIII-dependent inactivation of thrombin and factor Va, the inactivation of factor Va by APC, and the inactivation of factor V and Va enhanced by heparin and/or APC. Average $[T]_{max}$ and $[T]_{ss}$ values (Figure 54) suggested that efficiency of thrombin inactivation is in the order of TF/TM-Heparin > TF/TM+AT > TF/Heparin > TF+AT.

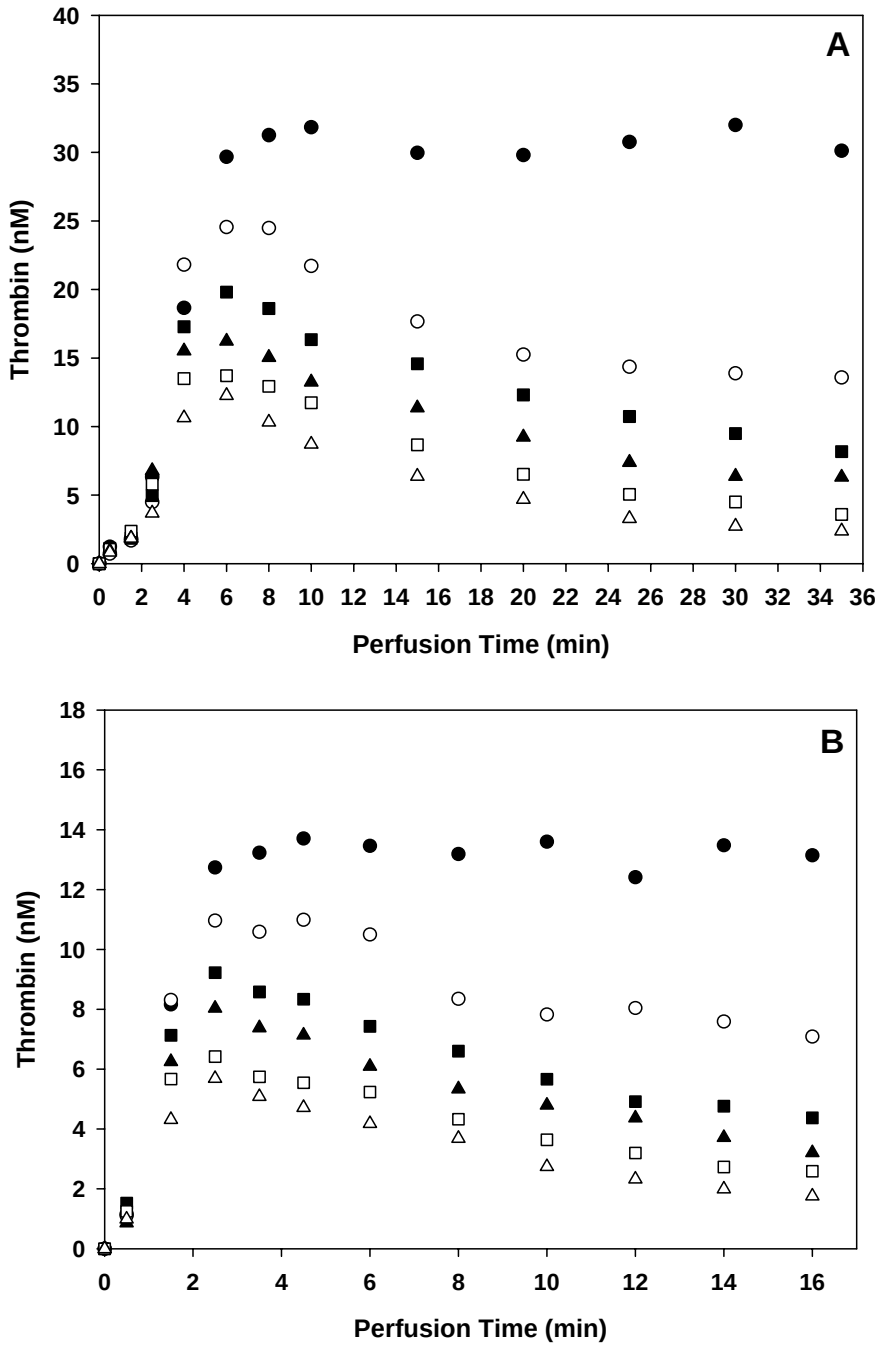

Figure 52 Thrombin generation at the reactor outlet over perfusion time from TF (●),TF/TM (○), TF + AT (■),TF/TM + AT (□), TF/Heparin (▲), and TF/TM-heparin (Δ) surfaces with TF positioned at the upstream at wall shear rates of (A) 50 sec^{-1} (B) 500 sec^{-1}. Each data point represents a mean value (n = 5) with a standard error less than 10% (see Table G1 in Appendix G).

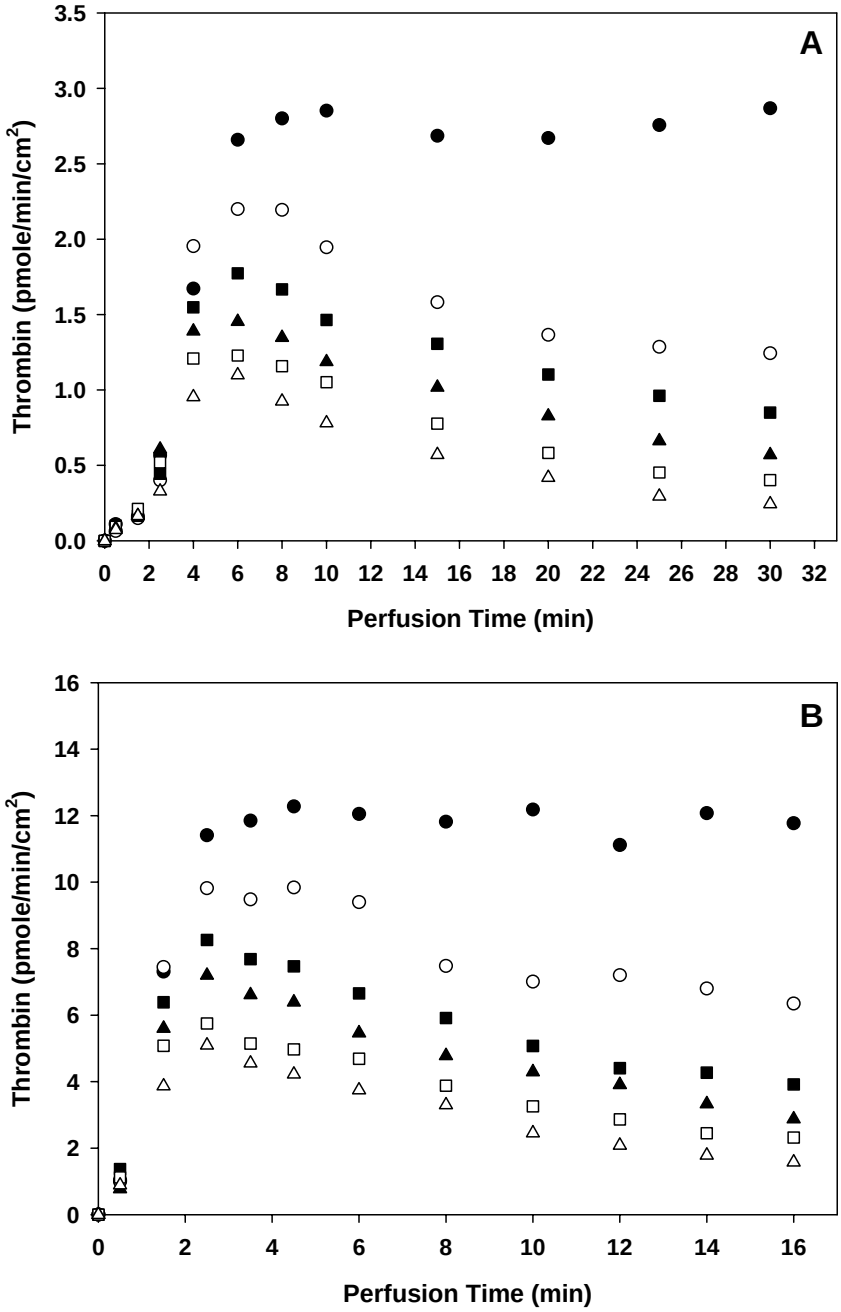

Figure 53 Rate of thrombin generation at the reactor outlet over perfusion time from TF (●),TF/TM (○), TF + ATIII (■), TF/TM + ATIII (□), TF/Heparin (▲), and TF/TM-heparin (Δ) surfaces with TF positioned at the upstream at wall shear rates of (A) 50 sec^{-1} (B) 500 sec^{-1}. Each data point represents a mean value (n = 5) with a standard error less than 10% (see Table G2 in Appendix G). Note: rate of reaction = thrombin generation (Figure 31) x flow rate / surface area of reactor (= 0.6 (W, cm) x 3.6 (L, cm) = 2.16 cm^2).

Since physiologic level of ATIII has dramatic impact on thrombin generation from TF surface, we examined all systems containing ATIII in order to differentiate the effect on inhibition of thrombin generation in the presence of surface TM and heparin. Specifically, equality of mean values of $[T]_{max}$ and $[T]_{ss}$ among TF+AT, TF/TM+AT, TF/Heparin, and TF/TM-Heparin were statistically analyzed using the F test from the analysis of variance (ANOVA) (Appendix H) (209). The test results concluded that not all mean values of $[T]_{max}$ and $[T]_{ss}$ are equal. The probability of a type I error, which is probability of accepting the null hypothesis, is less than 0.001 according to F-test results. Then we further determined the significance of the presence of surface bound TM and/or heparin using the Tukey multiple comparison procedure (Appendix I) (209). This procedure is commonly used for pairwise comparison and is a preferred method to give narrower confidence limits than others such as Scheffé and Bonferroni procedures. For example, in Bonferroni procedure, one can form m simultaneous confidence intervals for an overall confidence level 1- α, leading to an individual level 1- α/m. Consequently, the half-width of confidence intervals is enlarged to cause wider confidence limits.

Results of comprehensive analyses are summarized in Table 11. We found that the addition of surface bound TM induced a statistically significant ($P < 0.05$) reduction in both $[T]_{max}$ and $[T]_{ss}$ when compared to systems containing ATIII or heparin alone (Figure 54, 55). In contrast, the effect of adding surface bound heparin on $[T]_{max}$ and $[T]_{ss}$ was statistically insignificant ($P < 0.2$) when compared to systems, which already contained ATIII or surface bound TM. These results indicate that a membrane-mimetic film containing TM will likely have a greater antithrombogenic capacity than current

commercially available heparinized surface due to the capacity to actively inhibit thrombin generation rather than inactivate thrombin after it has already been produced.

We found that the addition of surface bound TM induced a statistically significant reduction in both $[T]_{max}$ and $[T]_{ss}$ when compared to systems containing ATIII or heparin alone. In contrast, the effect of adding surface bound heparin on $[T]_{max}$ and $[T]_{ss}$ was statistically insignificant when compared to systems, which already contained ATIII or surface bound TM. These results indicate that a membrane-mimetic film containing TM will likely have a greater antithrombogenic capacity than current commercially available heparinized surface due to its capacity to actively inhibit thrombin generation rather than inactivate thrombin after it has already been produced.

Table 10 Summary of thrombin responses from a variety of surface systems, including maximum thrombin generation ($[T]_{max}$, nM) and rate of reaction (RT_{max}, pmole/min/cm^2), steady state thrombin generation ($[T]_{ss}$, nM) and rate of reaction (RT_{ss}, pmole/min/cm^2), and drop % of thrombin generation (mean value comparison of $[T]_{max}$ or $[T]_{ss}$ with respect to $[T]_{TFss}$). Each data value for $[T]_{max}$, RT_{max}, $[T]_{ss}$, and RT_{ss} is presented as mean ± standard deviation (n = 5).

50 sec^{-1}	Surface Systems For Flow Studies					
	TF	TF/TM	TF+AT	TF/TM+AT	TF/Heparin	TF/TM-Heparin
$[T]_{max}$	29.76 ± 1.98	24.55 ± 1.88	19.26 ± 1.73	13.86 ± 1.26	16.38 ± 0.92	12.94 ± 0.84
RT_{max}	2.67 ± 0.27	2.20 ± 0.17	1.77 ± 0.18	1.23 ± 0.15	1.45 ± 0.11	1.10 ± 0.08
drop %	0	18	35	54	45	57
$[T]_{ss}$	29.76 ± 1.98	13.88 ± 1.95	8.45 ± 0.73	3.88 ± 1.03	6.29 ± 1.07	2.65 ± 1.16
RT_{ss}	2.67 ± 0.27	1.24 ± 0.18	0.75 ± 0.10	0.37 ± 0.06	0.62 ± 0.09	0.24 ± 0.06
drop %	0	53	72	86	77	91

500 sec^{-1}	Surface Systems For Flow Studies					
	TF	TF/TM	TF+AT	TF/TM+AT	TF/Heparin	TF/TM-Heparin
$[T]_{max}$	12.98 ± 1.69	10.98 ± 1.34	9.30 ± 0.98	6.59 ± 0.63	8.12 ± 0.89	5.74 ± 0.27
RT_{max}	11.63± 1.55	9.84 ± 1.20	8.26 ± 0.92	5.75 ± 0.70	7.20 ± 0.90	5.10 ± 0.53
drop %	0	16	29	51	38	56
$[T]_{ss}$	12.98 ± 1.69	7.18 ± 0.87	4.59 ± 0.94	2.70 ± 0.46	3.36 ± 0.54	1.92 ± 0.53
RT_{ss}	11.63± 1.55	6.42 ± 0.78	4.11 ± 0.84	2.42 ± 0.41	3.01± 0.58	1.72 ± 0.49
drop %	0	45	65	79	74	85

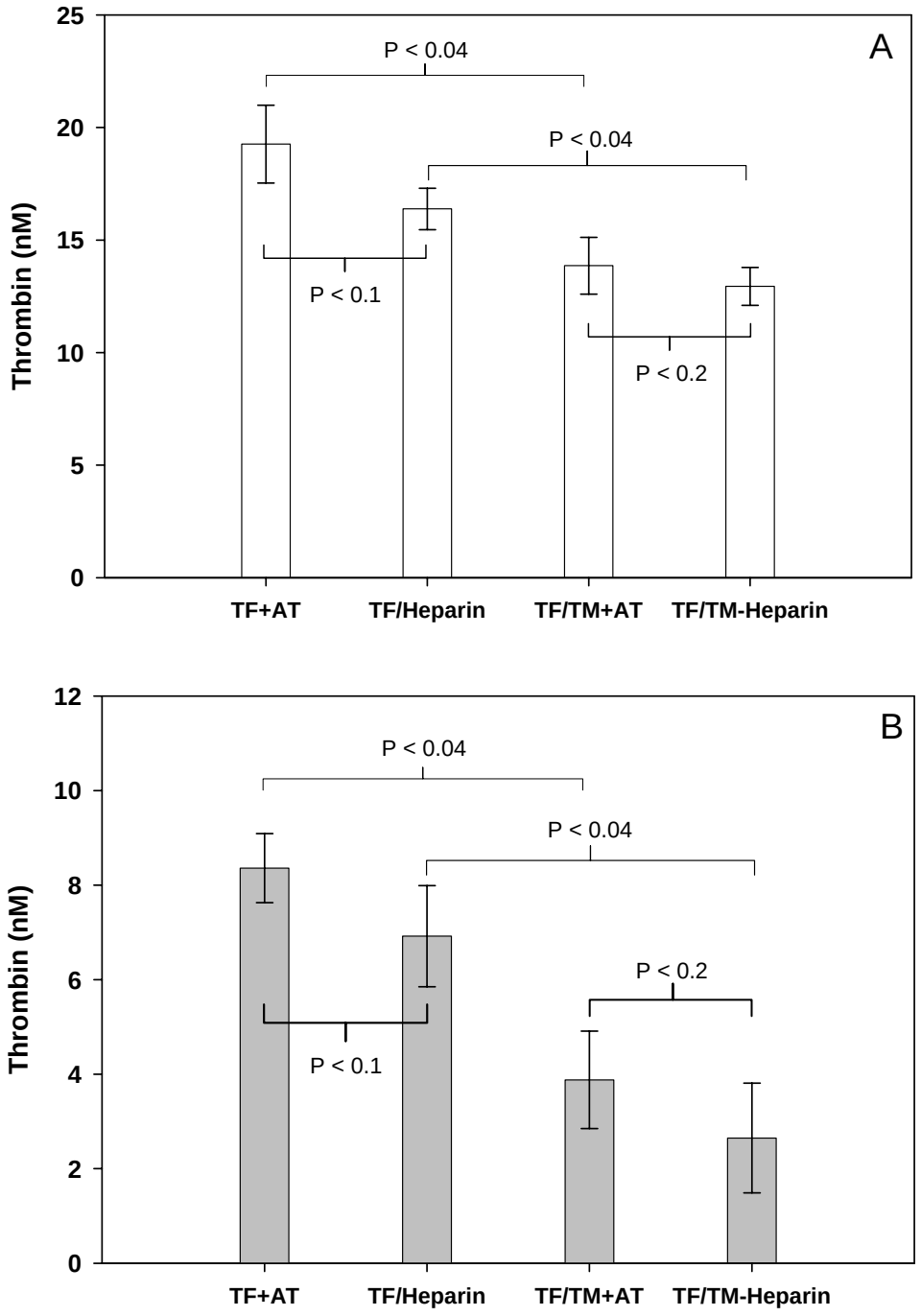

Figure 54 Thrombin responses at (A) peak ([T]max, nM) and (B) steady state ([T]ss, nM) levels from TF surfaces in the presence of ATIII only (TF+AT), surface heparin (TF/Heparin), surface TM (TF/TM+AT) and both surface heparin and TM (TF/TM-Heparin) at shear rates of 50 sec^{-1}. P values are analyzed from comparisons between surfaces in the absence and presence of TM (TF+AT vs. TF/TM+AT and TF/Heparin vs. TF/TM-Heparin), and between surfaces in the absence and presence of heparin, (TF+AT vs. TF/Heparin and TF/TM+AT vs. TF/TM-Heparin). The error bars represent standard deviation (n = 5).

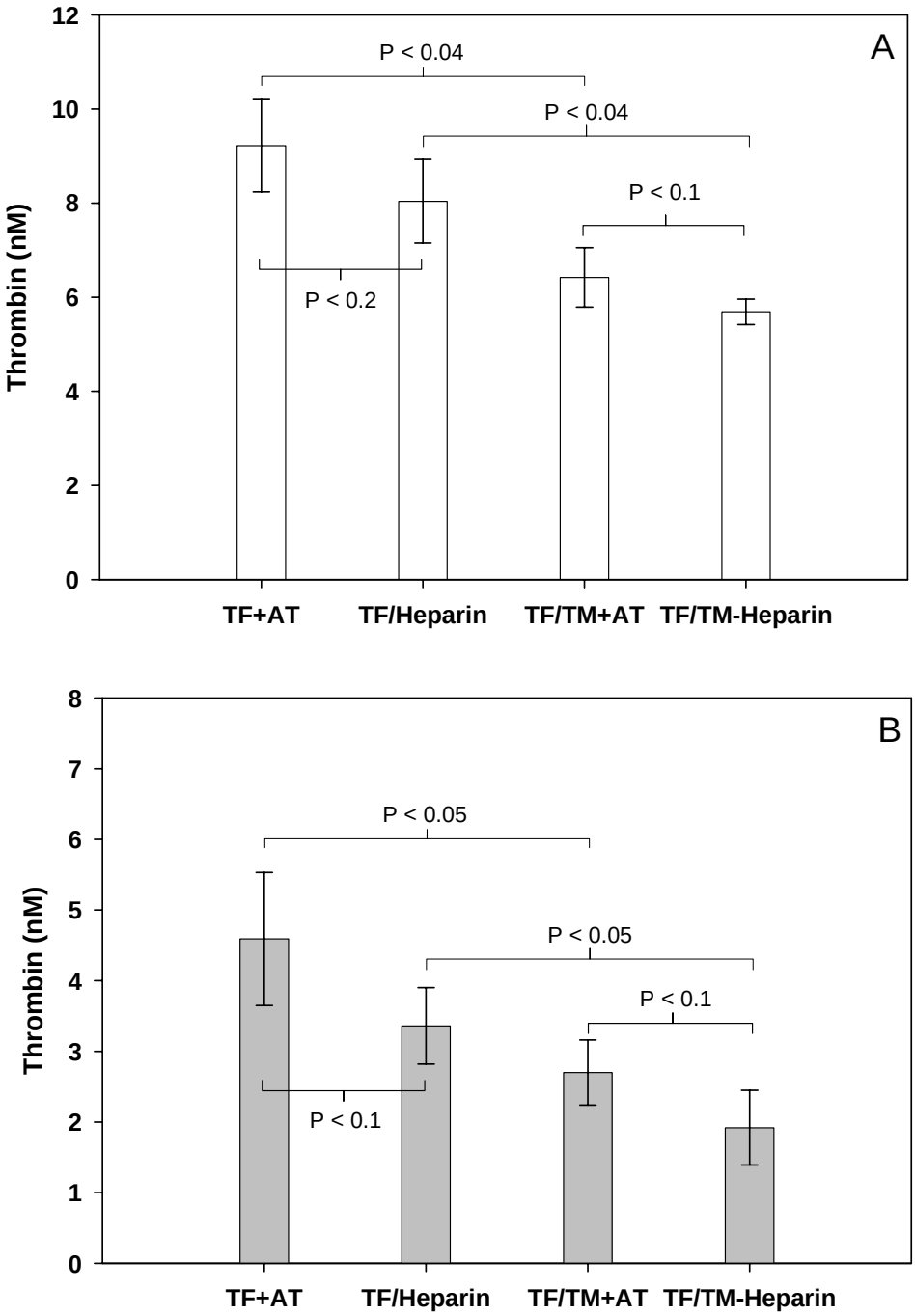

Figure 55 Thrombin responses at (A) peak ([T]max, nM) and (B) steady state ([T]ss, nM) levels from TF surfaces in the presence of ATIII only (TF+AT), surface heparin (TF/Heparin), surface TM (TF/TM+AT) and both surface heparin and TM (TF/TM-Heparin) at shear rates of 500 sec^{-1}. P values are analyzed from comparisons between surfaces in the absence and presence of TM (TF+AT vs. TF/TM+AT and TF/Heparin vs. TF/TM-Heparin), and between surfaces in the absence and presence of heparin, (TF+AT vs. TF/Heparin and TF/TM+AT vs. TF/TM-Heparin). The error bars represent standard deviation (n = 5).

Table 11 Comparisons of transient peak ([T]max) and steady state ([T]ss) using ANOVA with Tukey multiple comparison procedure between test surfaces in the absence and presence of TM (TF+AT vs. TF/TM+AT and TF/Heparin vs. TF/TM-Heparin), and between test surfaces in the absence and presence of heparin, (TF+AT vs. TF/Heparin and TF/TM+AT vs. TF/TM-Heparin). Confidence intervals (C.I.) indicate whether the comparison of [T]max is significantly different or not for confidence coefficient of 95 percent. A value of $P < 0.05$ was used to define statistical significance.

$[T]_{max}$, 50 sec^{-1}	TF+AT		TF/TM-Heparin	
TF/TM+AT	C.I.		C.I.	
	0.48	10.32	-0.81	2.65
	p value < 0.04		p value < 0.2	
TF/Heparin	C.I.		C.I.	
	-0.21	5.98	0.36	6.52
	p value < 0.1		p value < 0.04	

$[T]_{max}$, 500 sec^{-1}	TF+AT		TF/TM-Heparin	
TF/TM+AT	C.I.		C.I.	
	0.194	5.220	-0.141	1.845
	p value < 0.04		p value < 0.1	
TF/Heparin	C.I.		C.I.	
	-0.489	2.845	0.217	4.543
	p value < 0.2		p value < 0.04	

$[T]_{ss}$, 50 sec^{-1}	TF+AT		TF/TM-Heparin	
TF/TM+AT	C.I.		C.I.	
	0.345	8.256	-0.390	3.413
	p value < 0.04		p value < 0.2	
TF/Heparin	C.I.		C.I.	
	-0.073	2.958	0.527	8.020
	p value < 0.1		p value < 0.04	

$[T]_{ss}$, 500 sec^{-1}	TF+AT		TF/TM-Heparin	
TF/TM+AT	C.I.		C.I.	
	0.012	3.772	-0.187	1.739
	p value < 0.05		p value < 0.1	
TF/Heparin	C.I.		C.I.	
	-0.270	2.733	0.027	2.846
	p value < 0.1		p value < 0.05	

Effects of Mass Transfer on Thrombin Response In the Presence of Inhibitors

According to the experimental conditions, the reactions occurring under flow involve more than twenty steps (Scheme I) (14, 106, 178). Concentrations and transport rates of the coagulation proteins to and from bulk fluid and a catalytically active surface can in principle be derived from various forms of mass balances according to Navier-Stokes and continuity equations in mass transport coupled with reaction rates (210). Complete treatment of transport with surface reaction leads to an intractable set of nonlinear differential equations. Thus, we simplified our analysis using mass transfer coefficients and kinetic constants derived from previous studies (102, 103, 210-213) in order to interpret the results of our experimental studies.

It has been recognized that the most cases of interest transport resistance resides entirely within a thin concentration boundary layer (the Lévêque regime) (210-213), Characteristically, the concentration changes within the boundary layer are much more significant than those taking place in the bulk. Generally, the concentration boundary layer thickness (δ) is dependent of time (t) and longitudinal distance (x) from inlet of the flow system. Since δ is related to mass transfer coefficient (k_L: cm/sec), $k_L = D/\delta$ (D: diffusion coefficient, cm^2/sec), k_L is also a function of x and t. At the time of initial reaction, for example, the activation of factor X by TF:VIIa complex near $t = 0$, there is no transport resistance ($k_L \sim \infty$) due to the absence of boundary layer formation.

$TF + VIIa \leftrightarrow TF:VIIa$ (1)
$TF + VII \leftrightarrow TF:VII \rightarrow TF:VIIa$ (2)
$IX+TF:VIIa \leftrightarrow IX.TF:VIIa \rightarrow TF:VIIa+IXa$ (3)
$X+TF:VIIa \leftrightarrow X.TF:VIIa \rightarrow TF:VIIa+Xa$ (4)
$X + VIIIa:IXa \leftrightarrow X:VIIIa:IXa \rightarrow VIIIa:IXa + Xa$ (5)
$IX + X\ a \rightarrow X\ a + IXa$ (6)
$VIII + Xa \rightarrow Xa + VIIIa$ (7)
$V + Xa \rightarrow Xa + Va$ (8)
$V + IIa \rightarrow IIa + Va$ (9)
$VIII + IIa \rightarrow IIa + VIIIa$ (10)
$II + Va:Xa \leftrightarrow II:Va:Xa \rightarrow Va:Xa + mIIa$ (11)
$mIIa + Va:Xa \rightarrow Va.Xa + IIa$ (12)
$VIIIa + IXa \leftrightarrow VIIIa:IXa$ (13)
$Va+Xa \leftrightarrow Va:Xa$ (14)
$ATIII + Xa \leftrightarrow ATIII:Xa \rightarrow ATIII + Xai$ (15)
$ATIII + IIa \leftrightarrow ATIII:IIa \rightarrow ATIII + IIai$ (16)
$H + ATII \leftrightarrow H:ATIII$ (17)
$H:ATIII + Xa \leftrightarrow H:ATIII:Xa \rightarrow H:ATIII + Xa_i$ (18)
$H:ATIII + IIa \leftrightarrow H:ATIII:IIa \rightarrow H:ATIII + IIa_i$ (19)
$IIa + TM \leftrightarrow IIa:TM$ (20)
$PC + IIa:TM \leftrightarrow PC:IIa:TM \rightarrow IIa:TM + APC$ (21)
$APC + Va \leftrightarrow APC:Va \rightarrow APC + Va_i$ (22)
$APC + VIIIa \leftrightarrow APC:VIIIa \rightarrow APC + VIIIa_i$ (23)
$H + APC + V \leftrightarrow H:APC:V \rightarrow H:APC + V_i$ (24)

Roman numeral numbers: coagulation factors, subscript i: inactive form, II: prothrombin, IIa: thrombin, APC: activated protein C, H: heparin, PC: protein C, TF: tissue factor, TM: thrombomodulin.

Scheme I. Relevant reactions in regulation of blood coagulation

However, immediately after the initiation of the reactive event, k_L diminishes and δ increases rapidly and both reach steady state values, characteristic of a fully developed regime, within seconds (210). At this point, it is assumed that changes in k_L and δ with time are negligible. Under steady state conditions, δ is expressed as a function of x

$$\delta \approx \left(\frac{6xD}{\gamma_w} \right)^{1/3}$$

where L is length of the reactor (cm), γ_w is wall shear rate (sec^{-1}), x is distance from inlet (cm), and D is diffusivity (cm^2/sec).

Since δ is relatively small within a few millimeters from the inlet of the reactor, mass transport resistance is less in those areas. This may explain why rapid TF-initiated reactions occur for thrombin generation. From the expression of δ as a function of x, average boundary layer thickness (δ_{av}) becomes

$$\delta_{av} \approx 0.75 \left(\frac{6DL}{\gamma_w} \right)^{1/3}$$

In turn, given the geometry of the flow system and flow conditions, average mass transfer coefficient k_L (= D/δ_{av}) can be obtained. The higher the shear rate, the larger the mass transfer coefficient, which will cause a more rapid surface reaction (less effect of diffusion) and shorter induction period for thrombin generation (211).

In the classic Micahelis-Menten form, the Micahelis constant (K_m) represents the inherent kinetic property of an enzyme. However, in the case of immobilized enzymatic reactions under flow, an apparent Michaelis constant ($K_m$app) is used to replace K_m in the Michaelis-Menten equation, so as to incorporate transport effects. Specifically, Laidler et al. (102, 103) suggested that the apparent Michaelis constant vary with the reciprocal

cubic rot of the flow rate, indicating that $K_m$app is smaller at higher shear flow and consequently the rates of reaction is larger.

Net thrombin production is the result of a mass balance involving the transport of relevant coagulation proteins to/from reactive surface, reaction kinetics including activation of factor X by TF, positive feedback reactions catalyzed by tenase (IXa:VIIIa complex) and prothrombinase (Xa:Va complex), and negative feedback reactions including direct inactivation by antithrombin either alone or catalyzed by surface bound heparin, and surface bound TM-induced protein C activation. The general expression (210-212) for a set of differential equations can be presented as:

$$\frac{\delta}{2}\frac{d[P]}{dt} = k_L([P_0] - [P]) + \Sigma \pm R_P$$

where $[P_0]$ and $[P]$ are the protein concentrations in the bulk and at the surface, respectively, k_L is the mass transfer coefficient and R_P is the rate of enzymatic reaction. Model simulations of thrombin dynamics (211, 212) for common pathway of coagulation in the presence of antithrombin have revealed rapid initial thrombin generation, followed by transient maximum and subsequent steady state at a slightly lower level than the peak thrombin generation. These results are similar to our experimental observations with the exception that surface bound TM and heparin reduce both peak and steady state thrombin concentrations. The TM effect appears greater than heparin, although as complementary negative feedback systems the combined effect of both factors had the greatest impact. Numerical modeling studies of this system are ongoing and will be reported in a subsequent publication.

6.5 CONCLUSIONS

A vascular injury site was mimicked by fabricating membrane-mimetic assemblies containing tissue factor on a planar supporting substrate. Relipidated TF vesicles were tethered onto a membrane-mimetic thin film by a dip-coating process. Thrombin generation initiated by TF with surface density ranging from approximately 9 to 90 fmole/cm^2 was investigated by perfusion of a coagulation protein mixture over test surfaces at shear rates of 50 sec^{-1} and 500 sec^{-1}. Our results showed that thrombin production was initially rapid and then reached a steady state level. Steady state thrombin generation did not significantly increase in the presence of TF density more than 51.2 fmole/cm^2, indicating a transport limiting effect in the reaction. This TF surface density was selected to investigate effect of surface bound TM and heparin on thrombin production under flow.

In the presence of surface anticoagulants, kinetics of thrombin generation featured a rapid induction phase and a transient maximum that was followed by a gradual decrease to a steady state level. Initial thrombin production could not be completely inhibited, which is likely a result of minimal transport resistance for surface bound TF-mediated extrinsic coagulation pathway activation. However, peak and steady state values of thrombin were decreased by ATIII and surface bound heparin and TM. At physiologic concentrations of ATIII, thrombin activity was profoundly inhibited. Nonetheless, surface bound TM and heparin appear to have the potential to completely shut down thrombin generation. In particular, surface bound TM was superior to heparin in reducing thrombin generation. Admittedly, limitations of an experimental approach, which utilizes an artificial plasma protein solution, include the presence of existing natural inhibitors in

plasma or blood that could compromise the anticoagulant capacities of surface bound TM and heparin. For example, heparin can be inhibited by platelet factor 4 or potentially cleaved by endogenous heparanases and two serpins, α1-antitrypsin and the protein C inhibitor (PCI) are capable of inactivating APC. Of interest, PCI-catalyzed inhibition of APC can be enhanced when APC binds to heparin or heparan sulfate (214).

CHAPTER 7

DISCUSSION

Over the years, a substantial amount of research in designing nonthrombogenic surfaces has been performed to improve the biocompatibility of synthetic materials in contact with blood. Pharmacologically active compounds have been recognized and incorporated on surfaces as a design approach. Specifically, heparinization of artificial surfaces has been shown to be a successful strategy to prevent thrombus formation. For example, covalent bonding of nitrite-degraded heparin onto membrane oxygenators and tubings has made it possible to maintain a long-lasting extracorporeal circulation without systemic heparinization (53). It has been reported that the thrombogenic collagen becomes more thromboresistant in the presence of immobilized heparin (215). However, studies in animal or human models have demonstrated that heparin fails to prevent thrombosis (83, 216, 217) possibly due to the ineffectiveness of heparin/antithrombin III in preventing thrombin-induced platelet deposition. In addition, the findings of heparin limiting the spread of thrombus from the site of occlusion, lowering embolism recurrence, and reduceing mortality after prolonged treatment have been disputed (218). These have motivated us to design other potent antithrombogenic agent-immobilized surfaces.

There is growing evidence that the transmembrane protein thrombomodulin (TM) triggering the protein C pathway represents the major anticoagulant mechanism that is operative in both normal and injured blood vessels under physiologic conditions *in vivo* (84), which led to immobilization of TM as a antithrombogenic system. Several investigators have described the direct immobilization of thrombomodulin onto

polymeric surfaces in order to generate thromboresistant materials for blood contacting applications (54-59, 85, 86). Although these studies confirm that substrate bound TM has the potential to limit thrombus formation on synthetic surfaces, reduction in TM bioactivity was observed as evident by protein C activation rates, which were three orders of magnitude less than those when TM is evaluated as a component of either lipid vesicles or the endothelial cell surface. This emphasizes the importance of lipid membrane as an essential cofactor for protein bioactivity, leading to the design of membrane-mimetic systems incorporating biological substrates that can exhibit activities to mimic the functions of physiological regulators for blood coagulation.

In order to create membrane-membrane assemblies, we have developed an *in-situ* polymerization strategy using monoacrylate phospholipids as a means of stabilizing a self-assembled lipid monolayer on an alkylated surface supported by a hydrophilic polymeric cushion (77, 94, 219), and such a system showed limited thrombus formation and neointimal hyperplasia short term in vivo assays (77). Therefore, we believe that the inherent strength of a membrane-mimetic based approach is the capacity to incorporate within these systems a variety of physiologically significant processes relevant to the control of both blood coagulation and endothelial regeneration.

We observed TM-incorporated membrane-mimetic systems lipid membrane can exhibit bioactivity *in vitro* by catalyzing protein C activity. Significantly, surface bound TM was functional at physiologic shear rates and its activity was exceeded in the presence of high surface content due a transport-limiting effect. Surface TM activity showed at least short term stability in human plasma. Although stability of the surface bound TM has been confirmed, decrease in surface TM catalytic efficiency was noticed.

We suspect this is related to reduced membrane mobility and direct photoinactivation (79). In addition, activity of TM may be reduced due to limited molecular mobility and photoinactivation within the planar lipid membrane since immobilization of TM involves photopolymerization of acrylated lipids (79).

Since anticoagulant synergism of heparin and protein C pathway has been suggested (192-194), we designed a heparinized surface based on membrane-mimetic systems in order to incorporate with TM. Surface bound heparin is active by facilitating thrombin inactivation by antithrombin (ATIII). In a similar fashion to surface TM activity under flow, we observed surface heparin activity reached a limit in the presence of high surface content. Although stability of surface heparin was not exclusively examined, we assume the system was stabilized by the high affinity of biotin-streptavidin binding. In addition, surface heparin was resistant to high shear flow in short term. However, we do not exclude the possibility of loss of surface streptavidin due to competitive binding of biotinylated heparin in free from. We consider conducting long-term stability tests for the future work.

Based on the similar membrane-mimetic systems, tissue factor (TF) was incorporated to serve as a trigger for thrombin generation (15, 16). At shear flow conditions, we observed surface TF was functional by catalyzing factor Xa and thrombin generation. This provides a strategy to investigate antithrombogenic capacities of surface TM and heparin. Significantly, reduction in thrombin generation was observed in the presence of surface anticoagulants, demonstrating the potential to create an actively antithrombogenic surface. However, the major drawback of this system is that initial rapid thrombin production can not be effectively inhibited, which is similar to previous studies in static

models (14, 172, 200). This may lead to platelet (220) as well as coagulation protein activation when the surface is exposed to blood. In addition, other blood elements including natural inhibitors of anticoagulants may compromise the surface antithrombogenicity. More discussion comes in the following section when the model systems are investigated under blood flow.

There are certain important issues that need attention especially when applying the model surface *in vivo*. In order to investigate flow effect on surface enzyme activity, we approximated *in vivo* conditions by applying two shear rates of 50 and 500 sec^{-1} to simulate the conditions in vein and artery, respectively. Although the shear rates for the current *in vitro* systems are similar to most blood vessels in the human circulation, such as femoral artery and carotid (221), there is a broad range of shear rate outside these two values because physiologic wall shear rates can be lower than 50 sec^{-1} in larger vein, raise up to 1600 sec^{-1} in arteriole (221), or even extremely high more than 40,000 sec^{-1} in atherosclerotic vessels (222, 223). In addition, the hydrodynamic properties of the current *in vitro* system do not strictly apply to hemodynamic in the circulation for various reasons. Blood is not a homogeneous Newtonian fluid, and the velocity profiles are affected by flow rate and hematocrit. In the microcirculation, deviations from the parabolic profile are related to the effect of the erythrocytes on the flow. Given the shear conditions in the current *in vitro* systems, the entrance length is less than 1% of the total reactor length so that shear flow is considered to be fully developed over the whole flow-exposed area. For blood flow *in vivo*, the entrance length can be large enough so that it exceeds the lengths available before bifurcation occurs, leading to a non-fully developed flow condition. This explains why entrance effects are more operative in the aorta and

most of the major arteries than smaller vessels due to the larger Reynold's number and the vessel diameter. With increasing Reynold's number, particularly larger than the critical number ~ 2100, the stability of the flow decreases, resulting in turbulent flow due to the high energy dissipation associated with greater momentum losses from the random velocity fluctuations.

Moreover, instead of being unidirectional *in vitro*, flow is pulsatile and affected by branching and vessel curvature *in vivo*, where inertial effects result in the production of secondary flows having radial components, and sometimes in flow separation and eddy formation, which are likely present at aortic T-branches, at the carotid bifurcation, at the heart valves, and downstream of vascular stenoses. All these affect the transport of blood elements to interact with its contacting surface due to prolonged residence times and hence mechanisms of surface reactions.

Effects of blood elements including blood cells and inhibitors also limit the activity of surface anticoagulants. At increasing shear forces, inward migration of erythrocytes to the axis of the flow resulting in outward movement of platelets to the vessel wall occurs, which may explain that platelets play an important role in arterial thrombus formation (221, 224). In venous thrombus formation, fibrin and fibrin-trapped erythrocytes are the predominant thrombus building blocks. Platelets and leukocytes also provide procoagulant surfaces for local thrombin generation by assembling coagulation proteins and thereby amplifying coagulation activity on their surface (225-227). In addition, natural inhibitors of anticoagulants may compromise surface antithrombogenicity of the model system. For example, protein C inhibitor (PCI) inactivates activated protein C as well as the thrombin-thrombomodulin complex (113, 114). Homocystein, a sulfur

containing amino acid in plasma, can inactivate the cofactor activity of thrombomodulin by reducing the disulfide-bond rich epidermal growth factor-like structures of thrombomodulin (115). Heparin can be inhibited by platelet factor 4 or potentially cleaved by endogenous heparanases and two serpins, α1-antitrypsin. Moreover, PCI-catalyzed inhibition of APC can be enhanced when APC binds to heparin or heparan sulfate (214).

It has been suggested that the presence of the erythrocytes at volume concentration more than 40% considerably disturbs the transport of proteins and other blood cells. In flowing blood, the collisions between the blood cells induces a way of solute mixing, resulting in dispersion or effective diffusion coefficients which are two to three orders of magnitude greater than those due to Brownian motion and this mixing motion becomes the major mechanism for permitting cells and possibly certain larger proteins to interact with the surface.

CHAPTER 8

CONCLUSIONS

The use of synthetic materials for treatment of vascular disease is limited to larger diameter grafts due to the frequency of occlusion observed at diameters less than 5mm. It is recognized that the adverse events leading to the failure of vascular prostheses are related to maladaptive biological reactions at the blood-material and tissue-material interface. For example, many grafts occlude due to anastomotic restenosis, a condition caused by the maladaptive response to the implant and generated by the uncontrolled healing of the injured vessel. The ability of implanted materials to be compatible to the surrounding tissues and living cells is critical to the long-term patency of the implants. Among the approaches for improving the performance of the grafts, we postulate that biologically active membrane-mimetic assemblies, which are sufficiently robust for medical implant applications, can provide platforms for the presentation of biomolecular constructs that would exhibit antithrombogenic properties. In addition, such model materials may also assist in defining the extent to which the flow regime influences the catalytic efficiency of immobilized surface anticoagulants.

In attempt to test the hypothesis that membrane-mimetic films containing biologically functional regulators of the coagulation pathway can limit surface induced thrombus formation, we designed a system to determine the antithrombogenic capacities of immobilized surface anticoagulants, thrombomodulin and heparin. In the process, an *in vitro* equivalent of an *in vivo* vascular injury site was created that could be investigated under physiologic arterial and venous flow conditions. Test surfaces were fabricated and

characterized on planar supporting substrates including borosilicate glass and silicon wafers and flow studies were conducted using a parallel plate flow chamber.

The first step was to fabricate and characterize TM-containing membrane-mimetic surface. Fabrication of the construct involved layer-by-layer assembly of a polyelectrolyte multilayer containing poly-L-lysine and alginate, followed by coating of a terpolymer that consists (3-acryloyl-3-oxapropyl-3-(N,N-dioctadecyl-carbamoyl)-propionate))$_6$:(2-hydroxyethyl acrylate)$_3$:sodium styrene sulfonate$_1$ (AOD_6:HEA_3:SS_1) to present a hydrophobic alkylated basal layer on top of which TM-reconstituted acrylate phosphatidylcholine (AcPC, 1-palmitoyl-2-[12-(acryloyloxy) dodeca-noyl]-*sn*-glycero-3-phosphocholine) lipid vesicles (600 nm diameter) were fused to form lipid monolayer and subsequently stabilized by *in situ* polymerization. In the absence of surface TM, the membrane-mimetic surface constructs have been characterized by water contact angle measurement, infrared spectroscopy, scanning electronic microscopy, and ellipsometry. Films containing surface bound TM were characterized in a similar manner. In addition, surface TM density and catalytic activity under flow conditions were defined. TM surface content was quantified using ^{125}I-labeled TM and was found to be linearly correlated to the TM concentration in the lipid vesicle mixture used for membrane fusion: 6 to 300 nM of TM within 1.2 mM lipid vesicles lead to surface concentrations ranging between 66 to 1350 fmole/cm^2.

Flow studies demonstrated that TM induced activation of protein C reached a maximum at surface TM concentrations greater than 800 fmole per cm^2, indicating there is transport limitation on surface enzymatic reaction. The persistence of TM activity was

investigated by incubating test films in human plasma at 37^{o}C with periodic testing up to three months. Durable surface bound TM activity was observed.

In addition to incorporating TM into our model platform, we designed to accommodate a heparin containing membrane-mimetic system. In order to fabricate the heparinized surface, heparin was chemically modified by conjugation of biotin and anchored on a streptavidin functionalized membrane-mimetic surface which was composed of AcPC and biotin-conjugated AcPE (1-palmitoyl-2-(12-(acryloyloxy)dodecanoyl)-*sn*-glycero-3-phosphoethanolamine-biotin). Surface concentration of heparin was characterized using ^{3}H-labeled heparin and found to be directly related to the surface density of biotin-conjugated AcPE. Surface heparin activity was investigated by perfusion of a solution containing equal molar of thrombin and antithrombin at 30 nM. This study revealed that the steady state rate of thrombin inactivation could not be significantly increased beyond that obtained for surface composed of 4.4 pmole of heparin per cm^{2}, corresponding to 10 mol% of biotin-containing membrane-mimetic thin film.

In order to determine the relative capacity of surface bound TM and heparin to inhibit thrombin, we fabricated tissue factor-coated surfaces which triggered thrombin generation as a mimic of vascular injury. Briefly, TF was reconstituted into lipid vesicles (100 nm diameter) composed of 79 mole% egg PC (L-α-Phosphatidylcholine), 20 mole% brain PS (L-α-Phosphatidylserine), and 1 mole% biotin-PE (1,2-Dioleoyl-*sn*-Glycero-3-Phosphoethanolamine-N-Cap Biotinyl) which were tethered on a streptavidin functionalized membrane-mimetic surface. Prior studies had confirmed that films composed of 10 mol% of biotin-conjugated AcPE and 90 mol% of AcPC displayed

optimal activity of both surface TM and heparin in terms of protein C activation and thrombin inactivation, respectively.

In a similar fashion to heparinized and TM-coated surfaces, surface concentration of TF was determined using ^{125}I-labeled TF and was found linearly correlated to relipidated TF concentration: 6 to 120 nM TF/lipid vesicles (molar ratio of TF to liposome ranges from 1:8000 to 1: 160000) yielding in 9 to 90 fmole/cm^2 of TF surface density after 4 weeks of stability testing under static conditions in PBS at 37 °C. Surface bound TF was active due to its catalytic ability to initiate generation of factor Xa and thrombin under flow conditions. Both rates of factor Xa and thrombin generation were saturated at surface concentrations of TF equal to or greater than 50 fmole per cm^2. Similar responses of factor Xa and thrombin indicate that the thrombin generation is possibly dependent upon activation of factor X.

The final phase of our investigations focused on the antithrombogenic capacities of TM and heparin bound on surface alone and in a combined system. TF, TM and/or heparin (the implanted graft) were patterned on test surfaces with TF positioned at the upstream of flow. The TF–coated area was created using a dip-coating process. In the presence of TM, peak thrombin generation was reduced by 16% with an overall 50% reduction in steady state thrombin production.

A profound effect on thrombin inactivation was observed at physiologic concentrations of antithrombin. Without surface bound TM, peak thrombin concentrations were reduced by more than 30% and steady state levels decreased by more than 65%. With the addition of TM, peak values were reduced by more than 50% and steady state levels by 80%. Notably, thrombin inactivation was not significantly

influenced in the presence of surface heparin whether alone or in combination with TM. Nevertheless, thrombin production from TF/TM-heparin surface was the lowest among all test systems. Peak thrombin concentrations were reduced by 55% and steady state levels by 85%.

In addition to incorporating TM and heparin, the current membrane-mimetic system provides a platform that can potentially accommodate more biologically functional substances that improve antithrombogenicity of the surface. We believe that such surface modification strategies will help in the design of more robust materials for improving the performance of small caliber vascular prostheses.

CHAPTER 9

FUTURE WORK AND RECOMMENDATIONS

In this thesis, we addressed the issues dealing with biomaterials, biomolecular engineering, surface enzymatic reaction, and transport phenomena. Following the present work, we are looking forward to not only improving the performance of the model surface construct but also expanding its applicability to medical implants.

In the process of fabricating membrane-mimetic assemblies, formation of lipid monolayer, via vesicle fusion and *in situ* photopolymerization, on alkylated polyelectrolyte multilayer can retain the stability for at least short-term period.

Since most of the data presented in this thesis are results of empirical studies, we are looking forward to doing mathematical modeling based on the experimental conditions to not only validate the experimental results, but also simulating what can not be experimentally achieved, especially for detailed spatial and temporal dynamics of reactants and products involved in surface reactions under flow conditions. According to the flow studies on surface catalytic activity (immobilized TM, heparin, and TF), experimental results only revealed the product responses at the outlet of the flow reactor, including protein C activation, thrombin inactivation, and thrombin generation, representing the product concentrations in the bulk phase. Under flow conditions, surface enzymatic reaction which is generally assumed to occur only within the boundary layer of the reactive surface involves not only intrinsic kinetics between substrates and surface enzyme, but also transport of substrates to the catalytic sites and products removed from the surface. Mathematical simulation can assist to analyze dynamic behavior of reactants

and products within the boundary layer, which is extremely difficult to characterize experimentally.

As for TF-coated surface, we were focusing on making a TF functionalized system so that it can at least exhibit enzymatic activity. However, relipidated TF tethered on the membrane-mimetic assemblies needs to be further characterized, including size of lipid vesicles, surface structure, and stability of TF activity. Although the similar construct has been reported (148) that biotinylated lipid vesicles can bind intact on streptavidin functionalized surface, it is not yet clear that this technique can be applied to all lipids. We suggest using laser light scattering to determine vesicle size, ellipsometry to determine the thickness of anchored lipid vesicle layer, atomic force microscopy to examine the surface structure, and extensive flow studies on stability of TF activity. Through these scrutinized characterization process, we can have more consolidate understanding of such a system and further utilized for more applications such as incorporating more functionalized macromolecules for desired performances.

Ultimately, we are looking forward to successfully apply the current system to commercially available synthetic vascular grafts such as expanded poly-tetrafluoroethylene (ePTFE). Investigating graft performance using *ex vivo* models such as venous-arterial shunt studies or *in vivo* models by graft implantation for studies of long-term patency should be pursued.

APPENDIX A

Standard Protein Concentrations for Chromogenic Assay

Activated Protein C

A series of concentrations (ranging from 5 nM to 100nM) of activated protein C were prepared by diluting 1μM of APC in Tris-BSA (20mM Tris-HCl + 100 mM NaCl + 0.1 wt% BSA, pH 7.5) . The assay was conducted by adding 100 μL of each diluted APC to 200μL of Tris-BSA containing Spectrozyme PCa substrate (0.2 mM, final concentration) and monitoring absorbance change over time continuously at 405 nm for approximately 5 minutes. The standard curve was generated by plotting [APC] (nM) vs. Absorbance change/Time (Figure A1).

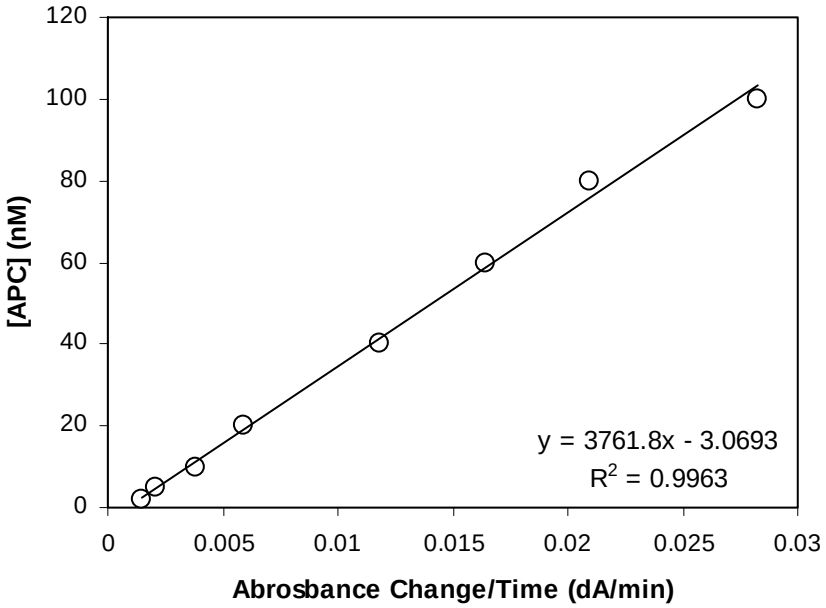

Figure A1 Standard curve of activated protein C. A linear relationship between [APC] (nM) and rate of absorbance change (dA/min) was observed: [APC] (nM) = 3761.8 (dA/min) – 3.0693.

Factor Xa

A series of concentrations (ranging from 2 nM ~ 100nM) of Factor Xa were prepared by diluting 1μM of factor Xa in HBSA (10 mM Hepes buffer + 140 mM NaCl + 0.1 wt% BSA, pH 7.5) . The assay was conducted by adding 16 μL of each diluted factor Xa to 384 μL of HBSA containing S-2222 substrate (0.2 mM, final concentration) and monitoring absorbance change over time continuously at 405 nm for approximately 5 minutes. The standard curve was generated by plotting [Xa] (nM) vs. Absorbance change/Time (Figure A2).

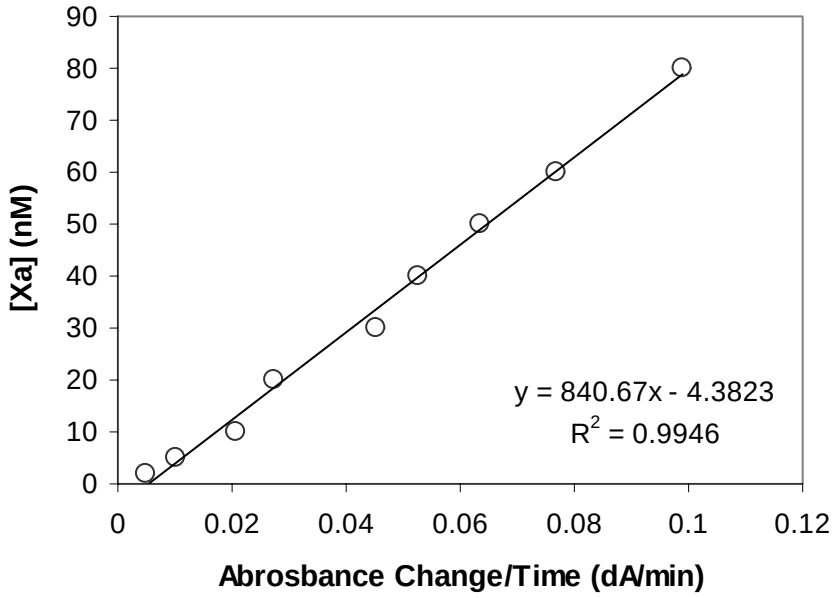

Figure A2 Standard curve of factor Xa. A linear relationship between [Xa] (nM) and rate of absorbance change (dA/min) was observed: [Xa] (nM) = 840.67 (dA/min) – 4.3823.

Thrombin

A series of concentrations (ranging from 2 nM to 500nM) of thrombin were prepared by diluting 5 μM of thrombin in Hepes buffer/BSA (20 mM Hepes + 150 mM NaCl, pH 7.4). The assay was conducted by adding 16 μL of each diluted factor Xa to 384 μL of Hepes buffer/BSA containing Spectrozyme TH substrate (0.2 mM, final concentration) and monitoring absorbance change over time continuously at 405 nm for approximately 2 minutes. The standard curve was generated by plotting [Thrombin] (nM) vs. Absorbance change/Time (Figure A3).

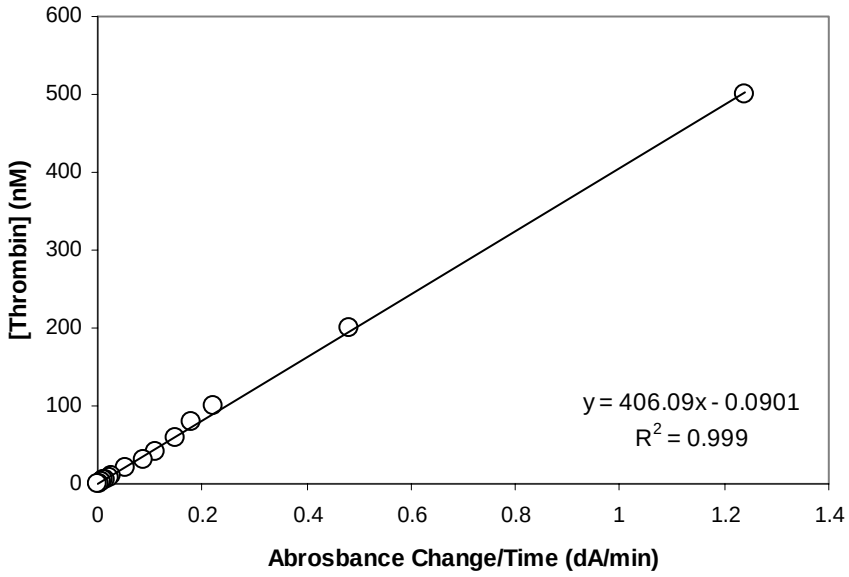

Figure A3 Standard curve of thrombin. A linear relationship between [thrombin] (nM) and rate of absorbance change (dA/min) was observed: [thrombin] (nM) = 406.09 (dA/min) – 0.0901.

APPENDIX B

Theoretical Considerations of Transport Effect on Surface Enzymatic Reactions

In order develop an expression to compute steady state rate of reaction for diffusion limited, laminar flow conditions, the following governing equation is considered:

$$D\frac{\partial^2 C}{\partial y^2} = v_z \frac{\partial C}{\partial z} \tag{1}$$

$$v_z = v_{\max}\left(1-\left(\frac{y}{B}\right)^2\right) \tag{2}$$

The appropriate boundary conditions at the surface and in the bulk fluid are:

B.C. 1: $C = C_0$ at $z = 0$ (at entrance) for all y (3)

B.C. 2: $C = 0$ at $y = \pm B$ for all z (4)

B.C. 3: $C = C_0$ everywhere but at $y \approx \pm B$ (5)

By introducing a coordinate system (x) emanating from the wall and for half the symmetrical reactor, we have:

$$x + y = B$$

then velocity in terms of x is

$$v_z = v_{\max}\left(2\left(\frac{x}{B}\right)-\left(\frac{x}{B}\right)^2\right)$$

which can be approximated to a linear form near the wall since $x/B \ll 1$ in that vicinity:

$$v_z \cong 2v_{\max}\left(\frac{x}{B}\right)$$

Thus, replacing y with x into the governing equation:

$$D\frac{\partial^2 C}{\partial x^2} = 2v_{\max}\left(\frac{x}{B}\right)\frac{\partial C}{\partial z}$$

subject to the boundary conditions

$$\text{At the entrance: } C = C_0 \quad \text{at} \quad z = 0,\ x > 0 \tag{3}$$

$$\text{At the wall: } C = 0 \qquad \text{at } x = 0 \text{ for all } z \tag{4}$$

For very thin layers near the wall, the bulk flow appears far away, so we write for short penetration:

$$C \rightarrow C_0 \quad \text{at } x \rightarrow \infty,\ z > 0 \tag{5}$$

The symmetry of the boundary conditions suggests a combination of variable approach. The similarity exists in the governing equation:

$$B\,D\,z \sim 2v_{\max}\,x^3$$

The combined variable in a convenient form is:

$$\eta = \frac{x}{\left(\frac{9B\,D\,z}{2v_{\max}}\right)^{1/3}}$$

By taking C = f (η) and the combined variable, the governing equation can be expressed:

$$\frac{\partial C}{\partial z} = \frac{\partial f}{\partial \eta}\frac{\partial \eta}{\partial z} = f'(\eta)\left(-\frac{1}{3}\eta\frac{1}{z}\right)$$

$$\frac{\partial C}{\partial x} = \frac{\partial f}{\partial \eta}\frac{\partial \eta}{\partial x} = f'(\eta)\left[\frac{1}{\left(\frac{9B\,D\,z}{2v_{\max}}\right)^{1/3}}\right]$$

$$\frac{\partial^2 C}{\partial x^2} = \frac{\partial}{\partial \eta}\left[f'(\eta) \frac{1}{\left(\frac{9BDz}{2v_{\max}}\right)^{1/3}} \right] \frac{\partial \eta}{\partial x} = f''(\eta) \frac{1}{\left(\frac{9BDz}{2v_{\max}}\right)^{2/3}}$$

Inserting the above into the governing equation shows

$$2v_{\max}\left(\frac{x}{B}\right)\left[f'(\eta)\left(-\frac{1}{3}\eta\frac{1}{z}\right)\right] = D f''(\eta) \frac{1}{\left(\frac{9BDz}{2v_{\max}}\right)^{2/3}}$$

$$\rightarrow \quad f''(\eta) + 3\eta^2 f'(\eta) = 0$$

with boundary conditions:

$f = C_0$ at $\eta = \infty$ ($z = 0$ or $x \rightarrow \infty$)

$f = 0$ at $\eta = 0$ ($z \rightarrow \infty$ or $x = 0$)

$$f'(\eta) = A\exp\left(-\eta^3\right) = \frac{df}{d\eta} \quad \rightarrow \quad f(\eta) = a\int \exp\left(-\eta^3\right) d\eta \; + \; b$$

evaluating a and b from boundary conditions:

$$a = \frac{C_0}{\int_0^\infty \exp\left(-\eta^3\right) d\eta}$$, b = 0

From the definition of Gamma function:

$$\Gamma(x) = \int_0^\infty t^{x-1} \exp\left(-t\right) dt$$

let $\eta^3 = t \rightarrow 3\eta^2 d\eta = dt$

$$\int_0^\infty \exp\left(-\eta^3\right) d\eta = \frac{1}{3}\Gamma\left(\frac{1}{3}\right) = \Gamma\left(\frac{4}{3}\right)$$

therefore, the concentration profile can be expressed as

$$C = f(\eta) = \frac{C_0 \int_0^{\eta} \exp\left(-\beta^3\right) d\beta}{\Gamma\left(\frac{4}{3}\right)}$$

The mass flux at the wall can be expressed as

$$N_0(z) = D\left[\frac{\partial C}{\partial x}\right]_{x=0} = D\left[\frac{\partial f}{\partial \eta}\right]_{\eta=0} \frac{\partial \eta}{\partial x} = \frac{D C_0}{\Gamma\left(\frac{4}{3}\right)}\left(\frac{2 v_{\max}}{9 B D z}\right)^{1/3}$$

The average rate of reaction, i.e. the average flux can be computed from

$$(r_p)_{diff} = \overline{N_0} = \frac{1}{L}\int_0^L N_0(z)\, dz = \frac{\frac{3}{2} D C_0}{\Gamma\left(\frac{4}{3}\right)}\left(\frac{2 v_{\max}}{9 B D L}\right)^{1/3}$$

Since average flow velocity: $v_{av} = \frac{Q}{2BW} = \frac{2}{3} v_{\max}$ and wall shear rate: $\gamma_w = \frac{3}{2}\frac{Q}{B^2 W}$,

Finally, average rate of reaction is expressed as a function of shear rate, length of flow reactor, and diffusivity and concentration of substrate.

$$(r_p)_{diff} = \frac{\frac{3}{2} C_0}{\Gamma\left(\frac{4}{3}\right)}\left(\frac{Q D^2}{6 B^2 W L}\right)^{1/3} = \frac{\frac{3}{2}}{\Gamma\left(\frac{4}{3}\right)}\left(\frac{\gamma_w D^2}{9 L}\right)^{1/3} C_0$$

$$\rightarrow \underline{(r_p)_{diff} = 1.68\left(\frac{\gamma_w D^2}{9 L}\right)^{1/3} C_0}$$

The steady state concentration of product, $[P]_{diff}$, at the outlet of the parallel plate reactor related to rate of reaction is expressed

$$[P]_{diff} = \frac{A(r_p)_{diff}}{Q} = \frac{W L (r_p)_{diff}}{\frac{2 B^2 W \gamma_w}{3}} \quad \rightarrow \quad \underline{[P]_{diff} = 1.21 \frac{C_0}{B^2}\left(\frac{D L}{\gamma_w}\right)^{2/3}}$$

APPENDIX C

Activated Protein C Generation Under Flow Conditions

Table C APC generation (nM) as a function of perfusion time at a series of TM surface concentrations (fmole/cm^2). Each data point represents the mean ± standard error (n = 5).

50 sec^{-1}	TM surface concentration (fmole/cm^2)						
Time (min)	1351	764	488	344	162	82	66
0	0.00	0.00	0.00	0.00	0.00	0.00	0.00
5	4.50 ± 0.16	3.14 ± 0.16	7.75 ± 0.63	7.98 ± 1.00	2.24 ± 0.41	2.66 ± 0.32	1.51 ± 0.12
15	17.99 ± 1.23	12.06 ± 1.01	17.32 ± 0.39	15.66 ± 0.90	16.66 ± 1.25	6.45 ± 0.59	5.06 ± 0.49
25	28.60 ± 1.31	22.19 ±0.80	23.43 ± 0.63	21.61 ± 0.87	22.78 ± 0.38	16.75 ± 0.71	12.34 ± 0.42
35	31.34 ± 1.15	28.72 ± 0.90	27.41 ± 0.59	24.44 ± 0.77	23.00 ± 0.77	18.65 ± 1.41	14.15 ± 1.32
45	34.64 ± 1.18	32.35 ± 1.21	30.25 ± 0.93	26.07 ± 1.58	23.60 ± 0.93	19.41 ± 0.81	13.23 ± 1.39
55	33.44 ± 1.34	32.60 ± 0.89	30.21 ± 0.94	27.58 ± 0.79	21.56 ± 0.86	18.06 ± 0.89	12.99 ± 0.56
65	33.38 ± 1.22	32.00 ± 1.01	30.17 ± 0.85	27.55 ± 0.62	22.49 ± 0.88	18.82 ± 0.65	13.32 ± 1.18
75	34.28 ± 1.25	31.57 ± 0.82	30.56 ± 1.13	26.77 ± 1.70	22.28 ± 0.94	19.07 ± 1.52	13.12 ± 1.19
85	33.81 ± 1.28	30.92 ± 0.98	31.00 ± 0.66	27.36 ± 1.40	22.72 ± 0.60	18.63 ± 0.89	13.64 ± 1.25
95	34.70 ± 1.12	31.87 ± 0.94	29.78 ± 1.04	26.78 ± 1.45	22.59 ± 1.01	18.14 ± 1.40	12.55 ± 1.20

500 sec^{-1}	TM surface concentration (fmole/cm^2)						
Time (min)	1351	764	488	344	162	82	66
0	0.00	0.00	0.00	0.00	0.00	0.00	0.00
1	2.72 ± 0.30	4.29 ± 0.51	3.14 ± 0.50	2.38 ± 0.50	1.82 ± 0.46	1.24 ± 0.31	1.28 ± 0.25
3	8.15 ± 1.03	8.16 ± 1.51	9.70 ± 0.72	8.01 ± 0.76	6.50 ± 0.63	3.88 ± 0.65	3.32 ± 0.35
5	12.62 ± 1.75	11.49 ± 1.12	12.19 ± 0.97	10.46 ± 0.64	7.06 ± 0.84	5.22 ± 0.58	3.98 ± 0.51
7	12.71 ± 2.06	12.45 ± 1.22	11.66 ± 1.43	9.97 ± 0.84	7.15 ± 0.83	4.85 ± 0.56	3.64 ± 0.79
9	12.85 ± 1.85	12.09 ± 1.45	12.91 ± 1.04	9.72 ± 1.12	7.21 ± 0.59	4.76 ± 0.53	3.94 ± 0.32
11	11.74 ± 2.01	11.78 ± 1.42	13.05 ± 1.29	9.74 ± 1.35	6.93 ± 0.44	5.14 ± 0.29	3.71 ± 0.56
13	12.21 ± 2.05	12.73 ± 1.49	12.49 ± 1.66	10.89 ± 0.73	6.43 ± 0.44	4.92 ± 0.59	3.75 ± 0.53
15	11.99 ± 2.13	11.87 ± 1.10	10.88 ± 1.15	9.65 ± 0.95	7.18 ± 0.77	4.99 ± 0.30	3.61 ± 0.83
17	12.39 ± 1.90	12.04 ± 1.35	12.43 ± 1.16	10.28 ± 0.65	7.40 ± 0.41	4.72 ± 0.50	3.68 ± 0.23
19	12.75 ± 2.15	11.88 ± 1.40	11.58 ± 1.18	9.35 ± 0.55	6.37 ± 0.38	4.99 ± 0.39	3.69 ± 0.57

APPENDIX D

Purification of Biotin-Conjugated Heparin Through Avidin Column

To purify the compound, a commercial kit called ImmunoPure® Immobilized Monomeric Avidin (Pierce) was used. The principle of the kit is using immobilized polymeric forms of avidin with strong binding characteristics to biotinylated molecules. In brief, these high affinity biotin-binding sites are first blocked with a biotin-containing buffer. Biotin molecules are eluted from the monomers with a glycine solution revealing only the reversible binding sites. The biotinylated molecule of interest may then be applied to the support for purification and then eluted by ligand competition using a biotin-containing buffer.

Materials:

Monomeric Avidin Column containing 2 ml of settled gel (support: 4% beaded agarose supplied as a 50% slurry, i.e., 4 ml of 50% slurry is equivalent to 2 ml of settled gel) with binding capacity ≥1.2 mg biotinylated BSA/ml settled gel. BupH™ Phosphate Buffered Saline (PBS) (0.1 M sodium phosphate, 0.15 M NaCl, pH 7.2 when reconstituted with 500 ml of sterilized deionized water). Biotin Blocking and Elution Buffer (200mL 2 mM D-biotin in PBS). Regeneration Buffer (250 ml 0.1 M glycine, pH 2.8).

Method:

1. Equilibrated kit components to room temperature.
2. Washed column with 8 ml PBS, followed by adding 6 ml Biotin Blocking and Elution Buffer to block any non-reversible biotin binding sites.

3. Removed biotin from the reversible binding sites by adding 12 ml Regeneration Buffer, followed by washing column with 8 ml PBS.
4. Placed at least twelve 12 x 75mm test tubes in a rack. Place the Monomeric Avidin Column in a tube and add 2mL biotinylated heparin (2mg/mL) by applying solution to the center of the disc.
5. When the entire sample has passed through the disc, 0.25 ml PBS was added to force sample completely into the gel bed.
6. Allowed the biotinylated heparin to incubate (cap the bottom and then the top of the column) in the column for 30min.
7. Placed column in a new tube and added 2.0 ml of PBS. Repeated PBS additions until a total of six 2.0 ml fractions have been collected. Samples were monitored by measuring the absorbance of the fractions at 280 nm (use PBS to obtain a baseline value). When absorbance value returns to baseline, non-bound protein has been removed (Figure D1 A).
8. Biotin Blocking and Elution Buffer was added to elute the bound biotinylated molecule, and collected at least six 2.0 ml fractions. Measure the absorbance of each fraction at 280 nm (Figure D1 B) and reserve the fractions of interest for further analysis, including dialysis and HABA assay to assure optimal binding capacity.
9. Regenerated the column by washing two times with 4 ml Regeneration Buffer, followed by washing column with 5 ml of PBS and stored the column at $4^{o}C$ for future use.

According to step 7 & 8, results from monitoring the desired eluted compound from avidin column were shown in Figure D1.

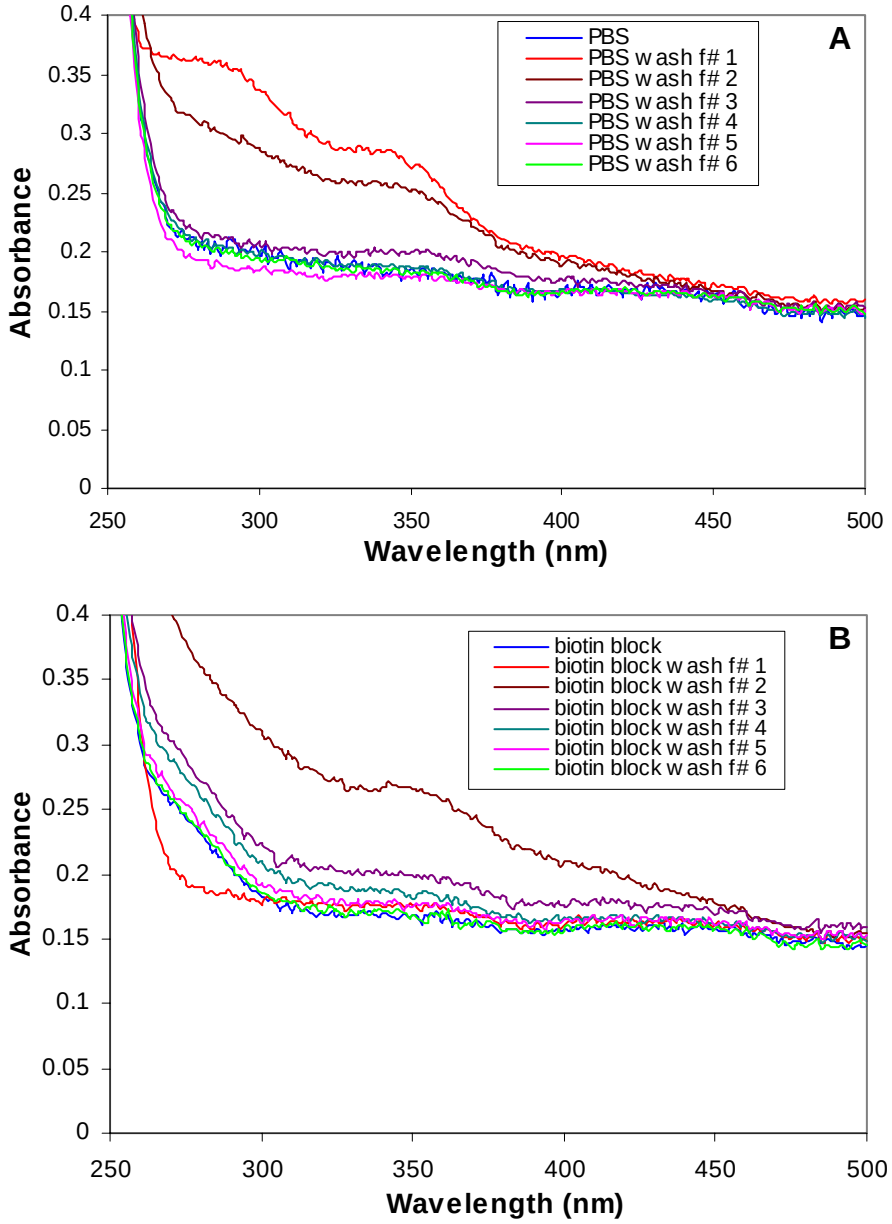

Figure D1 The UV-VIS scanning results demonstrate (A) the complete bound biotin-heparin in avidin column after washing with PBS (step 7) and (B) recovery of the bound compound after washing with Biotin Blocking and Elution Buffer (step 8). For PBS washing, non-bound material was completely removed after the third fraction collection (f#3). As for recovery of the biotin-heparin from the avidin column, scanning curves almost overlap with that of pure biotin blocking buffer after collecting fraction #5 (f#5), indicating the biotin-heparin was fully recovered.

APPENDIX E

Fact Xa and Thrombin Generation From TF-coated (Entire Flow-Exposed) Surface

Table E1 Factor Xa generation as a function of perfusion time at a series of TF surface concentrations (fmole/cm^2). Each data point represents the mean ± standard error (n = 5).

50 sec^{-1}	[TF] (nM) reconstituted within lipid vesicles				
Time (min)	6	30	60	90	120
0	0.00	0.00	0.00	0.00	0.00
2	2.04 ± 0.09	4.19 ± 0.36	5.11 ± 0.42	4.58 ± 0.63	6.29 ± 0.36
4	3.92 ± 0.14	6.86 ± 1.07	13.91 ± 0.06	16.85 ± 0.86	21.44 ± 3.39
6	8.89 ± 0.66	24.08 ± 1.34	28.00 ± 2.39	38.08 ± 2.72	41.73 ± 3.88
8	15.59 ± 1.04	35.99 ± 1.67	45.60 ± 0.97	51.14 ± 0.65	50.77 ± 2.76
10	21.26 ± 1.08	43.14 ± 1.96	49.19 ± 1.78	50.07 ± 2.03	49.84 ± 1.18
12	24.10 ± 1.87	43.59 ± 2.61	48.51 ± 1.19	53.41 ± 2.37	54.87 ± 4.70
14	25.63 ± 2.04	43.85 ± 0.80	51.88 ± 1.64	51.52 ± 0.73	45.96 ± 1.21
16	25.45 ± 2.39	42.06 ± 1.89	53.69 ± 2.55	50.55 ± 3.60	53.80 ± 2.68
18	24.26 ± 1.56	42.00 ± 1.65	46.53 ± 3.60	53.99 ± 0.97	51.78 ± 4.19
20	23.28 ± 1.64	40.92 ± 2.30	51.80 ± 2.68	53.82 ± 2.68	44.63 ± 1.20
22	23.08 ± 1.43	44.98 ± 1.58	53.12 ± 2.12	48.12 ± 1.98	52.76 ± 3.17
24	24.99 ± 1.72	42.21 ± 1.58	53.12 ± 2.12	49.78 ± 3.23	49.35 ± 2.01

500 sec^{-1}	[TF] (nM) reconstituted within lipid vesicles				
Time (min)	6	30	60	90	120
0	0.00	0.00	0.00	0.00	0.00
1	0.59 ± 0.04	1.27 ± 0.19	1.78 ± 0.04	1.71 ± 0.14	2.21 ± 0.17
2	1.01 ± 0.07	2.41 ± 0.10	3.76 ± 0.13	4.35 ± 0.35	4.63 ± 0.78
3	1.38 ± 0.21	4.17 ± 0.63	5.98 ± 0.71	7.87 ± 0.69	8.63 ± 0.92
4	2.44 ± 0.28	7.61 ± 0.30	9.54 ± 0.35	10.49 ± 1.07	11.97 ± 0.82
5	3.12 ± 0.51	8.25 ± 0.42	10.04 ± 0.50	11.86 ± 0.73	10.71 ± 0.51
6	4.24 ± 0.31	9.35 ± 0.53	11.31 ± 1.25	10.66 ± 1.07	9.51 ± 0.78
7	4.82 ± 0.25	9.46 ± 1.18	11.39 ± 1.42	12.50 ± 0.75	11.35 ± 0.52
8	4.78 ± 0.35	9.18 ± 0.64	11.11 ± 1.25	11.53 ± 0.71	10.95 ± 0.35
9	5.54 ± 0.40	8.42 ± 0.63	11.82 ± 0.54	9.83 ± 1.05	11.55 ± 0.33
10	4.88 ± 0.45	9.31 ± 1.13	11.20 ± 1.00	11.17 ± 0.35	10.59 ± 0.25
12	5.56 ± 0.52	8.77 ± 0.56	10.86 ± 0.72	11.69 ± 0.77	11.11 ± 0.40
14	4.39 ± 0.44	9.162 ± 0.51	10.12 ± 0.70	12.83 ± 0.89	11.82 ± 0.44

Table E2 Thrombin generation as a function of perfusion time at a series of TF surface concentrations (fmole/cm^2). Each data point represents mean ± standard error (n = 5).

50 sec^{-1}	[TF] (nM) reconstituted within lipid vesicles				
Time (min)	6	30	60	90	120
0	0.00	0.00	0.00	0.00	0.00
2	17.40 ± 0.67	23.39 ± 1.57	25.00 ± 2.68	25.63 ± 2.72	28.56 ± 3.37
4	20.64 ± 2.92	31.16 ± 3.38	40.20 ± 2.67	20.11 ± 1.87	50.00 ± 4.32
6	48.89 ± 4.57	155.93 ± 12.98	194.36 ± 11.62	201.54 ± 10.19	224.52 ± 18.79
8	136.62 ± 8.25	241.13 ± 17.23	316.26 ± 18.85	280.02 ± 12.65	335.01 ± 19.61
10	195.69 ± 14.70	350.27 ± 31.79	400.53 ± 22.14	408.60 ± 13.16	383.15 ± 16.41
12	218.94 ± 18.85	375.17 ± 24.26	484.33 ± 15.81	440.40 ± 19.49	492.43 ± 25.30
14	256.57 ± 21.64	368.73 ± 27.43	443.73 ± 26.32	463.70 ± 25.18	478.30 ± 15.81
16	266.14 ± 18.57	415.42 ± 23.62	495.42 ± 28.46	480.42 ± 19.49	432.20 ± 18.97
18	209.28 ± 13.38	400.67 ± 35.16	470.67 ± 22.14	460.56 ± 15.81	505.29 ± 12.65
20	246.91 ± 16.54	372.49 ± 22.38	472.49 ± 22.14	444.91 ± 22.14	479.39 ± 25.77
22	269.58 ± 20.82	410.40 ± 26.23	490.40 ± 25.30	471.80 ± 26.44	448.40 ± 19.49
24	209.13 ± 15.40	396.62 ± 30.45	476.62 ± 22.14	495.20 ± 31.29	476.48 ± 18.06

500 sec^{-1}	[TF] (nM) reconstituted within lipid vesicles				
Time (min)	6	30	60	90	120
0	0.00	0.00	0.00	0.00	0.00
1	11.71 ± 1.58	31.22 ± 2.52	54.44 ± 4.04	70.66 ± 3.81	78.72 ± 6.58
2	29.67 ± 3.16	59.73 ± 6.05	89.21 ± 7.62	118.73 ± 9.09	133.34 ± 10.06
3	49.15 ± 4.52	110.32 ± 11.38	160.43 ± 12.56	172.80 ± 13.12	168.32 ± 12.58
4	55.03 ± 4.72	145.00 ± 13.63	177.28 ± 16.32	185.71 ± 16.62	201.92 ± 17.11
5	65.23 ± 6.34	153.25 ± 9.49	198.71 ± 13.87	195.49 ± 10.34	191.92 ± 20.44
6	65.36 ± 5.28	160.24 ± 12.38	195.90 ± 18.32	186.52 ± 18.01	205.84 ± 14.57
7	84.73 ± 8.92	154.44 ± 13.02	181.12 ± 19.49	197.83 ± 12.87	204.97 ± 11.88
8	59.53 ± 6.10	148.33 ± 10.54	197.78 ± 12.32	184.10 ± 13.03	188.92 ± 18.31
9	78.96 ± 6.56	148.88 ± 13.73	171.96 ±15.25	201.81 ± 22.16	185.71 ± 12.66
10	66.84 ± 5.87	159.42 ± 14.74	192.30 ± 18.84	181.88 ± 19.16	197.57 ± 14.16
12	71.33 ± 6.78	163.51 ± 17.08	182.50 ± 15.77	188.72 ± 13.21	193.97 ± 14.66
14	57.76 ± 6.03	148.93 ± 10.21	188.96 ± 16.98	196.04 ± 14.02	180.57 ± 17.25

APPENDIX F

Tissue Factor Surface Density

Table F1 Tissue factor surface density (fmole/cm^2) as a function of TF concentration (nM)[a] within lipid vesicles (1mM of egg PC/brain PS/ biotin-PE, 79:20:1 molar ratio). Stability of TF coated surface was assessed by incubating the sample with PBS at 37 °C over a 28-day period. The samples were transferred to fresh PBS at indicated time points and radioactivity measured in a gamma counter. Each data point represents mean ± standard deviation (n = 6).

TF (nM)[a]	Day1	Day 3	Day 7	Day 14	Day 28
6	15.34 ± 5.95	11.71 ± 3.91	9.97 ± 4.29	9.21 ± 3.13	9.40 ± 4.64
12	28.70 ± 8.17	20.91 ± 7.86	19.26 ± 8.32	16.04 ± 6.54	15.56 ± 7.63
30	54.22 ± 7.81	38.42 ± 6.90	31.37 ± 6.87	26.19 ± 5.55	27.28 ± 6.06
60	108.62 ± 13.72	83.97 ± 14.17	66.08 ± 12.48	57.39 ± 10.23	51.16 ± 9.86
90	150.75 ± 13.02	115.18 ± 8.33	86.07 ± 10.24	73.29 ± 5.21	69.88 ± 8.65
120	175.44 ± 12.16	141.01 ± 15.44	113.49 ± 15.98	97.70 ± 9.49	88.56 ± 7.55

APPENDIX G

Thrombin Generation From TF-Coated (Localized at the Upstream) Surface

Table G1 Thrombin generation (nM, mean ± standard error, n = 5) vs. perfusion time for a variety of composite surfaces including TF, TF/TM, TF/heparin, and TF/TM-heparin systems.

50 sec^{-1}						
Time (min)	TF	TF/TM	TF+ ATIII	TF/TM + ATIII	TF/Heparin	TF/TM-Heparin
0	0	0	0	0	0	0
0.5	1.23 ± 0.14	0.73 ± 0.06	1.12 ± 0.15	1.05 ± 0.10	0.93 ± 0.07	0.82 ± 0.08
1	1.81± 0.14	1.67 ± 0.19	1.84 ± 0.21	2.36 ± 0.19	1.86 ± 0.24	1.92 0.21
2	6.32 ± 0.33	4.48 ± 0.33	4.96 ± 0.29	5.80 ± 0.47	6.78 ± 0.37	3.68 ± 0.34
4	18.66 ± 1.44	21.80 ± 0.82	17.28 ± 0.73	13.49 ± 0.55	15.52 ± 0.35	10.64 ± 0.79
6	29.68 ± 1.06	24.55 ± 0.84	19.26 ± 0.88	13.86 ± 0.72	16.38 ± 0.56	12.94 ± 0.38
8	31.25 ± 2.17	24.48 ± 0.82	18.61 ± 0.47	12.93 ± 0.57	15.04 ± 53	10.33 ± 0.47
10	31.83 ± 1.51	21.72 ± 1.00	16.35 ± 0.55	11.74 ± 0.48	13.25 ± 0.44	8.71 ± 0.40
15	29.97 ± 2.42	17.66 ± 0.86	14.58 ± 0.59	8.67 ± 0.52	11.36 ± 0.63	6.38 ± 0.52
20	29.80 ± 2.15	15.24 ± 0.85	12.31 ± 0.69	6.52 ± 0.47	9.23 ± 0.55	4.69 ± 0.32
25	30.76 ± 2.15	14.35 ± 1.11	10.73 ± 0.67	5.05 ± 0.37	7.39 ± 0.52	3.30 ± 0.39
30	32.00 ± 2.04	13.88 ± 0.87	8.49 ± 0.69	4.50 ± 0.36	6.37 ± 0.55	2.73 ± 0.26
35	30.11 ± 2.51	13.58 ± 1.13	8.16 ± 0.37	3.58 ± 0.11	6.30 ± 0.40	2.38 ± 0.18

500 sec^{-1}						
Time (min)	TF	TF/TM	TF+ ATIII	TF/TM + ATIII	TF/Heparin	TF/TM-Heparin
0	0	0	0	0	0	0
0.5	1.16 ± 0.12	1.10 ± 0.11	1.36 ± 0.18	1.25 ± 0.18	0.86 ± 0.10	0.99 ± 0.09
1.5	8.16 ± 0.31	8.31 ± 0.31	7.13 ± 0.36	5.67 ± 0.41	6.25 ± 0.31	4.32 ± 0.26
2.5	12.73 ± 0.58	10.96 ± 0.44	9.30 ± 0.46	6.59 ± 0.35	8.12 ± 0.45	5.74 ± 0.28
3.5	13.22 ± 1.05	10.59 ± 0.27	8.58 ± 0.50	5.74 ± 0.32	7.38 ± 0.34	5.08 ± 0.44
4.5	13.70 ± 0.64	10.98 ± 0.60	8.34 ± 0.50	5.55 ± 0.18	7.13 ± 0.33	4.72 ± 0.45
6	13.45 ± 0.56	10.49 ± 60	7.43 ± 0.48	5.24 ± 0.17	6.09 ± 0.33	4.18 ± 0.20
8	13.19 ± 1.12	8.34 ± 0.63	6.60 ± 0.63	4.33 ± 0.30	5.34 ± 0.26	3.68 ± 0.22
10	13.60 ± 1.10	7.82 ± 0.56	5.66 ± 0.32	3.64 ± 0.32	4.79 ± 0.28	2.74 ± 0.25
12	12.41 ± 1.22	8.04 ± 0.28	4.92 ± 0.23	3.20 ± 0.40	4.37 ± 0.41	2.33 ± 0.23
14	13.48 ± 0.53	7.59 ± 0.34	4.76 ± 0.36	2.73 ± 0.21	3.72 ± 041	1.99 ± 0.25
16	13.14 ± 0.44	7.09 ± 0.44	4.37 ± 0.47	2.59 ± 0.21	3.21 ± 0.19	1.76 ± 0.09

Note: red-marked values contain more than 10% of standard error.

Table G2 Rate of thrombin generation (pmole/min/cm^2, mean ± standard error, n = 5) vs. perfusion time for a variety of composite surfaces including TF, TF/TM, TF/heparin, and TF/TM-heparin systems.

50 sec^{-1}						
Time (min)	TF	TF/TM	TF+ ATIII	TF/TM + ATIII	TF/Heparin	TF/TM-Heparin
0	0	0	0	0	0	0
0.5	0.110 ± 0.013	0.065 ± 0.006	0.100 ± 0.013	0.094 ± 0.009	0.084 ± 0.007	0.074 ± 0.007
1	0.162 ± 0.013	0.150 ± 0.017	0.165 ± 0.019	0.212 ± 0.017	0.166 ± 0.022	0.173 ± 0.019
2	0.566 ± 0.029	0.401 ± 0.030	0.445 ± 0.026	0.520 ± 0.042	0.607 ± 0.033	0.330 ± 0.030
4	1.672 ± 0.130	1.953 ± 0.074	1.548 ± 0.066	1.209 ± 0.050	1.391 ± 0.031	0.953 ± 0.071
6	2.659 ± 0.095	2.199 ± 0.075	1.774 ± 0.079	1.229 ± 0.065	1.454 ± 0.050	1.099 ± 0.034
8	2.800 ± 0.195	2.193 ± 0.074	1.667 ± 0.042	1.159 ± 0.051	1.348 ± 0.047	0.925 ± 0.042
10	2.851 ± 0.135	1.946 ± 0.090	1.464 ± 0.050	1.052 ± 0.043	1.187 ± 0.039	0.781 ± 0.036
15	2.685 ± 0.217	1.582 ± 0.077	1.306 ± 0.053	0.777 ± 0.047	1.018 ± 0.056	0.571 ± 0.047
20	2.670 ± 0.193	1.365 ± 0.077	1.103 ± 0.062	0.584 ± 0.043	0.827 ± 0.049	0.420 ± 0.029
25	2.755 ± 0.190	1.286 ± 0.099	0.962 ± 0.060	0.453 ± 0.033	0.662 ± 0.047	0.295 ± 0.035
30	2.867 ± 0.183	1.243 ± 0.078	0.850 ± 0.062	0.403 ± 0.033	0.571 ± 0.049	0.245 ± 0.023
35	2.697 ± 0.225	1.216 ± 0.101	0.731 ± 0.033	0.231 ± 0.010	0.475 ± 0.036	0.213 ± 0.016

500 sec^{-1}						
Time (min)	TF	TF/TM	TF+ ATIII	TF/TM + ATIII	TF/Heparin	TF/TM-Heparin
0	0	0	0	0	0	0
0.5	1.037 ± 0.103	0.989 ± 0.101	1.220 ± 0.166	1.119 ± 0.165	0.773 ± 0.091	0.887 ± 0.080
1.5	7.308 ± 0.282	7.442 ± 0.275	6.387 ± 0.321	5.077 ± 0.368	5.600 ± 0.276	3.867 ± 0.236
2.5	11.408 ± 0.515	9.817 ± 0.392	8.261 ± 0.411	5.751 ± 0.313	7.198 ± 0.402	5.096 ± 0.249
3.5	11.847 ± 0.938	9.483 ± 0.240	7.683 ± 0.446	5.146 ± 0.287	6.611 ± 0.307	4.554 ± 0.390
4.5	12.277 ± 0.573	9.840 ± 0.537	7.469 ± 0.445	4.968 ± 0.162	6.391 ± 0.265	4.225 ± 0.401
6	12.053 ± 0.501	9.400 ± 0.540	6.656 ± 0.431	4.691 ± 0.152	5.460 ± 0.292	3.744 ± 0.181
8	11.814 ± 1.004	7.475 ± 0.562	5.914 ± 1.271	3.875 ± 0.266	4.780 ± 0.237	3.301 ± 0.198
10	12.180 ± 0.982	7.008 ± 0.504	5.072 ± 0.568	3.260 ± 0.288	4.292 ± 0.250	2.454 ± 0.222
12	11.117 ± 1.096	7.203 ± 0.254	4.404 ± 0.290	2.865 ± 0.355	3.911 ± 0.369	2.084 ± 0.206
14	12.072 ± 0.478	6.798 ± 0.302	4.268 ± 0.320	2.448 ± 0.184	3.329 ± 0.365	1.786 ± 0.224
16	11.770 ± 0.395	6.349 ± 0.398	3.918 ± 0.418	2.319 ± 0.186	2.872 ± 0.173	1.576 ± 0.085

Note: red-marked values contain more than 10% of standard error.

APPENDIX H

F Test for Equality of $[T]_{max}$ and $[T]_{ss}$ means among TF+AT, TF/TM+AT, TF/Heparin, and TF/TM-Heparin Systems

It is customary to begin the preliminary analysis of whether all the mean values of $[T]_{max}$ and $[T]_{ss}$ among the test systems containing ATIII are equal before pairwise comparison. The hypotheses we consider are"

H_0: all mean values are equal

H_a: not all mean values are equal

The test statistic is *F* test based on analysis of variance (ANOVA). When F is larger than its distributed form, F (1- α; r -1, n_T – r), we conclude H_a. Since we have four systems, there are four mean values (n = 5). Therefore, r and n_T are equal to 4 and 20, respectively. For 95 percentile (α = 0.05) of F distribution, F (0.95; 3, 16) is less than F (0.95; 3, 15), which is equal to 3.29. Mean values of $[T]_{max}$ and $[T]_{ss}$ at shear rates of 50 sec^{-1} and 500 sec^{-1} were statistically analyzed using ANOVA model and the results were computed by MINITAB (Release 13.1). All F values are much larger than F (0.95; 3, 16), so we conclude H_a. Results of ANOVA computed by MINTAB are shown below:

$[T]_{max}$ at 50 sec^{-1}

```
Analysis of Variance
Source     DF        SS        MS        F        P
Factor      3    120.58     40.19    26.28    0.000
Error      16     24.47      1.53
Total      19    145.05

                                 Individual 95% CIs For Mean
                                 Based on Pooled StDev
Level       N      Mean     StDev  ---+---------+---------+---------+---
TF+AT       5    19.263     1.727                          (----*----)
TF/Heparin  5    16.380     0.916                (----*---)
TF/TM+AT    5    13.860     1.263     (---*----)
TF/TM-Hep   5    12.942     0.837  (----*---)
                                 ---+---------+---------+---------+---
Pooled StDev =    1.237           12.5      15.0      17.5      20.0
```

$[T]_{ss}$ at 50 sec^{-1}

Analysis of Variance

Source	DF	SS	MS	F	P
Factor	3	100.04	33.35	**32.70**	0.000
Error	16	16.32	1.02		
Total	19	116.36			

Level	N	Mean	StDev
TF+AT_1	5	8.457	0.728
TF/Heparin	5	6.291	1.073
TF/TM+AT	5	3.882	1.028
TF/TM-Hep	5	2.645	1.159
Pooled StDev =		1.010	

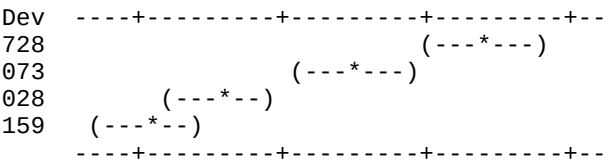

$[T]_{max}$ at 500 sec^{-1}

Analysis of Variance

Source	DF	SS	MS	F	P
Factor	3	37.635	12.545	**22.58**	0.000
Error	16	8.888	0.555		
Total	19	46.523			

Level	N	Mean	StDev
TF+AT_2	5	9.295	0.979
TF/Heparin	5	8.117	0.888
TF/TM+AT	5	6.588	0.634
TF/TM/Hep	5	5.736	0.269
Pooled StDev =		0.745	

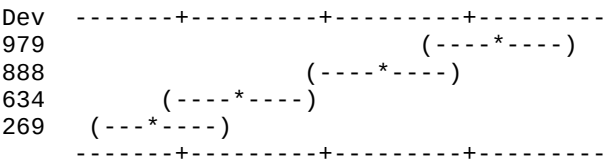

$[T]_{ss}$ at 500 sec^{-1}

Analysis of Variance

Source	DF	SS	MS	F	P
Factor	3	19.142	6.381	**15.29**	0.000
Error	16	6.678	0.417		
Total	19	25.820			

Level	N	Mean	StDev
TF+AT_3	5	4.5876	0.9365
TF/Heparin	5	3.3558	0.5444
TF/TM+AT	5	2.6958	0.4607
TF/TM-Hep	5	1.9198	0.5328
Pooled StDev =		0.6461	

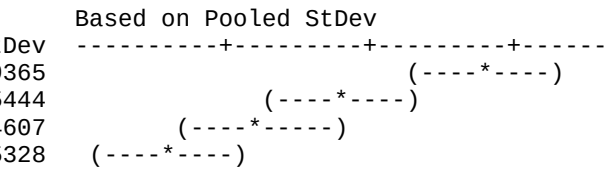

APPENDIX I

Tukey Multiple Comparison Procedure

To test whether the presence of surface TM causes significant difference in transient peak values of thrombin generation between TF+AT and TF/TM+AT at shear rate of 50 sec^{-1}, the hypotheses for comparison of $[T]_{TF+AT\ max}$ and $[T]_{TF/TM+AT\ max}$ are

H_o : μ of $[T]_{TF+AT\ max}$ = μ of $[T]_{TF/TM+AT\ max}$ (μ: mean value)

H_a : μ of $[T]_{TF+AT\ max}$ ≠ μ of $[T]_{TF/TM+AT\ max}$

The pairwise confidence limits are expressed as

$$D \pm Ts\{D\}$$

where

D: μ difference between $[T]_{TF+AT\ max}$ and $[T]_{TF/TM+AT\ max}$ = 19.26-13.86 = 5.40

$s\{D\}$: $\sqrt{\frac{MSE}{(1/n_1 + 1/n_2)}}$

MSE: error mean square = SSE/(n_T – r), r = 2 for two levels of factor

(SSE: error sum of squares, $n_T = n_1 + n_2$)

$T = q\,(1-\alpha; r; n_T - r)/(2^{1/2})$

q: the required percentile of the studentized range distribution

Data from each case has five replicates, meaning that $n_1 = n_2 = 5$. For confidence coefficient of 95 percent (1- α = 0.95), q (0.95; 2; 8) = 3.26, so we obtain T = 2.31. From the calculated MSE, which is 11.41, $s\{D\}$ is equal to 2.14, leading to $Ts\{D\}$ = 4.92. Therefore, the confidence limits are 5.40 ± 4.92 and confidence interval falls between 0.48 and 10.32. Since confidence interval does not include 0, conclusion H_a is reached,

meaning the difference between the maximum thrombin generation from TF+AT and that from TF/TM+AT is statistically significant.

REFERENCES

1. Graves, E., *Detailed diagnoses and procedures, National Hospital Discharge Survey, 1992. Series 13: Data from the National Hospital Survey.* Vital Health Stat, 1994. **13**(118): p. 1-281.

2. Eberhart, R.C., Huo, H-H, Nelson, K., Cardiovascular materials. MRS Bulletin, 1991. **19**: p. 50-4.

3. Chaikof, E.L., Merrill, E.W., Coleman, J.E., Ramberg, K., Connolly, R.J., Callow, A.D., *"Platelet interaction with poly(ethylene oxide)-polysiloxane networks". AIChEJ*, 1990. **36**: p. 994-1002.

4. Greisler, H.P., *New biologic and synthetic vascular protheses.* Austin: RG Landes Co., 1991.

5. Claggett, G.P., Burkel, W.E., Sharefkin, J.B., Ford, J.W., Hufnagel, H., Vinter, D.W., *Platelet reactivity in vivo in dogs with arterial prostheses seeded with endothelial cells.* Circulation, 1984. **69**: p. 632-9.

6. Pratt, G.H., *"Use of Teflon in replacement aortic and arterial segments". Am. J. Surg.*, 1984. **1**: p. 136-148.

7. Rutherford, R.B., Jones, D. N., Bergentz, S. E., Bergqvist, D., Comerota, A. J., Dardik, H., Flinn, W. H., Fry, W. J., McIntyre, K., Moore, W. S. and et al., *Factors affecting the patency of infrainguinal bypass. J Vasc Surg*, 1988. **8**(3): p. 236-46.

8. Hunink, M.G., Wong, J. B., Donaldson, M. C., Meyerovitz, M. F., Harrington, D. P., *Patency results of percutaneous and surgical revascularization for femoropopliteal arterial disease. Med Decis Making*, 1994. **14**(1): p. 71-81.

9. Goldberg, L., Bosco, P., Shors, E., Klein, S., Nelson, R., White, R., *Effect of surface porosity on early thrombogenicity using vascular grafts with two surfaces in sequence. Trans Am Soc Artif Intern Organs*, 1981. **27**: p. 517-21.

10. Itoh, T., Kambayashi, J., Tsujinaka, T., Sakon, M., Ohshiro, T., Mori, T., *Pathogenesis of early thrombus formation in experimental vein graft. Thromb Res*, 1989. **53**(4): p. 357-65.

11. Wu, M.H., Kouchi, Y., Onuki, Y., Shi, Q., Yoshida, H., Kaplan, S., Viggers, R. F., Ghali, R., Sauvage, L. R., *Effect of differential shear stress on platelet aggregation, surface thrombosis, and endothelialization of bilateral carotid-femoral grafts in the dog. J Vasc Surg*, 1995. **22**(4): p. 382-90; discussion 390-2.

12. Murugesan, G., Rani, M. R., Ransohoff, R. M., Marchant, R. E., Kottke-Marchant, K., *Endothelial cell expression of monocyte chemotactic protein-1, tissue factor, and thrombomodulin on hydrophilic plasma polymers. J Biomed Mater Res*, 2000. **49**(3): p. 396-408.

13. Carson, S.D., Brozna, J. P., *The role of tissue factor in the production of thrombin.* Blood Coagul Fibrinolysis, 1993. **4**(2): p. 281-92.

14. Butenas, S., Mann, K. G., *Blood coagulation.* Biochemistry (Mosc), 2002. **67**(1): p. 3-12.

15. McVey, J.H., *Tissue factor pathway.* Baillieres Best Pract Res Clin Haematol, 1999. **12**(3): p. 361-72.

16. Morrissey, J.H., *Tissue factor: an enzyme cofactor and a true receptor. Thromb Haemost*, 2001. **86**(1): p. 66-74.

17. Kirchhofer, D., Nemerson, Y., *Initiation of blood coagulation: the tissue factor/factor VIIa complex.* Curr Opin Biotechnol, 1996. **7**(4): p. 386-91.

18. Neuenschwander, P.F., M.M. Fiore, and J.H. Morrissey, *Factor VII autoactivation proceeds via interaction of distinct protease-cofactor and zymogen-cofactor complexes. Implications of a two-dimensional enzyme kinetic mechanism.* J Biol Chem, 1993. **268**(29): p. 21489-92.

19. Eichinger, S., Mannucci, P. M., Tradati, F., Arbini, A. A., Rosenberg, R. D., Bauer, K. A., *Determinants of plasma factor VIIa levels in humans.* Blood, 1995. **86**(8): p. 3021-5.

20. Silverberg, S.A., Nemerson, Y., Zur, M., *Kinetics of the activation of bovine coagulation factor X by components of the extrinsic pathway. Kinetic behavior of two-chain factor VII in the presence and absence of tissue factor.* J Biol Chem, 1977. **252**(23): p. 8481-8.

21. Bom, V.J., Bertina, R. M., *The contributions of Ca2+, phospholipids and tissue-factor apoprotein to the activation of human blood-coagulation factor X by activated factor VII.* Biochem J, 1990. **265**(2): p. 327-36.

22. Komiyama, Y., Pedersen, A. H., Kisiel, W., *Proteolytic activation of human factors IX and X by recombinant human factor VIIa: effects of calcium, phospholipids, and tissue factor.* Biochemistry, 1990. **29**(40): p. 9418-25.

23. Lawson, J.H., Mann, K. G., *Cooperative activation of human factor IX by the human extrinsic pathway of blood coagulation.* J Biol Chem, 1991. **266**(17): p. 11317-27.

24. Butenas, S., van 't Veer, C., Mann, K. G., *Evaluation of the initiation phase of blood coagulation using ultrasensitive assays for serine proteases.* J Biol Chem, 1997. **272**(34): p. 21527-33.

25. van 't Veer, C., Golden, N.J., Kalafatis, M., Mann, K.G., *Inhibitory mechanism of the protein C pathway on tissue factor-induced thrombin generation. Synergistic effect in combination with tissue factor pathway inhibitor.* J Biol Chem, 1997. **272**(12): p. 7983-94.

26. Lawson, J.H., Kalafatis, M., Stram, S., Mann, K. G., *A model for the tissue factor pathway to thrombin. I. An empirical study.* J Biol Chem, 1994. **269**(37): p. 23357-66.

27. Rand, M.D., Lock, J. B., van't Veer, C., Gaffney, D. P., Mann, K. G., *Blood clotting in minimally altered whole blood.* Blood, 1996. **88**(9): p. 3432-45.

28. Papahadjopoulos, D., Hanahan, D. J., *Observations on the Interaction of Phospholipids and Certain Clotting Factors in Prothrombin Activator Formation.* Biochim Biophys Acta, 1964. **90**: p. 436-9.

29. Nesheim, M.E., Taswell, J. B., Mann, K. G., *The contribution of bovine Factor V and Factor Va to the activity of prothrombinase.* J Biol Chem, 1979. **254**(21): p. 10952-62.

30. Kalafatis, M., Swords, N. A., Rand, M. D., Mann, K. G., *Membrane-dependent reactions in blood coagulation: role of the vitamin K-dependent enzyme complexes.* Biochim Biophys Acta, 1994. **1227**(3): p. 113-29.

31. Pieters, J., Lindhout, T., Hemker, H. C., *In situ-generated thrombin is the only enzyme that effectively activates factor VIII and factor V in thromboplastin-activated plasma.* Blood, 1989. **74**(3): p. 1021-4.

32. Bailey, K., Bettelheim, F. R., Lorand, L., Middlebrook, W. R., *Action of thrombin in the clotting of fibrinogen.* Nature, 1951. **167**(4241): p. 233-4.

33. Mosesson, M.W., *The roles of fibrinogen and fibrin in hemostasis and thrombosis.* Semin Hematol, 1992. **29**(3): p. 177-88.

34. Naski, M.C., Lorand, L., Shafer, J. A., *Characterization of the kinetic pathway for fibrin promotion of alpha-thrombin-catalyzed activation of plasma factor XIII.* Biochemistry, 1991. **30**(4): p. 934-41.

35. Lorand, L., Konishi, K., *Activation of the Fibrin Stabilizing Factor of Plasma by Thrombin.* Arch Biochem Biophys, 1964. **105**: p. 58-67.

36. Olson, S.T., Bjork, I., Shore, J. D., *Kinetic characterization of heparin-catalyzed and uncatalyzed inhibition of blood coagulation proteinases by antithrombin.* Methods Enzymol, 1993. **222**: p. 525-59.

37. Jordan, R.E., Oosta, G. M., Gardner, W. T., Rosenberg, R. D., *The kinetics of hemostatic enzyme-antithrombin interactions in the presence of low molecular weight heparin. J Biol Chem*, 1980. **255**(21): p. 10081-90.

38. Olson, S.T., Bjork, I., Sheffer, R., Craig, P. A., Shore, J. D., Choay, J., *Role of the antithrombin-binding pentasaccharide in heparin acceleration of antithrombin-proteinase reactions. Resolution of the antithrombin conformational change contribution to heparin rate enhancement.* J Biol Chem, 1992. **267**(18): p. 12528-38.

39. Lollar, P., Owen, W. G., *Clearance of thrombin from circulation in rabbits by high-affinity binding sites on endothelium. Possible role in the inactivation of thrombin by antithrombin III.* J Clin Invest, 1980. **66**(6): p. 1222-30.

40. Busch, C., Owen, W. G., *Identification in vitro of an endothelial cell surface cofactor for antithrombin III. Parallel studies with isolated perfused rat hearts and microcarrier cultures of bovine endothelium.* J Clin Invest, 1982. **69**(3): p. 726-9.

41. Marcum, J.A., Rosenberg, R. D., *Heparinlike molecules with anticoagulant activity are synthesized by cultured endothelial cells.* Biochem Biophys Res Commun, 1985. **126**(1): p. 365-72.

42. Marcum, J.A., McKenney, J. B., Rosenberg, R. D., *Acceleration of thrombin-antithrombin complex formation in rat hindquarters via heparinlike molecules bound to the endothelium.* J Clin Invest, 1984. **74**(2): p. 341-50.

43. Stern, D., Nawroth, P., Marcum, J., Handley, D., Kisiel, W., Rosenberg, R., Stern, K., *Interaction of antithrombin III with bovine aortic segments. Role of heparin in binding and enhanced anticoagulant activity.* J Clin Invest, 1985. **75**(1): p. 272-9.

44. Girard, T.J., Warren, L. A., Novotny, W. F., Likert, K. M., Brown, S. G., Miletich, J. P., Broze, G. J., Jr., *Functional significance of the Kunitz-type inhibitory domains of lipoprotein-associated coagulation inhibitor. Nature*, 1989. **338**(6215): p. 518-20.

45. Rapaport, S.I., *The extrinsic pathway inhibitor: a regulator of tissue factor-dependent blood coagulation.* Thromb Haemost, 1991. **66**(1): p. 6-15.

46. Broze, G.J., Jr., et al., *The lipoprotein-associated coagulation inhibitor that inhibits the factor VII-tissue factor complex also inhibits factor Xa: insight into its possible mechanism of action.* Blood, 1988. **71**(2): p. 335-43.

47. Esmon, C.T., *The roles of protein C and thrombomodulin in the regulation of blood coagulation. J Biol Chem*, 1989. **264**(9): p. 4743-6.

48. Kisiel, W., *Human plasma protein C: isolation, characterization, and mechanism of activation by alpha-thrombin. J Clin Invest*, 1979. **64**(3): p. 761-9.

49. Kisiel, W., Canfield, W. M., Ericsson, L. H., Davie, E. W., *Anticoagulant properties of bovine plasma protein C following activation by thrombin.* Biochemistry, 1977. **16**(26): p. 5824-31.

50. Nemerson, Y., Turitto, V. T., *The effect of flow on hemostasis and thrombosis. Thromb Haemost*, 1991. **66**(3): p. 272-6.

51. Mohamed, M.S., Mukherjee, M., Kakkar, V. V., *Thrombogenicity of heparin and non-heparin bound arterial prostheses: an in vitro evaluation.* J R Coll Surg Edinb, 1998. **43**(3): p. 155-7.

52. Park, K.D., Okano, T., Nojiri, C., Kim, S. W., *Heparin immobilization onto segmented polyurethane-urea surfaces--effect of hydrophilic spacers. J Biomed Mater Res*, 1988. **22**(11): p. 977-92.

53. Mottaghy, K., Oedekoven, B., Poppel, K., Bruchmuller, K., Kovacs, B., Spahn, A., Geisen, C., *Heparin free long-term extracorporeal circulation using bioactive surfaces. ASAIO Trans*, 1989. **35**(3): p. 635-7.

54. Kishida, A., Ueno, Y., Maruyama, I., Akashi, M., *Immobilization of human thrombomodulin on biomaterials: evaluation of the activity of immobilized human thrombomodulin. Biomaterials*, 1994. **15**(14): p. 1170-4.

55. Kishida, A., Ueno, Y., Fukudome, N., Yashima, E., Maruyama, I., Akashi, M., *Immobilization of human thrombomodulin onto poly(ether urethane urea) for developing antithrombogenic blood-contacting materials. Biomaterials*, 1994. **15**(10): p. 848-52.

56. Kishida, A., Ueno, Y., Maruyama, I., Akashi, M., *Immobilization of human thrombomodulin onto biomaterials. Comparison of immobilization methods and evaluation of antithrombogenicity. Asaio J*, 1994. **40**(3): p. M840-5.

57. Kishida, A., Akatsuka, Y., Yanagi, M., Aikou, T., Maruyama, I., Akashi, M., *In vivo and ex vivo evaluation of the antithrombogenicity of human thrombomodulin immobilized biomaterials. Asaio J*, 1995. **41**(3): p. M369-74.

58. Sperling, C., Konig, U., Hermel, G., Werner, C., Muller, M., Simon, F., Grundke, K., Jacobasch, H. J., Vasilets, V. N., Ikada, Y., *Immobilization of human thrombomodulin onto PTFE. J Mater Sci Mater Med*, 1997. **8**(12): p. 789-91.

59. Vasilets, V.N., Hermel, G., Konig, U.,Werner, C., Muller, M., Simon, F., Grundke, K., Ikada, Y., Jacobasch, H. J., *Microwave CO2 plasma-initiated vapour phase graft polymerization of acrylic acid onto polytetrafluoroethylene for immobilization of human thrombomodulin. Biomaterials*, 1997. **18**(17): p. 1139-45.

60. Esmon, C.T., *Thrombomodulin as a model of molecular mechanisms that modulate protease specificity and function at the vessel surface. Faseb J*, 1995. **9**(10): p. 946-55.

61. Esmon, N.L., DeBault, L. E., Esmon, C. T., *Proteolytic formation and properties of gamma-carboxyglutamic acid-domainless protein C. J Biol Chem*, 1983. **258**(9): p. 5548-53.

62. Mann, K.G., Jenny, R. J., Krishnaswamy, S., *Cofactor proteins in the assembly and expression of blood clotting enzyme complexes. Annu Rev Biochem*, 1988. **57**: p. 915-56.

63. Kalafatis, M., Egan, J. O., van't Veer, C., Mann, K. G., *Regulation and regulatory role of gamma-carboxyglutamic acid containing clotting factors. Crit Rev Eukaryot Gene Expr*, 1996. **6**(1): p. 87-101.

64. Schnur, J., *Lipid tubules: A paradigm for moleculary engineerd structures.* Science, 1994. **262**: p. 1669-76.

65. Seifert, K., Fendler, K., Bamberg, E., *Charge transport by ion translocating membrane proteins on solid supported membranes. Biophys J*, 1993. **64**(2): p. 384-91.

66. Florin, E.L., Gaub, H.E.. *Painted supported lipid membranes.* Biophys J, 1993. **64**: p. 375-83.

67. Spinke, J., Yang, J., Wolf, H., Liley, M., Ringsdorf, H., Knoll, W., *Polymer-supported bilayer on a solid substrate.* Biophys J, 1992. **63**: p. 1667-71.

68. Ulman, A., *An introduction to ultrathin organic films from Langmuir-Blodgett to self-assembly. New York: Academic Press.* 1991.

69. Cevc, G., Marsh, D., *Phospholipid Bilayers.* New York: Wiley, 1987.

70. Helm, C.A., Knoll, W., Israelachvili, J. N., *Measurement of ligand-receptor interactions.* Proc Natl Acad Sci U S A, 1991. **88**(18): p. 8169-73.

71. Pearce, K.H., Hof, M., Lentz, B. R., Thompson, N. L., *Comparison of the membrane binding kinetics of bovine prothrombin and its fragment 1. J Biol Chem*, 1993. **268**(31): p. 22984-91.

72. Tendian, S.W., Lentz, B. R., Thompson, N. L., *Evidence from total internal reflection fluorescence microscopy for calcium-independent binding of prothrombin to negatively charged planar phospholipid membranes. Biochemistry*, 1991. **30**(45): p. 10991-9.

73. Ishihara, K., Tsuji, T., Kurosaki, T., Nakabayashi, N., *Hemocompatibility on graft copolymers composed of poly(2-methacryloyloxyethyl phosphorylcholine) side chain and poly(n-butyl methacrylate) backbone. J Biomed Mater Res*, 1994. **28**(2): p. 225-32.

74. Hayward, J.A., Chapman, D., *Biomembrane surfaces as models for polymer design: the potential for haemocompatibility. Biomaterials*, 1984. **5**(3): p. 135-42.

75. Hall, B., Bird, R. R., Kojima, M., Chapman, D., *Biomembranes as models for polymer surfaces. V. Thrombelastographic studies of polymeric lipids and polyesters. Biomaterials*, 1989. **10**(4): p. 219-24.

76. Chapman, D., *Biomembranes and new hemocompatible materials. Langmuir*, 1993. **9**: p. 39-45.

77. Marra, K.G., Winger, T.M., Hanson, S.R., and Chaikof, E.L., *Cytomimetic biomaterials. 1. In-situ polymerization of phospholipids on an alkylated surface. Macromolecules*, 1997. **30**: p. 6483-7.

78. Orban, J.M., Faucher, K.M., Dluhy, R.A., Chaikof, E.L., *"Cytomimetic Biomaterials. 4. In-Situ Photopolymerization of Phospholipids on an Alkylated Surface." Macromolecules*, 2000. **33**: p. 4205.

79. Feng, J., Tseng, P-Y., Faucher K.M., Orban J.M., Sun, X-L, Chaikof E.L., *"Functional Reconstitution of Thrombomodulin within a Substrate-Supported Membrane-Mimetic Polymer Film". Langmuir*, 2002. **18**: p. 9907-9913.

80. Faucher, K.M., Sun, Xue-Long, Chaikof, E.L., *"Fabrication and Characterization of Glycocalyx-Mimetic Surfaces". Langmuir*, 2003. **19**: p. 1664-1670.

81. Bourin, M.C., Lindahl, U., *Glycosaminoglycans and the regulation of blood coagulation. Biochem J*, 1993. **289**: p. 313-30.

82. de Agostini, A.I., Watkins, S. C., Slayter, H. S., Youssoufian, H., Rosenberg, R. D., *Localization of anticoagulantly active heparan sulfate proteoglycans in vascular endothelium: antithrombin binding on cultured endothelial cells and perfused rat aorta. J Cell Biol*, 1990. **111**(3): p. 1293-304.

83. Lollar, P., MacIntosh, S. C., Owen, W. G., *Reaction of antithrombin III with thrombin bound to the vascular endothelium. Analysis in a recirculating perfused rabbit heart preparation. J Biol Chem*, 1984. **259**(7): p. 4335-8.

84. Kalafatis, M., Egan, J. O., van 't Veer, C., Cawthern, K. M., Mann, K. G., *The regulation of clotting factors. Crit Rev Eukaryot Gene Expr*, 1997. **7**(3): p. 241-80.

85. Li, J.M., Singh, M. J., Nelson, P. R., Hendricks, G. M., Itani, M., Rohrer, M. J., Cutler, B. S., *Immobilization of human thrombomodulin to expanded polytetrafluoroethylene.* J Surg Res, 2002. **105**(2): p. 200-8.

86. Han, H.S., Yang, S. L., Yeh, H. Y., Lin, J. C., Wu, H. L., Shi, G. Y., *Studies of a novel human thrombomodulin immobilized substrate: surface characterization and anticoagulation activity evaluation. J Biomater Sci Polym Ed*, 2001. **12**(10): p. 1075-89.

87. Sperling, C., Salchert, K., Streller, U., Werner, C., *Covalently immobilized thrombomodulin inhibits coagulation and complement activation of artificial surfaces in vitro. Biomaterials*, 2004. **25**(21): p. 5101-13.

88. Lu, R.L., Esmon, N. L., Esmon, C. T., Johnson, A. E., *The active site of the thrombin-thrombomodulin complex. A fluorescence energy transfer measurement of its distance above the membrane surface. J Biol Chem*, 1989. **264**(22): p. 12956-62.

89. Yegneswaran, S., Smirnov, M. D., Safa, O., Esmon, N. L., Esmon, C. T., Johnson, A. E., *Relocating the active site of activated protein C eliminates the need for its protein S cofactor. A fluorescence resonance energy transfer study. J Biol Chem*, 1999. **274**(9): p. 5462-8.

90. Sadler, J.E., *Thrombomodulin structure and function. Thromb Haemost*, 1997. **78**(1): p. 392-5.

91. Galvin, J.B., Kurosawa, S., Moore, K., Esmon, C. T., Esmon, N. L., *Reconstitution of rabbit thrombomodulin into phospholipid vesicles. J Biol Chem*, 1987. **262**(5): p. 2199-205.

92. Xu, J., Esmon, N. L., Esmon, C. T., *Reconstitution of the human endothelial cell protein C receptor with thrombomodulin in phosphatidylcholine vesicles enhances protein C activation. J Biol Chem*, 1999. **274**(10): p. 6704-10.

93. Christiansen, W.T., Jalbert, L. R., Robertson, R. M., Jhingan, A., Prorok, M., Castellino, F. J., *Hydrophobic amino acid residues of human anticoagulation protein C that contribute to its functional binding to phospholipid Vesicles. Biochemistry*, 1995. **34**(33): p. 10376-82.

94. Sun, X.-L., Liu, H., Orban, J.M., Sun, L., Chaikof, E.L., *Synthesis and terminal functionalization of a polymerizable phosphatidylethanolamine. Bioconjug Chem*, 2001. **12**(5): p. 673-7.

95. Chon, J.H., Marra, K. G., Chaikof, E. L., *Cytomimetic biomaterials. 3. Preparation and transport studies of an alginate/amphiphilic copolymer/polymerized phospholipid film. J Biomater Sci Polym Ed*, 1999. **10**(1): p. 95-107.

96. Liu, H., Faucher, K.M. , Sun, X-L, Feng, J., Johnson, T.L., Orban, J.M., Apkarian, A.P., Dluhy, R.A., Chaikof, E.L., *A Membrane-Mimetic Barrier for Cell Encapsulation. Langmuir*, 2002. **18**(4): p. 1332.

97. Deen, W.M., *Analysis of transport phenomena*. 1998, New York ; Hong Kong: Oxford University Press. xix, 597 p.
98. Mann, K.G., Krishnaswamy, S., Lawson, J. H., *Surface-dependent hemostasis. Semin Hematol*, 1992. **29**(3): p. 213-26.

99. Tracy, P.B., Nesheim, M. E., Mann, K. G., *Coordinate binding of factor Va and factor Xa to the unstimulated platelet. J Biol Chem*, 1981. **256**(2): p. 743-51.

100. Lamphear, B.J., Fay, P. J., *Factor IXa enhances reconstitution of factor VIIIa from isolated A2 subunit and A1/A3-C1-C2 dimer. J Biol Chem*, 1992. **267**(6): p. 3725-30.

101. Chen, C., Ofenloch, J. C., Yianni, Y. P.,Hanson, S. R., Lumsden, A. B., *Phosphorylcholine coating of ePTFE reduces platelet deposition and neointimal hyperplasia in arteriovenous grafts. J Surg Res*, 1998. **77**(2): p. 119-25.

102. Kobayashi, T. and K.J. Laidler, *"Theory of the kinetics of reactions catalyzed by enzymes attached to membranes".* Biotechnol Bioeng, 1974. **16**(1): p. 77-97.

103. Laidler, K.J., Bunting, P. S., *"The kinetics of immobilized enzyme systems". Methods in Enzymology*, 1980. **64**: p. 227-48.

104. Geankoplis, C.J., *Transport processes and unit operations*. 3rd ed. 1993, Engelwood Cliffs, N.J.: PTR Prentice Hall. xiii, 921 p.
105. Polson, A., *J. Phys. Colloid Chem.*, 1950. **54**: p. 649.

106. Kuharsky, A.L., Fogelson A.L., *"Surface-mediated control of blood coagulation: the role of binding site densities and platelet deposition". Biophys J*, 2001. **80**(3): p. 1050-74.

107. Cussler, E.L., *Diffusion : mass transfer in fluid systems*. 2nd ed. 1997, New York: Cambridge University Press. xviii, 580 p.
108. Gleason, N.J. and J.D. Carbeck, *Measurement of enzyme kinetics using microscale steady-state kinetic analysis.* Langmuir, 2004. **20**(15): p. 6374-81.

109. Andree, H.A., Contino, P. B.,Repke, D.,Gentry, R.,Nemerson, Y., *"Transport rate limited catalysis on macroscopic surfaces: the activation of factor X in a continuous flow enzyme reactor".* Biochemistry, 1994. **33**(14): p. 4368-74.

110. Bailey, J.E., and Ollis, D.F., *Biochemical Engineering Fundamentals*. Second ed. Chemical Engineering. 1986: McGraw-Hill, Inc.
111. Billy, D., Speijer, H., Willems, G., Hemker, H. C., Lindhout, T., *Prothrombin activation by prothrombinase in a tubular flow reactor. J Biol Chem*, 1995. **270**(3): p. 1029-34.

112. Gemmell, C., Nemerson, Y., Turitto, V., *The effects of shear rate on the enzymatic activity of the tissue factor-factor VIIa complex.* Microvasc Res, 1990. **40**(3): p. 327-40.

113. Elisen, M.G., von dem Borne, P. A., Bouma, B. N., Meijers, J. C., *Protein C inhibitor acts as a procoagulant by inhibiting the thrombomodulin-induced activation of protein C in human plasma. Blood*, 1998. **91**(5): p. 1542-7.

114. Rezaie, A.R., Cooper, S. T., Church, F. C., Esmon, C. T., *Protein C inhibitor is a potent inhibitor of the thrombin-thrombomodulin complex. J Biol Chem*, 1995. **270**(43): p. 25336-9.

115. Hayashi, T., Honda, G., Suzuki, K., *An atherogenic stimulus homocysteine inhibits cofactor activity of thrombomodulin and enhances thrombomodulin expression in human umbilical vein endothelial cells. Blood*, 1992. **79**(11): p. 2930-6.

116. Liang, J.F., Li, Y. T., Yang, V. C., *Biomedical application of immobilized enzymes. J Pharm Sci*, 2000. **89**(8): p. 979-90.

117. Lindholm-Sethson, B., Nystrom, J., Geladi, P., Koeppe, R., Nelson, A., Whitehouse, C., *Are biosensor arrays in one membrane possible? A combination of multifrequency impedance measurements and chemometrics. Anal Bioanal Chem*, 2003. **377**(3): p. 478-85.

118. Walde, P., Ichikawa, S., *Enzymes inside lipid vesicles: preparation, reactivity and applications. Biomol Eng*, 2001. **18**(4): p. 143-77.

119. Best, C.H., *Preparation of heparin and its use in the first clinical cases. Circulation*, 1959. **19**(1): p. 79-86.

120. Olson, S.T., Bjork, I., *Regulation of thrombin activity by antithrombin and heparin. Semin Thromb Hemost*, 1994. **20**(4): p. 373-409.
121. Bjork, I., Lindahl, U., *Mechanism of the anticoagulant action of heparin. Mol. Cel Biochem.*, 1982. **48**(3): p. 161-82.

122. Nader, H.B., Dietrich, C.P., *Natural occurrence, and possible biological role of heparin. In: Heparin chemical and biological properties, clinical applications. Lane DA, Lindahl U (eds), Edward Arnold, London, 81-96*. 1988.

123. Rosenberg, R.D., *Biochemistry of heparin antithrombin interactions, and the physiologic role of this natural anticoagulant mechanism. Am J Med*, 1989. **87**(3B): p. 2S-9S.

124. Ersdal-Badju, E., Lu, A., Zuo, Y., Picard, V., Bock, S. C., *Identification of the antithrombin III heparin binding site. J Biol Chem*, 1997. **272**(31): p. 19393-400.

125. Desai, U.R., Petitou, M., Bjork, I., Olson, S. T., *Mechanism of heparin activation of antithrombin: evidence for an induced-fit model of allosteric activation involving two interaction subsites. Biochemistry*, 1998. **37**(37): p. 13033-41.

126. Beeler, D., Rosenberg, R., Jordan, R., *Fractionation of low molecular weight heparin species and their interaction with antithrombin. J Biol Chem*, 1979. **254**(8): p. 2902-13.

127. Griffith, M.J., *Measurement of the heparin enhanced-antithrombin III/thrombin reaction rate in the presence of synthetic substrate. Thromb Res*, 1982. **25**(3): p. 245-53.

128. Griffith, M.J., *Kinetics of the heparin-enhanced antithrombin III/thrombin reaction. Evidence for a template model for the mechanism of action of heparin.* J Biol Chem, 1982. **257**(13): p. 7360-5.

129. Olson, S.T., Bjork, I., *Predominant contribution of surface approximation to the mechanism of heparin acceleration of the antithrombin-thrombin reaction. Elucidation from salt concentration effects. J Biol Chem*, 1991. **266**(10): p. 6353-64.

130. Maaroufi, R.M., Jozefowicz, M., Tapon-Bretaudiere, J., Fischer, A.M., *"Mechanism of thrombin inhibition by antithrombin and heparin cofactor II in the presence of heparin". Biomaterials*, 1997. **18**(3): p. 203-11.

131. Nojiri, C., Okano, T., Park, K. D., Kim, S. W., *Suppression mechanisms for thrombus formation on heparin-immobilized segmented polyurethane-ureas. ASAIO Trans*, 1988. **34**(3): p. 386-98.

132. Ebert, C.D., Lee, E. S., Kim, S. W., *The antiplatelet activity of immobilized prostacyclin. J Biomed Mater Res*, 1982. **16**(5): p. 629-38.

133. Byun, Y., Jacobs, H. A.,K im, S. W., *Binding kinetics of thrombin and antithrombin III with immobilized heparin using a spacer. Asaio J*, 1992. **38**(3): p. M649-53.

134. Byun, Y., Jacobs, H. A., Kim, S. W., *Heparin surface immobilization through hydrophilic spacers: thrombin and antithrombin III binding kinetics. J Biomater Sci Polym Ed*, 1994. **6**(1): p. 1-13.

135. H Liu, K.F., XL Sun, J Feng, TL Johnson, JM Orban, RP Apkarian, RA Dluhy, EL Chaikof., *A Membrane-Mimetic Barrier for Cell Encapsulation. Langmuir*, 2002. **18**(4): p. 1332.

136. Tseng, P.-Y., Rele, S.S., Sun, X-L, and Chaikof, E.L., *Fabrication and Characterization of Heparin- Functionalized Membrane-Mimetic Assemblies.* Biomaterials, 2005 (in press).

137. Henrickson, K.P., et al., *"An avidin monomer affinity column for the purification of biotin-containing enzymes." Anal. Biochem.*, 1979. **94**: p. 366-70.

138. Green, N.M.a.T., E.J., *"The properties of subunits of avidin coupled to Sepharose." Biochem. J.*, 1973. **133**: p. 687-698.

139. RB Guchait, e.a., *"Acetyl coenzyme A carboxylase system of Escherichia coli. Purification and properties of the biotin carboxylase, carboxyltransferase, and carboxyl carrier protein components." J. Biol. Chem.*, 1974. **249**(6633-45).

140. Green, N.M., *"Spectrophotometric determination of avidin and biotin".* Methods Enzymol., 1970. **18A**: p. 418.

141. Griffith, M.J., *"The heparin-enhanced antithrombin III/thrombin reaction is saturable with respect to both thrombin and antithrombin III". J Biol Chem*, 1982. **257**(23): p. 13899-302.

142. Pletcher, C.H. and G.L. Nelsestuen, *The rate-determining step of the heparin-catalyzed antithrombin/thrombin reaction is independent of thrombin.* J Biol Chem, 1982. **257**(10): p. 5342-5.

143. Lindhout, T., Blezer, R., Schoen, P., Willems, G. M., Fouache, B., Verhoeven, M., Hendriks, M. Cahalan, L., and P.T. Cahalan, *"Antithrombin activity of surface-bound heparin studied under flow conditions". J Biomed Mater Res*, 1995. **29**(10): p. 1255-66.

144. Jordan, R.E., et al., *The binding of low molecular weight heparin to hemostatic enzymes.* J Biol Chem, 1980. **255**(21): p. 10073-80.

145. Olson, S.T., *"Transient kinetics of heparin-catalyzed protease inactivation by antithrombin III. Linkage of protease-inhibitor-heparin interactions in the reaction with thrombin". J Biol Chem*, 1988. **263**(4): p. 1698-708.

146. Jung, L.S., Nelson, K.E., Stayton, P.S., and Campbell, C.T., *Binding and Dissociation Kinetics of Wild-Type and Mutant Streptavidins on Mixed Biotin-Containing Alkylthiolate Monolayers. Langmuir*, 2000. **16**: p. 9421-9432.

147. Jung, L.S., Nelson, K.E., Campbell, C.T., Stayton, P.S., Yee, S.S., Luna, V.P., Lopez, G.P., *"Surface plasmon resonance measurement of binding and dissociation of wild-type and mutant streptavidin on mixed biotin-containing alkylthiolate monolayers".* Sensors and Actuators, 1999. **B54**: p. 137-144.

148. Jung, L.S., Shumaker-Parry, J.S., Campbell, C.T., Yee, S.S., Gelb, M.H., *"Quantification of Tight Binding to Surface-Immobilized Phospholipid Vesicles Using Surface Plasmon Resonance: Binding Constant of Phospholipase A2". J. Am. Chem. Soc.*, 2000. **122**: p. 4177-4184.

149. Spinke, J., Liley, M., Schmitt, F.J., Guder, J.H., Angermaier, L., Knoll, W., *"Molecular recognition at a self-assembled monolayers: optimization of surface functionalization". Journal of Chemical Physics*, 1993. **99(9)**: p. 7012-19.

150. Spinke, J., Liley, M., Guder, J.H., Angermaier, L., Knoll, W., *"Molecular recognition at self-assembled monolayers: the construction of multicomponent multilayers".* Langmuir, 1993. **9(7)**: p. 1821-5.

151. Knoll, W., Angermaier, L., Batz, G., Fritz, T., Fujisawa, S., Furuno, T., Guder, H.J., Hara, M., Liley, M., Niki, K., Spinke, J., *"Supramolecular engineering at functionalized surfaces ".* Synthetic Metals, 1993. **61**(1-2): p. 5-11.

152. Galyautdinov, G.S., Kornilova, Y.L., *"Antithrombin III: Physiology and clinical significance".* Thoracic and Cardiovascular Surgery, 2002.

153. Griffith, M.J., Carraway, T., White, G.C., Dombrose, F.A., *"Heparin cofactor activities in a family with hereditary antithrombin III deficiency: evidence for a second heparin cofactor in human plasma". Blood*, 1983. **61**(1): p. 111-8.

154. Murano, G., et al., *Some properties of antithrombin-III and its concentration in human plasma.* Thromb Res, 1980. **18**(1-2): p. 259-62.

155. Mann, K.G., van't Veer, C., Cawthern, K., Butenas, S., *The role of the tissue factor pathway in initiation of coagulation. Blood Coagul Fibrinolysis*, 1998. **9 Suppl 1**: p. S3-7.

156. Drake, T.A., Morrissey, J. H., Edgington, T. S., *Selective cellular expression of tissue factor in human tissues. Implications for disorders of hemostasis and thrombosis. Am J Pathol*, 1989. **134**(5): p. 1087-97.

157. Bevilacqua, M.P., Pober, J. S., Majeau, G. R., Cotran, R. S., Gimbrone, M. A., Jr., *Interleukin 1 (IL-1) induces biosynthesis and cell surface expression of procoagulant activity in human vascular endothelial cells. J Exp Med*, 1984. **160**(2): p. 618-23.

158. Bevilacqua, M.P., Pober, J. S., Wheeler, M. E., Cotran, R. S., Gimbrone, M. A., Jr., *Interleukin-1 activation of vascular endothelium. Effects on procoagulant activity and leukocyte adhesion. Am J Pathol*, 1985. **121**(3): p. 394-403.

159. Bevilacqua, M.P., Pober, J. S., Wheeler, M. E., Cotran, R. S., Gimbrone, M. A., Jr., *Interleukin 1 acts on cultured human vascular endothelium to increase the adhesion of polymorphonuclear leukocytes, monocytes, and related leukocyte cell lines. J Clin Invest*, 1985. **76**(5): p. 2003-11.

160. Bevilacqua, M.P., Pober, J. S., Majeau, G. R., Fiers, W., Cotran, R. S., Gimbrone, M. A., Jr., *Recombinant tumor necrosis factor induces procoagulant activity in cultured human vascular endothelium: characterization and comparison with the actions of interleukin 1. Proc Natl Acad Sci U S A*, 1986. **83**(12): p. 4533-7.

161. Taubman, M.B., Fallon, J. T., Schecter, A. D., Giesen, P., Mendlowitz, M., Fyfe, B. S., Marmur, J. D., Nemerson, Y., *Tissue factor in the pathogenesis of atherosclerosis. Thromb Haemost*, 1997. **78**(1): p. 200-4.

162. Rickles, F.R., Hair, G. A., Zeff, R. A., Lee, E., Bona, R. D., *Tissue factor expression in human leukocytes and tumor cells. Thromb Haemost*, 1995. **74**(1): p. 391-5.

163. Robson, S.C., Schulte am Esch, J., 2nd, Bach, F. H., *Factors in xenograft rejection. Ann N Y Acad Sci*, 1999. **875**: p. 261-76.

164. Morrissey, J.H., Macik, B. G., Neuenschwander, P. F., Comp, P. C., *Quantitation of activated factor VII levels in plasma using a tissue factor mutant selectively deficient in promoting factor VII activation. Blood*, 1993. **81**(3): p. 734-44.

165. Tsujioka, H., Suehiro, A., Kakishita, E., *Activation of coagulation factor VII by tissue-type plasminogen activator. Am J Hematol*, 1999. **61**(1): p. 34-9.

166. Masys, D.R., Bajaj, S. P., Rapaport, S. I., *Activation of human factor VII by activated factors IX and X. Blood*, 1982. **60**(5): p. 1143-50.

167. Seligsohn, U., Osterud, B., Brown, S. F., Griffin, J. H., Rapaport, S. I., *Activation of human factor VII in plasma and in purified systems: roles of activated factor IX, kallikrein, and activated factor XII. J Clin Invest*, 1979. **64**(4): p. 1056-65.

168. Kisiel, W., Fujikawa, K., Davie, E. W., *Activation of bovine factor VII (proconvertin) by factor XIIa (activated Hageman factor). Biochemistry*, 1977. **16**(19): p. 4189-94.

169. Radcliffe, R., Nemerson, Y., *Activation and control of factor VII by activated factor X and thrombin. Isolation and characterization of a single chain form of factor VII. J Biol Chem*, 1975. **250**(2): p. 388-95.

170. Rao, L.V., Rapaport, S. I., *Activation of factor VII bound to tissue factor: a key early step in the tissue factor pathway of blood coagulation. Proc Natl Acad Sci U S A*, 1988. **85**(18): p. 6687-91.

171. Nemerson, Y., Repke, D., *Tissue factor accelerates the activation of coagulation factor VII: the role of a bifunctional coagulation cofactor. Thromb Res*, 1985. **40**(3): p. 351-8.

172. van 't Veer, C., Mann, K. G., *Regulation of tissue factor initiated thrombin generation by the stoichiometric inhibitors tissue factor pathway inhibitor, antithrombin-III, and heparin cofactor-II.* J Biol Chem, 1997. **272**(7): p. 4367-77.

173. Andree, H.A., Nemerson, Y., *Tissue factor: regulation of activity by flow and phospholipid surfaces.* Blood Coagul Fibrinolysis, 1995. **6**(3): p. 189-97.

174. Gemmell, C.H., Turitto, V. T., Nemerson, Y., *Flow as a regulator of the activation of factor X by tissue factor.* Blood, 1988. **72**(4): p. 1404-6.

175. Gir, S., Slack, S. M., Turitto, V. T., *A numerical analysis of factor X activation in the presence of tissue factor--factor VIIa complex in a flow reactor. Ann Biomed Eng*, 1996. **24**(3): p. 394-9.

176. Nemerson, Y., *Tissue factor and hemostasis. Blood*, 1988. **71**(1): p. 1-8.

177. Mimms, L.T., Zampighi, G., Nozaki, Y., Tanford, C., Reynolds, J. A., *Phospholipid vesicle formation and transmembrane protein incorporation using octyl glucoside.* Biochemistry, 1981. **20**(4): p. 833-40.

178. Jones, K.C., Mann, K. G., *A model for the tissue factor pathway to thrombin. II. A mathematical simulation.* J Biol Chem, 1994. **269**(37): p. 23367-73.

179. van 't Veer, C., Hackeng, T. M., Delahaye, C., Sixma, J. J., Bouma, B. N., *Activated factor X and thrombin formation triggered by tissue factor on endothelial cell matrix in a flow model: effect of the tissue factor pathway inhibitor. Blood*, 1994. **84**(4): p. 1132-42.

180. Hall, C.L., Slack, S. M., Turitto, V. T., *A computational analysis of FXa generation by TF:FVIIa on the surface of rat vascular smooth muscle cells. Ann Biomed Eng*, 1998. **26**(1): p. 28-36.

181. Santucci, R.A., Erlich, J., Labriola, J., Wilson, M., Kao, K. J., Kickler, T. S., Spillert, C., Mackman, N., *Measurement of tissue factor activity in whole blood. Thromb Haemost*, 2000. **83**(3): p. 445-54.

182. Osterud, B., Rapaport, S. I., *Activation of factor IX by the reaction product of tissue factor and factor VII: additional pathway for initiating blood coagulation. Proc Natl Acad Sci U S A*, 1977. **74**(12): p. 5260-4.
183. Davie, E.W., Fujikawa, K., Kisiel, W., *The coagulation cascade: initiation, maintenance, and regulation. Biochemistry*, 1991. **30**(43): p. 10363-70.

184. Naito, K., Fujikawa, K., *Activation of human blood coagulation factor XI independent of factor XII. Factor XI is activated by thrombin and factor XIa in the presence of negatively charged surfaces. J Biol Chem*, 1991. **266**(12): p. 7353-8.

185. Gailani, D., Broze, G. J., Jr., *Factor XI activation in a revised model of blood coagulation.* Science, 1991. **253**(5022): p. 909-12.

186. Ohlin, A.K., Marlar, R. A., *The first mutation identified in the thrombomodulin gene in a 45-year-old man presenting with thromboembolic disease. Blood*, 1995. **85**(2): p. 330-6.

187. Healy, A.M., Rayburn, H. B., Rosenberg, R. D., Weiler, H., *Absence of the blood-clotting regulator thrombomodulin causes embryonic lethality in mice before development of a functional cardiovascular system. Proc Natl Acad Sci U S A*, 1995. **92**(3): p. 850-4.

188. Shing, Y., Folkman, J., Sullivan, R., Butterfield, C., Murray, J., Klagsbrun, M., *Heparin affinity: purification of a tumor-derived capillary endothelial cell growth factor. Science*, 1984. **223**(4642): p. 1296-9.

189. Rosenberg, R.D., Reilly, C., Fritze, L., *Atherogenic regulation by heparin-like molecules. Ann N Y Acad Sci*, 1985. **454**: p. 270-8.

190. Bengtsson-Olivecrona, G., Olivecrona, T., *Binding of active and inactive forms of lipoprotein lipase to heparin. Effects of pH. Biochem J*, 1985. **226**(2): p. 409-13.

191. Zucker, M.B., *Effect of heparin on platelet function. Thromb Diath Haemorrh*, 1975. **33**(1): p. 63-5.

192. Hirahara, K., Etoh, Y., Matsuishi, T., Suzuki, N., Kurata, M., *Synergistic effect of antithrombin III, activated protein C and heparin on the inhibition of the tissue thromboplastin-mediated coagulation. Chem Pharm Bull (Tokyo)*, 1989. **37**(3): p. 692-6.

193. Petaja, J., Fernandez, J. A., Gruber, A., Griffin, J. H., *Anticoagulant synergism of heparin and activated protein C in vitro. Role of a novel anticoagulant mechanism of heparin, enhancement of inactivation of factor V by activated protein C.* J Clin Invest, 1997. **99**(11): p. 2655-63.
194. Nicolaes, G.A., Sorensen, K. W., Friedrich, U., Tans, G., Rosing, J., Autin, L., Dahlback, B., Villoutreix, B. O., *Altered inactivation pathway of factor Va by*

activated protein C in the presence of heparin. Eur J Biochem, 2004. **271**(13): p. 2724-36.

195. De Cristofaro, R., De Candia, E., Landolfi, R., *Effect of high- and low-molecular-weight heparins on thrombin-thrombomodulin interaction and protein C activation. Circulation*, 1998. **98**(13): p. 1297-301.

196. Linder, R., Frebelius, S., Jansson, K., Swedenborg, J., *Inhibition of endothelial cell-mediated generation of activated protein C by direct and antithrombin-dependent thrombin inhibitors. Blood Coagul Fibrinolysis*, 2003. **14**(2): p. 139-46.

197. Pignataro, B., Steinem, C., Galla, H. J., Fuchs, H., Janshoff, A., *Specific adhesion of vesicles monitored by scanning force microscopy and quartz crystal microbalance.* Biophys J, 2000. **78**(1): p. 487-98.

198. Chiruvolu, S., Walker, S., Israelachvili J, Schmitt FJ, Leckband D, Zasadzinski JA., *Higher order self-assembly of vesicles by site-specific binding.* Science, 1994. **264**(5166): p. 1753-6.

199. Pashkov VN, T.G., Griko NB, Skopinskaya SN, Yarkov SP., *The use of streptavidin-biotin interaction for preparation of reagents for complement-dependent liposome immunoassay of proteins: detection of latrotoxin.* Anal Biochem, 1992. **207**(2): p. 341-7.

200. Jesty, J., Lorenz, A., Rodriguez, J., Wun, T. C., *Initiation of the tissue factor pathway of coagulation in the presence of heparin: control by antithrombin III and tissue factor pathway inhibitor.* Blood, 1996. **87**(6): p. 2301-7.

201. Lu, G., Broze, G. J., Jr., Krishnaswamy, S., *Formation of factors IXa and Xa by the extrinsic pathway: differential regulation by tissue factor pathway inhibitor and antithrombin III. J Biol Chem*, 2004. **279**(17): p. 17241-9.

202. Marciniak, E., *Factor-Xa inactivation by antithrombin. 3. Evidence for biological stabilization of factor Xa by factor V-phospholipid complex. Br J Haematol*, 1973. **24**(3): p. 391-400.

203. Rosenberg, R.D., Rosenberg, J. S., *Natural anticoagulant mechanisms. J Clin Invest*, 1984. **74**(1): p. 1-6.

204. Ruzicka, K., Wojta, J., Artemiou, O.,Birsan, T., Quehenberger, P., Kapiotis, S., Hofbauer, R., Speiser, W., *Human endothelial cells do not exert heparin like accelerating effects on thrombin-antithrombin-complex formation. Life Sci*, 1998. **63**(17): p. 1493-503.

205. Koyama, T., Parkinson, J. F., Sie, P.,Bang, N. U., Muller-Berghaus, G., Preissner, K. T., *Different glycoforms of human thrombomodulin. Their glycosaminoglycan-*

dependent modulatory effects on thrombin inactivation by heparin cofactor II and antithrombin III. Eur J Biochem, 1991. **198**(3): p. 563-70.

206. Hofsteenge, J., Taguchi, H., Stone, S. R., *Effect of thrombomodulin on the kinetics of the interaction of thrombin with substrates and inhibitors. Biochem J*, 1986. **237**(1): p. 243-51.

207. Bourin, M.C., Boffa, M. C., Bjork, I., Lindahl, U., *Functional domains of rabbit thrombomodulin. Proc Natl Acad Sci U S A*, 1986. **83**(16): p. 5924-8.

208. Bourin, M.C., Lundgren-Akerlund, E., Lindahl, U., *Isolation and characterization of the glycosaminoglycan component of rabbit thrombomodulin proteoglycan. J Biol Chem*, 1990. **265**(26): p. 15424-31.

209. Neter, J., Kutner, M.H., Nachtsheim, C.J., Wasserman, W., *Applied Linear Statistical Models*. 4th ed. 1996: IRWIN.
210. Basmadjian, D., *The effect of flow and mass transport in thrombogenesis. Ann Biomed Eng*, 1990. **18**(6): p. 685-709.

211. Baldwin, S.A., Basmadjian, D., *A mathematical model of thrombin production in blood coagulation, Part I: The sparsely covered membrane case. Ann Biomed Eng*, 1994. **22**(4): p. 357-70.

212. Basmadjian, D., Sefton, M. V., Baldwin, S. A., *Coagulation on biomaterials in flowing blood: some theoretical considerations. Biomaterials*, 1997. **18**(23): p. 1511-22.

213. Gregory, K., Basmadjian, D., *An analysis of the contact phase of blood coagulation: effects of shear rate and surface are intertwined. Ann Biomed Eng*, 1994. **22**(2): p. 184-93.

214. Friedrich, U., Blom, A. M., Dahlback, B., Villoutreix, B. O., *Structural and energetic characteristics of the heparin-binding site in antithrombotic protein C. J Biol Chem*, 2001. **276**(26): p. 24122-8.

215. Keuren, J.F., Wielders, S. J., Driessen, A., Verhoeven, M., Hendriks, M., Lindhout, T., *Covalently-bound heparin makes collagen thromboresistant.* Arterioscler Thromb Vasc Biol, 2004. **24**(3): p. 613-7.

216. Bossavy, J.P., Cadroy, Y., Sakariassen, K., Boneu, B. and A. Barret, *Nonfractionated heparin fails to inhibit arterial thrombosis in a human ex vivo thrombosis model.* Ann Vasc Surg, 1999. **13**(4): p. 393-401.

217. Bossavy, J.P., Sakariassen, K. S., Rubsamen, K., Thalamas, C., Boneu, B., Cadroy, Y., *Comparison of the antithrombotic effect of PEG-hirudin and heparin in a*

human ex vivo model of arterial thrombosis. Arterioscler Thromb Vasc Biol, 1999. **19**(5): p. 1348-53.

218. Silvers, L.W., Royster, T. S., Mulcare, R. J., *Peripheral arterial emboli and factors in their recurrence rate.* Ann Surg, 1980. **192**(2): p. 232-6.

219. Marra, K.G., Kidani, D.D.A, Chaikof, E.L., *Cytomimetic Biomaterials. 2. In-Situ Polymerization of Phospholipids on a Polymer Surface. Langmuir*, 1997. **13**: p. 5697-5701.

220. Hubbell, J.A., McIntire, L. V., *Platelet active concentration profiles near growing thrombi. A mathematical consideration.* Biophys J, 1986. **50**(5): p. 937-45.

221. Goldsmith, H.L., Turitto, V. T., *Rheological aspects of thrombosis and haemostasis: basic principles and applications. ICTH-Report--Subcommittee on Rheology of the International Committee on Thrombosis and Haemostasis. Thromb Haemost*, 1986. **55**(3): p. 415-35.

222. Strony, J., Beaudoin, A., Brands, D., Adelman, B., *Analysis of shear stress and hemodynamic factors in a model of coronary artery stenosis and thrombosis.* Am J Physiol, 1993. **265**(5 Pt 2): p. H1787-96.

223. Roux, S.P., Sakariassen, K. S., Turitto, V. T., Baumgartner, H. R., *Effect of aspirin and epinephrine on experimentally induced thrombogenesis in dogs. A parallelism between in vivo and ex vivo thrombosis models.* Arterioscler Thromb, 1991. **11**(5): p. 1182-91.

224. Aarts, P.A., ,van den Broek, S. A., Prins, G. W., Kuiken, G. D., Sixma, J. J., Heethaar, R. M., *Blood platelets are concentrated near the wall and red blood cells, in the center in flowing blood.* Arteriosclerosis, 1988. **8**(6): p. 819-24.

225. Weiss, H.J., Turitto, V. T., Baumgartner, H. R., *Role of shear rate and platelets in promoting fibrin formation on rabbit subendothelium. Studies utilizing patients with quantitative and qualitative platelet defects.* J Clin Invest, 1986. **78**(4): p. 1072-82.

226. Weiss, H.J., *Scott syndrome: a disorder of platelet coagulant activity.* Semin Hematol, 1994. **31**(4): p. 312-9.

227. Zwaal, R.F., Schroit, A. J., *Pathophysiologic implications of membrane phospholipid asymmetry in blood cells.* Blood, 1997. **89**(4): p. 1121-32.